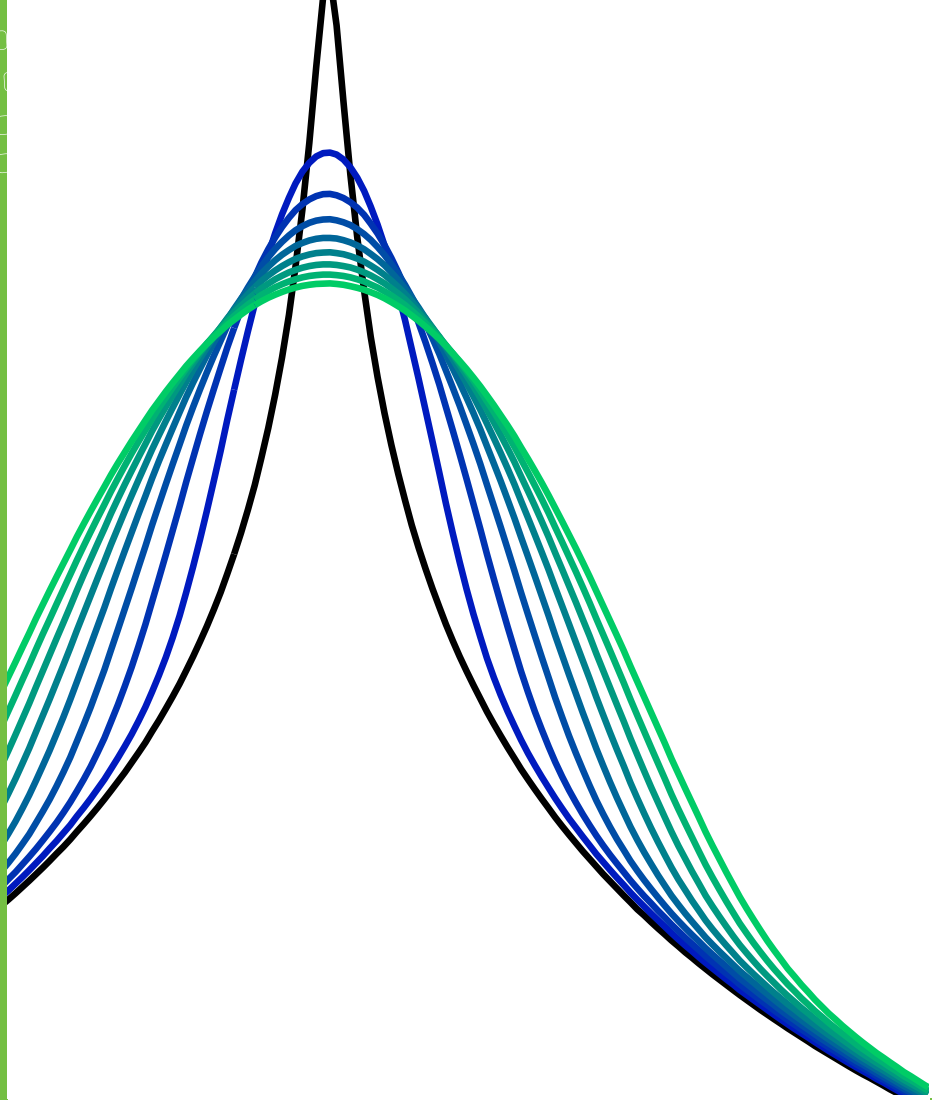

Development of a stochastic temperature treatment technique for Monte Carlo neutron tracking

Tuomas Viitanen

VISIONS • SCIENCE • TECHNOLOGY • RESEARCH HIGHLIGHTS

Dissertation
84

VTT SCIENCE 84

Development of a stochastic temperature treatment technique for Monte Carlo neutron tracking

Tuomas Viitanen

Thesis for the degree of Doctor of Science to be presented with due permission for public examination and criticism in Auditorium E, at Aalto University (Otakaari 1, Espoo, Finland), on the 8th of May, 2015, at 1 p.m.

ISBN 978-951-38-8242-6 (Soft back ed.)
ISBN 978-951-38-8243-3 (URL: http://www.vtt.fi/publications/index.jsp)

VTT Science 84

ISSN-L 2242-119X
ISSN 2242-119X (Print)
ISSN 2242-1203 (Online)

JULKAISIJA – UTGIVARE – PUBLISHER

Teknologian tutkimuskeskus VTT Oy
PL 1000 (Tekniikantie 4 A, Espoo)
02044 VTT
Puh. 020 722 111, faksi 020 722 7001

Teknologiska forskningscentralen VTT Ab
PB 1000 (Teknikvägen 4 A, Esbo)
FI-02044 VTT
Tfn +358 20 722 111, telefax +358 20 722 7001

VTT Technical Research Centre of Finland Ltd
P.O. Box 1000 (Tekniikantie 4 A, Espoo)
FI-02044 VTT, Finland
Tel. +358 20 722 111, fax +358 20 722 7001

Grano Oy, Kuopio 2015

Development of a stochastic temperature treatment technique for Monte Carlo neutron tracking

Tuomas Viitanen. Espoo 2015.

Abstract

Thermal motion of nuclides has a significant effect on the reaction probabilities and scattering kinematics of neutrons. Since also the nuclides in nuclear reactor materials are in constant thermal motion, the temperature-induced effects need to be taken into account in all neutron transport calculations. This task is notably complicated by the fact that the temperature distributions within operating power reactors are always non-uniform.

With conventional transport methods, accurate modeling of temperature distributions within a reactor is cumbersome. The temperature distributions that are in reality continuous in space need to be approximated with regions of uniform temperature. More importantly, pre-generated temperature-dependent data on reaction probabilities must be stored in the computer memory at each temperature appearing in the system, which restricts the feasible level of detail in the modeling of temperature distributions.

This thesis covers the previous development of a temperature treatment technique for modeling the effects of thermal motion on-the-fly during Monte Carlo neutron transport calculation. Thus, the Target Motion Sampling (TMS) temperature treatment technique is capable of modeling arbitrary temperature distributions such that the memory footprint of the interaction data is unaffected by the resolution of the temperature discretization. As a very convenient additional feature the TMS technique also provides for modeling of continuous temperature distributions as-is, making the discretization of temperature distributions unnecessary altogether.

The basic idea of the TMS technique is introduced, and the results are shown to be in accordance with reference solutions calculated with conventional neutron transport methods. The TMS method is developed further by optimizing its implementation, and the performance is compared against conventional neutron transport methods in different reactor systems. The results show that the TMS method significantly facilitates the modeling of complex temperature distributions in nuclear reactors without compromising the accuracy of the calculations. The method also proves to be well-feasible in terms of performance, especially as long as the number of temperature-dependent nuclides remains relatively small.

Keywords Monte Carlo, neutron tracking, temperature, Doppler-broadening, DBRC, Target motion sampling, TMS, temperature majorant cross section

Academic dissertation

Supervising professor	Prof. Filip Tuomisto Department of Applied Physics Aalto University, Finland
Thesis advisor	Adj. Prof. Jaakko Leppänen Nuclear Energy VTT Technical Research Centre of Finland Ltd
Preliminary examiners	Prof. Brian Kiedrowski Nuclear Engineering and Radiological Sciences University of Michigan
	Prof. Kord Smith Nuclear Science & Engineering Massachusetts Institute of Technology
Opponent	Prof. Sedat Goluoglu Department of Material Sciences & Engineering University of Florida

Acknowledgments

I wish to express my special appreciation and thanks to my instructor and mentor, the Father of Serpent, Dr. Jaakko Leppänen, for the inspiring research topic and all the invaluable guidance and support during the process. Having the opportunity to test and implement the new method as a part of Serpent has been extremely motivating, and, of course, the thesis would not exist without the ambitious Serpent code development project. Working together has also been a lot of fun.

I would like to thank my other colleagues at VTT for the great working atmosphere and for providing help whenever needed. I am especially grateful to our Team Leader, Dr. Petri Kotiluoto, and the Head of Research Area, Dr. Timo Vanttola, for their continuous support, and Dr. Maria Pusa for providing important comments on the key articles of the thesis.

I am obliged to Prof. Filip Tuomisto of the Department of Applied Physics, Aalto University, for acting as my supervisor and for Prof. Sedat Goluoglu of the Department of Material Sciences & Engineering, University of Florida, for acting as my opponent in the defense of this thesis. I wish to express my gratitude to the preliminary examiners Prof. Brian Kiedrowski, University of Michigan, and Prof. Kord Smith, Massachusetts Institute of Technology (MIT), for their careful work and insightful views on the thesis. I would like to thank also Prof. Benoit Forget (MIT) for hosting a short but very efficient and educative visit to MIT in the fall of 2013, during which this thesis took a giant step forward.

Finally, I want to thank the Polytech Choir for filling the musical void within for the past 9 years. Above all, I wish to thank thank my beloved wife Elina for her love and support during the long process.

This work has been funded through the Finnish Research Programme on Nuclear Power Plant Safety SAFIR and the Academy of Finland research program NUMPS.

List of publications

This thesis consists of the present article and the following seven publications.

I T. Viitanen and J. Leppänen, "Explicit treatment of thermal motion in continuous-energy Monte Carlo tracking routines", *Nucl. Sci. Eng.*, **171**, pp. 165-173, (2012).

II T. Viitanen and J. Leppänen, "Explicit temperature treatment in Monte Carlo neutron tracking routines — first results", *In proc.* PHYSOR-2012, Knoxville, TN, Apr. 15-20 2012, (2012).

III T. Viitanen and J. Leppänen, "Optimizing the implementation of the target motion sampling temperature treatment technique — How fast can it get?", *In proc.* M&C 2013, Sun Valley, ID, May 5-9 2013, (2013).

IV T. Viitanen and J. Leppänen, "Target motion sampling temperature treatment technique with elevated basis cross-section temperatures", *Nucl. Sci. Eng.*, **177**, pp. 77-89, (2014).

V T. Viitanen and J. Leppänen, "Temperature majorant cross sections in Monte Carlo neutron tracking", *Nucl. Sci. Eng.*, Accepted for publication Aug 31. 2014.

VI T. Viitanen and J. Leppänen "Effect of the target motion sampling temperature treatment method on the statistics and performance", *Ann. Nucl. Energy*, Accepted for publication Aug 21. 2014.

VII T. Viitanen, J. Leppänen and B. Forget, "Target motion sampling temperature treatment technique with track-length estimators in OpenMC — Preliminary results", *In proc.* PHYSOR-2014, Kyoto, Japan, Sep. 28-Oct 3. 2014, (2014).

Author's contribution

Publication I: Explicit treatment of thermal motion in continuous-energy Monte Carlo tracking routines

The author was responsible for all the theoretical considerations behind the TMS method, choosing the test problem and performing all the calculations. The article was written by the author apart from Sections I and III, which were written in collaboration by the two authors.

Publication II: Explicit temperature treatment in Monte Carlo neutron tracking routines — first results

The author was responsible for the implementation of the temperature treatment routine in Serpent reactor physics code, choosing of the test cases and performing the calculations. The article was written by the author with the exception that the description of the step-by-step example in Section III was written by the second author.

Publication III: Optimizing the implementation of the target motion sampling temperature treatment technique — How fast can it get?

All of the optimization techniques were developed by the author. The author also wrote the theoretical considerations, implemented the techniques in the Serpent code, performed the test calculations and was the main author of the article.

Publication IV: Target motion sampling temperature treatment technique with elevated basis cross-section temperatures

The author derived the theoretical considerations presented in the article, selected the test cases, performed the test calculations, analyzed the results and was the main author of the article.

Publication V: Temperature majorant cross sections in Monte Carlo neutron tracking

The author developed the new cut-off condition for thermal motion in the generation of TMS and DBRC majorants, implemented the new technique in Serpent, performed the test calculations, analyzed the results and was the main author of the article.

Publication VI: Effect of the target motion sampling temperature treatment method on the statistics and performance

The author tested the functionality of the reaction rate estimators together with the TMS method, studied the performance of the reaction rate estimators in four test cases, analyzed the results and was the main author of the article.

Publication VII: Target motion sampling temperature treatment technique with track-length estimators in OpenMC — Preliminary results

The author implemented the TMS technique in OpenMC, performed the test calculations, analyzed the results and was the main author of the article.

Contents

1. Introduction

Nuclear fission reactors play a very important role in contemporary society. As it is well known, most of the fission reactors around the world are harnessed to produce clean and carbon dioxide-free energy, but nuclear reactors serve also many less prominent but important purposes. Other common applications include materials research and production of artificial isotopes for various medical and industrial applications.

The operation of nuclear fission reactors is based on a self-sustaining fission chain reaction in fissile fuel material, typically uranium. The chain reaction is driven by neutrons that are released in each fission event and that are able to induce new fission reactions when interacting with fissile material. The power production of fission reactors is based on the fact that a significant amount of recoverable energy is released in each fission, while most of the other applications take advantage of excess neutrons present in the reactor core.

Safe and economical operation and design of nuclear fission reactors requires thorough understanding of their behavior in varying conditions. The behavior of an operating reactor is governed by the propagation of neutrons maintaining the fission chain reaction, and hence neutron transport studies constitute an essential part of practically all reactor analyses. For a couple of decades, reactor physics has been mainly analyzed with computer programs, "codes", that simulate neutron transport based on physical models and semi-empirical data describing the properties of reactor materials. Output from a neutron transport calculation includes for example the multiplication factor, which basically determines whether the neutron population in the system is increasing or decreasing, and the spatial power distribution.

The power distribution of the system affects the temperature and material density distributions within the system via heat transfer, but at the same time the transport of the neutrons is strongly affected by these distributions. Thus, an accurate solution for the state of the reactor can only be achieved by solving the neutronics and the thermal hydraulics simultaneously. Traditionally, the coupled solution has been achieved using an approximative scheme based on splitting the neutron transport calculation into two parts: First, the average properties of fuel assemblies are determined in accurate lattice physics calculations that are performed separately for a few different thermal hydraulic state points. Then, the averaged properties of the assemblies are

used as input in a more coarse, full-core thermal hydraulics/neutronics simulation such that the feedback to neutronics is modeled by interpolating between the state points.

This approach has been successfully used in the past and will probably be used also for many years to come, at least in production calculations in which fast calculation is a high priority. However, quite recently there has been a growing interest in performing high-fidelity multi-physics calculations in which both the thermal hydraulics and the neutronics are converged truly simultaneously. When applied with high-fidelity transport techniques like the continuous-energy Monte Carlo method, multi-physics simulations provide highly accurate reference solutions that can be used, for instance, in the validation of lighter calculation tools.

One non-trivial task in multi-physics calculations is the modeling of the temperature and density distributions, as obtained from the thermal hydraulics solver, within the neutron transport code. Traditional neutron transport methods can only be applied with material regions that are homogeneous in terms of material composition, density and temperature. Consequently, the temperature distributions that are factually continuous need to be approximated using spatial discretization[1]. This does not necessarily limit the accuracy of the transport calculation if the discretization is fine enough. However, splitting the geometry into numerous regions inflicts the performance of the transport calculations and increases the memory requirement, since nuclide interaction data needs to be stored separately at each temperature appearing in the system.

The main topic of the current thesis is a new technique for overcoming the challenges related to modeling the temperature distributions in continuous-energy Monte Carlo neutron transport calculations. The technique is discussed in Publications I-VII which are summarized in Chapter 5. Chapters 2–4 of the current article provide an introduction to the modeling of thermal motion in neutron transport calculations and neutron transport in general. The thesis is written strictly from the neutron physics point of view, i.e. assuming a given thermal-hydraulic state and nuclide composition within the system.

[1] The situation is, in fact, the same also with density distributions.

2. Physical background of neutron transport

Neutron transport analyses are required in the design and operation of all nuclear reactors. Practically all quantities studied in reactor physical analyses can be derived from the distribution of neutrons within the reactor in energy, space and time. Thus, solution of this distribution can be considered as the main goal of neutron transport calculations. Following the propagation of neutrons from birth at fission events to termination at the next generation fission events, absorptions or leakage requires a deep understanding of different phenomena affecting the transport process, as well as knowledge on the exact geometry, nuclide composition and thermal hydraulic state of the system. The most important concepts and phenomena related to the neutron transport are shortly introduced in the following.

2.1 Neutron interactions

The neutron interactions can be divided roughly into fission, scattering and capture reactions, the essentials of which are introduced in the current section.

2.1.1 Fission

In a fission reaction the target nucleus splits into two[2] lighter nuclides called fission fragments or fission products, releasing about 200 MeV of energy and a couple of fission neutrons, the average number of which depends on the energy of the incident neutron that induced the fission event. As it can be seen in Figure 2.1, at incident neutron energies lower than 100 keV the average number of neutrons emitted per fission, $\overline{\nu}_{\text{tot}}(E)$, is between two and three for the common fissile nuclides ^{235}U, ^{239}Pu and ^{241}Pu, but at higher energies the number of neutrons increases along with neutron energy. Even though it is hard to see in Figure 2.1 because of the logarithmic scale, the dependence of $\overline{\nu}_{\text{tot}}(E)$ on neutron energy is roughly linear.

Most of the energy released in the nuclear fission event is received by the fission fragments and ends up heating the nuclear fuel material. A small fraction of the energy is, however, received by the fission neutrons. The energy distribution of fission

[2] To be precise, also ternary and quaternary fissions, in which the fissile nuclide splits into three or four nuclides respectively, occurs but these reactions are relatively rare.

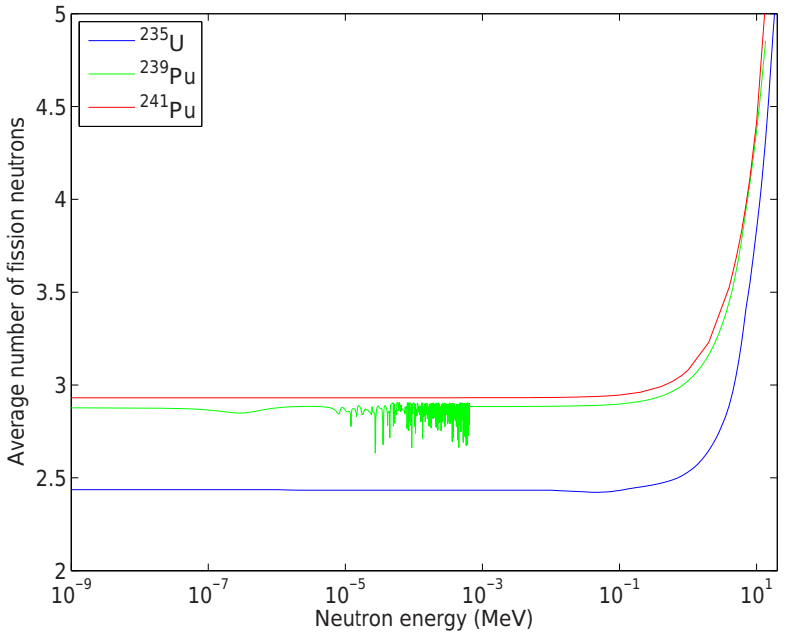

Figure 2.1. The average number of fission neutrons released in a fission event increases along with neutron energy [1].

neutrons is often described by a Maxwellian distribution with the peak of the distribution around 1 MeV. As can be seen in Figure 2.2, the exact shape of the distribution depends somewhat on the nuclide.

In fact, all of the fission neutrons are not released at the instant of the fission event, but following the beta decay of a special type of fission fragments called delayed neutron precursors. These precursor nuclides, for example ^{87}Br, may release a neutron immediately following their beta decay. Since the beta decay is a relatively slow process, the time difference between the *prompt neutrons* born in the fission event and the emission of the *delayed neutrons* makes a difference in reactor dynamics even though the proportion of delayed neutrons is very small. If the total number of fission neutrons $\overline{\nu}_{\text{tot}}(E)$ is divided into contributions from prompt and delayed neutrons, the proportion of $\overline{\nu}_{\text{delayed}}(E)$ at 1 eV is 0.66 % for ^{235}U, 0.23 % for ^{239}Pu and 0.55 % for ^{241}Pu [1]. Also the energy distribution of the delayed neutrons differs from the prompt neutron distribution.

Fission reactions are the primary neutron source in the fission reactors, and also the vast majority of the energy production originates from the fission reactions.

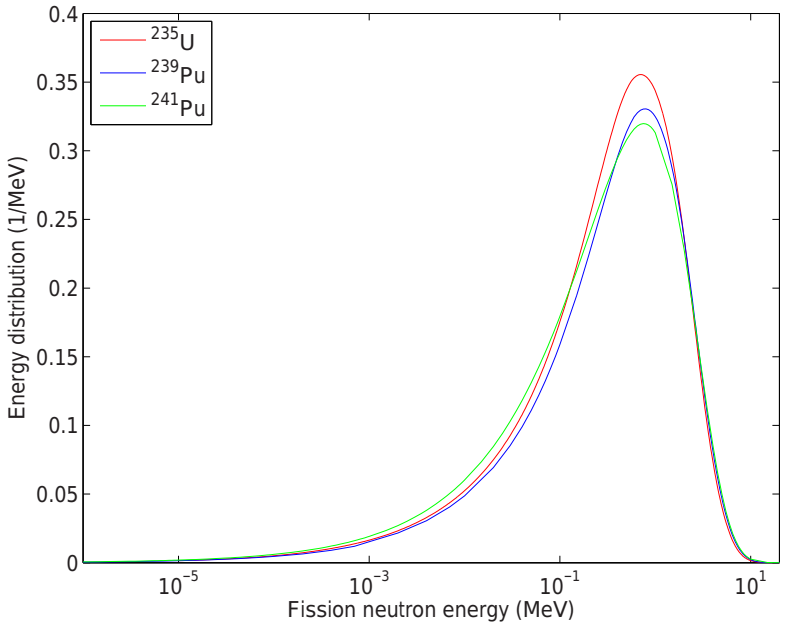

Figure 2.2. The energy distributions of fission neutrons are slightly different for each fissile nuclide, but the most probable energy is close to 1 MeV for all of the nuclides [1].

2.1.2 Capture

In this thesis capture reactions refer to all the interactions in which no secondary neutrons are emitted. The simplest of such interactions is called radiative capture (n,γ), in which the neutron is absorbed in the target nucleus, increasing its neutron number by one. In these interactions the daughter nuclide is born in an excited state, which is discharged via emission of a gamma photon. Other capture reactions include, for example, (n,p) and (n,α) interactions in which the neutron is absorbed in the target nucleus and a proton or an α particle is released, respectively.

Capture reactions are parasitic reactions that remove neutrons from the reactor system and consequently restrain the fission chain reaction. This effect can be used intentionally to regulate the operation of a nuclear reactor by inserting and removing absorbing materials to and from the reactor. On the other hand, the emergence of absorbing fission products introduces inevitable capture reactions in the reactor as the nuclear fuel gains burnup.

It should also be mentioned that some of the capture reactions produce useful nuclides. For instance the reaction chain

$$^{238}\mathrm{U(n,\gamma)}^{239}\mathrm{U} \xrightarrow[23.45\ \mathrm{min}]{\beta-} {}^{239}\mathrm{Np} \xrightarrow[2.365\ \mathrm{d}]{\beta-} {}^{239}\mathrm{Pu}$$

produces new fissile material in nuclear reactors and reaction ^{54}Fe(n, p)^{54}Mn is often used in the neutron dosimetry of pressure vessel materials.

2.1.3 Scattering

The scattering reactions can be divided further into elastic and inelastic scattering reactions, of which elastic scattering reactions dominate at energies below about 1 MeV and inelastic scattering occurs mainly at the MeV-range[3]. In an elastic scattering event a neutron collides with a target nucleus and scatters such that both the total kinetic energy and momentum are conserved in the collision, whereas only the momentum is conserved in inelastic scattering.

Assuming that the target is at rest, the collision kinematics of an elastic scattering event can be straightforwardly solved in the laboratory frame (L-frame). If the direction of the neutron is assumed to change by angle ϕ in the scattering process, the L-frame energy of the incident neutron is E and the mass of the target, MA_n, is expressed relative to the neutron mass M using atomic weight ratio A_n of the target nuclide n, equation

$$E^* = \frac{E}{(A_n + 1)^2}(\cos\phi + \sqrt{A_n^2 - \sin^2\phi})^2 \tag{2.1}$$

can be derived for the energy of the neutron after the scattering [2]. The equation follows straightforwardly from the conservation laws of energy and momentum in the L-frame, and it can be used to perceive some basic properties of the elastic scattering events.

However, in actual neutron transport calculations it is more practical to approach the scattering problem in center-of-mass frame (C-frame) in which the total momentum is always zero. There are basically two reasons for this:

- The L-frame equations are significantly complicated when the (thermal) motion of the target nuclide is taken into account.
- More importantly, the C-frame is the natural frame of reference for the solution of collision physics, specifically scattering angles. For instance, under certain conditions elastic scattering is isotropic in the C-frame, but the same does not apply to the L-frame.

The center-of-mass system is moving in the L-frame with velocity

$$\mathbf{V}_C = \frac{M\mathbf{v} + A_n M\mathbf{V}_t}{M + A_n M} = \frac{\mathbf{v} + A_n\mathbf{V}_t}{1 + A_n}, \tag{2.2}$$

where $\mathbf{v}$ is the velocity of the neutron and $\mathbf{V}_t$ is the velocity of the target. The L-frame

[3] To be precise, inelastic scattering may occur also at the keV-range from metastable nuclides like ^{242m}Am, but since the abundance of these nuclides in typical reactors is small, the keV-range inelastic scattering is of minor importance.

velocities can be converted to C-frame and vice versa using equations

$$\mathbf{v}_\mathrm{C} = \mathbf{v} - \mathbf{V}_\mathrm{C} = \frac{A_n(\mathbf{v} - \mathbf{V}_\mathrm{t})}{1 + A_n} \tag{2.3}$$

$$\mathbf{V}_{\mathrm{t,C}} = \mathbf{V}_\mathrm{t} - \mathbf{V}_\mathrm{C} = -\frac{\mathbf{v} - \mathbf{V}_\mathrm{t}}{1 + A_n}\,. \tag{2.4}$$

Using the classical relation between kinetic energy and velocity

$$E = \frac{1}{2}Mv^2\,, \tag{2.5}$$

the conservation laws for the energy and momentum can be written in the C-frame as

$$\frac{1}{2}v_\mathrm{C}^2 + \frac{1}{2}A_n V_{\mathrm{t,C}}^2 + Q_\mathrm{r} = \frac{1}{2}v_\mathrm{C}^{*2} + \frac{1}{2}A_n V_{\mathrm{t,C}}^{*2} \tag{2.6}$$

$$\mathbf{v}_\mathrm{C} + A_n\mathbf{V}_{\mathrm{t,C}} = \mathbf{v}_\mathrm{C}^* + A_n\mathbf{V}_{\mathrm{t,C}}^* = 0\,, \tag{2.7}$$

where $\mathbf{v}_\mathrm{C}{}^*$ and $\mathbf{V}_{\mathrm{t,C}}{}^*$ are the neutron and target velocities after the collision and Q_r is the amount of energy released in the reaction, which is zero in the case of elastic scattering and $Q_\mathrm{r} < 0$ in the case of inelastic scattering. In an inelastic scattering event the energy Q_r is absorbed by the target nucleus, which is left in an excited state after the interaction. From Equations (2.6)–(2.7) it is possible to derive the C-frame speed of the neutron after the scattering [3]

$$v_\mathrm{C}^* = \sqrt{v_\mathrm{C}^2 + \frac{2A_nQ_\mathrm{r}}{(A_n + 1)M}}\,. \tag{2.8}$$

It should be noted that in the case of an elastic scattering collision the C-frame speed of the neutron remains unchanged.

Instead, the scattering event affects the C-frame direction of the neutron. The change in direction is governed by two angles in the C-frame: cosine of the polar angle μ_C between the incident and exiting neutron directions and azimuthal angle θ_C, which describes the rotation of the velocity vector in the plane perpendicular to $\mathbf{v}_\mathrm{C}$. In general, angle θ_C changes isotropically in the scattering reactions, but the distribution of the cosine μ_C may be either isotropic or anisotropic. After rotating the C-frame velocity vector $\mathbf{v}_\mathrm{C}$ according to these angles, the L-frame velocity of the neutron is obtained with Equation (2.3).

The energy change of the neutron in an elastic scattering event can be easily studied with Equation (2.1) in the simplified case when the target nucleus is at rest. First of all, this equation shows that the neutron tends to lose a *proportion* of its energy in each elastic scattering event. Secondly, the energy change is the highest when $\phi = 180^\circ$ and Equation (2.1) simplifies to

$$E^* = E(\frac{A_n - 1}{A_n + 1})^2\,. \tag{2.9}$$

From this equation it can be seen that for a hydrogen target with $A \approx 1$ the energy change may reach even 100 % in a single collision, but for a heavy nuclide like ^{238}U

with $A \approx 238$ the theoretical maximum is less than 2 %. This property makes light nuclei like hydrogen in water very efficient materials for slowing down, or *moderating*, neutrons. Losing energy in elastic scattering collisions, *down-scattering*, is the primary slowing-down mechanism for the fission neutrons. The slowing-down can be facilitated by adding light moderator materials in the reactor, as it is done in all of the reactors based on fissions at the thermal energy range.

When the thermal motion of target nuclei is taken into account, the process becomes slightly more complicated and the neutron may also gain energy, *up-scatter*, in certain conditions. Thermal motion-induced effects are covered in Section 3.2 in detail.

Interactions denoted with (n,*x*n) do not quite fit in the previously mentioned reaction categories. In these reactions a neutron interacts with the target such that one ($x = 2$) or more ($x \geq 3$) additional neutrons are released from the nucleus. Part of the incident neutron energy is lost in the reaction, which makes these interactions somewhat similar to inelastic scattering reactions. However, the reactions also contribute to neutron multiplication, and the solution of the collision kinematics is complicated by the fact that the momentum and the kinetic energy are distributed among three or more particles.

2.2 Cross sections

The probabilities of the neutron interactions are described by cross sections, σ, which have the dimension of area. Usually cross sections are measured in barns such that one barn equals 10^{-24} cm^2. Physically they can be interpreted as the effective cross sectional area corresponding to a specific reaction of a nuclide. For example, the radiative capture cross section of nuclide n is designated $\sigma_{\gamma,n}$ and summing over all reaction cross sections of a nuclide results in the total cross section $\sigma_{\text{tot},n}$.

In addition to being nuclide- and reaction-dependent, the cross sections depend strongly on the energy of the incident neutron. The energy dependencies of two typical cross sections, namely the radiative capture and elastic scattering cross sections of ^{238}U, are depicted in Fig. 2.3. In this figure, several energy regions can be recognized: At the lowermost energies, in this case below about 10^{-6} MeV, the radiative capture cross section behaves as $1/v$, where v is the velocity of the incident neutron, while the elastic scattering cross section is constant. Between 10^{-6} MeV and 2×10^{-2} MeV the cross section curve contains peaks called resonances. It should be noted that the shape of the cross section curves around the resonances is somewhat different for the scattering and capture resonances: the scattering cross section drops right below the resonance energy and peaks above the energy, while the capture resonances have a purely increasing effect on the cross section. As can be seen in the figure, the cross section may increase more than by a factor of 10^4 in the vicinity of the resonances.

In Fig. 2.3 it seems that the resonances suddenly cease to exist when the energy of the incident neutron increases above 2×10^{-2}, but this not the real case. This energy corresponds to the boundary between the energy regions of resolved and un-

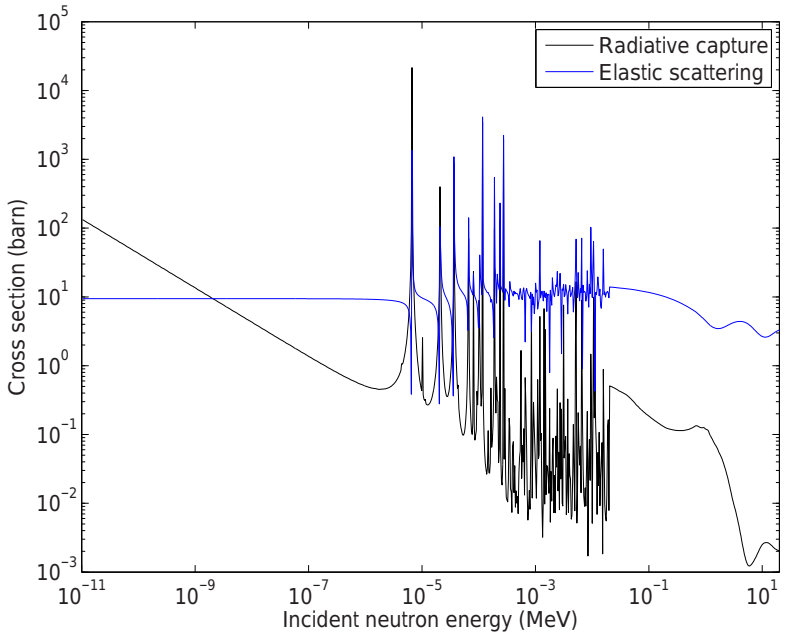

Figure 2.3. Radiative capture and elastic scattering cross sections of ^{238}U at 0 K temperature (cross section data from JEFF-3.1.2 [1]).

resolved resonances, an artificial boundary forced by practice. At the energy region of unresolved resonances, i.e. above the boundary, the relative energy difference between the adjacent resonances is so small that the resonances can no longer be distinguished from each other, but the resonances still have a significant effect on the reaction probabilities in practice. The unresolved resonances are usually described by average parameters for resonance spacing, resonance width and various other quantities, and their effect on reaction probabilities must be taken into account using special techniques. The smooth cross section curve plotted in Fig. 2.3 within this energy region represents energy-averaged or *infinitely dilute* cross sections that can only be applied to very thin geometries or very low abundances without compromising the accuracy of the transport calculations.

Even though it cannot be easily recognized in Fig. 2.3, the energy region of unresolved resonances also has an upper energy limit above which it is no longer necessary to take the effect of the resonance structure into account and the reaction probabilities can be again described as a smooth function of energy. In the case of ^{238}U from the JEFF-3.1.2 data library this boundary is at 3×10^{-1} MeV [1].

Not all nuclides or cross sections have all the previously mentioned regions in their cross section data. For example, cross section curves of the very lightest nuclides do not contain any resonances. It should also be mentioned that there are many *threshold reactions*, such as the (n,*x*n) reactions and the fission reactions of non-

fissile actinides, for which the cross section is zero below the threshold energy E_{thr}. Thus, these reactions cannot be induced by neutrons with energies $E < E_{\text{thr}}$.

2.3 Reaction rates

The microscopic cross sections σ that describe the probabilities for individual targets need to be multiplied by the atomic density of the target nuclide N_n to get macroscopic interaction probabilities in practical materials. The result

$$\Sigma_{i,n}(E) = N_n \sigma_{i,n}(E) \tag{2.10}$$

is the *macroscopic cross section* for reaction i of nuclide n and is expressed as cm^{-1}. In case a material consists of several nuclides, the macroscopic cross section of the material is simply the sum over nuclide-wise contributions

$$\Sigma_i(E) = \sum_n \Sigma_{i,n}(E)\,. \tag{2.11}$$

In the following, the macroscopic cross sections Σ without the subscript n refer to material total cross sections.

Because of the connection to the effective area, macroscopic cross section Σ_i can also be interpreted as the probability for reaction i to occur per unit path length. Hence, the probability distribution of the distance between the reactions P_i obeys the differential equation

$$\frac{dP_i(E,l)}{dl} = -\Sigma_i(E)P(E,l) \tag{2.12}$$

where l is the distance traveled within the material. Solving the equation and normalizing the distribution to unity yields

$$P_i(E,l) = \Sigma_i(E)e^{-\Sigma_i(E)l}\,, \tag{2.13}$$

which is also known as the probability density function of *exponential distribution*.

Reaction rates together with their derivatives constitute the main output of neutron transport calculations. When calculating the reaction rates within a reactor, it is practical to describe the density and velocity distribution of neutrons within the reactor with a quantity called *neutron flux*. It is defined as the neutron velocity (vector) multiplied by the corresponding neutron density $\rho_{\text{n}}(E,\mathbf{r})$. However, since this thesis only deals with the scalar form of the neutron flux, it is practical to remove the angular dependencies via integration over all spatial angles. The scalar neutron flux is designated $\Phi(E,\mathbf{r})$, where $\mathbf{r}$ is the spatial coordinate.

If the neutron flux and the macroscopic cross sections are known, the reaction rate R of reaction i within a volume V can be calculated with the double integral

$$R_i = \int_V \int_E \Sigma_i(E,\mathbf{r})\Phi(E,\mathbf{r})dEd^3r\,. \tag{2.14}$$

The energy integration is usually performed over all energies to get total reaction rates, but in some applications it is beneficial to calculate the contribution of a certain neutron energy interval to the total reaction rate, in which case the integration

limits are chosen according to the boundaries of this interval. For generality, the spatial dependence of Σ_i is added in Eq. (2.14) to allow spatial integration over inhomogeneous material regions.

2.4 Multiplication factor and criticality

As it was previously mentioned, the nuclear reactions are based on a fission chain reaction in which the fission neutrons from one fission generation induce the next generation of fission events. The properties of this chain reaction are of great importance when designing and operating nuclear reactors and, hence, it is necessary to introduce also some nomenclature describing the state of the chain reaction.

In case the chain reaction is exactly self-sustaining, meaning that the neutrons released in a fission event induce exactly one new fission reaction on average, the reactor is *critical* and the *multiplication factor*, defined as

$$k = \frac{\text{Number of neutrons in generation } n+1}{\text{Number of neutrons in generation } n} \tag{2.15}$$

is exactly $k = 1.0$. In case the neutron population and, thus, the fission power of the reactor are increasing, $k > 1.0$ and the reactor is referred to as *super-critical*, whereas the reactor is called *sub-critical* if $k < 1.0$. In addition to absolute units, k is often measured in pcms (*per cent mille*), one pcm corresponding to 10^{-5}.

3. Effects of thermal motion

Practical nuclear systems appear always at temperatures significantly above zero Kelvin. Usually the temperatures are at least around room temperature 300 K, but for example in operating light water reactors the temperature of the coolant is usually above 500 K, the center-line temperature of fuel rods often reaches 1200 K and in accident conditions the temperatures may even exceed 3000 K.

Whenever the temperature of a material is above zero Kelvin, the target nuclei are in constant thermal motion and the temperature determines the extent of the motion. In the case of free gases, the relation between the temperature and the energy distribution of the targets is given by the Maxwell-Boltzmann distribution

$$P_{\mathrm{MB}}(E,T) = 2\sqrt{\frac{E}{\pi}}\left(\frac{1}{k_{\mathrm{B}}T}\right)^{3/2} e^{-\frac{E}{k_{\mathrm{B}}T}} . \tag{3.1}$$

where k_{B} is the Boltzmann constant and T is the local temperature [4]. However, the same distribution has been traditionally applied for all reactor materials including crystalline solids and liquids, for the sake of practicality. The validity of this approximation has been studied by Lamb in Reference [5].

The thermal motion of targets affects neutron transport in several different ways, which are introduced in this chapter. Sections 3.1 and 3.2 discuss the effects on reaction rates and scattering kinematics, respectively, by assuming Maxwellian energy distribution for the thermal motion of targets. Section 3.3 covers the special case of bound atoms that do not obey the Maxwellian distribution and for which also the scattering kinematics is affected by molecular bonds.

3.1 Effect of thermal motion on reaction rates

Because of the thermal vibration of the target nuclei, the relative speed of the incident neutron to the target, v', may be either higher (target moving towards the neutron) or lower (target moving away from the neutron) than the L-frame velocity v. This affects the probabilities at which the neutrons interact with matter and, consequently, the reaction rates.

Perhaps the most intuitive way of examining the overall effect of thermal motion on reaction rates is via thermal-motion-averaged or *effective* cross sections. Using

effective cross sections Σ_{eff} must result in the correct reaction rates, i.e.

$$\Phi(E, \mathbf{r})\Sigma_{\text{eff},n}(E, T, A_n) \tag{3.2}$$

must be equal to the reaction rate calculated with zero Kelvin cross sections with the effect of thermal motion taken into account. By writing the neutron flux $\Phi(E, \mathbf{r})$ as the neutron density $\rho_{\text{n}}(E, \mathbf{r})$ multiplied by the neutron velocity v and by expressing all quantities in terms of neutron velocity rather than energy using Equation (2.5), the formula

$$\begin{aligned}
\rho_{\text{n}}(v, \mathbf{r})v\Sigma_{\text{eff},n}(v, T, A_n) &= \rho_{\text{n}}(v, \mathbf{r}) \int |\mathbf{v}'|\Sigma_n(|\mathbf{v}'|)P(\mathbf{V}_{\text{t}}, T, A_n)d\mathbf{v}' \Leftrightarrow \\
v\sigma_{\text{eff}}(v, T, A_n) &= \int |\mathbf{v}'|\sigma(|\mathbf{v}'|)P(\mathbf{V}_{\text{t}}, T, A_n)d\mathbf{v}' \Leftrightarrow \\
\sigma_{\text{eff}}(v, T, A_n) &= \frac{1}{v}\int |\mathbf{v}'|\sigma(|\mathbf{v}'|)P(\mathbf{V}_{\text{t}}, T, A_n)d\mathbf{v}'
\end{aligned} \tag{3.3}$$

is obtained for the effective cross section of nuclide n. In Equation (3.3) $\mathbf{V}_{\text{t}}$ is the target velocity, $P(\mathbf{V}_{\text{t}}, T, A_n)$ is the velocity distribution of the target nucleus and the integration is performed over all relative velocities. The target velocity $\mathbf{V}_{\text{t}}$ can be written also in terms of the two other velocities using the cosine law

$$\mathbf{V}_{\text{t}} = \mathbf{v} - \mathbf{v}' \tag{3.4}$$

$$V_{\text{t}} = |\mathbf{V}_{\text{t}}| = \sqrt{v^2 + v'^2 - 2vv'\nu}\,, \tag{3.5}$$

where $\nu = \cos\beta$ is the cosine of the angle between the neutron velocity and relative velocity vectors, as illustrated in Figure 3.1.

As it was previously mentioned, it is customary to describe the thermal motion of targets with Maxwell-Boltzmann distribution, which can be written in terms of velocity as

$$P_{\text{MB}}(\mathbf{V}_{\text{t}}, T, A_n) = \left(\frac{\gamma}{\sqrt{\pi}}\right)^3 e^{-\gamma^2(\mathbf{V}_{\text{t}}\cdot\mathbf{V}_{\text{t}})} = \left(\frac{\gamma}{\sqrt{\pi}}\right)^3 e^{-\gamma^2 V_{\text{t}}^2} = P_{\text{MB}}(V_{\text{t}}, T, A_n)\,, \tag{3.6}$$

where

$$\gamma(T, A_n) = \sqrt{\frac{A_n M}{2k_{\text{B}}T}} \tag{3.7}$$

and the dependence of γ on T and A_n is not explicitly shown for the sake of clarity. With the target velocity distribution defined, Equation (3.3) becomes

$$\sigma_{\text{eff}}(v, T, A_n) = \frac{1}{v}\left(\frac{\gamma}{\sqrt{\pi}}\right)^3 \int_0^\infty \int_0^\pi \int_0^{2\pi} v'\sigma(v')e^{-\gamma^2(v^2+v'^2-2vv'\cos\beta)}v'^2 \sin\beta d\theta d\beta dv'\,, \tag{3.8}$$

where the integration is performed in spherical coordinates and θ is the azimuthal angle. After performing the integration over θ and substituting $\cos\beta$ with ν, the equation reduces to

$$\sigma_{\text{eff}}(v, T, A_n) = \frac{2\pi}{v}\left(\frac{\gamma}{\sqrt{\pi}}\right)^3 \int_0^\infty \int_{-1}^1 v'^3\sigma(v')e^{-\gamma^2(v^2+v'^2-2vv'\nu)}d\nu dv'\,. \tag{3.9}$$

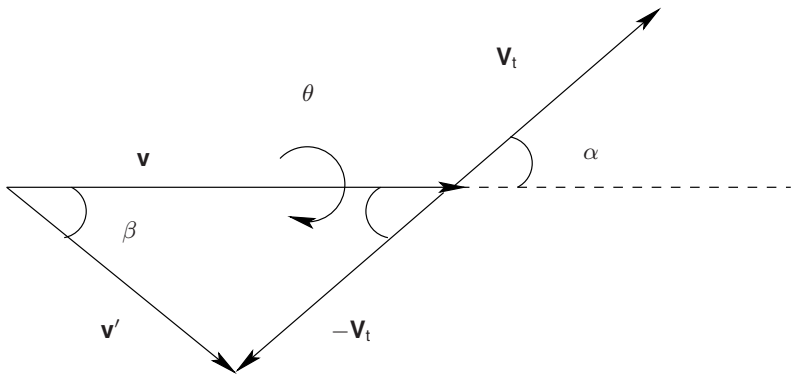

Figure 3.1. The vector diagram illustrates the symbol choices used in the integration over all relative velocities.

By further integrating over ν, the well-known kernel broadening equation

$$\sigma_{\text{eff}}(v, T, A_n) = \frac{\gamma}{v^2\sqrt{\pi}} \int_0^\infty v'^2 \sigma(v')(e^{-\gamma^2(v-v')^2} - e^{-\gamma^2(v+v')^2})dv' \tag{3.10}$$

emerges. The equation is sometimes also called the Solbrig's kernel according to its original developer [6].

This equation describes fully and accurately the effect of thermal motion on reaction probabilities through the concept of effective cross sections. What this means in practice is that the effects of thermal motion on reaction probabilities can be taken into account by simply replacing the zero Kelvin cross sections with effective cross sections in all basic equations, such as Equations (2.13) and (2.14). Additionally, Equation (3.10) is rather easy to apply in practice for all cross sections expressed in a continuous-energy format.

The following sections discuss the consequences of this equation in three different cases.

3.1.1 Thermal energy region

As it was noticed in 2.2, the elastic scattering and radiative capture cross sections of ^{238}U act quite predictably at energies below about 10^{-6} MeV: the elastic scattering cross section is constant and the (n,γ) cross section acts as $1/v$. This kind of behavior of cross sections is common to all nuclides excluding nuclides with strong resonances at low energies, such as ^{113}Cd and ^{135}Xe. For these special cases the low-energy capture cross sections increase slightly steeper than $1/v$ towards low energies and the shape of the elastic scattering cross section curve also is affected by the resonance.

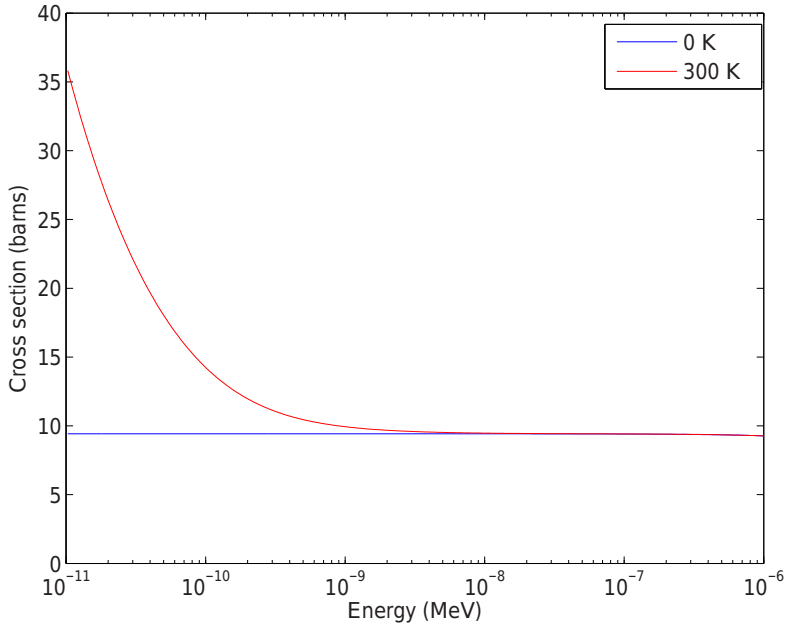

Figure 3.2. The elastic scattering cross section of ^{238}U increases at very low energies along with increasing material temperature.

By applying Equation (3.10) to a constant cross section $\sigma(E) = C$, formula

$$\sigma_{\text{eff}}(v, T, A_n) = C\left(\left(1 + \frac{1}{2\gamma^2 v^2}\right)\text{erf}(\gamma v) + \frac{e^{-\gamma^2 v^2}}{\sqrt{\pi}\gamma v}\right), \tag{3.11}$$

where erf is the error function, is obtained. The effect of this formula is demonstrated in Figure 3.2, in which the low energetic end of the elastic scattering cross section of ^{238}U has been plotted at both 0 K and 300 K.

As can be seen in the figure, thermal motion increases the cross section at very low energies. This phenomenon originates from an increase in potential scattering, or "billiard-ball scattering", in conditions where the thermal motion of the targets is significant compared to the speed of the neutron. This phenomenon can be understood by considering a stationary neutron within a scattering medium. The neutron cannot experience a collision with the surrounding targets in case also the targets are stationary, but if the surrounding targets are in thermal motion, a collision occurs certainly sooner or later. Remembering that the cross section corresponds to the reaction probability per unit neutron path length, which is zero for the stationary neutron, it is evident that in a medium with thermal motion the cross section approaches infinity as the velocity of the neutron approaches zero. The broader the thermal motion, the faster the approach.

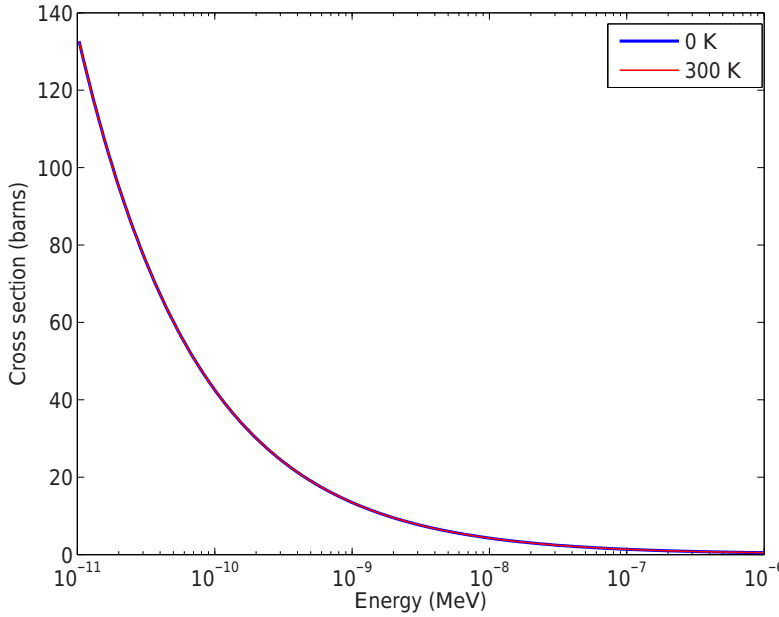

Figure 3.3. The $1/v$-shaped low-energy end of the radiative capture cross section of ^{238}U is unaffected by the thermal motion.

For an $1/v$ shaped cross section $\sigma(E) = D/v$ Equation (3.10) simplifies to

$$\begin{aligned}\sigma_{\text{eff}}(v, T, A_n) &= \frac{\gamma}{v^2\sqrt{\pi}} \int_0^\infty v'^2 \frac{D}{v'} (e^{-\gamma^2(v-v')^2} - e^{-\gamma^2(v+v')^2}) dv' \\ &= D\frac{\gamma}{v^2\sqrt{\pi}} \int_0^\infty v' (e^{-\gamma^2(v-v')^2} - e^{-\gamma^2(v+v')^2}) dv' \\ &= D/v\,, \end{aligned} \tag{3.12}$$

i.e. the cross section is unaffected by thermal motion. This is demonstrated in Figure 3.3 in which the radiative capture cross section of ^{238}U has been plotted in two temperatures.

This phenomenon can be explained by considering the physical meaning of $1/v$ cross sections. In case a cross section behaves as $1/v$, the reaction probability is in practice directly proportional to the *time* the neutron spends in the vicinity of the target nuclide. If thermal motion is moving the target towards the neutron, the time is reduced, and vice versa for a target moving away from the neutron. Since the thermal motion is isotropic in the L-frame, these two effects are in perfect balance. Consequently, the average time the neutron spends in the vicinity of the target nuclei is unaffected by thermal motion and, hence, the $1/v$ cross sections are not affected either.

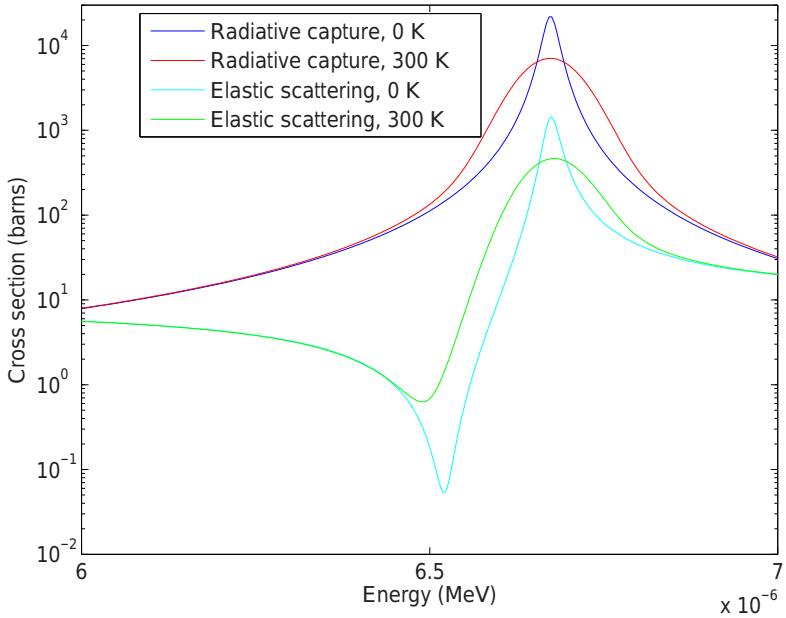

Figure 3.4. Thermal motion has a smoothing effect on the cross sections near resonances: the resonances are Doppler-broadened. This figure involves the elastic scattering and radiative capture cross sections of ^{238}U.

3.1.2 Energy region of resolved resonances

Thermal motion has a significant effect on the reaction rates near resonance energies. This effect has been demonstrated in Figure 3.4 by applying Equation (3.10) to the radiative capture and elastic scattering cross sections of ^{238}U.

As can be seen in Figure 3.4, the resonances become flatter and wider under the influence of thermal motion. Since the effect of thermal motion is analogous to the classical Doppler-effect, this phenomenon is called Doppler-broadening of resonances. In fact, the whole thermal-motion averaging procedure with Equation (3.10) is often called Doppler-broadening even though thermal motion has also other, yet less-important effects on the cross sections.

Doppler-broadening of resonances has a very important consequence considering the operation of nuclear reactors. As the resonances become wider, the probability of a neutron ending up under the influence of a resonance during the slowing-down process increases significantly, which has an increasing effect on reaction probabilities. On the other hand, flattening of the resonances decreases the reaction probabilities for neutrons that have energies very close to the resonance energy.

Unless studying very thin or dilute targets, the resonance flattening has only little practical effect on the reaction probabilities and from the reactor physics point of view

the broadening of the resonances is the dominant phenomenon affecting the reaction rates. In other words, increasing of the temperature tends to increase the probabilities of resonance reactions. The corresponding effect on reactor physics and, for example, the multiplication factor k depends on the composition of the material. For typical fuel materials with high ^{238}U abundance, the increase in parasitic resonance capture is the most important effect, and consequently an increase in fuel temperature tends to decrease k. This naturally occurring temperature feedback significantly facilitates the design and operation of nuclear reactors.

3.1.3 Energy region of unresolved resonances

Doppler-broadening of resonances occurs, naturally, also at the energy region of unresolved resonances. However, since the cross sections within this energy region are usually not expressed in continuous-energy format, it is not practical to perform Doppler-broadening using the Solbrig's kernel, Equation (3.10). Instead, the effects of thermal motion are usually taken into account with approximative methods that can be applied directly to the resonance formalism used at the unresolved energy region, without the need of reconstructing the cross sections in continuous-energy format [7].

Doppler-broadening of unresolved resonances is outside the topic of the current thesis and is, therefore, not discussed any further.

3.2 Effects on scattering kinematics

When considering a collision between two billiard balls A and B, it is quite easy to imagine that the post-collision velocity and angle of ball A depend on the velocity and direction of ball B prior to the collision. In a similar manner, thermal motion affects the kinematics of scattering events also on the microscopic scale.

In the special case of isotropic (in C-frame) elastic scatting, the basic effects of thermal motion on scattering kinematics can be described with Figure 3.5. The figure has been generated by studying the energy change in elastic scattering collisions with various equally probable scattering angles θ_C and target directions μ_C, using procedures described in Section 2.1.3. In the calculations it has been taken into account that the collision probabilities are directly proportional to the relative velocity between the neutron and the target v', which slightly increases the collision probabilities with targets moving towards the neutron compared to those moving away from them. The scattering cross sections are assumed to be constant.

Several conclusions can be drawn based on the minimum, maximum and average curves for the energy change, plotted in Figure 3.5. First of all, it can be seen that the curves are in accordance with Section 2.1.3: For the light nuclei the energy transfer in the elastic scattering process is high and the neutron may either receive all the kinetic energy of the target or lose all or nearly all of its energy to the target. The energy transfers are significantly lower for heavy nuclei, but both up- and down-scattering still occurs. Secondly, it can be seen that neutrons with energies higher than the

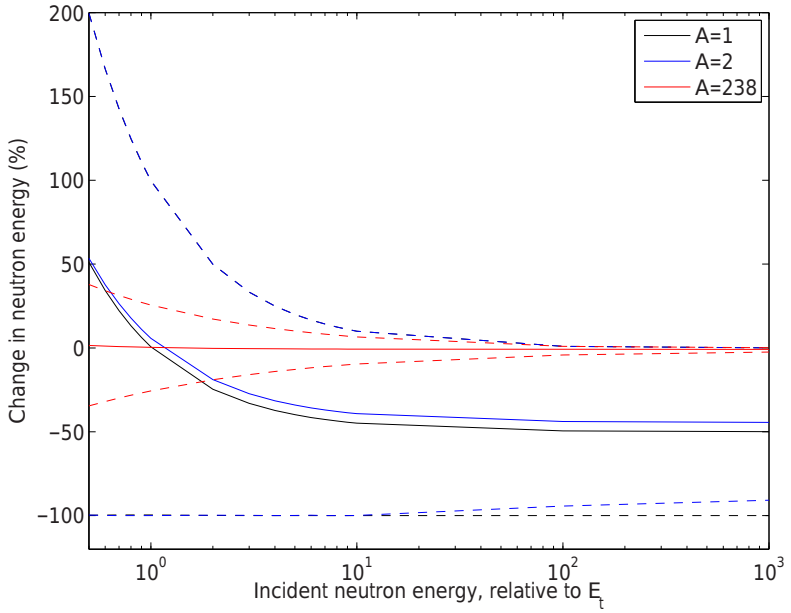

Figure 3.5. Average (solid lines), minimum and maximum (dashed lines) relative energy changes during isotropic elastic scattering when a neutron collides with a target that weights 1, 2 or 238 times the neutron mass.

target energy tend to lose energy during elastic scattering and, on the other hand, neutrons with small energies tend to gain energy. It should be noted that the solid lines describing the average behavior do not intersect at the relative incident neutron energy of $10^0 = 1$ because of the fact that the collision probabilities are proportional to v'.

The results of this simplified calculation model brought only little new information compared to the target-at-rest model discussed previously in Section 2.1.3. According to this model, thermal motion makes up-scattering possible and affects the secondary particle distributions from scattering events only slightly when the energy of the neutron is high compared to the target energy, i.e. during the slowing-process of fission neutrons. However, the effects of thermal motion become much more significant when the neutron energy is of the same order as the energy of the target, i.e. at *thermal* energy region.

The effects of thermal motion on scattering kinematics at the thermal energy region is discussed further in Section 3.2.1. It also turns out that the assumption on constant scattering cross sections, as in the simplified model, is not valid at the resonance energy region. The effect of resonances on scattering kinematics is discussed in Section 3.2.2.

3.2.1 Thermal peak

The most well-known consequence of thermal motion on the kinematics of elastic scattering occurs at thermal energies. As it was previously noticed, neutrons with energies lower than the target energy are likely to gain energy in the elastic scattering collisions and vice versa for neutrons with energies significantly higher than the target energy. In other words, it seems that the neutrons tend towards some kind of a thermal equilibrium with the surrounding matter.

In fact, using statistical mechanics it can be shown that in the absence of fast neutrons, absorbing reactions and leakage, the energy spectrum of neutrons eventually starts to obey the Maxwell-Boltzmann distribution as a result of repeated collisions with the surrounding matter [8, 9]. The temperature of the Maxwellian is the same as that of the matter. The neutron density spectrum, described by Equation (3.1), can be converted to the neutron flux spectrum by multiplying the spectrum with the neutron velocity v. Consequently, the thermal neutron flux is given by

$$\Phi_{\text{th}}(E) = 2E\sqrt{\frac{2}{M\pi}}\left(\frac{1}{k_{\text{B}}T}\right)^{3/2} e^{-\frac{E}{k_{\text{B}}T}} . \tag{3.13}$$

The *thermal peak*, described by Equation (3.13), is a good approximation of the thermal flux spectrum in thermal reactors. However, in practice the shape of the distribution is slightly affected by the presence of absorption reactions in realistic reactor systems. Because absorption reactions have (at least approximately) $1/v$ cross sections, neutrons are removed more efficiently from the low-energy tail of the distribution and, hence, the thermal flux spectrum is somewhat tilted in the direction of high energies compared to Equation (3.13). The tilt is emphasized in reactor systems with strong absorbers mixed together with the moderator material.

3.2.2 Effect of resonances

In the simplified scattering model, the results of which were given in Figure 3.5, the scattering cross sections were assumed to be constant. However, the scattering probability of a neutron with a target is not only proportional to the relative velocity of the neutron to the target, v', but also to the (zero Kelvin) scattering cross section of the target corresponding to this relative velocity. Since the scattering cross sections may vary by several orders of magnitude in the vicinity of strong resonances, the consequences on scattering kinematics are significant when it comes to scattering from heavy nuclides with strong resonances, for example ^{238}U.

This effect was for a long time omitted in reactor physical analyses either by assuming the target nuclei to be stationary when solving the scattering kinematics (asymptotic scattering kernel) or by assuming the scattering cross sections to be constant (cross section independent scattering kernel) like in the previous simplified model. Ouisloumen and Sanchez studied the importance of this effect by deriving a formula for the cross section-dependent scattering kernel, which provides the accurate energy and angle distributions of scattered neutrons from elastic scattering assuming Maxwellian velocity distribution of targets [10]. Later on, Rothenstein

developed this kernel into a more practical form, facilitating its use in everyday analyses [11].

The most important consequence of the cross section dependence of the scattering kernel concerns neutrons with energies corresponding to the wings of a scattering resonance (a Doppler-broadened scattering resonance of ^{238}U is shown in Figure 3.4). At these neutron energies, the scattering reactions tend to occur with targets that have a suitable velocity and direction in the sense that the relative velocity of the collision, v', corresponds to the elevated cross sections near the peak of the resonance. Consequently, when a neutron with energy right below the energy of a scattering resonance scatters from the target, the relative velocity v' of the collision is usually higher than the neutron velocity v, and vice versa for neutron energies right above the resonance. Since scattering with $v' > v$ on average leads to up-scattering in the case of heavy nuclides, this phenomenon increases resonance up-scattering from energies right below the resonance and, on the other hand, increases resonance down-scattering from energies right above the resonance.

This tendency of elastic scattering towards resonance energies increases the probability of resonance captures. Consequently, in typical reactor applications, taking the cross section dependence of the scattering kernel of ^{238}U into account usually decreases the multiplication factor estimates slightly.

3.3 Bound atoms

All of the previous results in the current chapter were derived from the properties of free gases. Thus, it was assumed that the target motion obeys the Maxwell-Boltzmann distribution, and that the chemical bonds and the lattice structure of the atoms do not affect the scattering kinematics. These assumptions cannot be applied for strongly bound atoms at neutron energies lower than the binding energy of the nucleus in the crystal lattice or molecule, typically a few electron volts. Below the binding energy, the chemical bonds affect both the scattering cross sections and kinematics significantly, necessitating a special treatment. The special treatment is, in practice, required for all common moderator materials in reactor systems involving neutron thermalization.

The effect of the chemical binding on cross sections is described in Figure 3.6 for hydrogen in water and for carbon in graphite. The cross sections of bound and free hydrogen are slightly different, and also the shape of the bound cross section curve differs from typical free atom cross sections within this energy region. The difference between the carbon cross sections is much more dramatic. The sharp edges in the cross section result from various lattice effects caused by the regular lattice structure of graphite.

When a neutron interacts with a bound atom, the scattering kinematics are also affected by the bond. For instance, in the case of graphite it is possible that the neutron interacts such that the neutron energy remains unchanged in the scattering, the classical counterpart of which would be elastic scattering from a target with an infinite mass.

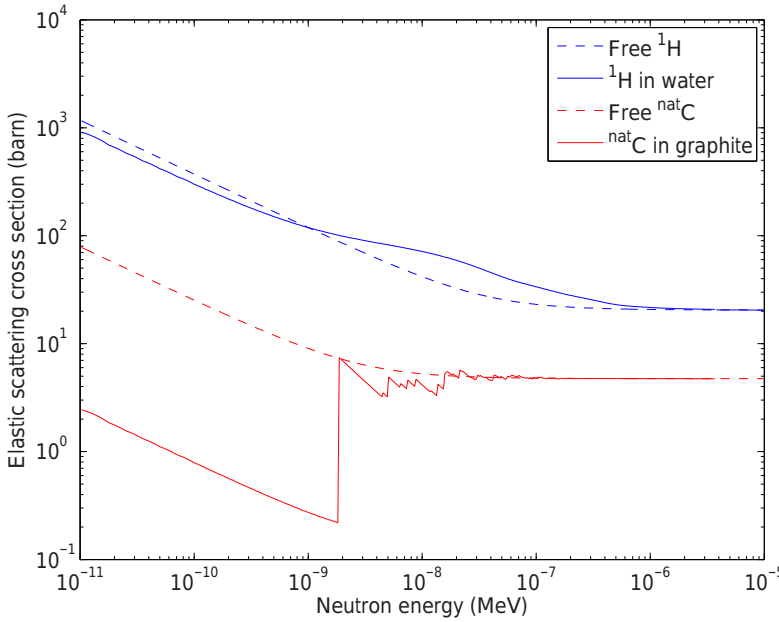

Figure 3.6. Chemical bonds affect the cross sections at low incident neutron energies.

4. Continuous-energy Monte Carlo neutron transport

Monte Carlo particle transport calculations are based on simulation of individual particle tracks within the problem geometry. The interaction sites, reactions and secondary particle distributions are randomly sampled from physically representative distributions, and thus the particle tracks correspond to the real-life transport process provided that the distributions are justified and the nuclear interaction data is accurate.

An individual particle track does not give almost any practical information on the properties of a system, but when numerous particle tracks are calculated, the distribution of the tracks can be used to estimate average properties of the system. The more particle tracks are simulated, the smaller is the statistical noise of the results. The number of simulated particles in neutron transport simulations usually varies between 10^6–10^{10}, depending on the size of the problem geometry, and the type and accuracy requirement of the quantities being calculated. In continuous-energy Monte Carlo the energy domain is treated continuously, as opposed to group-wise techniques in which the energy domain is divided into several energy groups and the physics treatment within each energy group is group-averaged.

Continuous-energy Monte Carlo is a very attractive method for modern neutron transport, because

- It is very general and well-applicable to all kinds of reactors.
- The simulations can be based on the most accurate available nuclear data with minimal approximations and processing.
- Specifically, continuous-energy Monte Carlo treats self-shielding effects inherently, making complicated self-shielding corrections unnecessary.
- The calculations can be easily made in parallel.

On the downside,

- Modeling of numerous neutron histories is computationally intensive.
- The memory footprint is relatively large compared to multi-group techniques.

- The results always involve statistical uncertainty.

Selected techniques behind continuous-energy Monte Carlo neutron transport are described in the current chapter. The processing of cross section data from standard nuclear data files to a more practical format is discussed in Section 4.1. The basics of the neutron tracking process are introduced in Section 4.2 and the calculation of different reactor physical quantities based on the simulated neutron tracks is described in Section 4.3. Sections 4.4 and 4.5 introduce two special techniques that deserve to be mentioned because of their strong relevance considering the topic of the current thesis.

4.1 Nuclear data processing

Standard nuclear data is distributed in ENDF (Evaluated Nuclear Data File) format. The file format is specified in Reference [12], and it includes standardized ways of interpreting all kinds of nuclear data including for example cross sections, angular distributions, thermal scattering data, decay data and covariance information.

The cross sections in ENDF format are represented as a combination of background cross sections and resonance parameters. There is in principle no reason why a Monte Carlo calculation tool could not utilize this data as-is, but it is by many means beneficial to process, or *reconstruct*, the basic data into a piece-wise linear format before use. This means that the energy dependence of cross sections is described by discrete energy-value pairs such that linear interpolation is assumed between the energy grid points. Pre-processing of the cross sections usually saves computational effort, since the once reconstructed cross sections can be utilized in multiple transport calculations.

The most common tool for cross section processing is called NJOY [7]. The RECONR module of NJOY is responsible of the cross section reconstruction. The energy grid of the cross section is chosen such that the relative error from the linear interpolation remains smaller than an input parameter called *reconstruction tolerance*, which is normally between 0.1–1 %.

It is also practical to perform Doppler-broadening for the cross sections, since the newly reconstructed zero Kelvin cross sections are often useless in practical calculations. This can be done using the BROADR module of NJOY, which is also capable of adjusting the energy grid so that the reconstruction tolerance is maintained despite the changes in the cross section curve. Since higher temperature leads to smoother cross section curves, Doppler-broadening actually decreases the number of grid points required for a certain reconstruction tolerance. Consequently, the Doppler-broadened cross sections consume less memory than the original zero Kelvin cross sections.

The cross section processing for Monte Carlo codes often proceeds with the generation of probability tables that are used in many Monte Carlo codes for a rigorous treatment of unresolved resonances [13]. This can be done using the PURR module of NJOY. Eventually, the cross section data may be converted to a Monte Carlo code-specific ACE file format using the module ACER. The ACE (A Compact ENDF)

format has been developed for the most widely used Monte Carlo particle transport code MCNP, developed at the Los Alamos National Laboratory [14]. The format is also used by a few other Monte Carlo codes, such as Serpent and OpenMC [15, 16].

4.2 Neutron tracking

In the absence of external sources, i.e. when performing *criticality source* simulations, all of the neutron tracks begin at fission sites and terminate because of capture or fission reactions, resulting in neutron absorption, or leakage. Monte Carlo neutron tracking involves basically four kinds of sampling all of which are discussed in the current section:

1. path length sampling that moves the neutron between collision sites,
2. reaction sampling that determines the reactions occurring at the collision points,
3. in the case of a fission reaction, sampling the number, type and energy of the fission neutrons or
4. in the case of a scattering or a (n,*x*n) reaction, sampling of the direction and energy of the scattered neutron or neutrons.

4.2.1 Path length sampling

In practice, the standard pseudo random number generators implemented in programming languages and Monte Carlo codes always produce random numbers ξ that are distributed uniformly on the unit interval [0,1). However, as it was discussed in Section 2.3, the distance between collisions obeys the exponential distribution with $\Sigma_i(E) = \Sigma_{\text{tot}}(E)$. Thus, to obtain valid path length samples, some kind of conversion is required for the uniformly distributed random variables ξ. The conversion can be based on the cumulative distribution function (CDF) of the exponential distribution, Equation (2.13)

$$P_{\text{CDF}}(E, l) = \int_0^l \Sigma_{\text{tot}}(E) e^{-\Sigma_i(E)x} dx = 1 - e^{-\Sigma_{\text{tot}}(E)l}, \tag{4.1}$$

which relates the path lengths l with cumulative probabilities. By denoting the cumulative probability with ξ and solving the inverse of this distribution, formula

$$l(E, \xi) = -\frac{\ln(1-\xi)}{\Sigma_{\text{tot}}(E)} \simeq -\frac{\ln(\xi)}{\Sigma_{\text{tot}}(E)} \tag{4.2}$$

is obtained for the conversion from uniformly distributed random variables to exponentially distributed path lengths l. This kind of *inversion sampling* is a standard technique for sampling non-uniformly distributed random variables in cases when the inverse of the CDF can be resolved [17].

If a neutron is at spatial coordinate $\mathbf{r_p}$ and is moving in direction $\mathbf{\Omega}$, the coordinates of the next collision are

$$\mathbf{r_{p+1}} = \mathbf{r_p} + l\mathbf{\Omega}\,, \tag{4.3}$$

where the path length l has been sampled with Equation (4.2). When modeling heterogeneous systems, it is possible that this collision point is no longer in the same material region as the starting point and, consequently, the total cross section $\Sigma_{\text{tot}}(E)$ that was used in the sampling of the collision point is not valid for the whole path length. In case l is greater than the distance to the next material boundary, the neutron is first moved to the material boundary and the tracking proceeds from this point by sampling of a new path length using the total cross section in the next material region.

This neutron tracking algorithm, in which the material cross sections are updated at each material interface, is often referred to as ray tracing or surface tracking. An alternative algorithm is introduced later in Section 4.4.

4.2.2 Reaction sampling

Since material total cross section Σ_{tot} is just the sum over the partial reaction cross sections, the probability of reaction i of nuclide n to occur at the collision point is simply

$$P_{i,n} = \frac{\Sigma_{i,n}(E)}{\Sigma_{\text{tot}}(E)}\,. \tag{4.4}$$

Consequently, the reaction and corresponding nuclide can be easily sampled by summing macroscopic reaction cross sections as long as

$$\xi < \sum_i \sum_n \frac{\Sigma_{i,n}(E)}{\Sigma_{\text{tot}}(E)} \tag{4.5}$$

and picking the reaction for which ξ was first exceeded.

If a capture or a fission reaction is sampled, the neutron path is terminated at the collision point. Fission reactions generate new fission neutrons the sampling of which is discussed in Section 4.2.3. The treatment of scattering and (n,xn) reactions is discussed in Section 4.2.4.

4.2.3 Fission neutrons

If a fission reaction occurs, the number and properties of the new source neutrons, generated in the fission event, need to be determined. In reactor physical applications it is not necessary to take into account the exact distribution of the number of fission neutrons, and the number of fission neutrons can thus be determined simply by ensuring that $\overline{\nu}_{\text{tot}}(E)$ neutrons are generated in each fission on average. Since $\overline{\nu}_{\text{tot}}(E)$ is not an integer, the decimal part must be handled using random sampling in analogous Monte Carlo simulation. The simplest method for sampling on average $\overline{\nu}_{\text{tot}}(E)$ fission neutrons at each fission site is to take the truncated integer value N_ν of $\overline{\nu}_{\text{tot}}(E)$ and sampling the number of fission neutrons as either N_ν or $N_\nu + 1$ according

to the probability given by the remaining decimal fraction $\overline{\nu}_{\text{tot}}(E) - N_\nu$. Thus, the number of fission neutrons is $N_\nu + 1$ at probability $\overline{\nu}_{\text{tot}}(E) - N_\nu$ and N_ν at probability $1 - (\overline{\nu}_{\text{tot}}(E) - N_\nu)$ [14].

Since $\overline{\nu}_{\text{tot}}(E)$ includes both prompt and delayed neutrons, the next step is to determine whether each of the sampled fission neutrons is a prompt or a delayed neutron. The probability of sampling a delayed neutron is simply

$$P_{\text{d}} = \frac{\overline{\nu}_{\text{delayed}}(E)}{\overline{\nu}_{\text{tot}}(E)} = \frac{\overline{\nu}_{\text{delayed}}(E)}{\overline{\nu}_{\text{prompt}}(E) + \overline{\nu}_{\text{delayed}}(E)} \tag{4.6}$$

and a prompt neutron is sampled with probability $1 - P_{\text{d}}$.

Finally, the energy of each fission neutron is sampled according to the fission energy distributions specific to the target nuclide, as provided in the ENDF data files. Different energy distributions are applied for the prompt and delayed neutrons, and the directions of the fission neutrons are sampled isotropically.

4.2.4 Kinematics of scattering and (n,*x*n) reactions

If the reaction sampling results in a scattering reaction, the energy and angle of the scattered neutron need to be resolved. More precisely, in most cases it is sufficient to determine only the angle of the scattered neutron, and the energy is determined by the conservation of total energy and momentum. The treatment of (n,*x*n) reactions is somewhat similar to scattering reactions, but the directions and energies need to be sampled for two or more neutrons instead of just one.

As it was discussed in Section 2.1.3, it is beneficial to solve the kinematics of elastic scattering events in the C-frame in which the collision cosine μ_{C} can be easily sampled, either isotropically or based on ENDF scattering laws in the case of anisotropic scattering. However, as it was learned in Section 3.2, thermal motion cannot, in general, be neglected in the solution of elastic scattering kinematics, and therefore it is necessary to take the velocity of the target into account when performing the coordinate transform from L-frame to C-frame and back. In Monte Carlo neutron transport this can be done by sampling the target velocity at each scattering event.

In Section 2.1.3, the basic properties of the target velocity distribution were already introduced: the probability of a neutron colliding with a target is directly proportional to the relative velocity of the neutron to the target v' and the zero Kelvin capture cross section. The velocity distribution is, however, usually written in a slightly different but practically equivalent form[4], in accordance with the Doppler-broadening equations. If the definition of effective cross section, Equation (3.3), is divided by the effective scattering cross section and the integration is performed over the cosine of the angle between the neutron and target velocity vectors $\mu = \cos\alpha$ (see Figure 3.1) such that

$$v' = \sqrt{v^2 + V_{\text{t}}^2 - 2vV_{\text{t}}\mu}\,, \tag{4.7}$$

[4] The differences affect only the normalization, not the shape of the distribution.

equation

$$1 = \int_0^\infty \int_{-1}^1 \frac{\sigma_s(v',0)}{\sigma_{\text{eff,s}}(v,T,A_n)} \frac{v'}{2v} P_{\text{MB}}(V_t,T,A_n) d\mu dV_t \,, \tag{4.8}$$

is obtained. This form of the integral reveals nicely the contribution of each target velocity and collision angle to the effective cross section corresponding to neutron velocity v. This contribution can also be interpreted as the probability that the neutron scatters from a target with a specific angle and energy, and the probability distribution of targets can thus be written

$$P_{\text{FGT}}(v,V_t,\mu,A_n) = \frac{\sigma_s(v',0)}{\sigma_{\text{eff,s}}(v,T,A_n)} \frac{v'}{2v} P_{\text{MB}}(V_t,T,A_n) \tag{4.9}$$

Traditionally, the energy dependence of the cross sections has been neglected by assuming [14]

$$\frac{\sigma_s(v',0)}{\sigma_{\text{eff,s}}(v,T,A_n)} \approx 1 \,, \tag{4.10}$$

after which the sampling of target velocities can be performed using a rather complicated sampling scheme, described in the original Reference [18]. Since the inversion of Equation (4.9) cannot be resolved in closed form, the sampling from this distribution must be based on more complicated techniques. The distribution can be written in the form

$$P_{\text{FGT}}(v,V_t,\mu,A_n) = C\left\{\frac{v'}{v+V_t}\right\}\left\{(2\gamma^4)V_t^3 e^{-\gamma^2 V_t^2} + B(4\gamma^3/\sqrt{\pi})V_t^2 e^{-\gamma^2 V_t}\right\}, \tag{4.11}$$

where C and

$$B = \frac{\gamma v\sqrt{\pi}}{2} \tag{4.12}$$

are constants that are independent of V_t. It turns out that sampling from distributions $V_t^3 e^{-\gamma^2 V_t^2}$ and $V_t^2 e^{-\gamma^2 V_t^2}$ is possible. Consequently, the correct velocity distribution for target velocity candidates can be obtained by first sampling the correct distribution out of the two candidates such that the first distribution is sampled with probability $1/(1+B)$ and the second with probability $B/(1+B)$. After sampling the velocity candidate from the sampled distribution and the collision cosine from a uniform distribution, the velocity sample is accepted or rejected using the criterion

$$\xi < \frac{v'}{v+V_t} \,, \tag{4.13}$$

where the right-hand side of the equation is always smaller than or equal to unity. In case the sample is rejected, the whole sampling procedure restarts from the beginning. These *rejection sampling* techniques were first suggested by Neumann in Reference [19].

This solution procedure for the kinematics of elastic scattering, including sampling from Equation (4.9) with the assumption of constant cross sections, coordinate transform to the C-frame, sampling the collision angles in this frame and transforming back to the L-frame, is usually called the *free gas treatment*. As it was discussed in Section 3.2.2, the energy dependence of the scattering cross sections in fact has

a significant effect on the velocity distribution and collision kinematics in some cases. A correction to this traditional sampling scheme is introduced later in Section 4.5.

Inelastic scattering and (n,*x*n) reactions occur at such high neutron energies that the accurate treatment of thermal motion is no longer necessary. Consequently, the L-frame velocity of the target can be assumed to be zero. The method of solution for the kinematics of these reactions depends on the nuclear data and the reaction. In the case of inelastic scattering the solution procedure is often similar to elastic scattering with the exception that the reaction Q_r value needs to be taken into account as a loss in the kinetic energy. However, in some cases the angle and energy of the exiting particle, or particles in the case of (n,*x*n) reactions, are sampled directly based on ENDF scattering laws.

As previously mentioned, scattering from bound atoms requires a special treatment at the thermal energy region. In bound-atom scattering the collision kinematics are sampled directly in the L-frame, using pre-calculated cosine or energy-cosine tables which are based on so called $S(\alpha, \beta)$ data available in a special set of ENDF files.

4.3 Result estimates

All kinds of information can be obtained from a system by simply performing a tracking calculation and looking at the reactions occurring during this calculation. For instance, it is possible to keep track of the fission reactions at each material zone during transport to get an approximative power distribution, or the multiplication factor can be estimated based on the size of the neutron population at the beginning and at the end of a simulated neutron generation. These *analog* estimators, based solely on the reactions and other phenomena observed during the tracking calculation, are, however, less efficient than *non-analog* estimators that contribute to the estimator value each time a neutron draws a track in a material zone (track-length estimators, Section 4.3.1) or collides with a target (collision estimators, Section 4.3.2). Consequently, the calculation of reaction rates in Monte Carlo transport codes is usually based on non-analog estimators.

The estimators can be used to calculate reaction rates and other integrals of the type

$$R = \int_V \int_E f(\mathbf{r}, E)\Phi(\mathbf{r}, E) dE d^3r \,, \tag{4.14}$$

where the integration is performed over volume and energy, $\Phi(\mathbf{r}, E)$ is the neutron flux and $f(\mathbf{r}, E)$ is a response. When calculating reaction rates, the response corresponds to the reaction cross section, the neutron flux is obtained with $f = 1$ et cetera. From these quantities it is possible to derive many of the output quantities of interest in reactor physical analyses. For example, the homogenized cross section for an

energy group bounded by energies E_1 and E_2 is defined

$$\Sigma_g = \frac{\int_V \int_{E_1}^{E_2} \Sigma(\mathbf{r}, E)\Phi(\mathbf{r}, E) dE d^3r}{\int_V \int_{E_1}^{E_2} \Phi(\mathbf{r}, E) dE d^3r} \tag{4.15}$$

and also the multiplication factor can be expressed using several reaction rates and $\overline{\nu}_{\text{tot}}$.

4.3.1 Track-length estimates of reaction rates

The basic idea behind track-length estimators is the fact that the integral of neutron flux over a volume and a time interval equals the total track length of the neutrons within this time interval in the volume. Consequently, the neutron track-lengths provide an estimate for the neutron flux. In analog Monte Carlo transport the track-length estimator scores are defined as

$$s_i = w f_i l_{\text{t},i} \,, \tag{4.16}$$

where $f_i = f(\mathrm{r}_i, E_i)$ is the value of the response function corresponding to the track length $l_{\text{t},i}$. In non-analog Monte Carlo simulation the scores are additionally multiplied by the neutron weight w.

The sum of the scores gives an estimate for the integral R. If the absolute value of a quantity is of interest, the result can be normalized for example with respect to total fission power. By binning the scores according to incident neutron energy or geometry region it is possible to gain information on the distribution of different quantities in energy or space.

4.3.2 Collision estimates of reaction rates

Since the collision density of neutrons in a material is the neutron flux multiplied by the total cross section within the material, the collisions in the Monte Carlo neutron transport can be used to estimate the neutron flux and other integral quantities. The collision estimator scores are defined

$$s_i = \frac{w f_i}{\Sigma_{\text{tot}}(E)} \,. \tag{4.17}$$

Naturally, the scores can be binned and the results can be normalized just like in the case of track-length estimators.

4.3.3 Estimator uncertainties and figures-of-merit

Because of the random nature of the Monte Carlo neutron transport process, all of the estimator results include statistical uncertainty. The amount of uncertainty can be estimated from the sample variance of the scores collected during the transport calculation. From basic statistical mathematics it follows that the amount of statistical

deviation in the average value of the scores is inversely proportional to the square root of the number of scores $\sqrt{n}$, given that the individual scores are independent of each other [20].

The statistical errors of a Monte Carlo calculation can be decreased by affecting the number of scores in the regions of interest. The apparent way for doing this is by increasing the number of neutron histories in the calculation: if the number of neutron histories is doubled, also the number of scores for each estimator doubles on average and the statistical deviances of the estimators are decreased by factor $1/\sqrt{2} \approx 0.7$. Since the errors tend to zero as n approaches infinity, the statistical error in Monte Carlo results can also be characterized as "The error from not calculating an infinite amount of neutron histories". It should be mentioned that there are also other significant error sources in the Monte Carlo calculations, for example uncertainties in the nuclear data and calculation models.

Since the Monte Carlo transport time depends linearly on the number of neutron histories, doubling the number of neutrons roughly doubles also the calculation time. Because of this apparent connection, the performance of a Monte Carlo simulation is often measured with figure-of-merit (*FOM*), defined

$$FOM = \frac{1}{s^2 \tau}, \tag{4.18}$$

where s is the standard deviation of an estimator and τ is the transport calculation time. *FOM* should be independent of τ because of the specific dependence of s on τ. In addition to being a good measure for comparing the performance of different transport algorithms, the figure-of-merit of an estimator can be used to estimate the calculation time required for a certain level of statistical accuracy in a specific computation environment.

4.4 Woodcock Delta-tracking

Woodcock Delta-tracking is a tracking technique that is an alternative to the ray tracing method introduced in Section 4.2.1. The main idea in Delta-tracking is that the tracking is based on a global majorant cross section Σ_{maj}, which is at all energies equal to the maximum total cross section within the whole system. Consequently, the tracking proceeds in smaller steps than in the ray tracing algorithm, but only a fraction of the collisions are accepted. The probability of accepting a collision point is determined by the ratio of the local total cross section to the majorant cross section. The rejected collision points which do not have any effect on the neutron track are called *virtual* collisions. The idea of the method has been introduced in Reference [21], by Woodcock et al.

The advantage of this kind of a tracking scheme is that the tracking does not have to stop at each material boundary, which makes Woodcock delta-tracking an efficient tracking technique when the geometry contains small details. On the downside, the proportion of virtual collisions may become very large at some energies if the geometry contains strong absorbers, which may significantly deteriorate the performance.

This drawback can, however, be avoided by using a combination of Delta-tracking and ray tracing in the neutron tracking.

The mathematical background of Woodcock tracking deserves to be discussed further. For the method to be valid, the path lengths between actual collisions must obey the same exponential distribution as in the case of ray tracing. In the case of average path lengths the equality of the two tracking techniques is easy to show: When sampling the distance to the next collision in Delta-tracking, the average path length is $1/\Sigma_{\text{maj}}$. As long as the neutron travels within a homogeneous material region, this path length is accepted with probability

$$P_{\text{acc}} = \frac{\Sigma_{\text{tot}}(E)}{\Sigma_{\text{maj}}(E)}\,, \tag{4.19}$$

and the average distance is obtained by dividing the average path length with the probability, i.e.

$$\frac{1}{\Sigma_{\text{maj}}(E)} \times \frac{\Sigma_{\text{maj}}(E)}{\Sigma_{\text{tot}}(E)} = \frac{1}{\Sigma_{\text{tot}}(E)}\,, \tag{4.20}$$

which corresponds to the average path length when using the ray tracing technique.

The equivalence is slightly more complicated to show in the case of the probability distribution of the path lengths. In Delta-tracking the path lengths are sampled from the exponential distribution

$$P_1(E,l) = \Sigma_{\text{maj}}(E) e^{-\Sigma_{\text{maj}}(E)l}\,. \tag{4.21}$$

Because of the rejection sampling scheme, the probability of sampling path length from this distribution is P_{acc}, assuming again that the neutron travels within a homogeneous material region. With probability $1 - P_{\text{acc}}$ the first sample is rejected and a new path length is sampled. In this case the total path length becomes (at least) the sum of the first path length and the second path length with the same distribution. The probability density distribution for the sum of j exponentially distributed random variables is given by the Erlang distribution [22]

$$P_j(E,l) = \frac{\Sigma_{\text{maj}}^j l^{j-1} e^{-\Sigma_{\text{maj}} l}}{(j-1)!}\,, \tag{4.22}$$

and the distribution for the sum of the first two path lengths is P_2. However, it is possible that also the second path length is rejected. Thus, the probability that the path length obeys P_2 is $P_{\text{acc}}(1 - P_{\text{acc}})$ and the rest of the probability is reserved for higher sums of exponentially distributed random variables.

Collecting the terms into a single formula yields

$$\begin{aligned} P_{\text{sum}}(E,l) &= P_{\text{acc}}\Sigma_{\text{maj}}(E)e^{-\Sigma_{\text{maj}}(E)l} + (1-P_{\text{acc}})\Big(\\ &\quad P_{\text{acc}}l\Sigma^2_{\text{maj}}(E)e^{-\Sigma_{\text{maj}}(E)l} + (1-P_{\text{acc}})\big(\\ &\quad \frac{1}{2}P_{\text{acc}}l^2\Sigma^3_{\text{maj}}(E)e^{-\Sigma_{\text{maj}}(E)l} + (1-P_{\text{acc}})(\ldots)\big)\Big) \\ &= \sum_{i=0}^{\infty}\frac{(1-P_{\text{acc}})^i P_{\text{acc}}l^i\Sigma^{i+1}_{\text{maj}}(E)e^{-\Sigma_{\text{maj}}(E)l}}{i!} \\ &= P_{\text{acc}}\Sigma_{\text{maj}}(E)e^{-\Sigma_{\text{maj}}(E)l}\sum_{i=0}^{\infty}\frac{\big((1-P_{\text{acc}})l\Sigma_{\text{maj}}(E)\big)^i}{i!}\,. \end{aligned} \tag{4.23}$$

The sum term can be recognized as the definition of the exponential function [20], and the equation simplifies to

$$\begin{aligned} P_{\text{sum}}(E,l) &= P_{\text{acc}}\Sigma_{\text{maj}}(E)e^{-\Sigma_{\text{maj}}(E)l}e^{(1-P_{\text{acc}})l\Sigma_{\text{maj}}(E))} \\ &= \frac{\Sigma_{\text{tot}}(E)}{\Sigma_{\text{maj}}(E)}\Sigma_{\text{maj}}(E)e^{-\Sigma_{\text{maj}}(E)l}e^{(1-\frac{\Sigma_{\text{tot}}(E)}{\Sigma_{\text{maj}}(E)})l\Sigma_{\text{maj}}(E)} \\ &= \Sigma_{\text{tot}}(E)e^{-\Sigma_{\text{maj}}(E)l+(\Sigma_{\text{maj}}(E)-\Sigma_{\text{tot}}(E))l} \\ &= \Sigma_{\text{tot}}(E)e^{-\Sigma_{\text{tot}}(E)l}\,, \end{aligned} \tag{4.24}$$

which is exactly the same distribution from which the track-lengths are sampled in the ray tracing algorithm. This derivation was first presented by Coleman in Reference [23].

The derivation can be straightforwardly generalized to a case where the neutron crosses a material boundary and P_{acc} changes along the neutron track. The only prerequisite for the Delta-tracking to provide the same results as the ray tracing method is that $\Sigma_{\text{maj}}(E) > \Sigma_{\text{tot}}(E)$ in which case the rejection sampling scheme is valid. Of course, this reproducibility applies only in a statistical sense. Delta-tracking results in a different random number sequence than ray tracing, i.e. the results are not exactly the same with the same random number seed as long as the number of neutron histories is finite.

4.5 Doppler-broadening rejection correction

In Section 3.2.2 it was mentioned that the cross section dependence of the scattering kernel increases scattering towards strong resonances. On the other hand, in Section 4.2.4 it was shown that in the traditional free gas treatment for elastic scattering kinematics the cross section dependence is omitted by assuming constant scattering cross sections or, more precisely,

$$\frac{\sigma_{\text{s}}(v',0)}{\sigma_{\text{eff,s}}(v,T,A_n)} \approx 1\,, \tag{4.25}$$

which effectively removes the dependence of the scattering kernel on $\sigma_{\text{s}}(v',0)$. Since the denominator of Equation 4.25 is independent of the target velocity V_{t}, it only contributes to the normalization of the probability distribution.

To make accurate solution of scattering physics possible in Monte Carlo neutron tracking, a couple of correction methods for the scattering kernel have been developed relatively recently. The methods by Lee et al., introduced in Reference [24], and Mori and Nagaya, introduced in Reference [25], rely on varying the particle weights and can only be applied together with non-analog Monte Carlo transport. Perhaps the most commonly used method for the cross section dependence is called Doppler-broadening rejection correction (DBRC), which is also applicable to analog Monte Carlo transport.

The DBRC method was first suggested by Rothenstein in Reference [26], and it has later been shown by Becker et al. in Reference [27] that the suggested technique is equivalent with the analytical version of the exact scattering kernel, studied in References [10, 11]. In the DBRC technique, an additional rejection sampling criterion is introduced in the sampling process of the target motion. To take into account the dependence of the target velocity distribution on the zero Kelvin scattering cross section, it is evident that the rejection criterion must be proportional to $\sigma_s(v', 0)$. Since the rejection criterion must be always smaller than unity for the rejection sampling to be possible, the rejection criterion must be normalized with a number that is greater than or equal to $\sigma_s(v', 0)$ for each L-frame neutron energy v. A safe bet for the denominator would be the global maximum scattering cross section

$$\max_{E \in [E_{\min}, E_{\max}]} \sigma_s(E, 0) \tag{4.26}$$

with $E_{\min} = 0.0$ and $E_{\max} = \infty$. However, as we remember from Section 2.2, the scattering cross section may vary by several orders of magnitude with the maximum cross sections being in the vicinity of very strong resonances. Consequently using the global maximum would lead to very poor sampling efficiencies in general, since the average sampling efficiency is determined by the average ratio of $\sigma_s(v', 0)$ to the denominator.

A much more practical choice is to take advantage of the fact that the high-energy tail of the Maxwellian distribution converges to zero relatively fast. Thus, it can be assumed that the target velocity is bounded by a maximum value and the range of relative velocity v' corresponding to each velocity v becomes finite. As a consequence, it is possible to determine the denominator as a function of v such that the rejection sampling is valid at a very high probability. Beckert et al. have chosen to determine the maximum target velocity using a cut-off criterion originally used in the Sigma1 Doppler-broadening code [28, 29], in which the maximum target energy is truncated to $16kT$ when calculating the Doppler-broadening integral in Equation (3.10). With this choice, the normalization function becomes

$$\sigma_{\text{maj,s}}(E, T, A_n) = \max_{E \in [E_{\min}, E_{\max}]} \sigma_s(E, 0)\,, \tag{4.27}$$

where

$$E_{\min}(E, T, A_n) = \left(\sqrt{E} - 4\sqrt{\frac{k_B T}{A_n}}\right)^2 \tag{4.28}$$

and

$$E_{\max}(E, T, A_n) = \left(\sqrt{E} + 4\sqrt{\frac{k_B T}{A_n}}\right)^2, \tag{4.29}$$

and the rejection sampling criterion can be written

$$\xi < \frac{\sigma_s(v', 0)}{\sigma_{\text{maj,s}}(E, T, A_n)} . \tag{4.30}$$

This “normalization function” is also called the *temperature majorant* cross section of the scattering cross section in this thesis. The majorant can be calculated either in the pre-processing phase or during the transport calculation. If the majorant cross section is pre-calculated and stored in the computer memory, it may be beneficial to choose the temperature T of the majorant cross section as the maximum temperature within the system. This way the majorant cross section needs to be stored only once regardless of the number of different temperatures, but on the downside the sampling efficiency of the rejection sampling criterion in Equation (4.30) is compromised.

In summary, with the Doppler-broadening rejection correction the target velocities are sampled from distribution

$$P_{\text{DBRC}}(v, V_t, \mu, A_n) = \frac{\sigma_s(v', 0)}{\sigma_{\text{maj,s}}(v, T, A_n)} \frac{v'}{2v} P_{\text{MB}}(V_t, T, A_n) . \tag{4.31}$$

Sampling from this distribution is otherwise similar to the standard free gas treatment, but the energy dependence of the scattering cross section is taken into account by introducing an additional rejection sampling. In case the target velocity is rejected in the DBRC sampling, the whole sampling process restarts from the beginning.

5. Development of on-the-fly temperature treatment methods

The conventional methodology for taking the thermal motion into account in continuous-energy Monte Carlo transport calculations was discussed in Chapter 4. In a nutshell, the effects of thermal motion on reaction rates and mean free paths are traditionally taken into account by using pre-calculated effective cross sections, which are stored in the computer memory during the transport calculation. The effects on scattering kinematics are modeled by solving the collision kinematics on-the-fly within the relevant energy region. This is done by first sampling the target velocity at each scattering event (Sections 4.2.4 and 4.5) and then solving the scattering kinematics taking into account the motion of the target (Section 4.2.4). In addition, the effects of thermal motion on the scattering of bound atoms and the reaction rates in the energy region of unresolved resonances must be handled using special techniques, which are not discussed further in the current thesis.

The memory footprint of the cross section data in problems involving burned fuel varies roughly between 0.1–30 GB per temperature (Reference [30] and Publication [IV]), depending strongly on the number of resonance absorber nuclides taken into account, accuracy of the cross section reconstruction and the way the cross sections are stored in the memory, which varies between Monte Carlo codes. Consequently, the standard approach works perfectly fine when modeling systems including only a few different temperatures: the memory capacity of modern workstations is large enough to contain the cross section data in at least a couple of temperatures, and the solution of the scattering kinematics is in any case based on temperature-independent data[5]. Instead, the memory footprint of the cross section data becomes a significant limitation when modeling systems with realistic temperature distributions, which is the case in multi-physics applications of Monte Carlo neutron transport, for example in coupled neutronics / thermal hydraulics calculations.

To overcome this limitation, different methods for reducing the memory footprint of the cross section data have been studied relatively recently. In practice, all of

[5] To be precise, the temperature majorant cross section required with the DBRC technique (Section 4.5) depends on the maximum temperature in the system, but the memory requirement is nevertheless unaffected by the number of temperatures.

the methods are based on making the temperature corrections on-the-fly during the transport calculation. These methods are generally called on-the-fly Doppler-broadening techniques, but the author prefers the term “on-the-fly temperature treatment” because of the nature of the Target Motion Sampling (TMS) technique developed in the current thesis. The current state-of-the-art of on-the-fly temperature treatment techniques is described in Section 5.1, and the development of the TMS temperature treatment technique, reported in Publications I–VII, is summarized in Section 5.2.

5.1 Overview of existing methods

This section provides an overview of selected on-the-fly temperature treatment techniques found in the literature. All of the techniques aim at resolving the effective cross sections during the Monte Carlo calculation based on different kinds of raw data and can, thus, be characterized as on-the-fly Doppler-broadening techniques.

5.1.1 Interpolation between data in different temperatures

The simplest way of handling the temperature dependence of effective cross sections is to interpolate between cross section data in different temperatures. Since the accuracy of this approach is determined by both the interpolation scheme and the spacing of the temperatures in the available cross section data, the main question considering the feasibility of this approach is the accuracy that can be reached with a reasonable amount of data stored in the memory.

The interpolation between temperatures can be done in at least two different ways. The first way is often called stochastic mixing or the pseudo materials approach. In this scheme the cross sections are actually not interpolated in any way, but the interpolation between temperatures is done by defining the material compositions as mixtures of nuclides in different temperatures. For example, a nuclide at temperature 325 K can be approximately modeled by mixing proportion X of this nuclide at 300 K with proportion $1 - X$ at 350 K.

The functionality of this approach has been studied for example in References [31, 32]. In Reference [31], using stochastic mixing introduced about 10–35 pcm biases in the multiplication factors when the cross section data was stored in 300 K steps. Instead, in Reference [32] the cross section data was stored in 100 K steps and the multiplication factors were in good agreement with the reference solutions, at least in the rather narrow temperature region studied in the article. Thus, the stochastic mixing seems to work fine as long as the spacing of the temperatures is relatively narrow, but it is hard to justify the use of this method in high-fidelity analyses because the physical background of the method is rather dubious.

Another interpolation approach, based on direct interpolation of cross section data, was studied by Trumbull in Reference [33] in which the effect of interpolation schemes and temperature spacing on the accuracy of the interpolated cross sections was studied. Out of the interpolation schemes studied in the article, log-log

interpolation performed the best. However, even with this interpolation scheme the 0.1 % accuracy goal of the interpolation could *not* be achieved with cross section data tabulated in 28 K intervals in the challenging case of ^{238}U.

Even with 28 K intervals, covering the roughly 600–1200 K temperature range of typical light water reactors would require storing the cross section data at more than 20 different temperatures, and many more temperatures are required before the 0.1 % accuracy goal is met. Whether or not this huge amount of data can be stored in a computer's memory depends on many factors, but in any case the memory consumption of the interpolation method can be considered very high. Because of this, the feasibility of the direct interpolation method is highly questionable.

5.1.2 Direct Doppler-broadening with Solbrig's kernel

Another straightforward solution to the on-the-fly Doppler-broadening problem is to simply calculate the Doppler-broadened cross sections during the transport calculation using a methodology similar to that normally used in the cross section pre-processing phase, i.e. based on Solbrig's kernel (Equation (3.10)). Because this method requires the cross section data in one temperature only, the memory footprint of the method is relatively small. The approach has been studied for example in Reference [34], which discusses a run-time Doppler-broadening implementation in the Monte Carlo neutron transport code MONK, and in Reference [30], where this approach is used in the calculation of a reference solution.

In both of the references, direct on-the-fly Doppler-broadening with the Solbrig's kernel slowed down the calculations substantially: in MONK the calculation times were 10 times higher than with pre-calculated cross sections, while the corresponding overhead in Reference [30] was approximately 40. Thus, even though direct Doppler-broadening is attractive considering the memory footprint of the approach, low performance makes the method practically useless in production calculations.

5.1.3 On-the-fly Doppler-broadening based on series expansions

Perhaps the most well-known on-the-fly Doppler-broadening technique has been introduced by Yesilyurt et al. in References [30, 35]. This method is based on fast Doppler-broadening of resonances using series expansions with pre-calculated coefficients, and the background of this technique is in the multi-level Adler-Adler formalism.

The method requires standard continuous-cross section data in 0 Kelvin and, additionally, a library of coefficients for the series expansions. In Reference [36] the size of the library is reported to be relatively small, only 3.25 GB for a full set of about 380 nuclides, and the memory consumption of the continuous-energy data is usually not a problem, as long as it needs to be stored in one temperature only. Hence, the memory consumption of the method is well-tolerable but not negligible.

The method has been implemented in the MCNP6 Monte Carlo transport code. For this implementation, the computational overhead from using the method is about

10–15 % in large problems and somewhat higher for smaller problems [36]. Hence, also the computational performance of the method is feasible and the method can be considered a practical solution for the on-the-fly Doppler-broadening of cross sections.

5.1.4 On-the-fly Doppler-broadening based on the multipole representation

Another promising on-the-fly technique has been introduced in Reference [37] and has been studied further in Reference [38]. This method relies on the multipole representation, which transforms the resonance parameters in the Reich-Moore formalism into a set of poles and residues which can be used for analytical Doppler-broadening. With this approach it is possible to represent the cross sections using resonance parameters only, without the need of storing the continuous-energy cross section data in a piece-wise linear format. Consequently, the memory requirement of the cross section data is significantly reduced.

The development of the method is still on-going and, hence, the performance of the method in practical Monte Carlo calculations remains to be seen in the future. Nevertheless, the results provided in Reference [38] indicate that the memory footprint of cross sections data can be reduced roughly by one decade compared to techniques relying on a piece-wise linear cross section format. With the windowed multipole approach studied in Reference [38] also the performance of the method seems very promising.

5.2 Target Motion Sampling (TMS) temperature treatment technique

The main topic of the current thesis is the development of the Target Motion Sampling (TMS) temperature treatment technique. It is a stochastic on-the-fly temperature treatment method which is based on sampling the thermal motion of target nuclides at each collision site and determining the reaction probabilities in the target-at-rest frame using cross sections at a temperature below that of the material or, originally, zero Kelvin. Since the effective cross sections are not calculated at any point of the transport calculation, this method is in fact *not* a Doppler-broadening technique.

When performing neutron transport with the TMS method, the total cross section becomes a distributed quantity, which needs to be handled using rejection sampling techniques, somewhat similar to the Woodcock Delta-tracking algorithm. The path lengths are sampled based on a temperature majorant cross section which takes into account the variation of the total cross section within the range of thermal motion. At each collision point candidate the thermal motion of the target is sampled from the same distribution that is also used in the ordinary free gas treatment, Equation (4.11). The collision point is accepted or rejected according to the ratio of the target-at-rest frame total cross section to the temperature majorant cross section. If the collision point is rejected, a new path length is sampled starting from the newly rejected collision point. Otherwise, a reaction is sampled based on the reaction probabilities in the target-at-rest frame. It should be noted that in this tracking scheme the normal

continuous-energy cross sections need to be stored at one temperature only and, on top of that, it is beneficial to pre-calculate and store a temperature majorant cross section for each nuclide. As a unique feature, the TMS method is capable of modeling geometry regions with inhomogeneous temperature profiles, which significantly facilitates the high-fidelity modeling of continuous temperature distributions.

The TMS method was introduced for the first time in English-written journals in Publication I under the initial name “Explicit treatment of thermal motion”, but it was learned later that a similar method was introduced already in 1984 in a Russian journal [39] and is routinely used, for example, in Russian Monte Carlo code PRIZMA [40]. After introduction of the TMS method, the main emphasis in development has been on the optimization of the method and studying its performance in different circumstances. The further development of the method is summarized in Sections 5.2.1 and 5.2.2.

5.2.1 Performance of the method

Shortly after the introduction of the method it was implemented in Serpent 2 Monte Carlo reactor physics code [15], and the first practical results of the method were reported in Publication II. In this first implementation the majorant cross section was expressed in multi-group format, since this approach provided for straightforward implementation of the method in Serpent. The multi-group majorant was expected to inflict the performance of the method since in multigroup representation the majorant is at all energies greater than or equal to a continuous-energy majorant. This excess conservativity in the majorant cross section reduces the right-hand side of the rejection sampling criterion

$$\xi < \frac{g(E)\sigma_{\mathrm{tot},n}(E')}{\sigma_{\mathrm{maj},n}(E)}\,, \tag{5.1}$$

where g is a normalization factor, E' is the target-at-rest energy of the neutron and $\sigma_{\mathrm{maj},n}$ is the temperature majorant cross section of the target nuclide n. Consequently, the sampling efficiency of the rejection sampling criterion is reduced and some CPU time is unnecessarily spent in the handling of extra virtual collisions.

Even with the very first implementation of the TMS method the slow-down from using the method was close to feasible: in the two test cases the overhead to conventional transport methods varied between 2–4 in a fair comparison. Nevertheless, it was decided to put some effort in the optimization of the method to make it more practical for production use.

The optimization of the method was mainly based on increasing the sampling efficiency defined by Equation (5.1). In practice this means increasing the right hand side of the equation by reducing the average gap between the total cross section and the majorant. Three different ways of increasing the sampling efficiency were shortly introduced in Publication III. The first of the techniques was changing to a continuous-energy majorant representation. The second technique involved increasing the temperature of the basis cross sections from 0 K to the minimum temperature

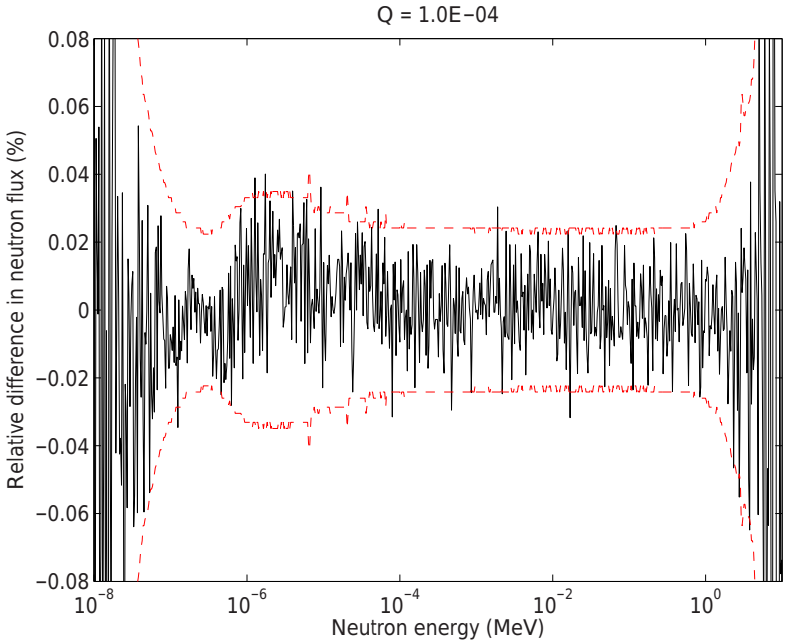

Figure 5.1. The neutron flux calculated with the TMS method corresponds to the reference solution, calculated with NJOY-based pre-broadened cross sections, within statistics. The red dashed curve corresponds to 2σ statistical deviation. The comparison corresponds to the PWR-BU case in Publication [V].

within the system. The justification of this approach and a more thorough study on its effects on performance were provided in Publication IV.

The third of the optimization techniques deals with the truncation of target velocity distribution. In the original implementation of the method, the cut-off for the target velocity was taken directly from the generation of temperature majorants for the DBRC method (Section 4.5), which again was adopted from the Sigma1 Doppler-broadening code [28]. Even though this cut-off condition is mathematically well-justified, in practice also less conservative cut-off conditions can be used without compromising the accuracy of the transport. In Publication V a revised cut-off condition is introduced and optimal levels of conservativity are determined for both the traditional and the revised majorant types by means of trial and error. The effect of the revised majorant generation was studied for both TMS and DBRC methods, and finally a value of 2×10^{-5} was chosen for the confidence level parameter Q when generating temperature majorant cross sections in Serpent 2. In Figure 5.1 it can be seen that the TMS method is able to reproduce the neutron spectrum of a NJOY -based reference calculation within statistical accuracy even with a less conservative majorant for which $Q = 10^{-4}$.

Table 5.1. Performance results for the TMS temperature treatment in three different thermal systems, compared to NJOY-based reference calculations. The performance of the TMS method in Serpent is compared against two different calculations: Serpent with reduced optimization (optimization mode 2, "fair" comparison) and Serpent with full optimization.

	Relative calculation time		
	PWR-Gd	PWR-BU	HTGR
Serpent 2, reference with full optimization	1.24	12.33	1.18
Serpent 2, reference with reduced optimization	0.89	1.36	0.84
OpenMC (preliminary results)	1.09	1.04	1.02

As a result of all the optimization techniques, the average sampling efficiency of the TMS method in PWR pin-cell problems could be increased from 26 % in the original implementation [III] to about 53 % in the optimized implementation [V]. The overhead from using the optimized TMS method varies between Monte Carlo codes, and in the case of the Serpent 2 code the performance comparison is also affected by the amount of optimization used in the calculation of the reference solution. Since pre-calculated material cross sections cannot be utilized together with the TMS method, the reference should be calculated using Serpent with reduced optimization (optimization mode 2) to get closer to an apples-to-apples comparison[6]. However, since Serpent 2 is usually run with full optimization, the slow-down observed by Serpent users is much higher than that seen in the fair comparison, especially in systems involving numerous resonance absorbers. The results of the calculation times relative to an NJOY-based reference solution, presented in Publications [V] and [VII], are summarized in Table 5.1. The results are provided for three systems: a pressurized water reactor (PWR-Gd) assembly including Gd-doped rods, the same assembly at 40 MWd/kgU burnup including about 250 nuclides (PWR-BU) and a high-temperature gas cooled reactor (HTGR) system. It should be noted that the implementation of the TMS method in OpenMC is not yet working properly (see Section 5.2.2 below) and the performance results must therefore be considered preliminary.

5.2.2 Reaction rate estimators

The performance of the method in terms of CPU time per calculated neutron, discussed in the previous section, is only a part of the whole truth. A much better measure for the true performance of a Monte Carlo calculation routine is the figure-of-merit, *FOM*, which describes the performance of a Monte Carlo calculation in the estimation of reaction rates. Using *FOM* instead of only the total calculation time in the performance comparisons is exceptionally relevant in the case of the TMS method, because the effective cross sections are not available during the transport

[6] Optimization mode 2 is, however, not a perfect reference either. In optimization mode 2 the Delta-tracking majorant cross sections are stored in multi-group format, which unnecessarily slows down the calculation, thus making the reference calculation slightly too slow for a true apples-to-apples comparison.

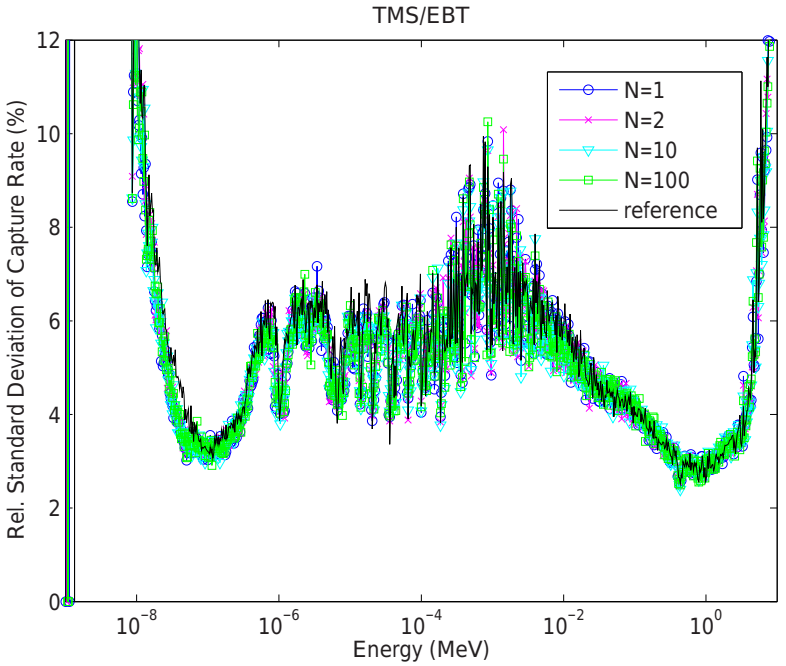

Figure 5.2. The standard deviation spectrum of TMS (N = 1) corresponds to the reference solution when the basis cross sections are at an elevated temperature. The figure is for the PWR-BU case in Publication [VI].

calculation and, as a consequence, the reaction rate estimators need to be scored using sampled cross section responses. The additional randomness in the estimator values may propagate also to the variances of the estimators and, thus, decrease the true performance of the transport calculation without affecting the calculation times.

Another important question considering the implementation of the TMS method in Monte Carlo codes other than Serpent is whether or not the track-length estimators can be scored with these sampled cross section responses altogether. Because Serpent in any case relies on collision estimators, this is of no concern for the implementation of the TMS method in Serpent 2.

The effect of the TMS method on the statistics of collision estimators was studied in Publication [VI]. The study was based on examining the standard deviation spectra of total and capture rate estimators in a few relevant systems. In these studies the "quality" of the responses was made variable by using an average of N cross section samples as the final response in the scoring, N = 1 corresponding to the normal use and N = 100 being already very close to scoring with effective cross sections. The results showed that with 0 Kelvin basis temperatures the standard deviations of the estimators are increased in the keV region, but when using TMS with basis

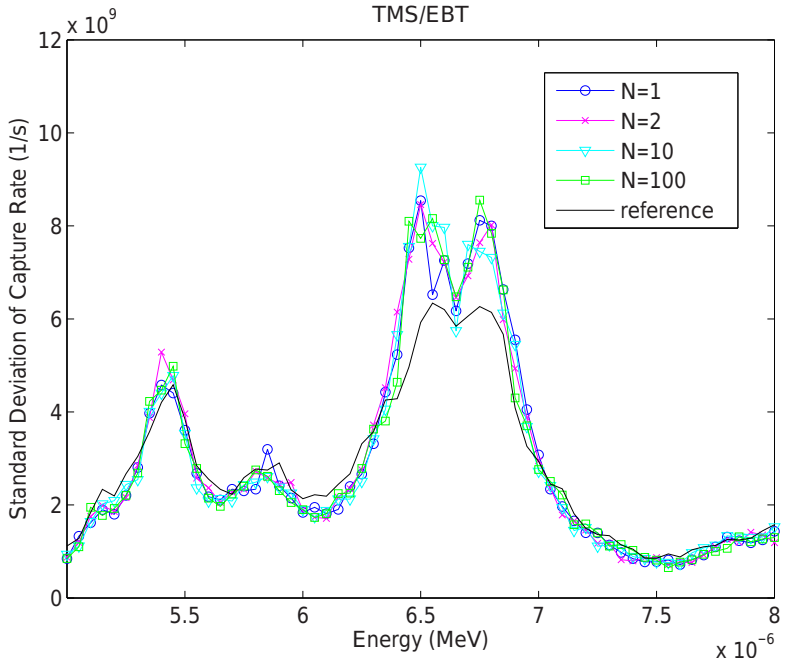

Figure 5.3. However, by looking closely at the surroundings of a strong resonance in Figure 5.2 it can be seen that the standard deviations are somewhat increased near strong resonances compared to the reference (Publication [VI]).

cross sections at an elevated temperature, i.e. the standard way, the method has no effect on the statistics of the estimators. This can also be seen in Figure 5.2. Hence, the effect of the TMS method on figures-of-merit is governed by the general slowing-down of the transport calculation.

As an exception to this conclusion it was found out that using the TMS method increases the statistical deviations of all estimators including the flux estimator near very strong resonances. This effect is demonstrated in Figure 5.3.

The applicability of the TMS method together with track-length estimators was studied in Publication [VII]. In this article, the TMS method was preliminarily implemented in the OpenMC Monte Carlo reactor physics code. Results calculated with the TMS were compared to NJOY-based reference solutions in three practical cases. At first glance, i.e. when looking at the multiplication factors of the fresh fuel cases, the implementation of the TMS method in OpenMC seemed to work fine. However, more thorough investigation of the reaction rate spectra revealed a small but statistically significant bias around the keV region. Thus, the implementation of the TMS method in OpenMC does not yet work properly. The bias is most probably related to the use of the TMS method together with track-length estimators.

6. Conclusions and future work

This thesis covers the previous development of a temperature treament technique for continuous-energy Monte Carlo neutron tracking. The method is able model the effects of thermal motion on mean free paths and reaction rates, also known as "Doppler-broadening" effects, on-the-fly during the transport calculation with only a small computational overhead. The method is based on sampling target velocities at each collision point and determining the reaction probabilities in the target-at-rest frame using cross sections at a temperature below the temperature of the matter. Since the total cross section becomes a distributed quantity, neutron transport is done using a rejection sampling scheme based on temperature majorant cross sections.

As it has been shown in the publications included in the thesis, the Target Motion Sampling temperature treatment technique is capable of accurately reproducing the results of conventional transport calculations based on NJOY -broadened cross sections, at least when using collision estimators for reaction rate calculation. Advantageously, the TMS method requires cross sections to be stored in the computer memory in one temperature only, regardless of the number of temperatures appearing in the transport problem. This saves significant amounts of computer memory in transport problems with realistic temperature distributions, compared to standard transport methods in which separate cross sections are required for each temperature appearing in the system. As a novel and very convenient feature considering the coupling of Monte Carlo transport codes with thermal hydraulics solvers, the TMS method is capable of modeling continuous temperature distributions as-is, without the need of approximating them with regions of uniform temperature.

Use of the TMS method increases the transport calculation times compared to normal transport with pre-broadened cross sections, because the sampling of target velocities at each collision point and the processing of additional virtual collisions consumes extra CPU time. Overhead from using the TMS method depends on the calculation code and the transport problem to which it is applied. In addition, the higher optimization modes of Serpent 2 include some optimization tweaks that cannot be applied with the TMS method, which makes defining of a fair reference solution complicated in Serpent. In an "unfair" comparison against Serpent with full optimization, the final implementation of the TMS method required 20 % more calculation

time than the NJOY-based reference when calculating systems with only a couple of nuclides. However, in a system with about 250 temperature-dependent nuclides, the TMS calculation required 12 times more time than the reference. The inability to use pre-calculated macroscopic cross sections together with the TMS method accounts for most of this considerable slow-down. In the preliminary and incomplete implementation of the TMS method in OpenMC the slow-down remained smaller than 10 % in all test cases, including a test case involving numerous resonance absorbers.

When considering a constant number of neutron histories, using TMS does not have an effect on the variances of estimators in practice. Hence, the TMS method affects the performance of reaction rate estimators, i.e. the figures-of-merit, mainly via the general slowing-down of the transport calculation.

In summary, the TMS method has proven to be a well-feasible and, in general, also an efficient method for on-the-fly temperature treatment. The method is especially well-suited for neutron transport codes based on collision estimators because of the ability to model continuous temperature distributions. This property cannot be taken advantage of with track-length estimators and, to be precise, the functionality of the TMS method together with track-length estimators has not yet been demonstrated either.

6.1 Future prospects

There are still many open questions and research topics left concerning the development of the TMS method. The most obvious deficiency in the present methodology is the unsolved bias that affects the reaction rate spectra when using the method with track-length estimators. Studying the cause for the bias and correcting the implementation of the method in OpenMC accordingly is a high-priority development topic.

Another important topic considering the practical use of the method in the Serpent 2 reactor physics code is the optimization of the method in burnup calculations involving numerous resonance absorber nuclides. The method is about as fast as it gets as long as all of the nuclides are treated temperature-dependently, but whether or not all the 250–300 nuclides need to be treated in a temperature dependent manner is a very important question considering the performance of the method. In case the temperature dependence can be neglected for part of the nuclei, the method can be optimized further.

It should also be noted that the applicability of the TMS method is currently limited to the energy region of resolved resonances and the thermal energy region in the case of free atom scattering. It should be relatively straightforward to extend the basic idea of the TMS method to the energy region of unresolved resonances in the future. Instead, bound-atom scattering is a rather complicated phenomenon, which currently requires solving of both the temperature-dependent cross sections and secondary particle distributions relying on special thermal scattering data, based on quantum mechanical models and experiments. Consequently, applying the basic idea of TMS to bound-atom scattering would require developing and implement-

ing very complicated models within the Monte Carlo calculation code, which is not considered reasonable in terms of performance or effort. At least with the currently available formalism for bound-atom scattering, the most practical way of handling the temperature dependence is by interpolating between data at different temperatures.

Bibliography

[1] A. Santamarina et al., "The JEFF-3.1.1 Nuclear Data Libary," ISBN 978-92-64-99076-6, Nuclear Energy Agency (2009).

[2] J. Lamarsh, *Introduction to Nuclear Engineering*, Addison-Wesley Publishing Company, Massachusetts (1983).

[3] J. Leppänen, "Development of a New Monte Carlo Reactor Physics Code," ISBN 978-951-38-7018-8, VTT Technical Research Centre of Finland (2007).

[4] M. Alonso and E. Finn, *Fundamental university physics, Volume III: Quantum and statistical physics*, Addison-Wesley Publishing Company, Reading, Massachusetts (1969).

[5] W.E. Lamb, Jr., "Capture of Neutrons by Atoms in a Crystal," *Phys. Rev.*, **55**, 190-197 (1939).

[6] J. A. W. Solbrig, "Doppler Effect in Neutron Absorption Resonances," *Am. J. Phys.*, **29**, 257-261 (1960).

[7] R. E. MacFarlane and D. W. Muir, "NJOY99.0 Code System for Producing Pointwise and Multigroup Neutron and Photon Cross Sections from ENDF/B Data," PSR-480, Los Alamos National Laboratory (2000).

[8] J. Lamarsh, *Introduction to Nuclear Engineering*, Addison-Wesley Publishing Company (1972).

[9] F. Reif, *Fundamentals of Statistical and Thermal Physics*, McGraw-Hill, New York (1965).

[10] M. Ouisloumen and R. Sanchez, "A Model for Neutron Scattering Off Heavy Isotopes That Accounts for Thermal Agiation Effects," *Nuc. Sci. Eng*, **107**, 189-200 (1991).

[11] W. Rothenstein, "Proof of the Formula for the Ideal Gas Scattering Kernel for Nuclides with Strongly Energy Dependent Scattering Cross Sections," *Ann. Nucl. Energy*, **31**, 9-23 (2004).

[12] C. S. E. W. Group, "ENDF-6 Formats Manual," BNL-90365-2009, Brookhaven National Laboratory (2009).

[13] L. Levitt, "The Probability Table Method for Treating Unresolved Neutron Resonances in Monte Carlo Calculations," *Nucl. Sci. Eng*, **49**, 450–457 (1972).

[14] X-5 Monte Carlo Team, "MCNP — a General Monte Carlo N-Particle Transport Code, Version 5," LA-UR-03-1987, Los Alamos National Laboratory (2003).

[15] "Serpent website," `http://montecarlo.vtt.fi`, Accessed: Jan 16. 2015.

[16] P. Romano and B. Forget, "The OpenMC Monte Carlo Particle Transport Code," *Ann. Nucl. Energy*, **51**, 274–281 (2013).

[17] I. Lux and L. Koblinger, *Monte Carlo Particle Transport Methods: Neutron and Photon Calculations*, CRC Press, Boca Raton, Florida (1990).

[18] R. Coveyou et al., "Effect of moderator temperature upon neutron flux in infinite, capturing medium," *J. Nuclear Energy*, **2**, 153–167 (1956).

[19] J. Neumann, "Various Techniques Used in Connection with Random Digits," volume 12, p. 36–38, National Bureau of Standards Applied Mathematics Series, U.S. Government, Printing Office, 1951.

[20] E. Kreyszig, *Advanced Engineering Mathematics, 8th edition*, John Wiley & Sons, inc., New York (1999).

[21] E. Woodcock et al., "Techniques used in the GEM code for Monte Carlo neutronics calculations in reactors and other systems of complex geometry," (1965).

[22] "Erlang distribution, Wikipedia," `http://en.wikipedia.org/wiki/Erlang_distribution`, Accessed: Jan 16. 2015.

[23] W. Coleman, "Mathematical Verification of a Certain Monte Carlo Sampling Technique and Applications of the Technique to Radiation Transport Problems," *Nucl. Sci. Eng*, **32**, 79–81 (1968).

[24] K. S. D. Lee and J. Rhodes, "The Impact of ^{238}U Resonance Elastic Scattering Approximations on Thermal Reactor Doppler Reactivity," *Ann. Nucl. Energy*, **36**, 274–280 (2009).

[25] T. Mori and Y. Nagaya, "Comparison of Resonance Elastic Scattering Models Newly Implemented in MVP Continuous-Energy Monte Carlo Code," *J. Nucl. Sci. Tech*, **46**, 793–789 (2009).

[26] W. Rothenstein, "Effect of Upscattering by Heavy Nuclides on Doppler Changes of Resonance Absorption," *Proc. ENS Conference 1994*, Tel Aviv, Israel, 23-26 January 1994, 1994.

[27] R. D. B. Becker and G. Lohnert, "Proof and implementation of the stochastic formula for ideal gas, energy dependent scattering kernel," *Ann. Nucl. Energy*, **36**, 470-474 (2009).

[28] D. Cullen, "Program SIGMA1 (version 79-1): Doppler broaden evaluated cross sections in the evaluated nuclear data file/version B (ENDF/B) format," UCRL-50400, Lawrence Livermore National Laboratory (1979) (1979).

[29] D. Cullen and C. Weisbin, "Exact Doppler Broadening of Tabulated Cross Sections," *Nucl. Sci. Eng*, **60**, 199–229 (1976).

[30] W. R. M. G. Yesilyurt and F. B. Brown, "On-the-Fly Doppler Broadening for Monte Carlo Codes," *Nucl. Sci. Eng.*, **171**, 239-257 (2012).

[31] J. Donnelly, "Interpolation of Temperature-Dependent Nuclide Data in MCNP," *Nucl. Sci. Eng*, **168**, 180–184 (2011).

[32] A. Ivanov et al., "High fidelity simulation of conventional and innovative LWR with the coupled Monte-Carlo thermal-hydraulic system MCNP-SUBCHANFLOW," *Ann. Nucl. Energy*, **262**, 264–275 (2013).

[33] T. Trumbull, "Treatment of nuclear data for transport problems containing detailed temperature distributions," *Nucl. Tech.*, **156**, 75–86 (2006).

[34] C. Dean et al., "Validation of Run-time Doppler Broadening in MONK with JEFF3.1," *J. Kor. Phys. Soc.*, **59**, 1162-1165 (2011).

[35] W. R. M. G. Yesilyurt and F. B. Brown, "On-the-Fly Doppler Broadening for Monte Carlo Codes," *Proc. M&C 2009*, Saratoga Springs, NY, May 3-7 2009, 2009.

[36] W. Martin et al., "On-The-Fly Neutron Doppler Broadening in MCNP," *Proc. SNA + MC 2013*, Paris, France, Oct. 27-31 2013, 2013.

[37] S. X. B. Forget and K. Smith, "Direct Doppler broadening in Monte Carlo simulations using the multipole representation," *Ann. Nucl. Energy*, **64**, 78–85 (2014).

[38] B. F. C. Josey and K. Smith, "Efficiency and accuracy evaluation of the windowed multipole direct doppler broadening method," *Proc. PHYSOR-2014*, Kyoto, Japan, Sep. 28-Oct 3. 2014, 2014.

[39] V. Ogibin and A. Orlov, "Majorized cross-section method for tracking neutrons in moving media," *Voprosy Atomnoj Nauki i Techniki, Metodoki i Programmy*, **2(16)**, 6–9 (1984), in Russian.

[40] Y. Kandiev et al., "PRIZMA Status," *Proc. SNA+MC2013*, Paris, France, Oct. 27-31 2013, 2013.

Errata

A few very unfortunate errors have been identified in the Publications after their publication. The author apologizes all the inconvenience these errors may have caused.

- Publication I, Page 168, Equation (22): The sign of the exponential term in the equation should be positive instead of negative. The correct formula is, thus

$$g(v,T,A) = \left(1 + \frac{1}{2\gamma(T,A)^2 v^2}\right)\mathrm{Erf}(\gamma(T,A)v) + \frac{e^{-\gamma(T,A)^2 v^2}}{\sqrt{\pi}\gamma(T,A),v},$$

  similar to Equation (3.11) in the current thesis.

- Publication II, Page 79, Equation (5): All γ symbols should be replaced with γ^2 in the equation. The correct formulation for the Maxwell-Boltzmann distribution is thus

$$P(\mathbf{V}_t, T, A)d\mathbf{V}_t = (\frac{\gamma}{\sqrt{\pi}})^3 e^{-\gamma^2(\mathbf{V}_t\cdot\mathbf{V}_t)}d\mathrm{V}_t \tag{6.1}$$

- Publication II, Page 84, Section V.A: The nuclides that were recognized to require a DBRC treatment to get correct results in a test case involving burned fuel were correctly identified in Fig. 3, but two plutonium isotopes are missing in the list of the DBRC nuclides within the text. The corresponding sentence should be written
  "The reference calculation was repeated such that the use of DBRC was extended to nuclides ^{95}*Mo,* ^{108}*Pd,* ^{131}*Xe,* ^{145}*Nd,* ^{147}*Pm,* ^{152}*Sm,* ^{239}*Pu,* ^{240}*Pu,* ^{242}*Pu and* ^{241}*Am, in addition to* ^{238}*U."*.
  This is the list of DBRC nuclides actually used in the calculations.

PUBLICATION I

Explicit treatment of thermal motion in continuous-energy Monte Carlo tracking routines

Nucl. Sci. Eng., **171**, pp. 165–173.

NUCLEAR SCIENCE AND ENGINEERING: **171**, 165–173 (2012)

Explicit Treatment of Thermal Motion in Continuous-Energy Monte Carlo Tracking Routines

Tuomas Viitanen* and Jaakko Leppänen

VTT Technical Research Centre of Finland
P.O. Box 1000, FI-02044 VTT, Finland

Received June 6, 2011
Accepted October 11, 2011

Abstract—*This paper introduces a new stochastic method for taking the effect of thermal motion into account on the fly in a Monte Carlo neutron transport calculation. The method is based on explicit treatment of the motion of target nuclei at collision sites and, consequently, requires simply cross sections at a temperature of 0 K regardless of the number of temperatures in the problem geometry. It utilizes rejection sampling techniques to manage the fact that total cross sections become distributed quantities. The method has a novel capability of accurately modeling continuous temperature distributions.*

The new stochastic method is verified using a simple test program, which compares its results to an analytical reference solution based on NJOY-broadened cross sections. Future implementation to Monte Carlo reactor physics code Serpent is also discussed shortly.

I. INTRODUCTION

Material temperature plays an important role in nuclear reactor analysis, as all reaction rates are affected by the thermal motion of nuclides in the medium. Temperature effects cannot be neglected in any application without inflicting serious errors in the results, but their role is particularly emphasized in coupled neutronics/thermal hydraulics calculations dealing with heat transfer and feedback between fission power and coolant flow. These applications are becoming increasingly important for continuous-energy Monte Carlo codes as well, along with the development of computer capacity.

The traditional approach to dealing with the temperature effects involves using pregenerated, Doppler-broadened cross sections. This approach is well sufficient for applications where materials are at constant temperature or where the distributions can be approximated by constant effective values. More rigorous description of temperature gradients requires dividing the materials into several homogeneous subregions, each assigned with a different set of cross sections. This, in turn, requires additional storage space, which may become a practical limitation if the number of subregions and nuclides is large.

One possibility to treat temperature distributions without excessive storage space requirements is to use interpolation between tabulated values.[1] This approach, however, requires relatively narrow spacing between the temperature points to reduce the interpolation errors to an acceptable level. The capability to use 0 K cross sections is another option that has been studied extensively within the past few years. Yesilyurt et al. have developed an efficient on-the-fly Doppler-broadening routine, based on series expansions and the multilevel Adler-Adler resonance representation.[2] Becker et al. have used another approach, relying on a stochastic algorithm for calculating effective integral and double-differential cross sections, which were utilized in the confirmation of the analytic scattering kernel.[3]

This paper presents another stochastic method for performing temperature corrections on reaction rates during the Monte Carlo transport simulation. The basic idea is very similar to Becker's method, but instead of performing stochastic Doppler broadening on the cross sections, the thermal motion of target nuclides is handled explicitly by making a coordinate transformation to target-at-rest frame (T-frame) at each collision point. The fact

*E-mail: tuomas.viitanen@vtt.fi

that material total cross sections become distributed quantities is handled using a rejection sampling routine on the neutron path lengths. As an additional feature, the use of this method also removes the homogeneity requirement and allows the modeling of continuous temperature distributions without approximations.

The current version of the method is unable to utilize the thermal scattering laws for bound atoms at thermal energies or probability table treatment at the unresolved resonance region, which somewhat limits the usability of the method in practical reactor calculations. The explicit treatment method also slightly complicates the implementation of flux estimators.

This paper considers only transport in a homogeneous material region with heterogeneous temperature, which is the simplest case that provides for proper verification of the method. However, the method can be straightforwardly generalized to transport in heterogeneous systems.

The methodology used in the calculation routines is introduced in Sec. II and demonstrated in Sec. III. The future implementation of the new method in the Serpent Monte Carlo code is discussed in Sec. IV, and Sec. V is left for the conclusions.

II. METHODS

The core of every Monte Carlo neutron transport code is the tracking routine, which simulates the random walk process by transporting neutrons through the geometry from one interaction to the next. The simulation is based on the fact that the free path length between two collision points is exponentially distributed, with the well-known probability density function (PDF) of the form

$$f(E,x) = \Sigma_{\text{tot}}(E) e^{-x\Sigma_{\text{tot}}(E)} \quad , \tag{1}$$

where Σ_{tot} is the macroscopic total cross section of the medium. The conventional approach to sampling neutron path lengths from this distribution is to use the inversion method, which requires calculating the cumulative distribution function (CDF) of Eq. (1),

$$F(E,x) = \int_0^x f(E,x')\,dx' = 1 - e^{-x\Sigma_{\text{tot}}(E)} \quad , \tag{2}$$

and using the inverse of the CDF with a uniformly distributed random variable ξ on the unit interval as a sample from f:

$$x = F^{-1}(E,\xi) = -\frac{1}{\Sigma_{\text{tot}}(E)} \ln(1-\xi) \quad . \tag{3}$$

The prerequisite of this technique is that the total cross section remain constant throughout the path. If this is not the case, the integration in Eq. (2) does not hold, and the sample in Eq. (3) is not statistically valid. This happens, for example, when the sampled collision point lies outside the material boundaries, in which case the neutron is stopped at the boundary surface and a new path length is sampled using the total cross section of the next material. The same limitation requires the geometry to be defined using homogeneous material regions without internal spatial variation in the total cross section.

II.A. Rejection Techniques for Sampling Neutron Path Length

It is important to notice that material homogeneity is a demand resulting from the use of the inversion sampling technique and not a characteristic of the Monte Carlo method itself. The limitation can be easily lifted by using rejection sampling techniques,[4] which are based on the use of two distribution functions: the original PDF and a majorant function satisfying

$$f_{\text{maj}}(z) \geq f(z) \tag{4}$$

for all values of the random variable and formed in such a way that values from f_{maj} can be sampled using the inversion method. According to the theory, values sampled from the majorant function and accepted with probability

$$P = \frac{f(z)}{f_{\text{maj}}(z)} \tag{5}$$

follow the distribution of f. Rejected values are discarded, and the procedure is repeated until a successful sample is obtained from Eq. (5).

A good example of using rejection techniques for sampling neutron path lengths is the Woodcock delta-tracking method,[5] which allows the random walk to be continued over one or several material boundaries without stopping the track at each boundary surface. The free path length is sampled using Eq. (3), with material total cross section replaced by the majorant cross section:

$$\Sigma_{\text{maj}}(E) \geq \Sigma_{\text{tot}}(E,x) \quad . \tag{6}$$

The collision point is accepted with probability

$$P(E,x) = \frac{\Sigma_{\text{tot}}(E,x)}{\Sigma_{\text{maj}}(E)} \quad . \tag{7}$$

If the point is rejected, the procedure is restarted by sampling a new path length using the majorant cross section.

This study deals with a very similar problem. Material total cross sections are not constant, but instead of discrete discontinuities at boundary crossings, the values are characterized by a continuous distribution. The variation in the value of Σ_{tot} results from the fact that reaction cross sections are evaluated in the T-frame at energy E', which depends not only on the neutron energy E in the laboratory frame (L-frame), but also on the thermal motion of the target nucleus. The rejection sampling

routine applied to the problem accounts for this variation by using a majorant cross section for sampling the neutron path lengths. Similar to in delta tracking, the actual value of Σ_{tot} is needed only at the tentative collision points. In delta tracking this value depends on the material where the collision occurs. In this case the velocity of the target nucleus is sampled from a Maxwellian-based distribution to make a transfer from L-frame to T-frame, and the result dictates the energy at which cross section is evaluated.

It should be noted that the explicit temperature treatment method only governs the way neutrons are transported inside a material region. Thus, the method is applicable to all kinds of tracking schemes including delta and surface tracking. As an additional remark, the track-length estimators—usually utilized with surface tracking—can only be used to calculate integrals of quantities that are homogeneous inside a material zone. Therefore, for example, reaction frequencies inside a region with an inhomogeneous temperature profile must be calculated using collision estimators. This is a limitation of the track-length estimator, not of the explicit temperature treatment itself.

II.B. Forming the Majorant Cross Section

The majorant cross section must be defined in such a way that the value is always greater than or equal to the T-frame total cross section at the collision point:

$$\Sigma_{maj}(E) \geq \Sigma^0_{tot}(E', x) \ , \tag{8}$$

where the superscript indicates that the cross sections are generated at absolute zero temperature. Since the T-frame energy is a distributed quantity, finding the maximum value requires determining the variation of relative velocity $v' \in [v'_{min}, v'_{max}]$, corresponding to relative energy E', as a function of L-frame velocity v, material temperature T, and nuclide mass $m = AM_n$.

If the velocity of the target nucleus equals V_t, the maximum of

$$v' = \sqrt{v^2 + V_t^2 - 2vV_t\mu} \tag{9}$$

corresponds to a parallel collision with $\mu = -1$. Relative velocity v' is minimal for a head-on collision with $\mu = 1$ unless $V_t > v$, in which case the velocity may reach arbitrarily small values. Thus,

$$v'_{max} = v + V_t \tag{10}$$

and

$$v'_{min} = \begin{cases} v - V_t \ , & \text{if } V_t \leq v \\ 0 \approx v_0 \ , & \text{if } V_t > v \ , \end{cases} \tag{11}$$

where v_0 corresponds to the lowest energy in the cross-section energy grid.[a]

Both of the extremities are obtained with the highest possible value of V_t. Target velocity V_t is assumed to obey the Maxwell-Boltzmann distribution

$$P_{MB}(V_t) = \frac{4}{\sqrt{\pi}} \gamma^3 V_t^2 e^{-\gamma^2 V_t^2} \tag{12}$$

and

$$\gamma(T, A) = \sqrt{\frac{AM_n}{2kT}} \ , \tag{13}$$

where k is the Boltzmann constant. To be precise, this assumption is only valid for ideal gases, not for example crystalline materials like UO_2. Hence, the sampling of target velocities from the Maxwell-Boltzmann distribution may cause bias in the results. This issue, however, concerns not only the current study but also many other calculation codes in which this very common assumption is made. For instance, all effective cross sections broadened by the SIGMA1 code (used in NJOY) have the same assumption built in.[6]

Since the distribution (12) has an infinite tail, it is impossible to determine an unambiguous maximum for the velocity, and therefore, an approximation must be introduced. If the approximative maximum is chosen too high, Σ_{maj} becomes inefficiently conservative, while too-small values may result in significant errors.

A convenient way of dealing with a similar problem was introduced in the SIGMA1 module of NJOY (Ref. 7) and was recently utilized in the creation of a majorant cross section for the Doppler broadening rejection correction method by Becker et al.[8] In SIGMA1, a target velocity of

$$V_t = \frac{4}{\gamma(T, A)} \tag{14}$$

was used as a cutoff value in the integrals of the Doppler-broadening algorithm. The same cutoff value is adopted as the maximum of V_t in the current study also. This approximation omits a proportion of 5×10^{-7} of the most energetic nuclei, which is considered a suitable compromise between efficiency and accuracy. For the majorant to be conservative, the temperature T in Eq. (13) must be chosen as the maximum T_{max} inside a material region in the case of nonuniform temperature distributions.

[a]Physically correct cross-section extrapolation to zero velocity would result in an unfeasible, infinite majorant in the case of $1/v$-shaped cross sections. Hence, cross sections for $v' \leq v_0$ are approximated with $\Sigma_{tot}(v_0)$ when forming the majorant. The effect of this approximation was studied and found insignificant.

To summarize the above discussion, Σ_{maj} for neutron energy E is obtained as the maximum of the 0 K total cross section Σ^0_{tot} within an interval $E' \sim v' \in [v'_{\min}, v'_{\max}]$ defined by Eqs. (10), (11), and (14).

II.C. Sampling Target Velocity

The tracking routine proceeds in the conventional way, the only difference being that the neutron path lengths are sampled using majorants instead of macroscopic total cross sections. Once the collision point x is reached, the T-frame energy E' is sampled based on distribution $P(V_t, \mu)$.

For the tracking routine to be consistent with the traditional transport methods relying on effective cross sections, it is obvious that the distribution $P(V_t, \mu)$ must satisfy relation

$$\iint \Sigma^0_i(v', x) P(V_t, \mu)\, dV_t\, d\mu = \Sigma_{\text{eff}}(v, x, T) \ , \qquad (15)$$

where $\Sigma_{\text{eff}}(v, x, T)$ is the effective cross section for temperature T, defined[9,10]

$$\Sigma_{\text{eff}}(v, x, T) = \frac{1}{v} \iint v' \Sigma^0_i(v', x) P_{\text{MB}}(V_t)\, dV_t\, d\frac{\mu}{2} \ . \qquad (16)$$

From Eqs. (15) and (16), it results that consistency is achieved if

$$P(V_t, \mu) = \frac{v'}{2v} P_{\text{MB}}(V_t) \ , \qquad (17)$$

which is exactly the same distribution that is used in the sampling of target velocities in the free gas thermal treatment of MCNP. Hence, also the sampling procedure is the same, as described in the following.

Because of the v' multiplier, direct sampling from the distribution Eq. (17) is problematic. Consequently, Eq. (17) is rewritten in the form

$$P(V_t, \mu) = C \left\{ \frac{v'}{v + V_t} \right\} \left\{ (2\gamma^4) V_t^3 e^{-\gamma^2 V_t^2} + B(4\gamma^3/\sqrt{\pi}) V_t^2 e^{-\gamma^2 V_t^2} \right\} \ , \qquad (18)$$

where constants C and

$$B = \frac{\gamma v \sqrt{\pi}}{2} \qquad (19)$$

are both independent of V_t. The nuclide velocity is sampled from $V^3 e^{-\gamma^2 V^2}$ distribution with probability $Q = 1/(1 + B)$ and from $V^2 e^{-\gamma^2 V^2}$ with probability $1 - Q$. The cosine between the velocity vectors is obtained from an isotropic distribution, and the sample is accepted with probability $v'/(v + V_t) \leq 1$. The sampling is repeated until an accepted v' is found.[11]

II.D. Rejection Sampling at Collision Point

The procedure continues by rejection sampling using the 0 K total cross section at energy E' corresponding to the sampled relative velocity v'. The collision point x is accepted with probability

$$P = \frac{\Sigma^0_{\text{tot}}(E', x)}{\Sigma_{\text{maj}}(E)} \ . \qquad (20)$$

If the point is rejected, the whole procedure restarts by sampling a new path length starting from x. The 0 K cross sections are also used for sampling the reaction mode. The probability of sampling reaction i is simply

$$P_i = \frac{\Sigma^0_i(E', x)}{\Sigma^0_{\text{tot}}(E', x)} \ . \qquad (21)$$

II.E. Normalization Factor for Low Energies

The explicit treatment of target motion, as introduced above, cannot fully account for the low-energy effects on effective cross sections, namely, the increase in potential scattering rate when $E \ll kT$. As the energy of a neutron approaches zero, the thermal motion of the surrounding nuclei becomes an increasingly important cause for collision events. Thus, the slower the velocity of the neutron, the more thermal-motion-initiated collisions occur per traveled path length, and consequently, the larger the apparent increase in effective potential scattering cross section. This effect does not affect the fission and capture cross sections that typically behave as $1/v$ at low energies.

A mathematical explanation for this phenomenon is concealed in Eq. (17) or, more precisely, the fact that Eq. (17) is not actually a distribution in the sense that its integral over V_t and μ differs significantly from unity if $E \ll kT$. The value of this integral depends on the L-frame velocity of the incident neutron v and equals

$$g(v, T, A) = \iint \frac{v'}{2v} P_{\text{MB}}(V_t)\, d\mu\, dV_t = \left(1 + \frac{1}{2\gamma(T,A)^2 v^2}\right) \text{erf}(\gamma(T,A) v) - \frac{e^{-\gamma(T,A)^2 v^2}}{\sqrt{\pi}\gamma(T,A) v} \ , \qquad (22)$$

which can be easily written also in terms of energy as $g(E, T, A)$ (Ref. 11).

Equation Eq. (17) is rewritten in the form

$$P(V_t,\mu) = g(v,T,A)P_1(V_t,\mu) \ , \tag{23}$$

where the integral of

$$P_1(V_t,\mu) = \frac{1}{g(v,T,A)} \frac{v'}{2v} P_{MB}(V_t) \tag{24}$$

equals unity for all v and, therefore, is the actual distribution used in the sampling of target velocity since only one nuclide is considered per collision. Taking this into account, Eq. (15) is corrected in accordance with the sampling procedure as

$$\iint g(v,T,A)\Sigma_i^0(v',x)P_1(V_t,\mu)\,dV_t\,d\mu = \Sigma_{eff}(v,x,T) \ . \tag{25}$$

Equation (25) points out that the low-energy phenomenon can be correctly accounted for by multiplying all the 0 K cross sections used in the transport simulation with factor $g(E,T,A)$. Correspondingly, the same correction must be applied also for the majorant cross sections with $T = T_{max}$, i.e.,

$$\Sigma_{maj,corr}(E) = g(E,T_{max},A)\Sigma_{maj}(E) \ , \tag{26}$$

where Σ_{maj} is as defined in Sec. II.B.

II.F. Materials Consisting of Multiple Nuclides

Since the distribution of target velocity depends on nuclide mass, the procedure introduced in Secs. II.B through II.E cannot be directly applied to materials consisting of multiple nuclides. The simplest way to solve this problem is to form a material-wise majorant cross section by summing over the nuclide-wise majorants in the composition

$$\Sigma_{maj,corr}(E) = \sum_n \Sigma_{maj,corr,n}(E) = \sum_n g(E,T_{max},A_n)\Sigma_{maj,n}(E) \ . \tag{27}$$

Neutron path lengths are sampled using $\Sigma_{maj,corr}$, and rejection sampling is divided into two parts. First, the target nuclide n is sampled with probability

$$P_n = \frac{\Sigma_{maj,corr,n}(E)}{\Sigma_{maj,corr}(E)} = \frac{g(E,T_{max},A_n)\Sigma_{maj,n}(E)}{\Sigma_{maj,corr}(E)} \ . \tag{28}$$

This selection is then followed by the sampling of T-frame energy E', rejection sampling with acceptance criterion

$$\xi < \frac{g(E,T(x),A_n)\Sigma^0_{tot,n}(E',x)}{g(E,T_{max},A_n)\Sigma_{maj,n}(E)} \ , \tag{29}$$

and, finally, the reaction sampling using the 0 K cross sections

$$P_i = \frac{g(E,T(x),A_n)\Sigma^0_{i,n}(E',x)}{g(E,T(x),A_n)\Sigma^0_{tot,n}(E',x)} = \frac{\Sigma^0_{i,n}(E',x)}{\Sigma^0_{tot,n}(E',x)} \ . \tag{30}$$

III. DEMONSTRATION

The validity of the new method is demonstrated with a test program. It uses the methodology described in Sec. II to sample next collision sites and reactions for neutrons with user-defined L-frame energies E. To demonstrate the capability of heterogeneous temperature modeling, the test calculations are performed for a one-dimensional single-material system in which neutron paths begin from $x = 0$, region $x \le x_0$ is at temperature T_1, and region $x > x_0$ is at temperature T_2.

Advantageous to the verification purpose, the neutron mean free path (mfp) can be analytically resolved in the chosen system. The mfp for a neutron with energy E is

$$l(E) = \frac{1}{\Sigma_{tot,1}(E)} + e^{-\Sigma_{tot,1}(E)x_0}\left(\frac{1}{\Sigma_{tot,2}(E)} - \frac{1}{\Sigma_{tot,1}(E)}\right) \ , \tag{31}$$

where $\Sigma_{tot,1}$ and $\Sigma_{tot,2}$ are the Doppler-broadened total cross sections for temperatures T_1 and T_2, respectively. The test program uses this result, together with reaction probabilities

$$P_i = (1 - e^{-\Sigma_{tot,1}(E)x_0})\frac{\Sigma_{i,1}(E)}{\Sigma_{tot,1}(E)} + e^{-\Sigma_{tot,1}(E)x_0}\frac{\Sigma_{i,2}(E)}{\Sigma_{tot,2}(E)} \ , \tag{32}$$

to provide analytical reference results. Sampling path lengths and reactions using the stochastic method should reproduce the same behavior with 0 K data, when the results are averaged over a large number of samples.

The medium in the test case consists of 8.3% enriched uranium oxide. Fuel material is at 900 K for $x \le x_0$ and at 1800 K for $x > x_0$. Temperature boundary x_0 is at 0.0197 cm, which corresponds to the lethargy-averaged mfp at 900 K. The calculations were performed with JEFF-3.1–based cross-section data.

In the specific test case, the sampling efficiency of acceptance criterion Eq. (29) varied between 0.2% at an energy point in the resonance region (186 eV) to almost 100% at energies close to 1 MeV. The average efficiency was 41% when the energies E were chosen in 500 equi-lethargy intervals from 10^{-11} to 15 MeV.

Selected results are presented in Fig. 1. The results in Fig. 1 are calculated using a cross-section library processed with NJOY using 0.003 reconstruction tolerance. Ten million samples were run per each energy E.

Comparison of the results is carried out for neutron mfp and fission, capture, and elastic scattering

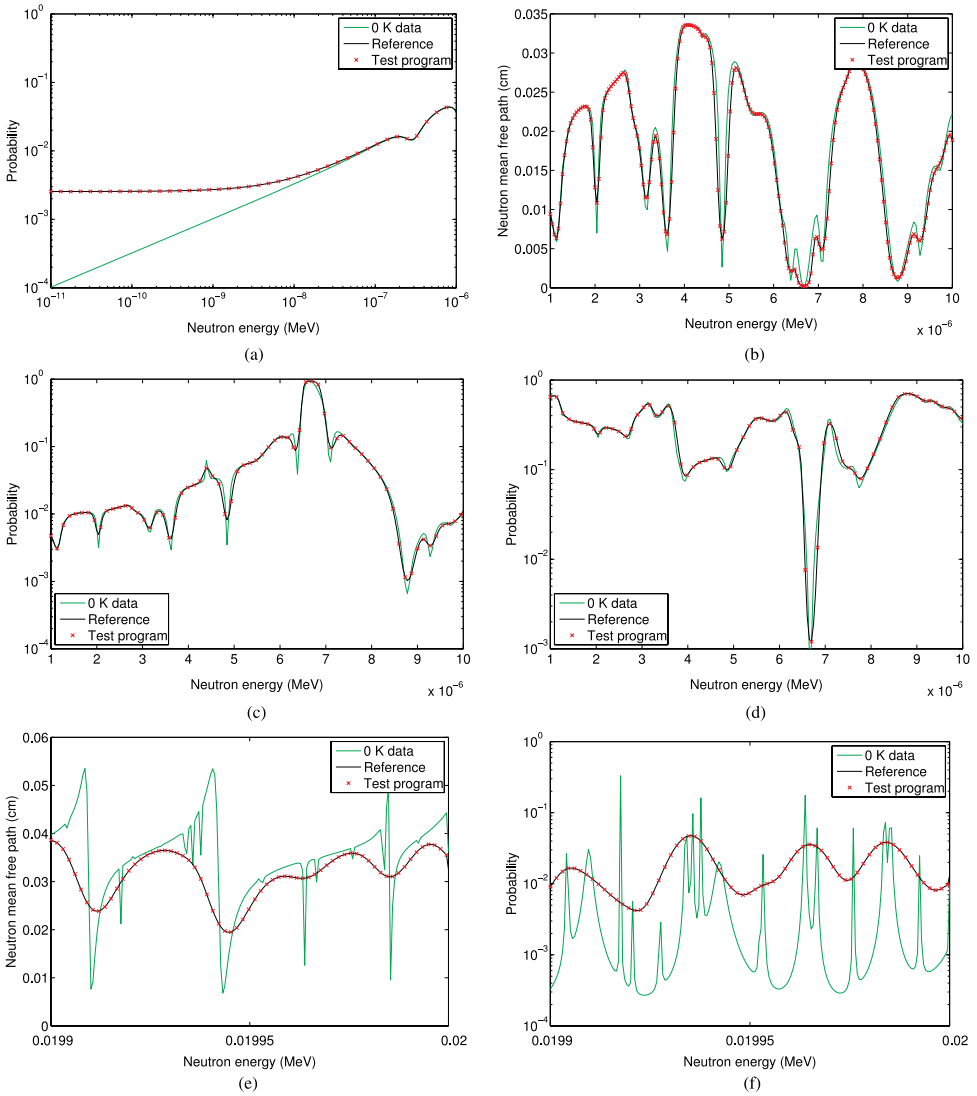

Fig. 1. The correspondence between the test routine and the NJOY-based reference results is excellent. (a) Elastic scattering probability of ^{16}O (thermal energy region). (b) Neutron mfp (low-resonance region). (c) Uranium-238 capture probability (low-resonance region). (d) Uranium-235 fission probability (low-resonance region). (e) Neutron mfp (high-resonance region). (f) Uranium-238 capture probability (high-resonance region).

probabilities of the uranium isotopes and ^{16}O. To distinguish the impact of thermal motion, analytical solutions are also provided at zero temperature. Three energy intervals are considered:

Thermal region: 1×10^{-11} to 1×10^{-6} MeV—This energy region lies below the first resonances and shows the low-energy behavior of elastic scattering cross sections.

Low resonance region: 1×10^{-6} to 1×10^{-5} MeV—This region covers the lowest resonance peaks of ^{235}U and ^{238}U.

High-resonance region: 19.9×10^{-3} to 20×10^{-3} MeV—This is the higher end of the resolved resonance region, just below unresolved resonances.

Neutron capture and fission are the dominant reaction modes at low energies. Since the cross sections of these reactions are unaffected by thermal motion, differences in neutron mfp remain small as well. Elastic scattering cross sections are increased, which is shown in the reaction probabilities. The curves for ^{16}O are plotted in Fig. 1a. The agreement is good and the differences clear when compared to 0 K data.

The low-resonance region covers the first high peak of ^{238}U and several lower humps of ^{235}U. The high capture resonance at 6.7 eV drops neutron mfp close to zero, as seen in Fig. 1b. Broadening of the resonance peaks is clearly shown in the reaction probabilities, and the effect is well reproduced by the stochastic model.

Resonances in the high end of the resolved region exhibit strong overlap when broadened to 900 or 1800 K temperature. Neutron mfp and ^{238}U capture probability in Figs. 1e and 1f barely resemble the 0 K data. The analytical and stochastic results are in good agreement.

Test calculations were also performed for the whole energy spectrum using two cross-section libraries of different reconstruction tolerances, namely, 0.010 and 0.003. To minimize the statistical errors, the number of neutrons per energy grid point was increased to one hundred million. Relative differences in mfp are plotted in Fig. 2 for both of the libraries.

In Fig. 2, a small negative bias can be recognized at energies below 10^{-7} MeV. It originates from the limited accuracy of the cross-section representation in which the cross sections between energy grid points are obtained via linear interpolation. NJOY chooses the energy grid so that the proportional error of linear interpolation does not exceed the reconstruction tolerance.[12] In the resonance region of a typical cross-section curve, the linear interpolation results occasionally in both too-high and too-small values. Instead, when a $1/v$-shaped cross-section curve is approximated with linear interpolation, the result is systematically larger than the actual cross section. Since the dominating fission and capture cross

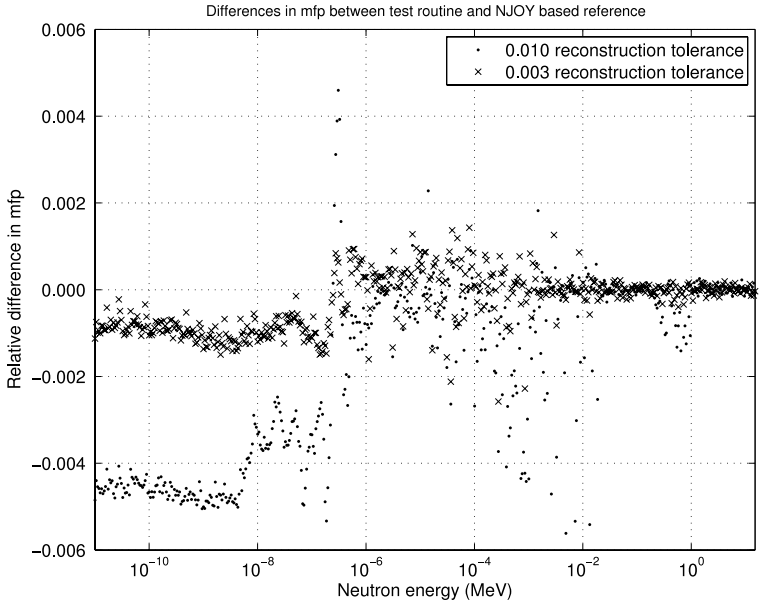

Fig. 2. The relative difference plot between the test routine and reference results points out a minor bias at thermal energies.

sections are $1/v$-shaped at low energies, the total cross section becomes positively biased, which results in a negative bias in the mfp.

As can be seen in Fig. 2, the proportional deviances in mfp are smaller than the reconstruction tolerances. In other words, the limited accuracy of the cross-section representation, together with an insignificant amount of statistical error, accounts for all the perceived errors in mfp. Thus, the new explicit temperature treatment method seems just as accurate as the available cross-section libraries, at least when compared to an NJOY-based benchmark.

IV. FUTURE IMPLEMENTATION IN SERPENT

Serpent is a three-dimensional continuous-energy Monte Carlo neutron transport code, specifically developed for reactor physics calculations.[b] The code uses multitemperature ACE format cross-section libraries that can be Doppler-broadened to an arbitrary temperature using a built-in preprocessor routine.[13,14] This approach is considered sufficient for most of the present applications, typically related to group constant generation, burnup calculation, and research reactor modeling, in which the number of material temperatures is usually very limited. The main reason for this study was to develop a method that could extend the temperature treatment to an arbitrary number of temperatures, which is a requirement encountered in coupled neutronics/thermal hydraulics calculations and other multiphysics applications.

The theoretical basis and demonstration discussed in this paper show the viability of the new method, but the practical implementation still requires much work. In addition to the transport routine, the on-the-fly sampling of cross sections must be compatible with the methods used for calculating various reaction rate tallies, needed for group constant generation and burnup calculation. We are currently investigating the best practices for implementing these routines in the Serpent code. This, and the performance of the new method, remain topics for future studies.

V. SUMMARY AND CONCLUSIONS

A new stochastic method for performing Doppler broadening on the fly in a Monte Carlo transport simulation is introduced. The method is based on explicit treatment of target motion at collision sites. A collision point candidate x is first sampled using a majorant cross section, the relative velocity of the collision nuclide to the incident neutron is sampled from a Maxwellian-based distribution, and finally, the collision point is accepted or rejected according to the 0 K cross section corresponding to the relative velocity. In case of a rejection the procedure restarts by sampling of a new path length starting from x.

The method is verified with a test program, which compares results of the stochastic algorithm to analytical reference results based on effective NJOY cross sections. The results of the algorithm are in good agreement with the reference. The minor differences between the results are recognized to originate from the finite accuracy of the reconstructed cross sections, not the method itself.

Sampling efficiency of the method varied substantially with neutron energy, but the average efficiency was a rather promising 41%. Nevertheless, no conclusions can be drawn on the practical efficiency or even feasibility of the method in a Monte Carlo transport routine before a thorough implementation in a transport code.

There are at least two significant advantages in the new method. First of all, as a common feature to all on-the-fly Doppler-broadening techniques including Ref. 2, merely 0 K cross-section libraries are required regardless of the number of different temperatures appearing in a problem geometry. Consequently, the processing and storage of cross-section libraries is reduced to one temperature. More importantly, only 0 K cross sections need to be stored in the computer memory during transport calculation, significantly decreasing the memory demand of multitemperature transport problems.

The second advantageous property is unique for the explicit temperature treatment method: It provides for accurate modeling of continuous temperature distributions. This property can be taken advantage of, for instance, in the verification of current methods used in the determination of effective fuel temperatures. The importance of accurate temperature modeling is also emphasized in coupled neutronics/thermal hydraulics and neutronics/fuel behavior calculations that are increasingly important applications for Monte Carlo reactor physics codes.

ACKNOWLEDGMENTS

This work was funded from the KÄÄRME project under the Finnish Research Programme on Nuclear Power Plant Safety SAFIR2014.

REFERENCES

1. T. H. TRUMBULL, "Treatment of Nuclear Data for Transport Problems Containing Detailed Temperature Distributions," *Nucl. Technology*, **156**, 75 (2006).

[b] A complete and up-to-date description of the Serpent code is found at the project Web site: http://montecarlo.vtt.fi (current as of June 6, 2011).

2. G. YESILYURT, W. R. MARTIN, and F. B. BROWN, "On-the-Fly Doppler Broadening for Monte Carlo Codes," *Proc. M&C 2009*, Saratoga Springs, New York, May 3–7, 2009.

3. B. BECKER et al., "An Alternative Stochastic Doppler Broadening Algorithm," *Proc. M&C 2009*, Saratoga Springs, New York, May 3–7, 2009.

4. I. LUX and L. KOBLINGER, *Monte Carlo Particle Transport Methods: Neutron and Photon Calculations*, CRC Press (1991).

5. E. R. WOODCOCK et al., "Techniques Used in the GEM Code for Monte Carlo Neutronics Calculations in Reactors and Other Systems of Complex Geometry," ANL-7050, Argonne National Laboratory (1965).

6. D. E. CULLEN and C. R. WEISBIN, "Exact Doppler Broadening of Tabulated Cross Sections," *Nucl. Sci. Eng.*, **60**, 199 (1976).

7. D. E. CULLEN, "Program SIGMA1 (version 79-1): Doppler Broaden Evaluated Cross Sections in the Evaluated Nuclear Data File/Version B (ENDF/B) Format," UCRL-50400 Part B, Lawrence Livermore National Laboratory (1979).

8. B. BECKER, R. DAGAN, and G. LOHNERT, "Proof and Implementation of the Stochastic Formula for Ideal Gas, Energy Dependent Scattering Kernel," *Ann. Nucl. Energy*, **36**, 470 (2009).

9. E. P. WIGNER and J. E. WILKINS, Jr., "Effect of the Temperature of the Moderator on the Velocity Distribution of Neutrons with Numerical Calculations with H as Moderator," AECD-2275, Clinton Laboratory (1944).

10. A. W. SOLBRIG, Jr., "Doppler Effect in Neutron Absorption Resonances," *Am. J. Phys.*, **29**, 257 (1961).

11. MCNP X-5 MONTE CARLO TEAM, "MCNP—A General Monte Carlo N-Particle Transport Code," Version 5, LA-UR-03-1987, Los Alamos National Laboratory (2003).

12. R. E. MacFARLANE and D. W. MUIR, "NJOY99.0 Code System for Producing Pointwise and Multigroup Neutron and Photon Cross Sections from ENDF/B Data," PSR-480, Los Alamos National Laboratory (2000).

13. T. VIITANEN, "Implementing a Doppler-Preprocessor of Cross Section Libraries in Reactor Physics Code Serpent," M.Sc. Thesis, Helsinki University of Technology (2009).

14. J. LEPPÄNEN and T. VIITANEN, "New Data Processing Features in the Serpent Monte Carlo Code," *J. Korean Phys. Soc.*, **59**, 1365 (2011).

PUBLICATION II

Explicit temperature treatment in Monte Carlo neutron tracking routines – first results

In proc. PHYSOR-2012, Knoxville, TN, Apr. 15–20 2012.

PHYSOR 2012 Advances in Reactor Physics Linking Research, Industry, and Education
Knoxville, Tennessee, USA, April 15-20, 2012, on CD-ROM, American Nuclear Society, LaGrange Park, IL (2012)

EXPLICIT TEMPERATURE TREATMENT IN MONTE CARLO NEUTRON TRACKING ROUTINES — FIRST RESULTS

Viitanen Tuomas and Leppänen Jaakko
VTT Technical Research Centre of Finland
P.O. Box 1000, FI-02044 VTT, Finland
tuomas.viitanen@vtt.fi; jaakko.leppanen@vtt.fi

ABSTRACT

This article discusses the preliminary implementation of the new explicit temperature treatment method to the development version Monte Carlo reactor physics code Serpent 2 and presents the first practical results calculated using the method. The explicit temperature treatment method, as introduced in [1], is a stochastic method for taking the effect of thermal motion into account on-the-fly in a Monte Carlo neutron transport calculation. The method is based on explicit treatment of the motion of target nuclei at collision sites and requires cross sections at 0 K temperature only, regardless of the number of temperatures in the problem geometry. The method includes a novel capability of modelling continuous temperature distributions.

Test calculations are performed for two test cases, a PWR pin-cell and a HTGR system. The resulting k_{eff} and flux spectra are compared to a reference solution calculated using Serpent 1.1.16 with Doppler-broadening rejection correction [2]. The results are in very good agreement with the reference and also the increase in calculation time due to the new method is on acceptable level although not fully insignificant. On the basis of the current study, the explicit treatment method can be considered feasible for practical calculations.

Key Words: Monte Carlo, tracking routine, rejection, on-the-fly, Doppler-broadening

1. INTRODUCTION

The traditional approach to temperature modelling in Monte Carlo neutron tracking routines is based on pre-generated, Doppler-broadened cross sections. Each material zone is associated with a temperature to which the cross section libraries are prepared beforehand using cross section processing codes such as NJOY [3] or pre-processing techniques [4,5]. In case the user of a reactor physics code wants to increase the amount of detail in the temperature modelling, the geometry has to be split into smaller homogeneous zones, each assigned with a different set of cross sections that need to be stored in the computer memory. If the number of different temperatures or the number of nuclei appearing in the problem is large, the memory usage may become a practical limitation. The importance of detailed temperature modelling is emphasized in multiphysics calculations.

Different means of avoiding this memory limitation have been studied recently. Trumbull et al. studied a method in which cross sections at arbitrary temperatures are obtained by interpolating between tabulated values [6]. However, to reach high accuracy, this method requires a narrow spacing between the different temperatures. Yesilyurt et al. have developed an efficient on-the-fly Doppler-broadening method that is based on the multi-level Adler-Adler resonance representation [7]. This method is able to reach high accuracy in practically no extra calculation time, but requires the resonances to be presented using the Adler-Adler formalism.

This study deals with a new approach to the problem, introduced in [1]. This temperature treatment method is an on-the-fly tracking technique, which takes the thermal motion of target nuclei into account explicitly by making a coordinate transform to target-at-rest frame at each collision site. The fact that the total cross section becomes a distributed quantity is handled using rejection sampling techniques.

The new method is able to model arbitrary temperatures with only 0 K continuous-energy cross sections available. As a novel feature, the explicit treatment method removes the homogeneity requirement for cross section temperatures, consequently providing for rigorous modelling of continuous temperature distributions. Because of the way the target velocities are sampled and collision point candidates accepted, the target velocities at accepted collision sites can be re-utilized as such in the free gas thermal treatment for thermal scattering. The secondary particle distributions become automatically the same as if calculated using the free gas treatment with Doppler-broadening rejection correction (DBRC) [2].

Currently, the method is not compatible with the thermal scattering laws, which significantly limits its applicability to realistic reactor calculations. Also the usage of the method with the unresolved region probability table treatment is not yet discussed. In addition, the method is only applied in homogeneous temperature zones despite the capability to model continuous temperature distributions.

The current study discusses the preliminary implementation of the method to the development version of the Monte Carlo reactor physics code Serpent 2 [8] and presents the very first results calculated using the method. The explicit treatment method is shortly introduced in Section 2 and details of the first implementation are discussed in Section 3. The pin-cell and HTGR test cases together with simulation results are presented in Section 4 and the last Section 5 is left for conclusions.

2. EXPLICIT TREATMENT METHOD

In a nutshell, the explicit treatment method is based on sampling the neutron path lengths from a majorant cross section in which the effect of thermal motion on the variation of total cross section is taken into account (i.e. majorant at E equals the largest possible value assigned for the total cross section within the range of thermal motion around E). At each collision site the target nuclide is first sampled according to the nuclide-wise majorants. After this, the velocity of the target nuclide is sampled and the relative velocity of the incident neutron to the target nuclide is calculated. Finally, the collision point is rejected or accepted according to the nuclide-wise 0 K total cross section corresponding to the relative velocity. In the case of an accepted collision the procedure continues by reaction sampling using 0 K cross sections of the partial reactions.

This section introduces the methodology of the explicit treatment method as-is. A more detailed description with more thorough discussion can be found in Reference [1].

2.1. Calculating the majorant

The majorant used in the sampling of the path lengths must satisfy

$$\Sigma_{\mathrm{maj}}(E) > \sum_n g_n(E)\Sigma^0_{\mathrm{tot},n}(E', x) \qquad \forall E' \,, \tag{1}$$

where E is the energy of the incident neutron, Σ_{maj} is the majorant cross section of a material zone, $\Sigma^0_{\mathrm{tot},n}$ is the 0 K total cross section of nuclide n and E' is the energy corresponding to the relative velocity of the incident neutron to the target. The temperature-initiated increase in potential scattering cross section is taken into account using the correction factor

$$g_n(E,T) = \left(1 + \frac{1}{2\lambda_n(T)^2 E}\right) \mathrm{erf}\Big(\lambda_n(T)\sqrt{E}\Big) - \frac{e^{-\lambda_n(T)^2 E}}{\sqrt{\pi}\lambda_n(T)\sqrt{E}} \tag{2}$$

$$\lambda_n(T) = \sqrt{\frac{A_n}{kT}} \,, \tag{3}$$

where A_n is the weight ratio of nuclide n to the neutron mass M, k is the Boltzmann constant and T is the temperature of the material [9]. Since E' is a variable depending on the velocities of the neutron and target, its range of variation must be taken into account when calculating the majorant cross section.

The variation of E' depends strongly on the mass of the nuclide and, therefore, it is necessary to calculate the majorants for each nuclide separately. The nuclide-wise majorants $\Sigma^0_{\mathrm{tot},n}$ are formed in a similar manner as $\sigma_{\mathrm{s}}^{\max}(v_\xi, 0)$ in Reference [2]. Basically, the majorant for nuclide n satisfies

$$\Sigma_{\mathrm{maj},n}(E) = g_n(E) \max_{E_\xi \in [(\sqrt{E}-4/\lambda_n(T))^2, (\sqrt{E}+4/\lambda_n(T))^2)} \Sigma^0_{\mathrm{tot},n}(E_\xi) \tag{4}$$

for each incident neutron energy E. In case the temperature inside material zone is non-uniform, T in (4) must be chosen as the maximum temperature $T_{\max}$ within the material region.

The procedure in (4) involves an assumption that the kinetic energies of target nuclei remain smaller than $16/\lambda_i(T)^2$. If nuclide velocities are assumed to obey the Maxwell-Boltzmann (MB) distribution, this assumption omits about a proportion of $5 \cdot 10^{-7}$ of the most energetic nuclei. Consequently, the inequality in (1) does not necessarily apply for all E'. This cut-off condition was first introduced in the NJOY SIGMA1 module [10].

After the nuclide-wise majorants have been calculated using (4), the material majorant is obtained simply as the sum of the nuclide-wise majorants

$$\Sigma_{\mathrm{maj}}(E) = \sum_n \Sigma_{\mathrm{maj},n}(E) \,. \tag{5}$$

2.2. Sampling the target nuclide and velocity

Since the velocity of the target nuclide depends on its mass, the target nuclide has to be sampled at each collision site before the velocity sampling is possible. Target nuclide n is sampled with

probability

$$P_n = \frac{\Sigma_{\mathrm{maj},n}(E)}{\Sigma_{\mathrm{maj}}(E)} \,. \tag{6}$$

After this the target velocity V_t and cosine between the directions of the incident neutron and target μ are sampled from distribution

$$f(V_\mathrm{t}, \mu) = \frac{v'}{2v} f_\mathrm{MB}(V_\mathrm{t}) \,, \tag{7}$$

where v is the velocity of the neutron,

$$v' = \sqrt{v^2 + V_\mathrm{t}^2 - 2vV_\mathrm{t}\mu} \tag{8}$$

is the relative velocity of the neutron to the target nuclide and f_MB is the Maxwell-Boltzmann distribution

$$f_\mathrm{MB}(V_\mathrm{t}) = \frac{4}{\sqrt{\pi}} \gamma^3 V_\mathrm{t}^2 e^{-\gamma^2 V_\mathrm{t}^2} \tag{9}$$

$$\gamma(T, A_n) = \sqrt{\frac{A_n M}{2kT}} \,. \tag{10}$$

Distribution 7 is the same as that used in the free gas thermal treatment of MCNP and consequently also the sampling procedure is the same as described in [9].

It should be noted that here temperature T is the local temperature at the collision site x, i.e. $T(x)$.

2.3. Rejection and reaction sampling

The procedure continues with rejection sampling in which the 0 K total cross section corresponding to the sampled relative energy $E' \sim v'$ is compared to the nuclide-wise majorant. Again, the low-energy effects must be taken into account with the $g_n(E)$-factor for the 0 K cross section. The collision point is accepted with probability

$$P_\mathrm{acc} = \frac{g_n\Big(E, T(x), A_n\Big)\Sigma^0_{\mathrm{tot},n}(E', x)}{\Sigma_{\mathrm{maj},n}(E)} \,. \tag{11}$$

In the case of a rejection the procedure restarts from beginning by sampling of a new path length starting from the previous collision point candidate x.

If the collision point is accepted, the rejection sampling is followed by reaction sampling that is done in the target-at-rest frame using only the 0 K cross sections. Hence, the probability for reaction i is simply

$$P_i = \frac{g_n\Big(E, T(x)\Big)\Sigma^0_{i,n}(E', x)}{g_n\Big(E, T(x)\Big)\Sigma^0_{\mathrm{tot},n}(E', x)} = \frac{\Sigma^0_{i,n}(E', x)}{\Sigma^0_{\mathrm{tot},n}(E', x)} \,. \tag{12}$$

3. PRELIMINARY IMPLEMENTATION IN SERPENT

There are several ways in which the new method can be implemented in the Monte Carlo tracking routine, but the main requirements are that each nuclide is assigned with a majorant cross section (4), that accounts for the variation in the interaction probability due to thermal motion, and that the sampling of neutron path lengths is based on macroscopic cross sections (5), calculated by summing over these majorants for each material. The rejection sampling additionally requires microscopic 0 K cross sections, adjusted by the correction factor (2) at low energies.

While still studying the feasibility and the best practices for implementing the methodology in the Serpent code, it was decided to take a somewhat simplistic multi-group approach to the problem. The energy spectrum is divided into a number of discrete groups with equal lethargy width. Each nuclide total cross section is assigned with a multi-group majorant, defined by taking the maximum point-wise value within the group boundaries that are extended with the effect of thermal motion as in (4) (see Figure 3 below). Macroscopic material-wise totals are pre-calculated using the same multi-group structure, by summing over the constituent nuclei.

The tracking routine proceeds in the usual way, using the multi-group material totals for sampling path lengths, with additional rejection sampling performed with the probability given by the ratio of point-wise and multi-group total cross sections of the collided nuclide. The method works with and without the explicit temperature treatment. The only difference is that when the method is used, the thermal motion is taken into account in the calculation of the multi-group majorants and in the rejection sampling once the target nuclide is selected. The multi-group approach simplifies and speeds up the calculation of the majorant cross sections. It also enables the use of pre-calculated majorant data without significantly increasing the memory demand.* The majorant data is generated for each problem separately at runtime. In the present implementation a high number of 40000 energy groups was used for fast calculation. The number can be easily reduced in case memory consumption becomes a problem. The routine can also be implemented without any pre-calculated cross sections, but performing the same calculations during the tracking routine considerably increases the overall running time, especially if the number of nuclei is large.

The following step-by-step example illustrates the rejection sampling procedure when conventional surface-tracking is used for transporting the neutron to the next collision point. Assume that the neutron crosses the boundary surface of a UO_2 fuel pin in 900 K temperature and enters the material with 1 eV energy. The cross sections in the thermal energy range are plotted in Figure 3. The algorithm proceeds as follows:

1. The distance to the next collision site inside the material is sampled using the macroscopic total cross section of the medium. In this case, the value used is the multi-group total, at about 0.54 1/cm (black curve in Figure 3a).
2. Assuming that the sampled path length is shorter than the distance to the material boundary, the neutron is moved to the collision site. The target nuclide is selected, with probabilities given by the ratios of the corresponding multi-group totals. In this case, the probabilities of colliding with U-235, U-238 and O-16 are 27%, 40% and 33%, respectively.

*Memory usage per material region becomes important in large burnup calculation problems, involving thousands of depletion zones. Minimizing the memory demand is essential for extending the burnup calculation capabilities of the Serpent code from 2D lattice physics to 3D core-level calculations, which is one of the goals set for the development of Serpent 2.

3. Assume that the sample results in a collision with U-235. The relative velocity between the neutron and the target nuclide is sampled from distribution (7) with $T = 900$ K and $A_n = 235.04$. Coordinate transformation to target-at-rest frame essentially results in a new energy, at which the cross sections are evaluated from here on.
4. Rejection sampling is performed by correcting the zero-kelvin total cross section with the factor $g(1.0 \text{ eV}, 900 \text{ K}) = 1.0002$ (2) and comparing the result with the nuclide-wise multi-group majorant (black solid and dashed curves in Figure 3b). Assuming that the coordinate transformation results in a temperature-corrected energy of 1.1 eV, the probability of accepting the collision point is about 88%.
5. If the collision is rejected, the procedure restarts from step 1. If the collision is accepted, the reaction mode is sampled, with probabilities given by the ratios of the zero-kelvin microscopic cross sections. In this case the probabilities of fission, capture and elastic scattering are 17%, 74% and 9%, respectively.

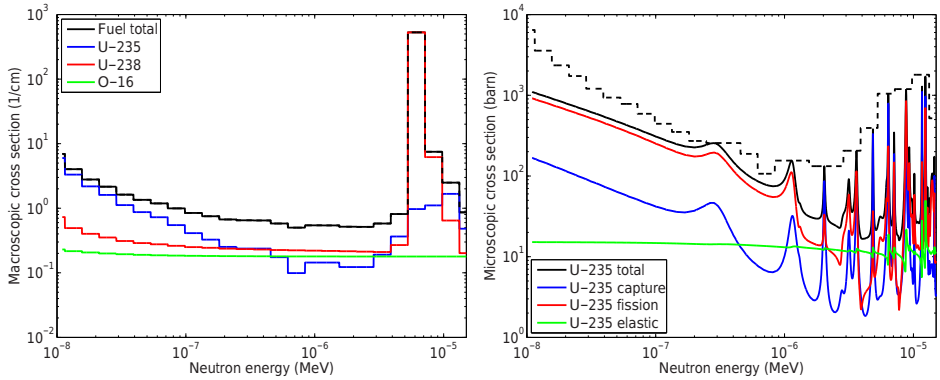

Figure 1. Left(a): Macroscopic multi-group cross sections used for sampling the target nuclide after collision in fuel. Right(b): Microscopic cross sections used for rejection sampling and selecting the reaction mode. The number of energy groups has been significantly reduced in this example for the sake of clarity.

As it was previously mentioned, the sampled target velocities can be used also in the calculation of the collision kinetics in case an elastic scattering occurs. It is, therefore, reasonable to take the target motion into account in elastic scatterings throughout the whole energy spectrum even though the free gas treatment is usually limited to energies lower than a cut-off value [8,9].

To get results consistent with NJOY-broadened effective cross sections and to save some calculation time, the velocity of the target nuclide is set to zero for threshold reactions, above the boundary of unresolved resonance region and at energies > 1 MeV [3]. The calculation of the low energy correction factor (2) was also slightly optimized in the implementation. Its value is approximated with 1 if $\lambda\sqrt{E} > 22$ and with

$$g_n(E) = 1 + \frac{1}{2\lambda_n^2 E} \tag{13}$$

if $\lambda\sqrt{E} > 2.57$. Otherwise, the factor is calculated the hard way, i.e. using Equation (2). The relative errors of these approximations remain smaller than 0.001. Quite similar approximations have been used also in MCNP5-1.40 [9].

Although the explicit temperature treatment offers a rigorous approach to the neutron transport problem using only zero-kelvin cross sections, it results in certain limitations regarding the Monte Carlo method and the procedures used in the Serpent code. The most significant methodological limitation is related to the use of the track-length estimate of neutron flux in the calculation of reaction rates, which is based on the assumption that cross sections remain constant over the sampled path length. This is not the case when the relative neutron energy becomes a statistically distributed quantity. To overcome the problem, flux integrals must be calculated using the collision estimator, which uses cross sections only at discrete collision points. Other limitations, related to Serpent-specific methods, are discussed with the example cases in Section 4.

4. TEST CASES AND RESULTS

The Serpent code is optimized for performance in lattice physics applications, and one of the methods used for speeding up the tracking routine and the calculation of macroscopic reaction rates for homogenization is the use of pre-calculated material-wise total cross sections (total, total absorption, total fission, etc.). These cross sections cannot be used with the explicit temperature treatment routine, which immediately reduces the performance when the code is used for group constant generation. In order to present a fair estimate for the overhead caused by the new routine, the performance comparisons should be carried out to calculations without similar optimization. The methodology is validated by comparing analog k_{eff} estimators and flux integrals, which doesn't require additional access to cross sections.

The validity of the method was tested by examining two thermal systems: a PWR pin-cell and a HTGR system consisting of 6 compacts around a coolant channel. The systems are modelled using Serpent 2 with the explicit temperature treatment method and the results are compared to a reference calculated with Serpent 1.1.16 [8]. Both of the cases were modelled without the probability table treatment for unresolved resonances and without thermal scattering libraries. Additionally, the Doppler-Broadening Rejection Correction method was used for $^{238}\mathrm{U}$ while generating the reference results.

The test calculations with the explicit treatment method were performed using a high-resolution JEFF-3.1.1 -based cross section data at 0 K, reconstructed using 0.001 tolerance for nuclei other than $^{238}\mathrm{U}$ for which a tolerance of 0.003 was used [†]. The reference results were calculated with JEFF-3.1.1 -based libraries with 0.001 reconstruction tolerance used for all nuclei. The same 0 K library with 0.001 / 0.003 reconstruction tolerances was also used together with DBRC in the reference calculations.

Performance measures for the test calculations are performed separately in subsection 4.3.

[†]For an unknown reason, NJOY 99.336 was not able to process $^{238}\mathrm{U}$ in 0 K temperature to reconstruction tolerances smaller than 0.003.

4.1. PWR pin-cell

The first of the test cases involves an ordinary PWR pin-cell in a square lattice. The linear power of the rod was assumed to be 254 W/cm and the corresponding temperature distribution was calculated with the VTT-modified version of the fuel performance code ENIGMA [11,12]. The fuel temperature is modelled by approximating the realistic continuous temperature profile with a 5-step profile.

Temperatures of the fuel zones were adjusted to the exact values using the Doppler-preprocessor of Serpent [5]. The fuel rod properties are listed in Table I and the step function for fuel temperature is defined in Table II. Altogether 250 million active neutron histories were calculated in 5000+20 cycles.

Table I. Properties for the PWR pin-cell test case.

Fuel radius	0.41443 cm	Cladding thickness	0.06365 cm
Fuel enrichment	3.48 w-% ^{235}U	Cladding material	Zr with 1 w-% Nb
Fuel centerline T	1329 K	Cladding T	579 K
Fuel surface T	738 K	Water density	0.7207 g/cm^3
Gas gap	0.00727 cm	Water temperature	579 K
Lattice pitch	1.295 cm		

Table II. Temperature distribution used in the modelling of the fuel in the pin-cell.

Zone	Outer radius	Temperature
1	0.16586 cm	1275 K
2	0.27638 cm	1129 K
3	0.33162 cm	983 K
4	0.38684 cm	865 K
5	0.41443 cm	772 K

The calculated flux spectrum of the pin-cell case is plotted and compared to reference in Figure 2. To put the accuracy of the method into perspective, the same comparison was performed against a Serpent 1.1.16 spectrum calculated without the DBRC. The analog estimate for k_{eff} was 1.34669 ± 0.00008 when calculated with the explicit treatment method and 1.34644 ± 0.00008 in the reference case. This corresponds to a reactivity difference of about 13 ± 9 pcm, which is of the same magnitude as the statistical deviation.

4.2. HTGR

The second test case is based on a High Temperature Gas Cooled Reactor (HTGR) benchmark [13]. The calculations were performed for fresh prismatic fuel for which the input file

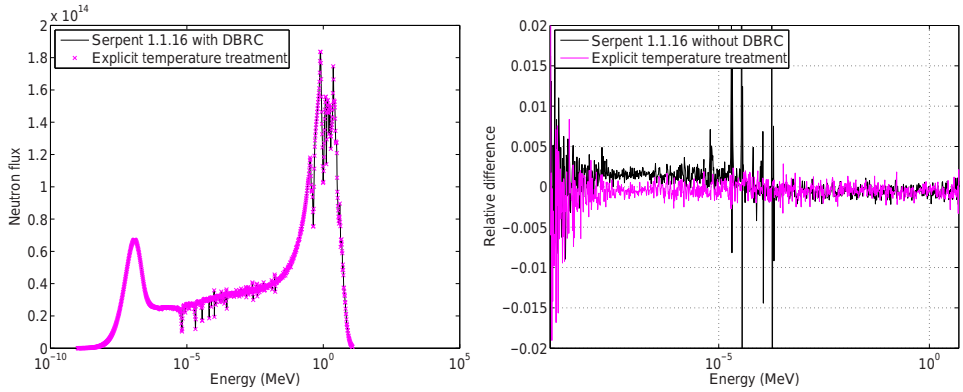

Figure 2. Left: Flux spectrum of the pin-cell case. Right: Differences in the flux spectra compared to Serpent 1.1.16 with DBRC.

is available at the Serpent website [8]. In this example case the lattice is modelled with 6 compacts in a graphite matrix surrounding a coolant channel full of helium. The lattice is extended to infinity using periodic boundary conditions. The material temperatures in the input were modified such that fuel in the fuel particles is in 1800 K temperature, all other solid materials are in 1200 K temperature and helium is in 900 K temperature.

While calculating the reference results, it was noticed that the 400 kT free gas treatment (FGT) threshold of Serpent, as adopted from MCNP [9], is too low for this test case and consequently causes significant bias in the results compared to the explicit treatment method in which the target motion is taken into account throughout the whole energy spectrum. Consequently, Serpent 1.1.16 was modified such that FGT was extended to all energies and this modified version was used to calculate the reference results. The HTGR simulations were carried out using 100 million active neutron histories in 5000+10 cycles.

The flux spectrum and differences in the spectra are plotted in Figure 3. Analog k_{eff} estimate for the HTGR case was 1.28296 ± 0.00010 in the reference calculation and 1.28266 ± 0.00010 when calculated with the explicit treatment method. The reactivity difference is, thus, about 18 ± 15 pcm which cannot be distinguished from the statistical deviation in practice.

4.3. Performance

To evaluate the feasibility of the method in practical calculations, it is worthwhile to compare the calculation times of the reference cases to those of the explicit treatment method. As it was mentioned earlier, the comparison between the explicit method and reference is fair when the optimization in Serpent is somewhat reduced. The righteous level of optimization is obtained when utilizing the optimization mode 2 in Serpent 2 [14]. However, to put the results into perspective, the running times are provided also for the reference cases calculated in Sections 4.1 and 4.2.

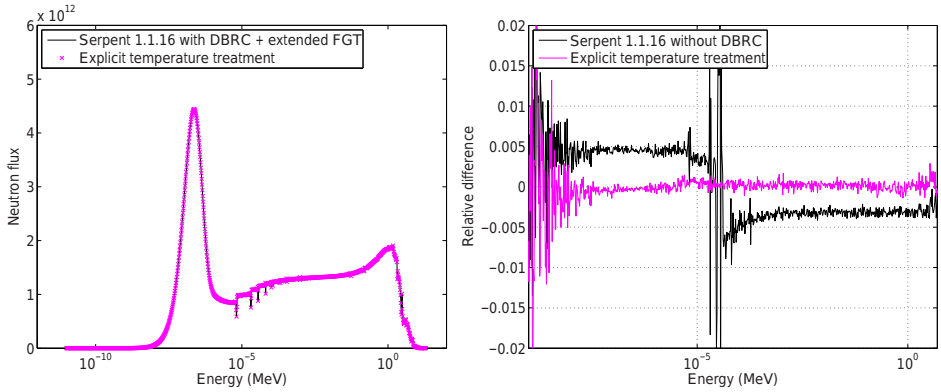

Figure 3. Left: Flux spectrum of the pin-cell HTGR case. Right: Differences in the flux spectra compared to Serpent 1.1.16 with DBRC and extended Free Gas Treatment.

The pin-cell cases were calculated using 250 million neutrons and the HTGR cases using 100 million neutrons. The calculation times presented in Table III are total CPU times in minutes. All the calculations were calculated using one 2.4 GHz Intel Core i5 CPU.

Table III. Total CPU times of the simulations.

Pin-cell			HTGR		
Case	Time	Ratio	Case	Time	Ratio
Serpent 2, explicit	1585.4	2.28	Serpent 2, explicit	3497.0	4.20
Serpent 2, optimiz. mode 2	696.3	1.00	Serpent 2, optimiz. mode 2	830.9	1.00
Serpent 1.1.16+DBRC	463.0	0.66	Serpent 1.1.16+DBRC+FGT	911.7	1.10
Serpent 1.1.16	425.9	0.61	Serpent 1.1.16	845.6	1.02

5. CONCLUSIONS

The present paper discusses the implementation of the explicit temperature treatment method, introduced in [1], to Monte Carlo Reactor Physics code Serpent. Also first results calculated with the method are presented in this paper. The method provides for modelling of arbitrary temperatures in neutron transport routines with only 0 K continuous-energy cross sections available. The explicit treatment method also provides inherently correct velocities for target nuclei that can be utilized when solving the kinetics of scattering events.

Results for two test cases, a PWR pin-cell and a HTGR system, are presented in Section 4. The results calculated with the explicit method are in very good agreement with the reference.

Differences in the multiplication factors are lost in statistical deviation in both of the test cases.

In the PWR pin-cell case the differences in neutron flux remain smaller than 0.003 throughout the whole energy spectrum excluding the very low energies with poor statistics (Figure 2). Since the Doppler-preprocessor of Serpent was used to adjust the cross section temperatures in the reference case, the expected amount of error in the cross section reconstruction is higher than that of the basis library (0.001). This, together with the fact that the 0 K cross section of $^{238}\mathrm{U}$ is reconstructed to 0.003 tolerance, explains the deviances observed in the flux spectra.

The slightly smaller differences seen in the HTGR spectra (Figure 3) support the previous conclusion. In this case the reference was calculated using unmodified NJOY cross sections for which the reconstruction tolerance is known to be exactly 0.001. In this case the differences in flux spectra are smaller than 0.002 if the high and low energy regions with low statistics are ignored. Especially in the HTGR case the importance of DBRC is easy to notice: the resonance absorption would be clearly underestimated if DBRC was not used in the calculation of reference results.

The efficiency of the explicit treatment method depends strongly on the rejection sampling efficiency in Equation (11). This, in turn, depends on the material maximum temperature used in the generation of the majorant. The higher the temperature, the larger the majorant cross section and, consequently, the higher the proportion of rejected collision points.

This can be also observed in the performance measures presented in Table III. In the pin-cell case, where the temperatures ranged from about 550 K to 1300 K the calculation took 2.3 times more time than Serpent 2 with optimization mode 2. In the HTGR case, where the fuel was in 1800 K and other solid materials in 1200 K temperature, the calculation time ratio was significantly higher 4.2. The performance of the method could be improved by optimizing the group structure of the majorant cross sections or by changing to continuous-energy majorants. The present implementation with 40000 equi-lethargy groups is most likely far from optimal.

As it was observed, the usage of the explicit treatment method slows down the transport calculation notably. However, the slow-down is of tolerable magnitude and the method can be considered well-feasible to practical calculations, at least what comes to its efficiency. More efficient implementation of the method requires future work, and so does the usage of flux and reaction rate estimators with continuously-varying temperature profiles that are needed to take full advantage of the method. The explicit treatment method should also be made compatible with the thermal scattering laws and unresolved region probability table treatment before it can be utilized on full scale. It should, however, be noted that it is possible to use the explicit thermal treatment for only part of the materials in the problem geometry. The problem thus exists only if thermal scattering laws or probability tables are required for the same materials for which the temperature treatment is used.

In summary, the explicit treatment proved accurate and fast enough for practical transport calculations. The method, however, requires more research to extend its capabilities to the thermal and unresolved resonance regions that are essential when simulating realistic reactors. Already now the method is a great tool for examining different temperature-related phenomena such as temperature-dependent scattering kernels.

ACKNOWLEDGEMENTS

This work was funded from the KÄÄRME project under the Finnish Research Programme on Nuclear Power Plant Safety SAFIR2014.

REFERENCES

[1] T. Viitanen and J. Leppänen, "Explicit Treatment of Thermal Motion in Continous-energy Monte Carlo Tracking Routines," *Nuc. Sci. Eng.*, in-press.

[2] B. Becker, R. Dagan and G. Lohnert, "Proof and implementation of the stochastic formula for ideal gas, energy dependent scattering kernel," *Ann. Nucl. Energy*, **36**, pp. 470–474 (2009).

[3] R. E. MacFarlane and D. W. Muir, "NJOY99.0 Code System for Producing Pointwise and Multigroup Neutron and Photon Cross Sections from ENDF/B Data," PSR-480, Los Alamos National Laboratory (2000).

[4] T. Mori, K. Okumura, Y. Nagaya and M. Nakagawa, "Application of continuous energy Monte Carlo code MVP to burn-up and whole core calculations using cross sections at arbitrary temperatures," *Proc. M&C'99*, Madrid, Spain, September 27–30, pp. 987–996, (1999).

[5] J. Leppänen and T. Viitanen, "New Data Processing Features in the Serpent Monte Carlo Code", *J. Korean Phys. Soc.*, **59**, 1365–1368 (2011).

[6] T. H. Trumbull, "Treatment of Nuclear Data for Transport Problems Containing Detailed Temperature Distributions," *Nucl. Technology*, **156**, 75–86 (2006).

[7] G. Yesilyurt, W. R. Martin and F. B. Brown, "On-the-fly Doppler Broadening for Monte Carlo Codes," *Proc. M&C 2009*, Saratoga Springs, New York, May 3–7 (2009).

[8] Serpent website, http://montecarlo.vtt.fi [referenced 27.10.2011]

[9] MCNP X-5 Monte Carlo Team, "MCNP — a General Monte Carlo N-Particle Transport Code," Version 5, LA-UR-03-1987, Los Alamos National Laboratory (2003).

[10] D. E. Cullen, "Program SIGMA1 (version 79-1): Doppler broaden evaluated cross sections in the evaluated nuclear data file/version B (ENDF/B) format," UCRL-50400 Part B., Lawrence Livermore National Laboratory (1979).

[11] V. Tulkki. "ENIGMA State of the Art Report.", VTT Research Report VTT-R-09938-10, Technical Research Centre of Finland VTT (2010).

[12] W. J. Kilgour, "The ENIGMA Fuel Performance Code, Users Guide, Version 5.8d", TD/NS/REP/0034, Berkeley Nuclear Laboratories (1992).

[13] M. D. DeHart and A. P. Ulses, "Benchmark Specification for HTGR Fuel Element depletion", NEA/NSC/DOC(2009)13, Nuclear Energy agency, Organization for Economic Cooperation and Development (2009).

[14] J. Leppänen and A. Isotalo, "Burnup Calculation Methodology in the Serpent 2 Monte Carlo Code", *Proc. PHYSOR 2012*, Knoxville, Tennessee, April 15–20 (2012).

PUBLICATION III

Optimizing the implementation of the target motion sampling temperature treatment technique – How fast can it get?

In proc. M&C 2013, Sun Valley, ID, May 5–9 2013.

International Conference on Mathematics and Computational Methods Applied to Nuclear Science & Engineering (M&C 2013)
Sun Valley, Idaho, USA, May 5-9, 2013, on CD-ROM, American Nuclear Society, LaGrange Park, IL (2013)

OPTIMIZING THE IMPLEMENTATION OF THE TARGET MOTION SAMPLING TEMPERATURE TREATMENT TECHNIQUE — HOW FAST CAN IT GET?

Viitanen Tuomas and Leppänen Jaakko
VTT Technical Research Centre of Finland
P.O. Box 1000, FI-02044 VTT, Finland
tuomas.viitanen@vtt.fi; jaakko.leppanen@vtt.fi

ABSTRACT

This article discusses the optimization of the target motion sampling (TMS) temperature treatment method, previously implemented in the Monte Carlo reactor physics code Serpent 2. The TMS method was introduced in [1] and first practical results were presented at the PHYSOR 2012 conference [2]. The method is a stochastic method for taking the effect of thermal motion into account on-the-fly in a Monte Carlo neutron transport calculation. It is based on sampling the target velocities at collision sites and then utilizing the 0 K cross sections at target-at-rest frame for reaction sampling. The fact that the total cross section becomes a distributed quantity is handled using rejection sampling techniques.

The original implementation of the TMS requires 2.0 times more CPU time in a PWR pin-cell case than a conventional Monte Carlo calculation relying on pre-broadened effective cross sections. In a HTGR case examined in this paper the overhead factor is as high as 3.6. By first changing from a multi-group to a continuous-energy implementation and then fine-tuning a parameter affecting the conservativity of the majorant cross section, it is possible to decrease the overhead factors to 1.4 and 2.3, respectively. Preliminary calculations are also made using a new and yet incomplete optimization method in which the temperature of the basis cross section is increased above 0 K. It seems that with the new approach it may be possible to decrease the factors even as low as 1.06 and 1.33, respectively, but its functionality has not yet been proven. Therefore, these performance measures should be considered preliminary.

Key Words: on-the-fly, Doppler, temperature, Monte Carlo, neutron tracking

1. INTRODUCTION

Recently, there has been a lot of interest in combining Monte Carlo reactor physics with thermal hydraulics or other multi-physics applications [3–6]. Multi-physics is also a major topic in the future development of Serpent*, involving developent of a universal multi-physics interface that will provide for information exchange with thermal hydraulics and fuel performance codes [7]. The long-term target is to develop Serpent into a competitive neutronics solver, capable of both steady-state and transient analyses including thermal-hydraulics feedback [8].

When examining the temperature dependence of system parameters, as is the case in multi-physics applications, it is often necessary to model the temperature distributions within a system in high detail. However, when using the conventional approach relying on pre-broadened effective cross sections, the cross section data must be stored in computer memory separately for each nuclide and temperature appearing in the problem geometry. The memory capacity becomes a major limitation if the number of different temperatures in the system is large.

*A complete and up-to-date description of the Serpent code is found at the project website: http://montecarlo.vtt.fi

As a solution to this issue, on-the-fly Doppler-broadening techniques have been developed, meaning that the effective cross sections are calculated as they are needed. The very efficient technique implemented in MCNP6 is based on calculating the temperature-dependent cross sections using series expansions with pre-calculated coefficients [9]. This paper is about another promising on-the-fly temperature treatment technique which, in fact, does not involve Doppler-broadening in the sense that effective cross sections are not calculated at any point of the transport calculation.

The target motion sampling temperature treatment method, discussed in this paper, was first introduced in [1] with the name "explicit treatment of thermal motion", and the first implementation and first practical results were presented at PHYSOR 2012 [2]. The method is based on taking the thermal motion of target nuclei into account explicitly at each collision site and dealing with the collisions in target-at-rest frame using cross sections at 0 K temperature. The fact that the total cross section becomes a distributed quantity is handled using rejection sampling techniques. As a novel feature the method provides for rigorous modelling of continuous temperature distributions within homogeneous material zones.

The preliminary multi-group implementation of the TMS method, for which results were presented in [2], resulted in a significant increase in calculation time when compared to traditional transport methods utilizing effective cross sections. In a PWR pin-cell case with realistic temperature distribution the calculation time increased by a factor of 2 and in a HTGR case, which was slightly different from the one examined in this paper, the overhead factor was 4.2. To make the method practical for everyday usage, some optimization is required.

This paper describes the optimization effort that has so far been put in the implementation of the target motion sampling method in Serpent. Results of the evolvement of the calculational overhead are also provided. The tracking scheme of the TMS method is shortly introduced in Section 2, the means of optimization covered in this paper are discussed in Section 3, performance results are provided in Section 4 and Section 5 is left for conclusions.

This paper only covers the efficiency of the method in the neutron transport calculation, basically CPU time required per transported neutron. The possible effect of the method on the variance of reaction rate estimators is left as a future topic.

2. TARGET MOTION SAMPLING METHOD FOR TEMPERATURE TREATMENT

Neutron tracking scheme of the TMS method is shortly introduced in the following on a step-by-step basis. More complete description of the scheme can be found in References [1] and [2]. Since the method only governs the way the neutrons are transported within material zones, discussion on the handling of material boundaries is omitted as irrelevant. In any case, the TMS method is compatible with all kinds of geometry routines, including the surface tracking and the Woodcock delta tracking methods.

1. The neutron transport begins from point x_i by sampling a path length l using a majorant cross section $\Sigma_{\mathrm{maj}}(E)$ at laboratory-frame energy of the neutron E. This is done by normal inversion sampling with equation

$$l = -\frac{1}{\Sigma_{\mathrm{maj}}} \ln(\xi)\,, \tag{1}$$

where ξ is a uniformly distributed random variable on unit interval.

2. At the new collision point candidate, $x_{i+1} = x_i + l$, collision nuclide is sampled based on nuclide-wise majorants such that probability of colliding with nuclide n is simply

$$P_n = \frac{\Sigma_{\mathrm{maj},n}(E)}{\Sigma_{\mathrm{maj}}(E)} = \frac{\Sigma_{\mathrm{maj},n}(E)}{\sum_n \Sigma_{\mathrm{maj},n}(E)} \,. \tag{2}$$

3. Velocity and direction of the target nuclide V_t μ are sampled from distribution

$$f(V_\mathrm{t}, \mu) = \frac{v'}{2v} f_{\mathrm{MB}}(V_\mathrm{t}) \,, \tag{3}$$

where v is the velocity of the neutron and μ is the cosine of the angle between the directions of the neutron and target,

$$v' = \sqrt{v^2 + V_\mathrm{t}^2 - 2vV_\mathrm{t}\mu} \tag{4}$$

is the relative velocity of the neutron to the target nuclide and f_{MB} is the Maxwell-Boltzmann (MB) distribution for target speed

$$f_{\mathrm{MB}}(V_\mathrm{t}) = \frac{4}{\sqrt{\pi}} \gamma^3 V_\mathrm{t}^2 e^{-\gamma^2 V_\mathrm{t}^2} \,, \tag{5}$$

where

$$\gamma(T, A_n) = \sqrt{\frac{A_n M}{2kT}} \,. \tag{6}$$

Target-at-rest-frame energy E' corresponding to the relative velocity calculated with Equation (4) is calculated and used from here on.

4. The collision is accepted or rejected according to rejection sampling criterion

$$\xi < \frac{g_n\Big(E, T(x_{i+1}), A_n\Big)\Sigma^0_{\mathrm{tot},n}(E')}{\Sigma_{\mathrm{maj},n}(E)} \,, \tag{7}$$

where $T(x_{i+1})$ is the local temperature at x_{i+1}, normalization factor g is obtained from equation[†]

$$g_n(E, T, A_n) = \left(1 + \frac{1}{2\lambda_n(T)^2 E}\right) \mathrm{erf}\Big(\lambda_n(T)\sqrt{E}\Big) + \frac{e^{-\lambda_n(T)^2 E}}{\sqrt{\pi}\lambda_n(T)\sqrt{E}} \,, \tag{8}$$

$$\lambda_n(T) = \sqrt{\frac{A_n}{kT}} \,, \tag{9}$$

and $\Sigma^0_{\mathrm{tot},n}$ is the total cross section of nuclide n at 0 Kelvin temperature. If the collision point is rejected, the procedure restarts from 1. with $i = i + 1$.

5. If the collision point is accepted, the procedure continues by reaction sampling using the relative energy E' and zero-Kelvin cross sections. Reaction r is sampled with probability

$$P_r = \frac{\Sigma^0_{r,n}(E')}{\Sigma^0_{\mathrm{tot},n}(E')} \tag{10}$$

and the transport proceeds according to the sampled reaction.

[†]The sign of the exponential term in this equation was erroneously negative in previous publications [1] and [2]. The authors apologize any inconvenience this may have caused.

The majorant cross section $\Sigma_{\mathrm{maj}}(E)$ is the maximum total cross section within the range of the target-at-rest energy E', which depends on the lab energy E and the thermal motion of the target nuclide. Since the MB distribution has an infinite tail, all possible nuclide velocities cannot be taken into account in the calculation of the majorant. As a quick and easy solution to this issue, a cut-off condition was adopted from the calculation of the Doppler-Broading Rejection Correction (DBRC) majorant [10]. This cut-off condition was first introduced in the SIGMA1 program [11] and is also used in the BROADR module of NJOY [12]. The majorant cross section is, thus, calculated according to equation

$$\Sigma_{\mathrm{maj},n}(E) = g(E, T_{\max}, A_n) \max_{E_\xi \in [(\sqrt{E}-\alpha)^2, (\sqrt{E}+\alpha)^2)} \Sigma^0_{\mathrm{tot},n}(E_\xi)\,, \tag{11}$$

where

$$\alpha = \frac{4}{\lambda_n(T_{\max})} \tag{12}$$

determines the proportion of nuclides that are omitted in the calculation of the majorant. It should be noted that in case a nuclide appears in the problem at different temperatures, the maximum of these temperatures $T_{\max}$ must be used in the calculation of the majorant to assure conservativity within the whole system.

A significant advantage of the TMS method is that the transport routine sees the temperature variable only through an arbitrary function $T(x)$, which can be continuous in both space and time.

3. DIFFERENT MEANS OF OPTIMIZATION

The performance of the TMS method is ultimately defined by the efficiency of the rejection sampling criterion (7). In this equation it can be seen that the probability of a successful sample depends on the ratio of the total 0 K cross section at target-at-rest energy E', multiplied by the g-factor that only depends on the L-energy of the neutron, to the majorant cross section. It should be noted that E' is a distributed quantity and, therefore, the true sampling efficiency for neutron energy E cannot be obtained directly from (7).

In practice the optimization of the TMS method is, thus, about decreasing the differences between the total cross section and the majorant cross section, which can be done in a few different ways. Two different means of decreasing the majorant are discussed in Sections 3.1–3.3. In addition, a new but not yet fully implemented optimization approach of increasing the temperature of the basis cross section above zero Kelvin is introduced in 3.4.

3.1. From Multi-group to Continous-energy Implementation

In the preliminary implementation the majorant cross section was constructed on a multi-group energy grid mainly because this way of implementation required the least changes in the source code. Since the multi-group energy grid is rather coarse, the majorant at an energy point corresponds to the maximum total cross section within quite a broad energy interval, thus making the majorant unnecessarily conservative.

Evidently, the efficiency of the majorant can be increased by adding grid points in its energy grid. The more grid points are used, the less conservative the majorant becomes. However, in practice there exists a limit after which adding new points does not anymore speed up the overall calculation. This is because after some point more CPU time will be lost in dealing with a very fine energy grid than what is saved due

to a less conservative majorant. Naturally, increasing the number of grid points also affects the memory requirement of the majorant cross sections.

As a comfortable compromise between efficiency and practicality, it was decided to generate the majorants on the unionized continuous-energy grid on which all of the cross sections are constructed in Serpent.

3.2. Energy Range Boundaries of the Majorant

Before proceeding to the next logical step of further decreasing the conservativity by manipulating parameter α, defined in Equation (12), it was noticed that the current "DBRC way" of choosing the energy boundaries for the majorant is not necessarily the best possible method for this purpose. The energy range boundaries, as determined by Equation (11), are basically the minimum and maximum target-at-rest energy corresponding to a collision with a target nuclide with velocity equal to the SIGMA1 cut-off condition. The condition, for its part, is based on the MB distribution such that the chosen value for the α parameter omits about a proportion of 5×10^{-7} of the most energetic nuclei.

However, the velocity distribution of a target nucleus interacting with a neutron with velocity v differs from the MB distribution by factor v'/v (see Equation (3)). This should also be taken into account in the generation of the majorant for the majorant to be optimal. Above thermal energies the deviance from the MB distribution is negligible, because the v'/v factor approaches unity, but at low energies with $v \sim V_\mathrm{t}$ the difference can be recognized. Particularly, the difference affects the high-energy tail of the distribution that specifies the energy boundaries of the majorant.

One way of choosing the energy range boundaries is to use the same confidence level $Q/2$ for each upper (E_max) and lower (E_min) majorant energy boundary associated with neutron L-frame energy E. In other words, a proportion of $Q/2$ of the least probable target velocities are omitted when determining both the upper and the lower boundary of the energy energy range in this approach.

The boundaries can be resolved from the velocity distribution of the target nuclide (3). The minimum target-at-rest energy is obtained for a parallel collision with $\mu = 1$ for which the unnormalized cumulative distribution is

$$
\begin{aligned}
f_1(x) \quad &= \int_x^\infty \frac{\sqrt{v^2 + V_\mathrm{t} - 2vV_\mathrm{t}}}{2v} f_\mathrm{MB}(V_\mathrm{t}) dV_\mathrm{t} \\
&= \begin{cases}
-\frac{1}{2\gamma\sqrt{\pi}v}\Big(-4e^{-\gamma^2 v^2} + \gamma\sqrt{\pi}v + e^{-\gamma^2 x^2}(2 + 2\gamma^2 x(x-v)) \\
\qquad\qquad - 2\gamma\sqrt{\pi}v\,\mathrm{erf}(\gamma v) + \gamma\sqrt{\pi}v\,\mathrm{erf}(\gamma x)\Big) & \text{if } \; v > x \\
\frac{1}{2}\Big(\frac{e^{-\gamma^2 x^2}(2 + 2\gamma^2 x(x-v))}{\gamma v\sqrt{\pi}} + \mathrm{erf}(\gamma x) - 1\Big) & \text{if } \; v \leq x
\end{cases}
\end{aligned}
$$

The corresponding distribution for the maximum energy resulting from a head-on collision with $\mu = -1$ is

$$f_{-1}(x) = \int_x^\infty \frac{\sqrt{v^2 + V_\mathrm{t} + 2vV_\mathrm{t}}}{2v} f_\mathrm{MB}(V_\mathrm{t}) dV_\mathrm{t} = \frac{e^{-\gamma^2 x^2}(1 + \gamma^2 x(v + x))}{\gamma v \sqrt{\pi}} + \frac{1}{2} \operatorname{erfc}(\gamma x) \,.$$

Using conditions

$$\frac{f(x)}{f(0)} = \frac{Q}{2} \tag{13}$$

it is possible to numerically resolve the boundaries x for the target velocity and, furthermore, the corresponding boundary energies E_min and E_max. Determining the boundaries this way increases the complexity and computational cost of the majorant generation compared to the much simpler DBRC method, but advantageously the majorant is based on the same distribution from which the target velocities are actually sampled, and a uniform and easily adjustable cut-off condition can be used throughout the energy spectrum. The advantages of these properties are emphasized in the next phase, described in Section 3.3, in which the conservativity of the majorant will be decreased by manipulating the Q parameter.

3.3. Energy Range Width of the Majorant

The proportion Q, as introduced in the previous section, is by definition the expected proportion of target-at-rest energy samples outside the energy region used in the generation of majorant cross sections for the two extreme cases of a head-on and a parallel collision. Hence, it also gives a very conservative upper limit for the proportion of unphysical or erroneous samples P_err at which the sampled total cross section exceeds the majorant. In practice $P_\mathrm{err} \ll Q$, because only a small fraction of all collisions are close to head-on or parallel collisions and, additionally, the total cross section at an "erroneously sampled" target-at-rest energy E' quite rarely exceeds the majorant cross section.

The Q parameter has a large effect on the efficiency of the majorant. The larger the Q parameter, the higher the sampling efficiency, but on the other hand the laws of physics are broken more often due to increasing P_err. Thus, the Q parameter should be given as high a value as possible such that the proportion of erroneous samples P_err still remains small enough not to, in practice, distract the solution of neutronics. Since playing with the Q parameter is basically cheating and too large values result in serious errors, the final value for the parameter should be chosen conservatively.

3.4. Increasing the Temperature of the Basis Library

The range of temperatures appearing in reactor conditions is not very wide. Usually, the smallest temperature appearing in reactor physical calculations is that of the coolant material, which is almost always larger than room temperature, about 300 K. On the other hand, the fuel temperature may reach a few thousand degrees, but in many cases the range of different fuel temperatures appearing in a system is quite narrow. Considering this, it is quite obvious that the current approach of using the basis cross sections at zero Kelvin and at each collision making the on-the-fly correction to temperatures above 300 K might

not be an optimal one. A much better idea would be to apply the on-the-fly Doppler-broadening to a cross section at the minimum temperature of a nuclide. For example, in PWR conditions this would spare about 700–800 K of on-the-fly Doppler-broadening "effort" (as seen through a lowered rejection sampling efficiency) at each collision in the fuel region.

In fact, increasing of the temperature of the basis library above zero Kelvin is quite straightforward with the TMS method. This is due to the fact that the well-known definition of the effective cross section [13]

$$\sigma_{\mathrm{eff}}(v) = \frac{1}{v} \int |\mathbf{v} - \mathbf{V}_{\mathrm{t}}| \sigma_0(|\mathbf{v} - \mathbf{V}_{\mathrm{t}}|) f_{MB}(\mathbf{V}_{\mathrm{t}}, T) \mathbf{d}\mathbf{V}_{\mathrm{t}} \tag{14}$$

on which also the TMS method is based, allows the increasing of the cross section temperature in two or more steps, i.e. the cross section temperature can first be risen from 0 K to T' and then from T' to T utilizing basically the same methodology. This can be shown using either Fourier transform techniques [13] or with straightforward calculation [14]. There is, however, one drawback in the splitting of the Doppler-broadening in two parts: the sampled target velocities can no longer be recycled in the solution of scattering kinetics, somewhat decreasing the elegance of the TMS method. The theoretical considerations behind this optimization approach are under examination and to be published in the near future.

A quick-and-dirty implementation purely for performance studying purposes was implemented in Serpent by making the following modifications:

1. Every nuclide appearing in the problem is associated with a minimum and maximum temperature such that $T_{\max} = T_{\min} + \Delta T$.
2. The cross sections of each nuclide are Doppler-broadened to $T_{\min}$ in the pre-processing phase using the Doppler-preprocessor of Serpent [15].
3. The majorant cross sections are calculated similar to Equation (11), but using effective cross sections at $T_{\min}$ instead of zero Kelvin and ΔT instead of $T_{\max}$ in the generation.
4. The tracking routine is modified such that the target velocities are sampled from a distribution corresponding to temperature $T - T_{\min}$ instead of T.

The solving of scattering kinetics is based on the standard free gas treatment without Doppler-Broadening Rejection Correction in this very first implementation. For this reason, the results are not even expected to match perfectly with the benchmark.

4. EFFECTS ON PERFORMANCE

The performance of the TMS method with different levels of optimization is measured with the following key parameters:

- REA_SAMPLING_EFF, a standard output parameter of Serpent 2 that describes the proportion of accepted reactions, i.e. the average rejection sampling efficiency of (7). Denoted with η_{rea} in the following.

- The measure t_{rel}, defined as the ratio of the transport cycle calculation time to that of a Serpent 2 calculation and NJOY-broadened effective cross sections, free gas thermal treatment at all energies and Doppler-Broadening Rejection Correction used between 0.4 eV and 210 eV for $^{238}\mathrm{U}$.

- Proportion of erroneous samples, P_{err}, for which the majorant is exceeded at least by a factor of 1E-3, i.e. $\Sigma^0(E') > 1.001\ \Sigma_{\mathrm{maj}}(E)$.

Results are provided for two test cases: a PWR pin cell and a HTGR system. The PWR pin cell test case is identical to that used in the PHYSOR2012 paper [2]. The temperature of the coolant water and the cladding in the PWR pin-cell model is 579 K and the temperature distribution within the fuel pin is modelled with a step function ranging from 772 to 1275 K. The HTGR system was changed from the PHYSOR test case to an infinite cubic lattice of TRISO-particles, because, with the current version of Serpent, the TRISO system was found to reflect much better the effect of the tracking method on performance[‡]. The exact composition of the TRISO particles is described in Table I and the lattice pitch is 0.16341 cm.

Table I. Composition of the TRISO particle used in the HTGR test case.

Outer radius cm	Density g/cm^3	Temperature K	Material
0.0125	10.4	1800 K	UO_2 enriched to 8.2 w-% ^{235}U with 1 ppm boron
0.0250	10.4	1200 K	UO_2 enriched to 8.2 w-% ^{235}U with 1 ppm boron
0.0340	1.05	1200 K	carbon
0.0380	1.90	1200 K	pyrolytic carbon
0.0415	3.18	1200 K	silicon carbide
0.0455	1.90	1200 K	pyrolytic carbon
surroundings	1.75	1200 K	graphite

All of the calculations were made using a JEFF-3.1.1 based cross section library with 0.001 reconstruction tolerance. Results for performance comparison are presented in Tables II and III for a PWR pin cell and a HTGR system, respectively. Ten million active neutron histories were calculated in these test cases.

The statistics of these calculations are poor, leading to high statistical deviations in k_{eff}. DBRC was not used when calculating the results with the elevated basis cross section temperature, which causes significant bias in the corresponding eigenvalues. It should also be noted that the η_{rea} parameter is scored at all collisions also in the EBT case. Thus, also the collisions with nuclides appearing in one temperature only, for which the reaction sampling efficiency is 100 %, affect the η_{rea} parameter.

To show the effect of parameter Q on the calculation, differences in flux spectra compared to a NJOY-based benchmark are plotted in Figure 1 for both of the cases and three different values of Q. The temperatures of the cross sections were adjusted using the Doppler-preprocessor routine in the PWR case, while the HTGR case was based purely on NJOY-broadened cross sections. The number of active neutron histories used in the spectrum comparisons was 2.5 billion in the PWR case and 1 billion in the HTGR case.

[‡]The computational cost of the boundary condition handling routine of Serpent was slightly increased in version 2.1.8. Due to high number of boundary crossings in the original HTGR test case the effect of the tracking routine was blurred.

Table II. Performance measures for a PWR pin-cell calculation are provided in this table. Results are calculated with Serpent 2 and NJOY cross sections, multi-group (MG) on-the-fly method introduced in [2] and continuous-energy (CE) on-the-fly with different means of optimization as described in this paper, including the optimization method involving an elevated basis cross section temperature (EBT). The statistical deviations Δk_{eff} correspond to one sigma.

Case	Q	η_{rea}	t_{rel}	P_{err}	k_{eff}	Δk_{eff} (pcm)
NJOY XS, opti 2	-	0.99[§]	1.00	0	1.34604	40
MG on-the-fly	-[¶]	0.26	2.00	0.0E+0	1.34686	40
CE on-the-fly	1E-6	0.27	1.82	5.7E-9	1.34714	40
CE on-the-fly	1E-5	0.29	1.78	2.3E-8	1.34693	40
CE on-the-fly	1E-4	0.32	1.68	7.4E-8	1.34724	40
CE on-the-fly	1E-3	0.36	1.57	2.5E-7	1.34704	39
CE on-the-fly	1E-2	0.43	1.43	3.3E-6	1.34724	40
CE on-the-fly	1E-1	0.53	1.29	7.7E-5	1.34785	42
CE on-the-fly + EBT	1E-6	0.72	1.06	0.0E+0	1.35013	41
CE on-the-fly + EBT	1E-5	0.75	1.05	2.7E-9	1.35029	39
CE on-the-fly + EBT	1E-4	0.77	1.01	5.5E-9	1.34957	39
CE on-the-fly + EBT	1E-3	0.79	1.00	2.2E-7	1.34894	40
CE on-the-fly + EBT	1E-2	0.82	0.98	3.0E-6	1.34909	42

The benchmark calculation of the PWR case resulted in an analog k_{eff} estimate of $1.34651 \pm 2\ \mathrm{pcm}$, while the TMS method with $Q = 10^{-6}$ resulted in a 51 pcm larger value, $1.34702 \pm 2\ \mathrm{pcm}$. In the HTGR case the corresponding estimates were $1.20271 \pm 5\ \mathrm{pcm}$ and $1.20298 \pm 4\ \mathrm{pcm}$, the difference being 27 pcm. The multiplication factors of the TMS with Q-values 10^{-6} and 10^{-2} were equal within statistical accuracy.

In Figure 1 it can be seen that deviance curves for Q values 10^{-6} and 10^{-2} are practically the same over the whole energy spectrum, but when Q is increased to 10^{-1}, the spectrum starts to differ from the two other cases. This indicates that a value of $Q = 10^{-2}$ leading to P_{err} of magnitude 10^{-7}–10^{-6} seems tolerable, because with this proportion of erroneus samples the results of the transport calculation are still unaffected. On the other hand, 10^{-1} is evidently too high a value for the Q parameter and the transport calculation is notably disturbed if P_{err} exceeds 10^{-5}.

The PWR case with elevated basis temperature and the largest acceptable Q-value 10^{-2} performed, surprisingly, even better than normal Serpent in optimization mode 2. This is due to the fact that DBRC was not used in the calculations with EBT. Since the slow-down of DBRC in this PWR case is about 8 % [2], t_{rel} for the on-the-fly + EBT case with $Q = 10^{-2}$ is expected to become about 1.06 after introduction of DBRC. In the HTGR case the slow-down of DBRC is about 14 % and the expected t_{rel} for the fastest $Q = 10^{-2}$ case is 1.33.

[§] Since optimization mode 2 involves a combined multi-group/continuous-energy tracking scheme with rejection sampling, the reaction sampling efficiency differs from 1.00.

[¶] Multi-group on-the-fly uses the DBRC cut-off condition as defined in Equation (11).

Table III. Performance measures for a HTGR system.

Case	Q	η_{rea}	t_{rel}	P_{err}	k_{eff}	Δk_{eff} (pcm)
NJOY XS, opti 2	-	0.99	1.00	0	1.20281	38
MG on-the-fly	-	0.67	3.62	0.0E+0	1.20288	40
CE on-the-fly	1E-6	0.68	3.24	0.0E+0	1.20323	40
CE on-the-fly	1E-5	0.69	3.11	0.0E+0	1.20279	38
CE on-the-fly	1E-4	0.72	2.92	0.0E+0	1.20223	38
CE on-the-fly	1E-3	0.75	2.77	3.0E-8	1.20348	39
CE on-the-fly	1E-2	0.78	2.50	4.3E-7	1.20345	39
CE on-the-fly	1E-1	0.83	2.26	1.8E-5	1.20419	40
CE on-the-fly + EBT	1E-6	0.96	1.32	0.0E+0	1.21097	39
CE on-the-fly + EBT	1E-5	0.96	1.29	0.0E+0	1.21043	39
CE on-the-fly + EBT	1E-4	0.96	1.28	3.4E-9	1.21065	38
CE on-the-fly + EBT	1E-3	0.97	1.23	6.6E-8	1.21093	38
CE on-the-fly + EBT	1E-2	0.97	1.17	6.0E-7	1.21079	40

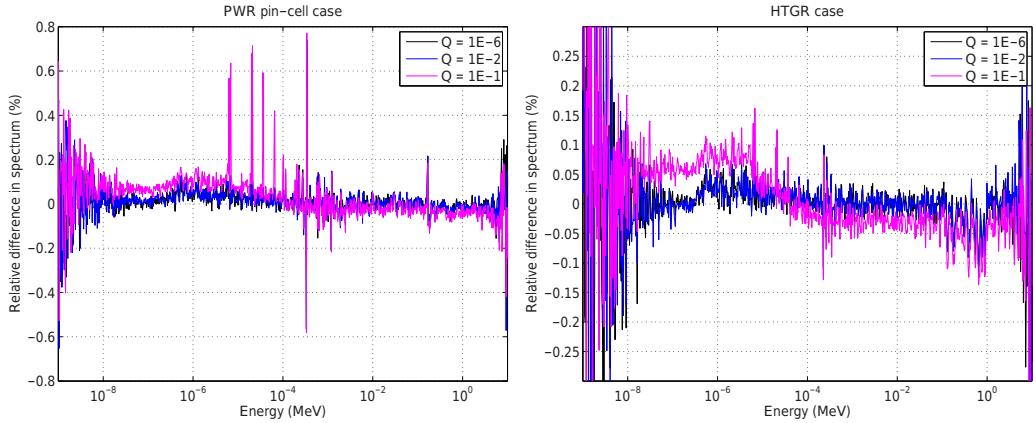

Figure 1. Spectra corresponding to 0 Kelvin basis temperature and three different Q-values are compared to a benchmark solution calculated using Serpent 2.1.9 with NJOY-broadened cross sections. Results are provided for two cases: a PWR pin-cell and a HTGR system.

5. CONCLUSIONS

In Figure 1 it can be seen that even with the lowest values of the Q parameter there is some systematical difference between the spectrum calculated with the on-the-fly treatment and the benchmark. The comparison of the results at this accuracy is unreasonable in the PWR case, since the accuracy of the cross section libraries is unknown due to the usage of the Doppler-preprocessor of Serpent. The preprocessor does not modify the energy grid of the cross section during Doppler-broadening and, hence, the reconstruction tolerance of the resulting cross section is higher than in the original one. In the HTGR case, small deviances can be recognized around energy intervals 2E-7–1E-5 MeV and 1E-1–1E0 MeV, which was found to result in a significant 27 pcm difference in the multiplication factor. These deviances most likely originate from small methodological differences combined with the limited accuracy of the cross section representation, but more results are needed for confirmation. The differences existed already in the previous multi-group implementation, but were not paid attention to before now.

From the performance measures it can be seen that the effect of changing from multi-group to continuous-energy majorant reduces the required CPU time about 5–10 %, depending on the case. By increasing the value of the Q parameter, which controls the conservativity of the majorant cross section, to 10^{-2} the CPU time savings increases to 28–30 %. With these means of optimization the relative calculational effort of the TMS method to an ordinary transport calculation can be decreased from 2.0–3.6 to 1.4–2.5 in the specific test cases.

The most significant enhancement in performance is, however, achieved with the still incomplete method of raising the temperature of the basis library above 0 K. Since the results obtained with the elevated basis library temperature do not match with the benchmark yet, it is too early to make any final conclusions about the efficiency of the method. Nevertheless it seems that, after introduction of DBRC, this means of optimization may decrease the relative calculational effort even as low as 1.06–1.33 in the specific test cases. This is still somewhat worse than the incredible efficiency of the on-the-fly methodology used in MCNP [9], but this level of slow-down can in many cases be considered acceptable and sometimes even negligible.

In the results it seemed that the value of Q may be chosen surprisingly large: even as high value as 10^{-2} was small enough not to affect the transport calculation significantly. Before hard-coding any values in the implementation, more systems should be investigated. It is possible that in some systems the Q parameter must be chosen smaller than 10^{-2}, deteriorating the performance of the method. The efficiency of the method should also be investigated with a system containing burned fuel. The performance of the method may drop dramatically if the number of nuclides in a material increases to several hundreds.

The optimization method based on elevated basis library temperature will be completed and implemented in the official version of Serpent 2 in the near future. Thereafter, the main topics for future research considering the TMS method involve the implementation of reaction rate estimators, the resonance treatment at the unresolved region and the handling of bound-atom scattering.

ACKNOWLEDGEMENTS

This work was partly funded through the NUMPS project of the Finnish Academy and KÄÄRME project of the Finnish Research Programme on Nuclear Power Plant Safety, SAFIR2014.

REFERENCES

[1] T. Viitanen and J. Leppänen, "Explicit Treatment of Thermal Motion in Continuous-energy Monte Carlo Tracking Routines," *Nucl. Sci. Eng.*, **171**, pp. 165–173 (2012).

[2] T. Viitanen and J. Leppänen, "Explicit Temperature Treatment in Monte Carlo Neutron Tracking Routines – First Results," *Proc. PHYSOR-2012*, Knoxville, TN, 15–20 April (2012).

[3] D. Kotlyar, et al., "Coupled neutronic thermo-hydraulic analysis of full PWR core with Monte-Carlo based BGCore system," *Nucl. Eng. Design*, **241**, pp. 3777–3786 (2011).

[4] M. Vazquez, et al., "Coupled neutronics thermal-hydraulics analysis using Monte Carlo and sub-channel codes," *Nucl. Eng. Design*, **250**, pp. 403–411 (2012).

[5] A. Ivanov, V. Sanchez and J. E. Hoogenboom, "Single Pin BWR Benchmark problem for Couled Monte Carlo – Thermal Hydraulics Analysis," *Proc. PHYSOR-2012*, Knoxville, TN, 15–20 April (2012).

[6] F. P. Espel, et al., " New developments of the MCNP/CTF/NEM/NJOY code system Monte Carlo based coupled code for high accuracy modeling," *Ann. Nucl. Energy*, **51**, pp. 18–26 (2013).

[7] J. Leppänen, T. Viitanen and V. Valtavirta, "Multi-physics Coupling Scheme in the Serpent 2 monte Carlo Code", *Trans. Am. Nucl. Soc.*, **107**, pp. 1165–1168 (2012).

[8] J. Leppänen, "Development of a Dynamic Simulation Mode in Serpent 2 Monte Carlo Code", *Proc. M&C 2013*, Sun Valley, ID, 5–9 May, (2013).

[9] G. Yesilyurt, W. R. Martin and F. B. Brown, "On-the-Fly Doppler Broadening for Monte Carlo Codes", *Nucl. Sci. Eng.*, **171**, pp. 239–257 (2012).

[10] B. Becker, R. Dagan and G. Lohnert, "Proof and implementation of the stochastic formula for ideal gas, energy dependent scattering kernel," *Ann. Nucl. Energy*, **36**, pp. 470–474 (2009).

[11] D. E. Cullen, "Program SIGMA1 (version 79-1): Doppler broaden evaluated cross sections in the evaluated nuclear data file/version B (ENDF/B) format," UCRL-50400 Part B., Lawrence Livermore National Laboratory (1979).

[12] R. E. MacFarlane and D. W. Muir, "NJOY99.0 Code System for Producing Pointwise and Multigroup Neutron and Photon Cross Sections from ENDF/B Data," PSR-480, Los Alamos National Laboratory (2000).

[13] R. V. Meghreblian and D. K. Holmes, *Reactor analysis*, pp. 137140, McGraw-Hill Book Company, New York (1960).

[14] T. Viitanen, "Implementing a Doppler-Preprocessor of Cross Section Libraries in Reactor Physics Code Serpent", Masters thesis, Helsinki University of Technology (2009).

[15] T. Viitanen and J. Leppänen, "New Data Processing Features in the Serpent Monte Carlo Code," *J. Korean Phys. Soc.*, **59**, pp. 1365–1368 (2011).

PUBLICATION IV

Target motion sampling temperature treatment technique with elevated basis cross-section temperatures

Nucl. Sci. Eng., **177**, pp. 77–89.

NUCLEAR SCIENCE AND ENGINEERING: **177**, 77–89 (2014)

Target Motion Sampling Temperature Treatment Technique with Elevated Basis Cross-Section Temperatures

Tuomas Viitanen* and Jaakko Leppänen

VTT Technical Research Centre of Finland
P.O. Box 1000, FI-02044 VTT, Finland

Received May 15, 2013
Accepted August 25, 2013
http://dx.doi.org/10.13182/NSE13-37

Abstract—*The target motion sampling (TMS) temperature treatment technique, previously known as "explicit treatment of target motion," is a stochastic method for taking the effect of thermal motion on reaction rates into account on-the-fly during Monte Carlo neutron tracking. The method is based on sampling target velocities at each collision site and dealing with the collisions in the target-at-rest frame using cross sections below the actual temperature of the nuclide or, originally, 0 K. Previous results have shown that transport with the original implementation of the TMS method requires about two to four times more CPU time than conventional transport methods, depending on the case. In the present paper, it is observed that the overhead factor may increase even above 10 in cases involving burned fuel. To make the method more practical for everyday use, some optimization is required.*

This paper discusses a TMS optimization technique in which the temperatures of the basis cross sections are elevated above 0 K. Comparisons show that the TMS method is able to reproduce the NJOY-based reference results within statistical accuracy, both with and without the newly implemented optimization technique. In the specific test cases, the optimization saved 35% to 83% of the calculation time, depending on the case.

I. INTRODUCTION

Neutron transport in the conventional Monte Carlo approach relies on prebroadened effective cross sections. This means that the cross-section data must be stored in computer memory separately for each nuclide and temperature appearing in the problem geometry. Memory capacity becomes a major limitation when modeling systems involving burned fuel and temperature feedback, which is the case with actual nuclear reactors in operation.

To overcome the limitations in memory capacity, on-the-fly temperature treatment techniques have been developed. The idea behind these methods is that the effect of thermal motion on reaction rates is calculated during the transport calculation, i.e. "on the fly," and consequently the effective cross sections no longer need to be stored in computer memory, at least not for all temperatures appearing in the problem geometry. Perhaps the most well-known on-the-fly technique at present was introduced by Yesilyurt et al.[1,2] and has recently been implemented in MCNP6. The technique is based on fast Doppler broadening of cross sections using series expansions with precalculated coefficients.

Recently, a novel on-the-fly temperature treatment was suggested by the present authors.[3–5] The target motion sampling (TMS) temperature treatment technique is a stochastic on-the-fly temperature treatment method for Monte Carlo neutron tracking routines. The main idea of the method is to sample target velocities at collision sites according to the thermal motion and to handle the collisions in the target-at-rest frame using cross sections below the actual temperature of the target nuclide. The fact that in this tracking scheme the total cross section becomes a distributed quantity is accounted for by applying rejection sampling on the particle path lengths. An advantage of this approach is that it provides for rigorous modeling of temperature distributions that may

*E-mail: tuomas.viitanen@vtt.fi

vary continuously in both time and space, independent of the material boundaries in the problem geometry. It is also convenient that the method relies on ordinary pointwise continuous-energy cross sections and does not require any additional precomputed data.

The method was first introduced with the name "explicit treatment of thermal motion"[3] but was recently renamed TMS because after the modifications discussed in this paper, the sampled target velocities no longer correspond to the actual, or "explicit," target motion. The preliminary implementation of the method in the continuous-energy Monte Carlo reactor physics code Serpent 2 together with the first practical results were presented in Ref. 4. This implementation involved multigroup majorant cross sections and required about four times more CPU time in a high-temperature gas-cooled reactor (HTGR) calculation than a conventional Monte Carlo calculation with effective, prebroadened cross sections. In Ref. 5, a few different ways of optimizing the method were introduced, with good preliminary results. These optimization tweaks involved changing to a continuous-energy majorant, adjusting the conservativity of this majorant, and incorporating a new and so-far incomplete idea of elevating the basis temperature of cross sections above 0 K.

This paper continues with the topic of elevating the basis cross-section temperatures above 0 K. The 0 K version of the TMS method, as introduced in Ref. 3, is first summarized in Sec. II, and the TMS method with elevated basis temperatures is introduced and justified in Sec. III. The new methodology is implemented in Serpent 2.1.14, and results considering the performance and accuracy of the TMS method with and without the elevated basis temperature optimization are provided in Sec. V. Conclusions are given in Sec. VI.

Topics that are intentionally omitted from this paper include the generation of an optimal majorant cross section and the efficiency of reaction rate estimators in TMS transport. Both of these important topics will be covered in separate papers as soon as possible. There are also plans to extend the TMS capability to the energy region of unresolved resonances and to make the method compatible with bound-atom scattering in the more distant future.

II. TEMPERATURE TREATMENT WITH TMS

To introduce readers to the TMS method and to provide some background information for the upcoming analyses, the concept of the TMS method is first summarized. This summary is strongly based on the first paper written on the subject.[3] The very heart of the method, the TMS tracking scheme, is described in Sec. II.A, and the connection between the stochastically broadened cross sections of the TMS method and effective cross sections, used in traditional Monte Carlo transport, is shown in Sec. II.B.

II.A. Basic TMS Tracking Scheme

The tracking scheme of the TMS governs the way in which the neutrons are transported within material zones. It is emphasized that in this first version of the tracking scheme the basis cross sections are at a temperature of 0 K.

1. The neutron path lengths l are sampled using the standard inversion sampling method as

$$l = -\frac{1}{\Sigma_{\text{maj}}} \ln \xi , \tag{1}$$

where ξ is a random variable uniformly distributed on the unit interval. The sampling is based on a majorant cross section Σ_{maj} that takes into account the variations in the total cross sections within the range of thermal motion.[a] The next collision occurs at $\mathbf{r}_{n+1} = \mathbf{r}_n + l\hat{\mathbf{\Omega}}$, where $\mathbf{r}_n$ is the previous collision site corresponding to collision number n and $\hat{\mathbf{\Omega}}$ is the direction vector of neutron motion.

The majorant cross section is similar to the majorant used with the Doppler-broadening rejection correction (DBRC) method,[6] and hence, it can be generated using the same criteria. Basically, the majorant at energy E is chosen as the maximum total cross section within the range of possible target-at-rest energies in a collision between a neutron with laboratory-frame (LAB) energy E and a target nuclide with energy $16k_{\text{B}}T_{\text{max}}$, where k_{B} is the Boltzmann constant and T_{max} is the maximum temperature of the target nuclide. The $16k_{\text{B}}T$ cutoff condition for thermal motion has been adopted from the SIGMA1 Doppler-broadening code.[7] The majorant is further multiplied by a normalization factor $g_{\text{E}}(E, T_{\text{max}}, A)$ that is introduced later in Sec. II.B.

2. At each collision point candidate $\mathbf{r}_{n+1}$, the target nuclide is first sampled. The probability of sampling nuclide i is

$$\frac{\Sigma_{\text{maj},i}(E, \mathbf{r}_{n+1})}{\Sigma_{\text{maj}}(E, \mathbf{r}_{n+1})} = \frac{\Sigma_{\text{maj},i}(E, \mathbf{r}_{n+1})}{\sum_j \Sigma_{\text{maj,j}}(E, \mathbf{r}_{n+1})} , \tag{2}$$

where E represents the LAB energy of the neutron. The material-wise majorant cross section Σ_{maj} is obtained by summing over the nuclide-wise majorants.

3. The target velocity is then sampled from a Maxwellian-based distribution $P_1(T)$, the exact form and

[a]If the transport routine is based on the Woodcock delta-tracking method, this majorant cross section also takes into account the variation in reaction probability when the neutron crosses a boundary between two materials. The TMS methodology also works with the more commonly used surface tracking, in which case the majorant only accounts for the variation in microscopic cross sections within a single material.

justification of which are presented later in Sec. II.B. The temperature T corresponds to the local temperature at the collision point, i.e., $T=T(\mathbf{r}_{n+1})$.

4. The collision point is accepted or rejected according to the criterion

$$\xi < \frac{g_{\mathrm{E}}(E,T,A)\Sigma_i^0(E',\mathbf{r}_{n+1})}{\Sigma_{\mathrm{maj},i}(E,\mathbf{r}_{n+1})}\ , \tag{3}$$

where $\Sigma_i^0(E',\mathbf{r}_{n+1})$ is the 0 K cross section of nuclide i at target-at-rest energy E'.

5. If the collision is rejected, the procedure restarts from 1 by sampling of a new path length starting from the newly rejected collision point $\mathbf{r}_{n+1}$. If the collision is accepted, a reaction is sampled based on 0 K cross sections at E', and the tracking proceeds according to the sampled reaction.

As previously mentioned, the temperature may vary arbitrarily in space and time, i.e., $T=T(\mathbf{r},\ t)$, when using the TMS method in neutron tracking. Another very convenient feature is that in the case that a scattering reaction is sampled at step 5, the kinematics of the scattering event can be resolved using the already-sampled target velocity. The secondary particle distributions calculated this way correspond to the temperature-dependent scattering kernel and are thus equivalent to those calculated with the normal free gas treatment involving DBRC. In fact, the implementation of the TMS technique in Serpent takes advantage of this feature and solves the kinematics of elastic scattering events accurately for all energies and nuclides when the transport is based on 0 K cross sections.

II.B. Stochastically Broadened Versus Effective Cross Sections

The traditional tracking methodology is based on effective cross sections that are basically 0 K cross sections averaged over the thermal motion of target nuclei. The analysis presented in Secs. II.B through III.B discusses the Doppler broadening of the cross sections of an individual nuclide, appearing at homogeneous density and temperature. Since there are consequently no $\mathbf{r}$ or i dependences involved, the dependence of the cross sections on these parameters is, for simplicity, not explicitly shown in the equations. The definition of effective cross sections follows straightforwardly from the condition of constant reaction rates and can be written in vector form as

$$\Sigma_{\mathrm{eff}}(v,T,A)=\frac{1}{v}\int |\mathbf{v}-\mathbf{V}_{\mathrm{t}}|\Sigma^0(|\mathbf{v}-\mathbf{V}_{\mathrm{t}}|)P(\mathbf{V}_{\mathrm{t}},T,A)\ d\mathbf{V}_{\mathrm{t}}\ , \tag{4}$$

where

$v=|\mathbf{v}|$ = speed of the neutron,

$\mathbf{V}_{\mathrm{t}}$ = target velocity, and

$P(\mathbf{V}_{\mathrm{t}},T,A)$ = probability density function of target velocities at temperature T (Ref. 8).

Traditionally, the thermal motion is assumed to follow the Maxwell-Boltzmann distribution

$$P_{\mathrm{MB}}(\mathbf{V}_{\mathrm{t}},T,A)\ d\mathbf{V}_{\mathrm{t}}=\left(\frac{\gamma}{\pi}\right)^{3/2}e^{-\gamma(\mathbf{V}_{\mathrm{t}}\cdot\mathbf{V}_{\mathrm{t}})}\ d\mathbf{V}_{\mathrm{t}}\ , \tag{5}$$

where

$$\gamma(T,A)=\sqrt{\frac{AM_{\mathrm{n}}}{2k_{\mathrm{B}}T}}, \tag{6}$$

M_{n} = neutron mass, and

A = ratio of target mass to M_{n}, also known as the atomic weight ratio.

The integration in Eq. (4) can be performed in at least two practical ways, leading to two different formulations for the effective cross section, both of which can be found useful for different purposes. When actually Doppler-broadening the cross sections, for example, in NJOY or the Doppler preprocessor of Serpent (Refs. 7, 9, and 10), it is beneficial to integrate over the relative speed

$$v'=|\mathbf{v}'|=|\mathbf{v}-\mathbf{V}_{\mathrm{t}}| \tag{7}$$

and the cosine of the angle between $\mathbf{v}'$ and $\mathbf{v}$, $\nu=\cos\ \beta$, as illustrated in Fig. 1. With these integration variables, the well-known kernel-broadening equation

$$\begin{aligned}\Sigma_{\mathrm{eff}}(v,T,A)=&\\ &\frac{1}{v}\frac{2}{\sqrt{\pi}}\gamma^3\int_0^\infty\int_{-1}^1 v'^3\Sigma^0(v')e^{-\gamma^2(v^2+v'^2-2vv'\nu)}\,dv'\,d\nu\\ &=\frac{1}{v^2}\frac{\gamma}{\sqrt{\pi}}\int_0^\infty v'^2\Sigma^0(v')\left(e^{-\gamma^2(v'-v)^2}-e^{-\gamma^2(v'+v)^2}\right)dv'\end{aligned} \tag{8}$$

is obtained. We will return to this formulation later in Sec. III.A.

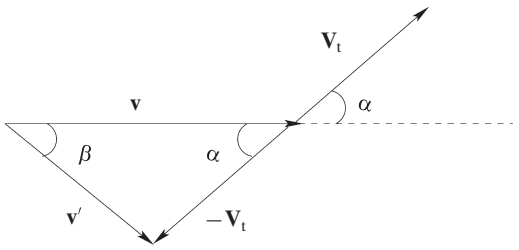

Fig. 1. Vector diagram illustrating the notation used in this paper: $\mathbf{v}$ is the velocity of the neutron, $\mathbf{V}_{\mathrm{t}}$ is the velocity of the target, and $\mathbf{v}'$ is the relative velocity.

The second form of Eq. (4), which is more useful in the following considerations because of more practical variable choices, involves integration over V_t and the cosine of the angle between $\mathbf{v}$ and $\mathbf{V}_t$, $\mu = \cos\alpha$ (Fig. 1). The equation for effective cross sections corresponding to these integration variables is

$$\Sigma_{\text{eff}}(v,T,A) = \frac{1}{v}\int_0^\infty \int_{-1}^{1} v'\Sigma^0(v')P_{\text{MB}}(V_t,T,A)\, dV_t\, d\frac{\mu}{2}, \tag{9}$$

where

$$P_{\text{MB}}(V_t,T,A)\, dV_t = \frac{4}{\sqrt{\pi}}\gamma^3 V_t^2 e^{-\gamma^2 V_t^2}\, dV_t \tag{10}$$

is the Maxwell-Boltzmann distribution written for the target speed V_t. The speed of the neutron relative to the target, v', is related to V_t, v, and μ via the equation

$$v' = \sqrt{v^2 + V_t^2 - 2vV_t\mu}\,. \tag{11}$$

In Ref. 3, it was reasoned that the neutron tracking with the TMS method corresponds, on average, to a conventional transport calculation with effective cross sections only if the 0 K cross sections at sampled target-at-rest velocities conform to the effective cross sections on average. This condition can be considered also the only fundamental requirement for the TMS method to function correctly; otherwise, the TMS method, as described in Sec. II.A, is only about sampling techniques that allow path length sampling using a distributed total cross section. The condition was also expressed in mathematical terms as

$$\int_0^\infty \int_{-1}^{1} g(v,T,A)\Sigma^0(v')P_1(V_t,\mu,T,A)dV_t d\mu = \Sigma_{\text{eff}}(v,T,A), \tag{12}$$

where $P_1(V_t,\mu,T,A)$ is the target velocity distribution and

$$\begin{aligned} g(v,T,A) &= \int_0^\infty \int_{-1}^{1} \frac{v'}{2v} P_{\text{MB}}(V_t,T,A)\, dV_t\, d\mu \\ &= \left(1 + \frac{1}{2\gamma^2 v^2}\right)\text{erf}(\gamma v) + \frac{e^{-\gamma^2 v^2}}{\sqrt{\pi}\,\gamma v} \end{aligned} \tag{13}$$

is a normalization factor for the distribution P_1 or, in practice, the Doppler-broadening integral for constant cross section.[b] Usually, for instance, in Eq. (3), it is more practical to write Eq. (13) in terms of energy as[11]

$$g_{\text{E}}(E,T,A) = \left(1 + \frac{k_B T}{2AE}\right)\text{erf}\left(\sqrt{\frac{AE}{k_B T}}\right) + \sqrt{\frac{k_B T}{\pi AE}}\, e^{-AE/(k_B T)}. \tag{14}$$

By comparing Eq. (12) with the effective cross-section formula (9) involving μ, it was concluded that the target velocities must be sampled from the distribution

$$P_1(V_t,\mu,T,A)\, dV_t\, d\mu = \frac{1}{g(v,T,A)}\frac{v'}{2v} P_{\text{MB}}(V_t,T,A)\, dV_t\, d\mu \tag{15}$$

for the neutron tracking to be consistent with traditional transport methods relying on effective cross sections.

III. TMS METHOD WITH ELEVATED BASIS TEMPERATURE

In Ref. 5, it was noted that the efficiency of the rejection sampling criterion (3) could be significantly increased by elevating the temperature of the basis cross section above 0 K. The increase in efficiency is caused by the smoothing effect of Doppler broadening, which very efficiently flattens the sharp resonance peaks of the total cross sections at 0 K, together with the fact that the amount of thermal motion involved in the majorant generation is smaller with higher cross-section basis temperatures. Both of these effects reduce the gaps between the majorant and the total cross section, which effectively increases the performance of the TMS method. Because of the "Doppler smoothening," the CPU time savings should be notable for all systems in which the minimum temperature of nuclides is significantly above 0 K. The increase in performance is greatest in systems with narrow temperature ranges.

The following considerations show why and how the TMS method can also be utilized to raise the temperature of an already-broadened cross section. First, an important and well-known property of the kernel-broadening equation is shown in Sec. III.A, the functionality of the TMS method with elevated basis temperatures (EBT) is justified in Sec. III.B, and the differences between EBT and 0 K transport are discussed in Sec. III.C.

III.A. Rebroadening of Effective Cross Sections

The well-known definition of effective cross sections, as written in Eq. (4), relates the reaction rate at temperature T to the reaction rate at 0 K. However, as shown in Ref. 8, basically the same formula can be used to relate reaction rates at an arbitrary temperature T to those at a lower temperature $T' \geq 0$ K in general. In other words, the same equation can be used to raise the temperatures of already-broadened effective cross sections.

[b] In the original paper,[3] the sign of the exponential term in Eq. (13) was erroneously negative. The authors apologize for any inconvenience this may have caused.

This property is briefly demonstrated in the following, beginning from the kernel-broadening equation (8). To explicitly show the temperature dependences, a new auxiliary variable

$$a(A)=\sqrt{\frac{AM_{\mathrm{n}}}{2k}}=\gamma(T,A)\sqrt{T} \tag{16}$$

is introduced, and Eq. (8) becomes

$$\Sigma_{\mathrm{eff}}(v,T,A)= \frac{1}{v^2}\frac{a}{\sqrt{\pi T}}\int_0^\infty v'^2\Sigma^0(v')\left(e^{-a^2(v'-v)^2/T}-e^{-a^2(v'+v)^2/T}\right)\,dv' . \tag{17}$$

If this equation is applied with $T=T_2$ to an effective cross section already at temperature T_1, then recursive application of the formula yields

$$\begin{aligned}&\frac{1}{v^2}\frac{a}{\sqrt{\pi T_2}}\int_0^\infty v'_2{}^2\,\Sigma_{\mathrm{eff}}(v'_2,T_1,A)\\ &\quad\times\left(e^{-a^2(v'_2-v)^2/T_2}-e^{-a^2(v'_2+v)^2/T_2}\right)\,dv'_2\\ &=\frac{1}{v^2}\frac{a^2}{\pi\sqrt{T_1T_2}}\int_0^\infty v'_1{}^2\,\Sigma^0(v'_1)\\ &\quad\times\int_0^\infty\left(e^{-a^2(v'_1-v'_2)^2/T_1}-e^{-a^2(v'_1+v'_2)^2/T_1}\right)\\ &\quad\times\left(e^{-a^2(v'_2-v)^2/T_2}-e^{-a^2(v'_2+v)^2/T_2}\right)\,dv'_1\,dv'_2 .\end{aligned} \tag{18}$$

After integrating this formula with respect to dv'_2, a familiar-looking equation emerges:

$$\frac{1}{v^2}\frac{a}{\sqrt{\pi(T_1+T_2)}}\int_0^\infty v'_1{}^2\,\Sigma^0(v'_1)\left(e^{-a^2(v'_1-v)^2/(T_1+T_2)}-e^{-a^2(v'_1+v)^2/(T_1+T_2)}\right)\,dv'_1 . \tag{19}$$

By comparing this equation with the kernel-broadening formula (17), it can be seen that rebroadening a cross section at temperature T_1 by temperature T_2 has exactly the same effect as broadening a cross section from 0 K to T_1+T_2 in one step, at least in analytical terms. Since the choice of the integration variables is arbitrary as long as the integration is performed over all $\mathbf{V}_{\mathrm{t}}$, the result applies also for the Doppler-broadening formula (9), in which the integration is performed over μ.

III.B. Sampling Target Velocities with Elevated Basis Temperature

Analogous to the reasoning in Ref. 3 that was summarized in Sec, II.B, the cross sections sampled with the TMS should correspond to effective cross sections on average also if the temperature of the basis library is above 0 K, say, $T_{\mathrm{base}}<T$. If we forget at first about the normalization of the distribution of target velocities when dealing with elevated basis temperatures P_{EBT}, then the relation between sampled and effective cross sections is

$$\int_0^\infty\int_{-1}^1\Sigma_{\mathrm{eff}}(v',T_{\mathrm{base}},A)P_{\mathrm{EBT}}(V_{\mathrm{t}},\mu,T,A)\,dV_{\mathrm{t}}\,d\mu =\Sigma_{\mathrm{eff}}(v,T,A) . \tag{20}$$

Based on the discussion in Sec. III.A, the effective cross section on the right side can be written

$$\Sigma_{\mathrm{eff}}(v,T,A)=\frac{1}{v}\int_0^\infty\int_{-1}^1 v'\,\Sigma_{\mathrm{eff}}(v',T_{\mathrm{base}},A) \times P_{\mathrm{MB}}(V_{\mathrm{t}},T-T_{\mathrm{base}},A)\,dV_{\mathrm{t}}\,d\frac{\mu}{2}. \tag{21}$$

By comparing Eq. (21) with Eq. (20), it can be seen that the consistency of the TMS with conventional tracking methods is achieved by sampling the target velocities from the distribution

$$\begin{aligned}P_{\mathrm{EBT}}(V_{\mathrm{t}},\mu,T,T_{\mathrm{base}},A)&=\frac{v'}{2v}P_{\mathrm{MB}}(V_{\mathrm{t}},T-T_{\mathrm{base}},A)\\ &=P(V_{\mathrm{t}},T-T_{\mathrm{base}},A) .\end{aligned} \tag{22}$$

Thanks to the simple relation between P_{EBT} and P, the normalization issues can also be solved based on the 0 K case. The integral of Eq. (22) over all target velocities and collision cosines equals $g(v,T-T_{\mathrm{base}},A)$ as defined in Eq. (13). Thus, the actual distribution used in the nuclide sampling is

$$\begin{aligned}&P_{\mathrm{EBT},1}(V_{\mathrm{t}},\mu,T,T_{\mathrm{base}},A)\\ &=\frac{1}{g(v,T-T_{\mathrm{base}},A)}\frac{v'}{2v}\,P_{\mathrm{MB}}(V_{\mathrm{t}},T-T_{\mathrm{base}},A)\\ &=P_1(V_{\mathrm{t}},\mu,T-T_{\mathrm{base}},A),\end{aligned} \tag{23}$$

and the effective cross sections used in the TMS transport must be multiplied by the same factor for Eq. (21) to hold, i.e.,

$$\int_0^\infty\int_{-1}^1 g(v,T-T_{\mathrm{base}},A)\Sigma_{\mathrm{eff}}(v',T_{\mathrm{base}},A) \times P_{\mathrm{EBT},1}(V_{\mathrm{t}},\mu,T,T_{\mathrm{base}},A)\,dV_{\mathrm{t}}\,d\mu=\Sigma_{\mathrm{eff}}(v,T,A) . \tag{24}$$

III.C. Tracking with Elevated Basis Temperatures

It is practical to associate each nuclide appearing in the problem with a minimum and maximum temperature such that

$$T_{\max} = T_{\min} + \Delta T , \quad (25)$$

where $\Delta T \geq 0$. Since the TMS temperature treatment can only be used to raise the temperatures of cross sections, the basis cross-section temperature T_{base} cannot exceed $T_{\min}$.

The tracking with EBT is very similar to the $T_{\text{base}} = 0$ K case. The track lengths and collision nuclides are again sampled from majorant cross sections. The target velocities are sampled from the distribution $P_1\left(V_t, \mu, T(\mathbf{r}_{n+1}) - T_{\text{base}}, A\right)$, and the rejection sampling criterion becomes

$$\xi < \frac{g_E\left(E, T(\mathbf{r}_{n+1}) - T_{\text{base}}, A\right)\Sigma_{\text{eff},i}(E', \mathbf{r}_{n+1}, T_{\text{base}}, A)}{\Sigma_{\text{EBT,maj},i}(E, \mathbf{r}_{n+1})} . \quad (26)$$

The nuclide-wise majorant cross section $\Sigma_{\text{EBT,maj},i}(E, \mathbf{r}_{n+1})$ is analogous to the 0 K case, and consequently, the majorant can be generated based on the same methodology. The only difference is that the 0 K cross section is replaced by the effective cross section $\Sigma_{\text{eff}}(E', \mathbf{r}_{n+1}, T_{\text{base}}, A)$ at temperature T_{base}. Naturally, also the $16k_B T_{\max}$ cutoff condition in the majorant generation is replaced with $16k_B(T_{\max} - T_{\text{base}})$, and the multiplier of the majorant becomes $g_E(E, T_{\max} - T_{\text{base}}, A)$, because $T_{\max} - T_{\text{base}}$ is the maximum temperature difference that can be encountered when sampling target velocities from the distribution in Eq. (23).

It should be noted that the temperature difference $T_{\max} - T_{\text{base}}$ significantly affects the rejection sampling efficiency in Eq. (26): The smaller the temperature difference, the closer the majorant is to the effective cross section and the higher the efficiency. Thus, the best performance in a multitemperature system is achieved if $T_{\text{base}} = T_{\min}$. If cross-section libraries are not readily available at this minimum temperature, the temperature of the library cross section can be adjusted with Doppler preprocessing.[10]

When keeping the basis cross section at 0 K, the sampled target velocities correspond to the actual thermal motion of the target nuclei. Thus, the sampled velocities can be reused when calculating the kinematics of scattering events. However, when the basis temperature is elevated above zero, the sampled target velocities no longer have any practical physical meaning, and the target velocities can no longer be reused. Thus, the situation becomes exactly the same as with conventional neutron tracking methods: When a scattering reaction occurs, the target velocity must be sampled using the free gas treatment, in some cases completed with the DBRC, which can be used to take into account the effect of an energy-dependent scattering cross section on the scattering kernel.[6] Alternatively, the collision kinetics could be resolved using recently introduced direct sampling methods for the secondary neutron velocity,[12] or the problem could be treated using weight-reduction techniques[13,14] in the case that the particle weights are allowed to vary in the Monte Carlo transport. Neither of these alternative techniques is, however, currently implemented in Serpent, so the target velocity sampling in this paper is based on the free gas treatment + DBRC scheme.

IV. TEST CASES

The calculations are performed for four fuel assemblies with different neutron spectra to determine the performance of the TMS method in diverse conditions.

IV.A. Pressurized Water Reactor Assembly

The first case, PWR-Gd, involves a 17×17 pressurized water reactor (PWR) fuel assembly with 16 gadolinium-doped fuel rods in an infinite two-dimensional lattice. The geometry and material definitions of the fuel assembly are from a Nuclear Energy Agency (NEA) benchmark.[15] The only differences from the benchmark specifications are related to temperatures: The moderator temperature is increased to 600 K for simplicity, and the originally flat temperature profiles of the fuel rods are replaced with three-step distributions such that the pellets are divided into three equally thick annular regions with temperatures 600, 900, and 1200 K from the outside in.

The temperature profile is of an unrealistic shape, but the temperatures are of the same magnitude as in an ordinary PWR fuel rod operating at a rather high linear power.[4] However, the same does not apply for the fresh Gd fuel rods, which are, in reality, considerably cooler because of lower power densities. In any case, the chosen temperature distributions represent well enough the actual temperatures appearing in fuel rods and, above all, act as a good test case for the TMS method.

IV.B. PWR-Gd Assembly at 40 MWd/kgU Burnup

The second case, PWR-BU, features the PWR-Gd bundle introduced in Sec. IV.A irradiated to 40 MWd/kgU burnup. The irradiated material compositions were obtained by running a separate burnup calculation using Serpent 2.1.14. The resulting compositions contain 241 actinide and fission product nuclides with cross sections available in the data libraries. Serpent burnup routines are optimized in such way that the large number of cross sections is usually not a major factor for the overall calculation time, which, however, is no longer the case with TMS.

IV.C. High-Temperature Gas-Cooled Reactor System

The HTGR test case consists of tristructural-isotropic (TRISO) particles within a graphite matrix in an infinite three-dimensional lattice. The specifications of the TRISO

particles and the composition of the graphite matrix are based on an NEA benchmark for HTGR fuel depletion,[16] and the lattice pitch is 0.16341 cm.

The fuel kernel in the spherical TRISO particles is divided in two equally thick parts such that the innermost 0.0125 cm is at temperature 1800 K and the outer layer is at 1200 K. The temperature of all other materials is 1200 K.

IV.D. Sodium-Cooled Fast Reactor Assembly

The last of the test cases, SFR, involves a fuel assembly from the sodium-cooled fast reactor JOYO in an infinite two-dimensional lattice. The specifications of the assembly can be found in Ref. 17. The geometry and material definitions correspond to the benchmark definition for the 250°C core.

Again, the fuel temperature is modified such that the inner half of the fuel pellets is at 1200 K and the outer half is at 900 K. All other materials are at temperature 600 K in the model.

V. RESULTS

All of the calculations are made using Serpent 2.1.14 with the previously described TMS + EBT methodology implemented. The implementation is tested using three variants of the TMS:

1. basis cross sections at 0 K
2. basis cross sections at a library temperature $T_{base} = T_{min} - 300$ K
3. basis cross sections at T_{min}.

The second of the variants is introduced only to judge whether or not the adjustment of the basis cross-section temperatures with Doppler preprocessing is reasonable in a case where the cross sections are available in 300 K steps, which has been the case with Serpent 1 cross-section libraries. As mentioned previously, it should be possible to gain some efficiency by adjusting the cross-section temperatures to exactly T_{min} before the transport calculation, but if the gain in performance is not significant, the adjustment makes no sense.

The TMS treatment is used for fuel materials of the test cases, and effective cross sections are used for other materials. The results are compared with reference calculations in which NJOY-broadened cross sections are used for all materials.[9] It is emphasized that the Doppler preprocessor of Serpent (Ref. 10) was *not* used to adjust the temperature of the basis cross-section library in any of the calculations.

The Serpent transport routine is optimized for performance using pregenerated material-wise total cross sections to avoid summation over material compositions during tracking.[18] This method results in a considerable speedup in calculation, especially when modeling irradiated fuels, typically consisting of more than 200 actinide and fission product isotopes. Since the values of the microscopic cross sections are not defined before the velocity of the target nuclide is sampled, the same optimization cannot be used with TMS. This drawback in itself lowers the performance compared with a "typical" Serpent calculation. The reference calculations without TMS were therefore also run without precalculated total cross sections, using one of the lower optimization modes developed for Serpent 2 for the purpose of saving memory in large burnup calculations.[19] Even so, the comparison of running times is subject to factors not directly related to TMS, and the performance indicators presented in the following should not be taken too literally.

The cross-section library is JEFF-3.1.1 based and processed using a rather low 0.001 reconstruction tolerance. Free gas thermal treatment with DBRC for the scattering of ^{238}U was used from 0.4 eV to the unresolved resonance region boundary at 20 keV.[c] Since the TMS temperature treatment cannot yet handle probability table sampling, the method was not used in the reference calculations either.

The use of the high-resolution cross-section library and the free gas treatment at a wide energy range leads to a deterioration in the performance of the calculations. On the other hand, the results are not compromised in almost any way, which is favorable for validation purposes. Because all the calculations are made using the same library and free gas treatment parameters, the performance measures are highly comparable.

All of the calculations were made using 10 OpenMP threads on Intel Xeon X5690 CPUs running at 3.47 GHz.

V.A. Comparison of Accuracy

The multiplication factors of the different variants of the TMS method are compared with an ordinary Serpent calculation with optimization mode 2 and NJOY-broadened cross sections in Table I. Because the multiplication factor does not necessarily reveal all differences between the methods, the accuracy is also examined by comparing the differences in the neutron flux spectra. Comparison is made with the NJOY-based reference solution in Figs. 2 through 5 using 1000 energy bins of equal lethargy width. Each of the figures shows results for all three variants of the TMS. The dashed lines in the figures represent 1σ statistical deviations.

In the results of the PWR-BU test case, significant differences in the flux spectra can be observed between the 0 K basis case and the reference solution. Also, the eigenvalues differ in this case by 19 pcm. It should be

[c]Too low an upper energy limit for DBRC was afterward found to be the most significant error source in Ref. 5, so it was decided to be cautious in the current paper.

TABLE I

Results of the Test Calculations Using Serpent 2.1.14*

	PWR-Gd	PWR-BU	HTGR	SFR
Number of active neutron histories	10^9	5×10^8	5×10^8	10^9
NJOY-based benchmark				
k_{eff}	1.15522	0.93486	1.20241	1.78804
Δk_{eff} (pcm)	4	6	6	5
Transport time (h)	7.5	23.6	10.7	17.0
Memory requirement (GBytes)	2.1	69.7	0.5	2.1
TMS with $T_{\text{base}} = 0$ K				
$k_{\text{TMS}} - k_{\text{NJOY}}$ (pcm)	6 ± 6	$\mathbf{-19 \pm 8}$	4 ± 8	11 ± 7
Absolute transport time (h) / relative transport time	19.7 / 2.62	295.2 / 12.50	29.7 / 2.79	17.7 / 1.04
Absolute memory requirement (GBytes) / relative memory requirement	1.5 / 0.72	40.6 / 0.58	0.5 / 1.10	2.0 / 0.95
Sampling efficiency (%)	9	9	6	50
TMS with $T_{\text{base}} = T_{\text{min}} - 300$ K				
$k_{\text{TMS}} - k_{\text{NJOY}}$ (pcm)	-6 ± 6	3 ± 9	4 ± 8	5 ± 7
Absolute transport time (h) / relative transport time	9.7 / 1.29	78.5 / 3.32	13.2 / 1.24	12.0 / 0.70
Absolute memory requirement (GBytes) / relative memory requirement	1.5 / 0.70	31.1 / 0.45	0.5 / 1.01	1.7 / 0.85
Sampling efficiency (%)	29	28	30	94
TMS with $T_{\text{base}} = T_{\text{min}}$				
$k_{\text{TMS}} - k_{\text{NJOY}}$ (pcm)	-6 ± 6	-1 ± 8	9 ± 8	8 ± 7
Absolute transport time (h) / relative transport time	7.4 / 0.98	50.2 / 2.13	10.9 / 1.02	11.4 / 0.67
Absolute memory requirement (GBytes) / relative memory requirement	1.4 / 0.67	29.4 / 0.42	0.5 / 1.00	1.7 / 0.83
Sampling efficiency (%)	39	38	38	96

*The relative transport times and memory requirements are calculated with respect to the NJOY-based reference. The errors in reactivity eigenvalues correspond to 1σ statistical deviation.

noted that in the $T_{\text{base}} = 0$ K case, the sampled target velocities are always utilized in the solution of the kinetics of elastic scattering events, which effectively corresponds to using free gas treatment with DBRC for all nuclides at all energies. Since in the reference solution the DBRC is used only for ^{238}U, the $T_{\text{base}} = 0$ K TMS calculation is more detailed than the reference in this sense.

Indeed, the lack of DBRC for certain nuclides in the reference solution was found to be the reason for the observed differences. The nuclides that cause the difference peaks in flux spectra are identified in Fig. 3a. It was additionally noticed that using DBRC for ^{239}Pu has some effect on the k_{eff}, even though no clear difference peaks in the flux spectrum were observed for this nuclide. The reference calculation was repeated such that the use of DBRC was extended to nuclides ^{95}Mo, ^{108}Pd, ^{131}Xe, ^{145}Nd, ^{147}Pm, ^{152}Sm, ^{239}Pu, and ^{241}Am, in addition to ^{238}U. The TMS calculation with 0 K basis is compared with this more detailed reference solution in Fig. 6. The extended list of DBRC nuclides was applied also to the TMS calculation with $T_{\text{base}} = T_{\text{min}}$ and compared with the reference in Fig. 7. The corresponding differences in k_{eff} for the 0 K basis and the EBT case were 2 ± 8 and 8 ± 8 pcm, respectively.

To further validate the results, the same comparisons were performed against an NJOY-based reference solution in which DBRC was applied to all 241 nuclides in the fuel material. The results were practically the same as those presented in Figs. 6 and 7; i.e., no differences could be distinguished from the statistical noise. This indicates that all the nuclides for which the DBRC treatment is necessary in the PWR-BU case are included in the previously presented list of nuclides, or at least new nuclides cannot be identified with the current level of statistical accuracy.

V.B. Comparison of Performance

The performance measures of the TMS and reference calculations are also provided in Table I. As expected, the use of on-the-fly temperature treatment methods decreases

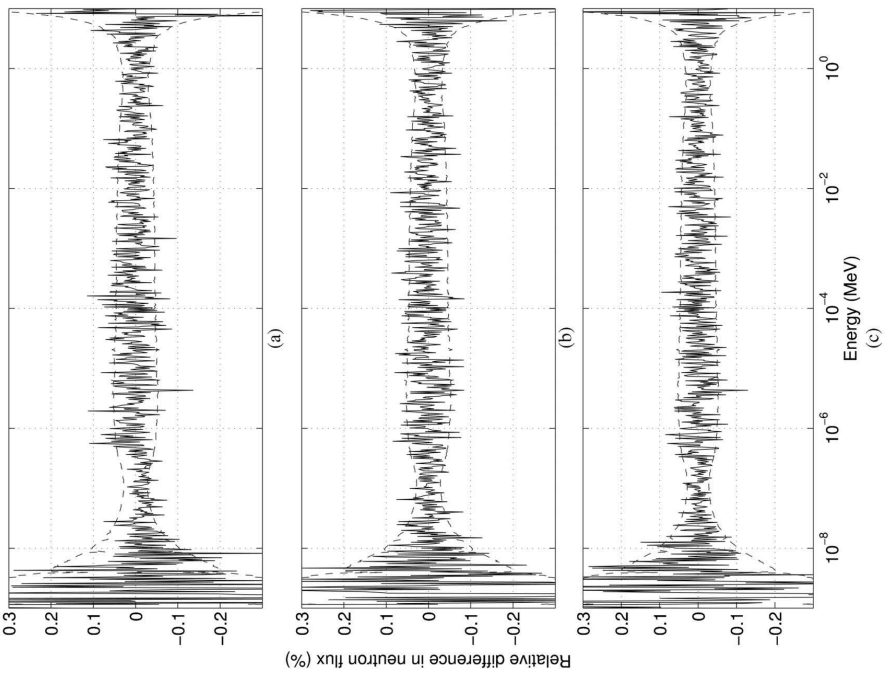

Fig. 2. Differences in neutron spectra of the PWR-Gd case for three different variants of the TMS method: (a) $T_{\text{base}} = 0$ K, (b) $T_{\text{base}} = T_{\text{min}} - 300$ K, and (c) $T_{\text{base}} = T_{\text{min}}$. The spectra are compared with a reference solution based on NJOY generated cross sections.

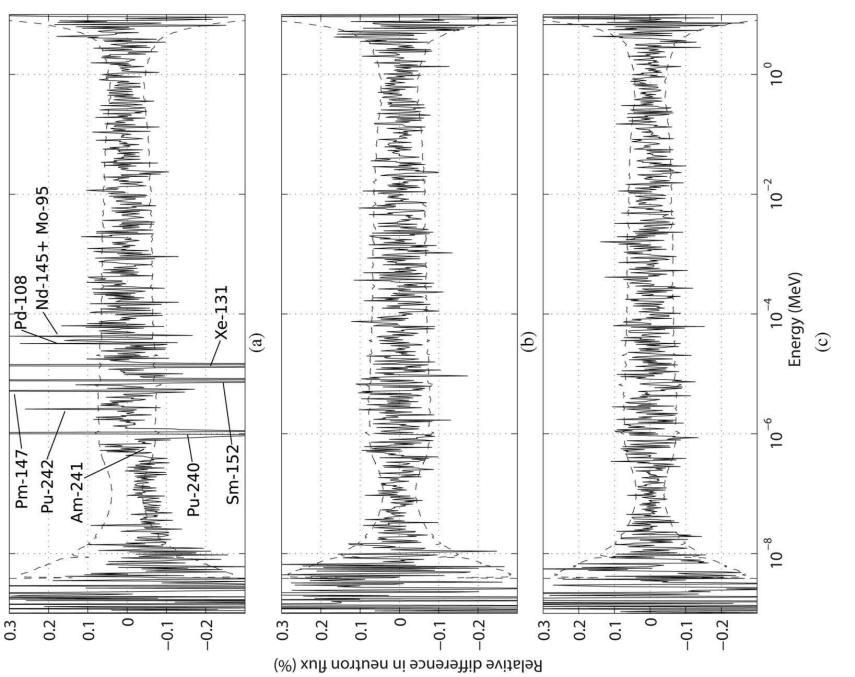

Fig. 3. Differences in neutron spectra of the PWR-BU case for three different variants of the TMS method: (a) $T_{\text{base}} = 0$ K, (b) $T_{\text{base}} = T_{\text{min}} - 300$ K, and (c) $T_{\text{base}} = T_{\text{min}}$. The nuclides corresponding to the difference peaks originating from the inaccurate scattering kernel have been identified in (a). The highest of these peaks, corresponding to ^{152}Sm, extends to 2%.

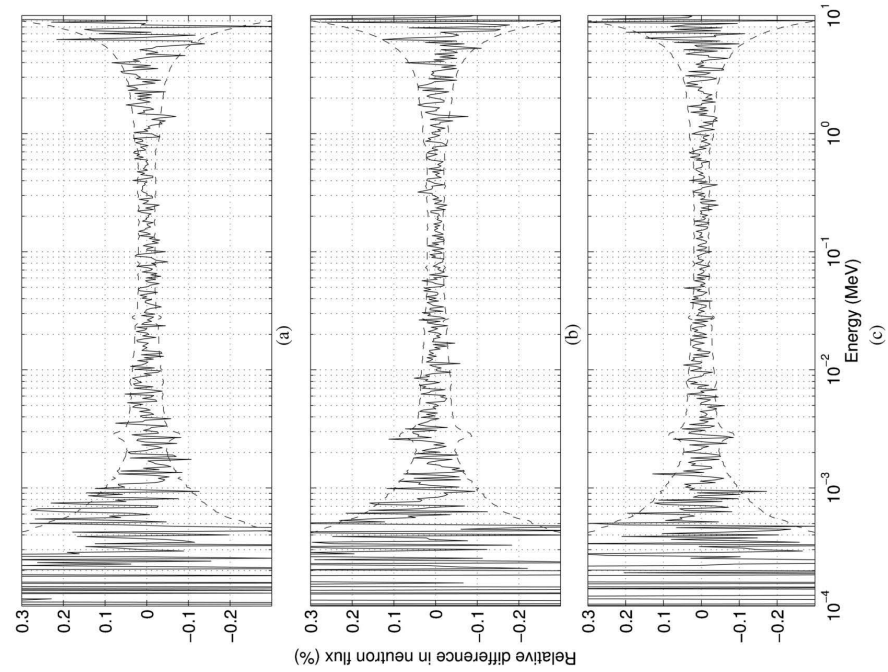

Fig. 5. Differences in neutron spectra of the SFR case for three different variants of the TMS method: (a) $T_{\text{base}} = 0$ K, (b) $T_{\text{base}} = T_{\text{min}} - 300$ K, and (c) $T_{\text{base}} = T_{\text{min}}$.

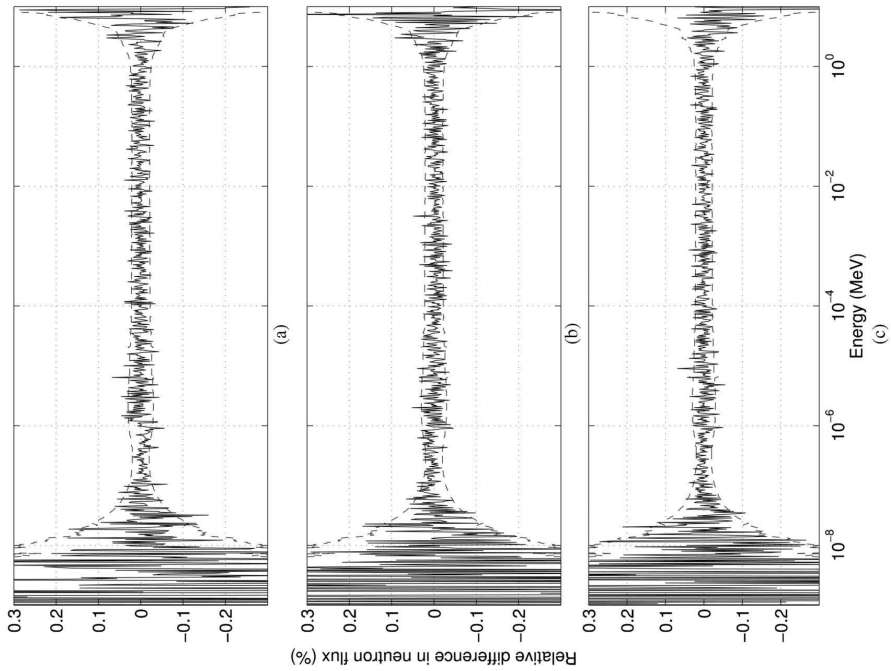

Fig. 4. Differences in neutron spectra of the HTGR case for three different variants of the TMS method: (a) $T_{\text{base}} = 0$ K, (b) $T_{\text{base}} = T_{\text{min}} - 300$ K, and (c) $T_{\text{base}} = T_{\text{min}}$.

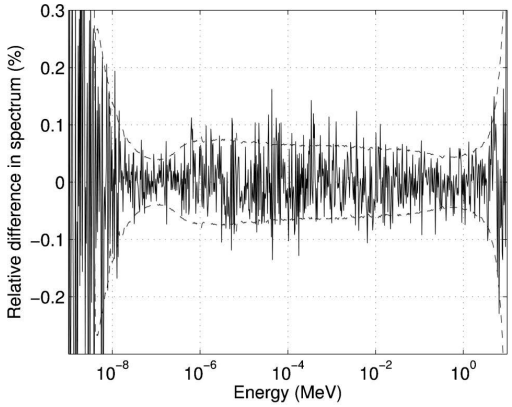

Fig. 6. Differences in neutron spectra of the PWR-BU case between the $T_{base} = 0$ K variant and the reference after introducing ten new nuclides in the list of DBRC nuclides in the reference solution.

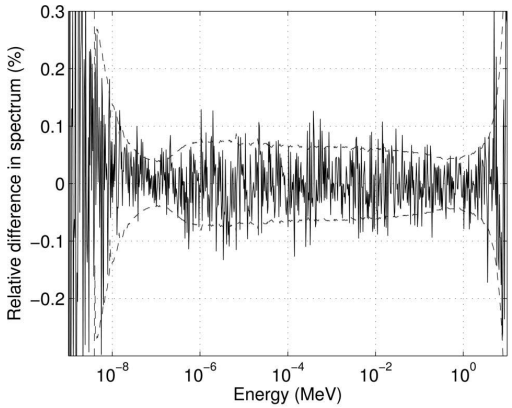

Fig. 7. Differences in neutron spectra of the PWR-BU case between the $T_{base} = T_{min}$ variant and the reference after introducing ten new nuclides in the list of DBRC nuclides in the reference solution.

the memory consumption in most of the cases because cross sections of the fuel materials need to be stored in one temperature only. However, in the HTGR case, it seems that storing the continuous-energy majorant cross sections consumes more memory than is saved in storing the basis cross sections. This is due to the relatively low number of nuclides appearing in the fresh HTGR fuel. Also, the dependence of the number of energy grid points on temperature can be recognized in the figures: The higher the temperature of the basis cross section, the fewer grid points are needed to reproduce the cross section at a specific tolerance and the less memory is required. This effect is greatest in the PWR-BU case, where the EBT variant consumes almost 30% less memory than the 0 K calculation.

From the calculation times in Table I, it can be seen that in most cases transport with the TMS method requires somewhat more calculational effort than conventional tracking methods. This is, however, not the case with the SFR cases and the PWR-Gd case with the highest basis temperature. In these cases, the multigroup tracking scheme of the reference calculation in optimization mode 2 is slower than TMS, which is based on continuous-energy majorant cross sections. The slowdown factors are greatest (2.13 to 12.50) in the case involving burned fuel. With numerous nuclides in the fuel composition, the sampling of nuclides at each collision site starts to take significant amounts of time, and the calculation slows down. The slowdown is emphasized in the 0 K case, in which the TMS sampling efficiency is rather poor. The differences in the performance results compared with earlier measures presented in Ref. 5 are due to two reasons: First, the majorant is chosen in a different way and, second, a bug that made the majorant cross section overly efficient at high energies in Ref. 5 has been fixed. In addition, it should be noted that the PWR-Gd case examined in the present paper involves Gd-doped rods, which seems to slow down the TMS calculations.

The advantages of elevating the basis cross-section temperatures can be easily seen in the performance measures: The calculation times decrease significantly with increasing cross-section temperature. By increasing the basis cross-section temperature from 0 K to T_{min}, the calculation time drops to 38% in the PWR-Gd case, 17% in the PWR-BU case, 37% in the HTGR case, and 64% in the SFR case. The effect is also seen in the significantly higher sampling efficiencies. It can also be concluded that a 300 K elevation in the cross-section temperature is enough to increase the efficiency quite notably. Hence, it might be a good idea to combine the TMS method with cross-section prebroadening in the case that the cross-section libraries are available only in ≥ 300 K steps.

VI. SUMMARY AND CONCLUSIONS

In this paper, the performance and accuracy of the target motion sampling temperature treatment technique were examined using three different variants of the technique. The first of the variants, as introduced in Ref. 3, involves cross sections at 0 K temperature. The idea behind the two other variants, in which the basis temperature is elevated above 0 K, was first presented in Ref. 5, and the theoretical background behind the idea was introduced in the present paper.

The accuracy of the three different TMS variants was studied through criticality eigenvalues and spectra of the systems by comparing the results with a reference in

which all cross sections were Doppler-broadened with NJOY. The TMS calculations were in very good agreement with the reference, and statistically significant differences existed in only one of the test cases. This case involved a PWR fuel assembly at 40 MWd/kgU burnup, modeled with the 0 K variant of the TMS.

It was found that the differences originated from the different treatment of the elastic scattering kernels: The 0 K TMS takes the effect of an energy-dependent cross section inherently into account for all nuclides and energies, whereas DBRC is used only for scattering from ^{238}U in the reference solution and the other TMS variants. After increasing the accuracy of the reference calculation by extending the usage of DBRC to several other nuclides, a perfect match between the results was obtained.

The elevation of the basis cross-section temperature above 0 K was found to increase the performance in terms of both calculation time and memory consumption. The calculation time savings compared with the 0 K TMS varied from 36% to 83%, depending on the case. It was also found out that a 300 K elevation in the basis temperature already brings a significant increase in performance. Thus, some calculation time could be saved by adjusting the cross-section temperatures before the TMS transport calculation using Doppler preprocessing. With regard to the memory consumption, the elevation of the basis temperature reduced the memory requirement by almost 30% in the PWR-BU test case, but in other cases the memory savings was insignificant.

In summary, the thermal treatment technique based on TMS has been successfully implemented in Serpent 2.1.14, and the use of elevated basis temperatures, the main topic of the present paper, brings a very welcome increase in the performance of the technique. The current implementation of the method reproduced the reference results, calculated using NJOY-broadened cross sections, within statistical accuracy. The method is very competitive for neutron transport in materials consisting of a moderate number of nuclides, and the method is feasible also for calculations involving numerous resonance absorbers.

ACKNOWLEDGMENTS

This work was partly funded from the NUMPS project of the Academy of Finland and the KÄÄRME project under the Finnish Research Program on Nuclear Power Plant Safety, SAFIR2014.

REFERENCES

1. G. YESILYURT, W. R. MARTIN, and F. B. BROWN, "On-the-Fly Doppler Broadening for Monte Carlo Codes," *Proc. 2009 Int. Conf. Mathematics, Computational Methods and Reactor Physics (M&C 2009)*, Saratoga Springs, New York, May 3–7, 2009, American Nuclear Society (2009).

2. G. YESILYURT, W. R. MARTIN, and F. B. BROWN, "On-the-Fly Doppler Broadening for Monte Carlo Codes," *Nucl. Sci. Eng.*, **171**, 239 (2012); http://dx.doi.org/10.13182/NSE11-67.

3. T. VIITANEN and J. LEPPÄNEN, "Explicit Treatment of Thermal Motion in Continuous-Energy Monte Carlo Tracking Routines," *Nucl. Sci. Eng.*, **171**, 165 (2012); http://dx.doi.org/10.13182/NSE11-36.

4. T. VIITANEN and J. LEPPÄNEN, "Explicit Temperature Treatment in Monte Carlo Neutron Tracking Routines—First Results," *Proc. PHYSOR 2012*, Knoxville, Tennessee, April 15–20, 2012, American Nuclear Society (2012).

5. T. VIITANEN and J. LEPPÄNEN, "Optimizing the Implementation of the Explicit Treatment of Thermal Motion—How Fast Can It Get?" *Proc. 2013 Int. Conf. Mathematics and Computational Methods Applied to Nuclear Science and Engineering (M&C 2013)*, Sun Valley, Idaho, May 5–9, 2013, American Nuclear Society (2013).

6. B. BECKER, R. DAGAN, and G. LOHNERT, "Proof and Implementation of the Stochastic Formula for Ideal Gas, Energy Dependent Scattering Kernel," *Ann. Nucl. Energy*, **36**, 470 (2009); http://dx.doi.org/10.1016/j.anucene.2008.12.001.

7. D. E. CULLEN and C. R. WEISBIN, "Exact Doppler Broadening of Tabulated Cross Sections," *Nucl. Sci. Eng.*, **60**, 199 (1976); http://dx.doi.org/10.13182/NSE76-1.

8. R. V. MEGHREBLIAN and D. K. HOLMES, *Reactor Analysis*, pp. 137–140, McGraw-Hill Book Company, New York (1960).

9. R. E. MacFARLANE and D. W. MUIR, "NJOY99.0 Code System for Producing Pointwise and Multigroup Neutron and Photon Cross Sections from ENDF/B Data," PSR-480, Los Alamos National Laboratory (2000).

10. J. LEPPÄNEN and T. VIITANEN, "New Data Processing Features in the Serpent Monte Carlo Code," *J. Korean Phys. Soc.*, **59**, 1365 (2011); http://dx.doi.org/10.3938/jkps.59.1365.

11. "MCNP—A General Monte Carlo *N*-Particle Transport Code," Version 5, LA-UR-03-1987, Los Alamos National Laboratory (2003).

12. E. E. SUNNY and W. R. MARTIN, "On-The-Fly Generation of Differential Resonance Scattering PDF," *Trans. Am. Nucl. Soc.*, **107**, 1124 (2012).

13. D. LEE, K. SMITH, and J. RHODES, "The Impact of ^{238}U Resonance Elastic Scattering Approximations on Thermal Reactor Doppler Reactivity," *Ann. Nucl. Energy*, **36**, 274 (2009); http://dx.doi.org/10.1016/j.anucene.2008.11.026.

14. T. MORI and Y. NAGAYA, "Comparison of Resonance Elastic Scattering Models Newly Implemented in MVP Continuous-Energy Monte Carlo Code," *J. Nucl. Sci.*

Technol., **46**, 793 (2009); http://dx.doi.org/10.1080/18811248.2007.9711587.

15. B. ROQUE et al., "Specification for the Phase 1 of a Depletion Calculation Benchmark Devoted to Fuel Cycles," NEA/NSC/DOC(2004)11, Nuclear Energy Agency, Organisation for Economic Co-operation and Development (2004).

16. M. D. DEHART and A. P. ULSES, "Benchmark Specification for HTGR Fuel Element Depletion," NEA/NSC/DOC(2009)13, Nuclear Energy Agency (2009).

17. "Japan's Experimental Fast Reactor Joyo Mk-I Core: Sodium-Cooled Uranium-Plutonium Mixed Oxide Fueled Fast Core Surrounded by UO_2 Blanket," in "International Handbook of Evaluated Reactor Physics Benchmark Experiments," NEA/NSC/DOC(2006)1, Nuclear Energy Agency (2006).

18. J. LEPPÄNEN, "Two Practical Methods for Unionized Energy Grid Construction in Continuous-Energy Monte Carlo Neutron Transport Calculation," *Ann. Nucl. Energy*, **36**, 878 (2009); http://dx.doi.org/10.1016/j.anucene.2009.03.019.

19. J. LEPPÄNEN and A. ISOTALO, "Burnup Calculation Methodology in the Serpent 2 Monte Carlo Code," *Proc. PHYSOR 2012*, Knoxville, Tennessee, April 15–20, 2012, American Nuclear Society (2012).

PUBLICATION V

Temperature majorant cross sections in Monte Carlo neutron tracking

Nucl. Sci. Eng., Accepted for publication Aug 31, 2014.

Temperature Majorant Cross Sections in Monte Carlo Neutron Tracking

Revised version: March 31, 2015

(Mr.) Tuomas Viitanen and (Dr.) Jaakko Leppänen

VTT Technical Research Centre of Finland

tuomas.viitanen@vtt.fi, jaakko.leppanen@vtt.fi

Send Correspondence to:

Tuomas Viitanen

VTT Technical Research Centre of Finland

P. O. Box 1000, FI-02044 VTT, Finland

Email: tuomas.viitanen@vtt.fi

Telephone: +358 40 763 1963

No. of pages: 35

No. of tables: 3

No. of figures: 8

Temperature Majorant Cross Sections in Monte Carlo Neutron Tracking

Tuomas Viitanen and Jaakko Leppänen

Abstract

This article discusses the generation of temperature majorant cross sections, the type of cross sections required by two separate techniques related to Monte Carlo neutron tracking, namely the Doppler-broadening rejection correction (DBRC) and Target Motion Sampling (TMS) temperature treatment methods. In the generation of these cross sections the theoretically infinite range of thermal motion must be artificially limited by applying some sort of a cut-off condition, which affects both the accuracy and the performance of the calculations. In this article, a revised approach for limiting the thermal motion is first introduced and, then, optimal cut-off conditions are determined for both the traditional majorant, commonly used in DBRC implementations and old implementations of the TMS method, and the revised majorant.

It turns out that using the revised type of temperature majorant cross sections increases the performance of the TMS method slightly, but no practical difference is observed with the DBRC method. It is also discovered that in ordinary reactor physical calculations the cut-off conditions originally adopted from the SIGMA1 Doppler-broadening code can be significantly relieved without compromising the accuracy of the results. By updating the cut-off conditions in the majorant generation, the CPU time requirement of Serpent 2.1.17 is reduced by 8–23 % in TMS calculations and by 1–6 % in problems involving DBRC.

Keywords: Monte Carlo, DBRC, on-the-fly, Doppler-broadening, temperature majorant cross section

I. Introduction

Thermal motion affects the neutronics of a reactor system in basically two ways. First, the thermal oscillation of nuclei changes the probabilities at which neutrons interact with matter, affecting the reaction rates and mean free paths within the system. Second, thermal motion also has impact on the collision physics of scattering events.

In conventional Monte Carlo neutron transport, the effects on reaction rates are taken into account by using effective, Doppler-broadened cross sections that are prepared before the transport calculation. The effect of thermal motion on scattering is usually modeled during the transport calculation by sampling the target motion from a Maxwellian-based distribution each time an elastic scattering occurs, and solving the kinetics of the event according to the sampled velocity. The same procedures cannot be directly applied for bound nuclides (for instance H in H_2O) in the thermal energy region, so for these nuclides the Doppler-broadening and elastic scattering models have to be completed using additional thermal scattering data consisting of special bound scattering cross sections and so-called $S(\alpha, \beta)$ data for secondary particle distributions [1].

Previously, two separate but loosely related techniques that supplement the conventional way of modeling the thermal motion have been introduced. Doppler-broadening rejection correction (DBRC) method, as described in Ref. [2], accounts for the effect of thermal motion induced variation of scattering cross sections on the secondary particle distributions of elastic scattering events. This effect has been traditionally omitted by assuming energy-independent scattering cross sections, but the effect is known to be important especially in case of heavy nuclides with significant resonances in the epithermal energy region. The Target Motion Sampling (TMS) temperature treatment technique, for its part, is a neutron tracking method for taking the effect of thermal motion on reaction rates into account on-the-fly during a Monte Carlo neutron tracking calculation. On-the-fly temperature treatment techniques in general can be used to reduce the memory consumption of transport problems involving materials at numerous temperatures, for example in multi-physics applications of Monte Carlo. The TMS method has been introduced in English by the authors in Refs. [3,4], but it was recently learned that a similar method has been previously presented in a Russian journal [5] and has been routinely used, for example, in the Monte Carlo transport code PRIZMA for many years [6].

The TMS and DBRC methods have two features in common. First, both of the methods are based on rejection sampling and, second, the rejection sampling techniques of both

methods require a special type of cross sections, called temperature majorant cross sections in the current article. The generation of these cross sections is otherwise straightforward, but the generation process involves determining of a finite range for the relative velocity between the neutron and the target nucleus, which is physically not bounded by any maximum value. Hence, some kind of approximation must be applied in the generation process and this approximation is open to discussion. Traditionally, the thermal motion has been limited by simply truncating the Maxwellian velocity distribution of the target and using the corresponding maximum and minimum relative velocity to determine the energy range of thermal motion. The cut-off condition commonly used in the current implementations of the DBRC method is 16 $k_{\mathrm{B}}T$, where k_B is the Boltzmann constant and T is the temperature of the target nucleus. This condition has been adopted from the SIGMA1 Doppler-broadening code (Ref. [7]) by the developers of the DBRC method [2], and the same condition has been further also used in the implementation of the TMS method in Monte Carlo reactor physics code Serpent[a] due to historical reasons [3].

It has been shown by Becker et al. that using the SIGMA1 cut-off condition results in the correct scattering kernel [2], but no studies were found on the practicality of this cut-off condition. Since both DBRC and TMS are based on rejection sampling, their performance is strongly dependent on the truncation of the thermal motion. Hence, the cut-off deserves a thorough discussion. The previous results in Ref. [8] and the fact that a less-conservative 9 $k_{\mathrm{B}}T$ cut-off has been successfully used together with the on-the-fly temperature treatment method in PRIZMA give rise to a suspicion that the 16 $k_{\mathrm{B}}T$ cut-off is overly conservative and, thus, leads to a waste of computing resources at least when applied with the TMS method.

A new approach for truncating the thermal motion was previously introduced by the authors in the M&C 2013 conference [8]. This idea is refined in the current article, and the properties of this "revised" majorant are compared to the "traditional" majorants. In addition, suggestions for the cut-off conditions to be used with both of the majorant types are determined by applying the majorants in practical calculations involving TMS and DBRC. Since the field of application for the TMS and DBRC methods is limited to free atoms at thermal and resolved resonance energy regions, bound-atom scattering and the unresolved resonance region are left outside the current article.

An introduction to the temperature majorant cross sections and their applications in Monte Carlo neutron tracking is provided in Section II., and the two methods for limiting the range of thermal motion in the majorant generation are presented in Section III. In

[a]For a complete and up-to-date description, visit Serpent website — http://montecarlo.vtt.fi

Section IV., properties of the majorant types are first studied and, then, optimal values of the corresponding cut-off conditions are determined for reactor applications. Serpent 2 is updated in light of the new results and final performance measures are also provided in the same Section. The last Section V. is left for summary and conclusions.

II. Temperature Majorants in Monte Carlo Neutron Tracking

The temperature majorant Σ_{maj} of a cross section Σ is defined

$$\Sigma_{\mathrm{maj}}(E) = \max_{E' \in [E_{\mathrm{min}}, E_{\mathrm{max}}]} \Sigma(E') \,, \tag{1}$$

where E' represents the relative (or target-at-rest) energies between a neutron with laboratory frame-of-reference (L-frame) energy E and a target nucleus in thermal motion[b]. The energy range of E' is limited by energies E_{min} and E_{max} that define the range of thermal motion.

With DBRC, the cross section Σ in Eq. (1) is always an elastic scattering cross section at zero Kelvin, $\Sigma_{\mathrm{s}}(E', 0\ \mathrm{K})$. With TMS method the majorant is based on the total cross section, which may be either a zero Kelvin cross section or a Doppler-broadened effective cross section at an above-zero temperature. Thus, the majorant cross section depends on both the temperature of the basis cross section, T_{base}, and the temperature difference between the T_{base} and the majorant, ΔT. By including the explicit temperature dependencies in Eq. (1), definition

$$\Sigma_{\mathrm{maj}}(E, \Delta T, T_{\mathrm{base}}) = \max_{E' \in [E_{\mathrm{min}}, E_{\mathrm{max}}]} \Sigma(E', T_{\mathrm{base}}) \,, \tag{2}$$

is obtained. Temperature majorant cross sections are illustrated in Figure 1.

The only open question in the majorant generation is related to the choosing of the energy range of the target-at-rest energies E' in Eq. (2). It is practical to approach this problem via velocities, which can be easily converted to energies using the classical relation between the kinetic energy and the velocity

$$E' = \frac{1}{2} M_{\mathrm{n}} v'^2 \,, \tag{3}$$

where M_n is the neutron mass. The relative velocity of the neutron to the target, also known as the target-at-rest velocity, can be obtained from equation

$$v' = \sqrt{v^2 + V_{\mathrm{t}}^2 - 2 v V_{\mathrm{t}} \mu} \,, \tag{4}$$

[b]To be precise, also each cross section Σ_x for which $\Sigma_x(E) \geq \Sigma_{\mathrm{maj}}(E)$ can be considered a temperature majorant cross section of $\Sigma(E')$, but usually it is practical to choose the majorant according to Eq. (1).

where v is the velocity of the neutron, V_t is the velocity of the target and μ is the cosine between the directions of the neutron and the target motion. The target velocity distribution is traditionally assumed to obey the Maxwell-Boltzmann distribution

$$P_\mathrm{MB}(V_\mathrm{t}, T, A)dV_\mathrm{t} = \frac{4}{\sqrt{\pi}}\gamma(T,A)^3 V_\mathrm{t}^2 e^{-\gamma(T,A)^2 V_\mathrm{t}^2} dV_\mathrm{t}\,, \tag{5}$$

where

$$\gamma(T, A) = \sqrt{\frac{AM_\mathrm{n}}{2k_\mathrm{B}T}}\,, \tag{6}$$

A is the ratio of the nuclide mass to M_n.

It should be noted that the distribution in Eq. (5) has an infinite tail and, consequently, an unambiguous maximum velocity for the target cannot be specified. Hence, to get a finite interval for the target-at-rest velocity v' and the corresponding energy, some kind of approximation is required. Two different ways, namely a traditional and a new, revised way, of limiting the thermal motion are presented in Section III. Before going into details of these approximations, the application of the temperature majorant cross sections with the DBRC and TMS methods is shortly presented in Sections II.A. and II.B., respectively.

II.A. Doppler-broadening Rejection Correction

In Monte Carlo neutron tracking, the kinetics of the elastic scattering events can be solved using a few different approaches. The simplest way to treat elastic scattering from free atoms is to assume that the target nucleus is at rest or, in other words, at zero Kelvin temperature. This approximation corresponds to so-called asymptotic scattering kernel, which omits all up-scattering effects, but acts as a reasonable approximation at relatively high neutron energies.

At lower energies, the thermal motion of the target nuclei must be taken into account to correctly model the slowing-down of neutrons. In the conventional free gas treatment, when an elastic scattering event occurs, the velocity of the target nuclide i is first sampled from distribution [9]

$$P_\mathrm{FGT}(V_\mathrm{t}, \mu, T, A_i)dV_\mathrm{t}d\mu = C\Big\{\frac{v'}{2v}P_\mathrm{MB}(V_\mathrm{t}, T, A_i)\Big\}dV_\mathrm{t}d\mu\,, \tag{7}$$

where C is a constant, and the kinetics are then solved conserving the energy and momentum. This sampling scheme involves the assumption that the scattering cross section of the target nuclide is constant and, thus, the secondary particle distributions correspond to a cross section independent scattering kernel.

More detailed description of the elastic scattering requires that also the energy dependence of the scattering cross section is taken into account. This can be done by inserting an additional rejection in the conventional sampling procedure[c]. With this so-called Doppler-broadening rejection correction the target velocity distribution becomes [2]

$$P_{\mathrm{DBRC}}(V_{\mathrm{t}},\mu,T,A_i)dV_{\mathrm{t}}d\mu = C'\Big\{\frac{\Sigma_{\mathrm{s},i}(v',0)}{\Sigma_{\mathrm{maj,s},i}(v,T,0)}\Big\}\Big\{\frac{v'}{2v}P_{\mathrm{MB}}(V_{\mathrm{t}},T,A_i)\Big\}dV_{\mathrm{t}}d\mu\,, \tag{8}$$

where the cross sections $\Sigma_{\mathrm{s},i}(v',0)$ and $\Sigma_{\mathrm{maj,s},i}(v,T,0)$ are the zero Kelvin elastic scattering cross section of nuclide i and its temperature majorant, respectively. In practice, the relative velocity of the neutron to target, v', is first sampled from Eq. (7) and the sample is accepted or rejected according to the ratio of the zero Kelvin cross section to the majorant. The whole sampling procedure is repeated until a successful sample for v' is obtained.

II.B. TMS Temperature Treatment Technique

The target motion sampling (TMS) temperature treatment technique is a Monte Carlo neutron tracking technique that takes the effect of thermal motion on reaction rates into account on-the-fly during transport calculation. The method was introduced for the first time in English-written journals in Ref. [3] by the authors. It was, however, recently found out that a similar method has been introduced already in 1984 in a Russian journal [5] and that the method is routinely used in at least two Russian Monte Carlo codes [6, 16]. The optimization of the TMS method has been covered in recent articles [4, 8] and the usage of the method together with reaction rate estimators has been studied in Refs. [17, 18]. These references provide a complete description of the method, while only the parts essential to the current article are shortly summarized in the following.

In the TMS tracking scheme the path lengths of neutrons are sampled based on a macroscopic majorant cross section

$$\Sigma_{\mathrm{maj,TMS}}(v) = \sum_i \Sigma_{\mathrm{maj,TMS},i}(v) \tag{9}$$

$$= \sum_i g(v, T_{\mathrm{max},i} - T_{\mathrm{base}}, A_i)\Sigma_{\mathrm{maj},i}(v, T_{\mathrm{max},i} - T_{\mathrm{base}}, T_{\mathrm{base}})\,, \tag{10}$$

[c]Also other ways of dealing with the energy dependence have been introduced: in Ref. [10] a technique based on direct sampling of the secondary neutron velocity has been examined, while in Refs. [11, 12] the correction is done by varying the particle weights. It is also possible to include the effect by using $S(\alpha,\beta)$ tables based on the analytical scattering kernel, which has been covered in sequential Refs. [13–15].

where index i runs over all nuclides in a material zone,

$$\begin{aligned} g(v,T,A_i) &= \int_0^\infty \int_{-1}^1 \frac{v'}{2v} P_{\mathrm{MB}}(V_\mathrm{t},T,A_i) dV_\mathrm{t} d\mu \\ &= \left(1+\frac{1}{2\gamma(T,A_i)^2 v^2}\right) \mathrm{erf}\Big(\gamma(T,A_i)v\Big) + \frac{e^{-\gamma(T,A_i)^2 v^2}}{\sqrt{\pi}\gamma(T,A_i)v} \end{aligned} \tag{11}$$

is the Doppler-broadening integral for constant cross section, erf is the error function, $T_{\mathrm{max},i}$ is the maximum temperature of nuclide i and $\Sigma_{\mathrm{maj},i}$ is the temperature majorant cross section of nuclide i. It should be noted that that the TMS majorant cross sections are otherwise similar to any temperature majorants, but the TMS majorant is additionally multiplied by the g-factor[d].

As a result of the path length sampling, a new collision point candidate is obtained. At each collision point, the target nuclide is first sampled based on the nuclide-wise majorant cross sections. Thus, probability of sampling nuclide i is

$$P_i = \frac{\Sigma_{\mathrm{maj,TMS},i}(v)}{\Sigma_{\mathrm{maj,TMS}}(v)}. \tag{12}$$

Then, the velocity of the nuclide is sampled from distribution in Eq. (7) with T equal to the local temperature at the collision point, and the target-at-rest energy corresponding to the collision v' is calculated. Finally, the collision point is accepted or rejected according to rejection sampling criterion

$$\xi < \frac{g(v,T-T_\mathrm{base},A_i)\Sigma_{\mathrm{tot},i}(v',T_\mathrm{base})}{\Sigma_{\mathrm{maj,TMS},i}(v)} = \frac{g(v,T-T_\mathrm{base},A_i)}{g(v,T_{\mathrm{max},i}-T_\mathrm{base},A_i)} \frac{\Sigma_{\mathrm{tot},i}(v',T_\mathrm{base})}{\Sigma_{\mathrm{maj},i}(v,T_{\mathrm{max},i}-T_\mathrm{base},T_\mathrm{base})}, \tag{13}$$

where ξ is a uniformly distributed random variable on the unit interval. If the sample is rejected, the tracking procedure restarts by sampling of a new path length beginning from the newly rejected collision point. In case the collision point is accepted, a reaction is sampled based on the reaction cross sections at T_base corresponding to the target-at-rest velocity v'. The neutron tracking proceeds according to the sampled reaction.

[d]The multiplication is required for correct modeling of the reaction rates at low energies and is related to the fact that the integral of the distribution from which the target velocities are sampled (Eq. (7)) is greater than unity at low energies. This modification is perhaps the most intuitive in case of potential scatterers with constant low-energy cross sections: these cross sections are increased in the Doppler-broadening process, but the corresponding increase in the reaction rates could not be captured in the TMS transport without multiplying the cross sections by g.

III. Truncation of Thermal Motion in Temperature Majorant Generation

In both of the applications studied in this article, introduced in Sections II.A. and II.B., the temperature majorant cross sections are applied with rejection sampling techniques. When using DBRC, the temperature majorant related rejection criterion is

$$\xi < \frac{\Sigma_{\mathrm{s},i}(v',0)}{\Sigma_{\mathrm{maj,s},i}(v,T,0)} \tag{14}$$

and the rejection sampling criterion of TMS is shown in Eq. (13). These rejection sampling criteria set the one and only basic requirement for the majorant cross section: For the rejection sampling to be valid, the sampled cross sections in Eqs. (13) and (14) shall not exceed the majorant cross section or, in practice, the exceedings must be rare. The majorant exceedings are a sign that part of the target velocity samples (DBRC) or collision points (TMS) may be accepted even though they should be rejected, which introduces bias in the secondary particle distributions of elastic scattering events and the neutron path lengths.

At the same time, the efficiency of the rejection sampling depends strongly on the conservativity of the majorant cross section: if the majorant cross section is large compared to the sampled cross sections, the proportion of accepted samples is small. Hence, determining the cut-offs for thermal motion in the temperature majorant generation is all about balancing between efficiency and accuracy. An optimal majorant would be as small as possible such that the proportion of majorant violations still does not introduce error in the results.

III.A. Traditional Method

The traditional approach for choosing the limits for the target-at-rest velocity v' in the temperature majorant generation has been used in DBRC implementations and in the implementations of the TMS or TMS-like methods in Serpent and PRIZMA [5]. For the DBRC implementations, the exact cut-off condition dates back to an article by Rothenstein, Ref. [19], which started the long journey towards the present DBRC technique. In this article Rothenstein suggested that "a finite range of energies near the neutron energy E can be used in the same manner as in the Doppler broadening code of Cullen", referring to the SIGMA1 code [7]. In the appendix of Ref. [7] it is discussed that since most of the contribution to the Doppler-broadening integral comes from relative velocities x that are close to the neutron velocity y (both dimensionless quantities), the integration can be optimized by limiting the range of x to a narrow region around y. It is, then, shown that if the integration range is chosen as $x \in [y-4, y+4]$, the error from truncation will remain smaller than 0.1 % even if the cross

sections vary by four orders of magnitude in the vicinity of y.

The same cut-off was later on adopted by Becker et al. to determine the energy ranges used in the generation of temperature majorant cross sections for the DBRC [2] method. The integration limits of Cullen can be interpreted as, first, truncating the Maxwellian velocity distribution of the target to a maximum value of

$$V_{\mathrm{t,max}} = h\sqrt{\frac{2k_{\mathrm{B}}\Delta T}{AM_{\mathrm{n}}}} \tag{15}$$

(converted into conventional units) with $h = 4.0$ and, then, determining the range of relative velocities or energies accordingly. Thus, the maximum target-at-rest energy E' corresponds to a head-on collision with $\mu = -1$ in Eq. (4) and the minimum energy is obtained for a parallel collision with $\mu = 1$. For nuclide i and neutron energy E the energy range of thermal motion is bounded by

$$E_{\min}(E, \Delta T, A_i) = \left(\sqrt{E} - h\sqrt{\frac{k_{\mathrm{B}}\Delta T}{A_i}}\right)^2 \tag{16}$$

and

$$E_{\max}(E, \Delta T, A_i) = \left(\sqrt{E} + h\sqrt{\frac{k_{\mathrm{B}}\Delta T}{A_i}}\right)^2. \tag{17}$$

As mentioned in the introduction, the cut-off $h = 4.0$ corresponds to a target energy of 16 $k_{\mathrm{B}}T$.

Needless to say, the original $h = 4.0$ truncation of Cullen is very well justified in the calculation of effective cross sections. Since this cut-off is in any case used when Doppler-broadening the scattering cross sections with NJOY [20], using the same cut-off in the generation of the temperature majorants for DBRC ensures that the kinetics of the elastic scattering events are resolved in consistence with other parts of the neutron transport, specifically reaction rates of scattering events. Hence, the $h = 4.0$ truncation, as adopted by Becker et al., is a logical and safe choice also for the DBRC majorant generation.

In practice it is, however, possible to use also other cut-off conditions for the DBRC majorants without disturbing the neutron transport. The justification for the original truncation, presented in Ref. [7], basically means that with $h = 4.0$ the energy of the target is outside the limits specified by Eqs. (16) and (17) with a probability smaller than 0.1 % even in the worst case scenario when the cross section increases by four orders of magnitude just outside the limits corresponding to the neutron energy E. Since the neutrons end up at these worst-case energies only rarely in normal criticality source calculations and since the error estimate is conservative, the proportion of target samples violating the limits is in practice decades smaller than 0.1 %, i.e. extremely small. When this is combined with the fact that small

errors in the secondary particle distributions have only minor effect on the neutron transport as a whole, reducing the value of the h parameter seems feasible.

Similar reasoning applies also for the TMS majorants with the exception that the errors arising from truncation lead to falsely accepted collision points, which affects the neutron transport in a different way than errors in the secondary neutron distributions. In the implementation of the TMS-like method in PRIZMA the cut-off $h = 3.0$, corresponding to 9 $k_{\mathrm{B}}T$ in terms of energy, has been successfully used [5]. Also this indicates that the conservativity could be, in practice, significantly reduced from the original value of $h = 4.0$ for the TMS majorants.

III.B. Revised Method

The "traditional" way of generating temperature majorant cross sections works perfectly well in practice, but by examining the applications of the temperature majorants, more arguable ways of choosing the energy boundaries can be figured out. In both of the rejection sampling criteria, Eqs. (14) and (13), the value of the sampled cross section depends on v', which is in both cases sampled based on the distribution in Eq. (7). Hence, also the range of sampled cross sections depends on this distribution and, consequently, the energy boundaries in the majorant generation should be based on the distribution in Eq. (7), not the Maxwell-Boltzmann distribution. It is also practical to associate the majorant with a confidence level, $1-Q$, to study the effect of the conservativity of the majorant on the results and performance.

This was the basic idea behind the method introduced in Ref. [8], where different confidence levels were used to determine the maximum target velocities corresponding to a head-on and a parallel collision. However, a more natural way for choosing the boundaries was found after a second consideration. Namely, the confidence level can also be associated directly with the relative velocities such that all possible collision angles are properly taken into account. When defined this way, the physical meaning of the confidence level is much clearer than with the method in Ref. [8].

The two extremes of the relative velocity corresponding to the new energy boundaries, $v'_{\mathrm{min,rev}}$ and $v'_{\mathrm{max,rev}}$, can be resolved by integrating the probability distribution of target velocities, Eq. (7). However, to provide for direct determination of the boundaries for the relative energy, the integration must be done with respect to the relative velocity v' and the cosine between the relative velocity vector and the neutron direction, ν. By comparing Eqs. (7) and (11) it can be seen that the normalization factor C in front of Eq. (7) is, in fact, just the inverse of $g(v, T, A)$. By replacing C with this factor and changing to the previously

mentioned integration variables, equations

$$\begin{aligned} P(v' < z) &= \frac{1}{g(v, \Delta T, A)} \int_0^z \int_{-1}^1 \frac{2}{\sqrt{\pi} v} \gamma^3 v'^3 e^{-\gamma^2 (v^2 + v'^2 - 2vv'\nu)} dv' d\nu \\ &= \frac{1}{g(v, \Delta T, A)} \Big\{ \frac{1}{2\gamma\sqrt{\pi} v^2} \Big(e^{-\gamma^2 (v+z)^2} (z - v) - e^{-\gamma^2 (v-z)^2} (v + z) + 2e^{-\gamma^2 v^2} v \Big) \\ &\quad + (\frac{1}{2} + \frac{1}{4\gamma^2 v^2}) \Big(\mathrm{erfc}\big((v - z)\gamma\big) + \mathrm{erfc}\big((v + z)\gamma\big) - 2\mathrm{erfc}\big(v\gamma\big) \Big) \Big\} \end{aligned} \tag{18}$$

and

$$\begin{aligned} P(v' > z) &= \frac{1}{g(v, \Delta T, A)} \int_z^\infty \int_{-1}^1 \frac{2}{\sqrt{\pi} v} \gamma^3 v'^3 e^{-\gamma^2 (v^2 + v'^2 - 2vv'\nu)} dv' d\nu \\ &= \frac{1}{g(v, \Delta T, A)} \Big\{ \frac{1}{2\gamma\sqrt{\pi} v^2} \Big(e^{-\gamma^2 (v+z)^2} (v - z) + e^{-\gamma^2 (v-z)^2} (v + z) \Big) \\ &\quad + (\frac{1}{2} + \frac{1}{4\gamma^2 v^2}) \Big(\mathrm{erf}\big((v - z)\gamma\big) + \mathrm{erf}\big((v + z)\gamma\big) \Big) \Big\} \end{aligned} \tag{19}$$

are obtained for the tail probabilities. In these equations, erfc is the complementary error function and the dependence of γ on ΔT and A, as specified in Eq. (6), is not explicitly shown for clarity. Furthermore, by using conditions

$$P(v' < v'_{\mathrm{min,rev}}) = \frac{Q}{2} \tag{20}$$

and

$$P(v' > v'_{\mathrm{max,rev}}) = \frac{Q}{2} \tag{21}$$

it is possible to numerically resolve the range of relative velocities corresponding to the confidence level Q, using for example the Newton's method [21]. The relative velocities v' can, further, be converted to the energy range boundaries using Eq. (3).

The small difference between the revised and the traditional energy boundaries in the majorant generation is demonstrated in Figure 2, where the differences in E_{min} and E_{max} between the traditional and the revised majorant with $Q = 1.541 \times 10^{-8}$ are plotted for ^{238}U. The specific Q-value was chosen such that the widths of the energy ranges $E_{\mathrm{max}} - E_{\mathrm{min}}$ are roughly equal at 6.7 eV.

As it can be seen in Figure 2, if the width of the energy range is matched at the low resonance region, the revised method leads to somewhat wider energy ranges than the traditional method at low energies below about 1 eV and at high energies above about 1 keV. While the widths of the energy ranges are similar at the resonance region, the usage of the revised

method shifts both the upper and the lower energy boundaries upwards by about one milli-eV compared to the traditional method.

IV. Results

Serpent version 2.1.15 with a few modifications is used as the testing platform in the calculations performed in Sections IV.B.–IV.D., and the results in Section IV.E. are calculated with a newly-updated version, Serpent 2.1.17. In all of the calculations, the energy threshold for free gas treatment is increased to infinity such that the target velocities are sampled for each elastic scattering event, regardless of the neutron energy. Doppler-broadening rejection correction (DBRC) is applied to ^{238}U between 0.4 eV and 20 keV in all of the calculations. Due to the findings in Ref. [4], usage of DBRC is extended to nuclides ^{95}Mo, ^{108}Pd, ^{131}Xe, ^{145}Nd, ^{147}Pm, ^{152}Sm, ^{239}Pu, ^{240}Pu, ^{242}Pu and ^{241}Am in addition to ^{238}U in the PWR-BU case.

The cross section library is based on JEFF-3.1.1 and has been processed using 0.001 reconstruction tolerance for high accuracy. All of the calculations are performed using 12 OpenMP threads on Intel Xeon X5690 CPUs running at 3.47 GHz.

IV.A. Test Cases

The effect of the temperature majorants on performance is examined in three realistic test cases with slightly different characteristics. The test cases are the same as the thermal systems in Refs. [4] and [17].

Gd-doped Pressurized Water Reactor Assembly (PWR-Gd)

The first "PWR-Gd" case involves a 17x17 PWR fuel assembly with 16 Gadolinium-doped fuel rods in an infinite two dimensional lattice. The geometry and material definitions of the fuel assembly are from a NEA benchmark [22]. The only differences to the benchmark specifications are related to temperatures: the moderator temperature is risen to 600 K for simplicity and the originally flat temperature profiles of the fuel rods are replaced with 3-step distributions such that the pellets are divided into three equi-thick annular regions with temperatures 600 K, 900 K and 1200 K from outside in.

PWR-Gd Assembly at 40 MWd/kgU burnup (PWR-BU)

The second case is abbreviated "PWR-BU" and features the previously introduced "PWR-Gd" bundle irradiated to 40 MWd/kgU burnup. The irradiated material compositions were

obtained by running a separate burnup calculation using Serpent 2.1.14. The resulting compositions contain 241 actinide and fission product nuclides with cross sections available in the data libraries.

High Temperature Gas Cooled Reactor System (HTGR)

The "HTGR" test case consists of TRISO particles within graphite matrix in an infinite three dimensional lattice. The specifications of the TRISO particles and the composition of the graphite matrix are based on a NEA benchmark for HTGR fuel depletion [23], and the lattice pitch is 0.16341 cm. The fuel kernel in the spherical TRISO particles is divided in two equally thick parts such that the innermost 0.0125 cm is at 1800 K temperature and the outer layer is at 1200 K. The temperature of all other materials is 1200 K.

IV.B. Traditional Versus Revised Majorant

Since the revised way of choosing the majorant energies differs substantially from the traditional way, comparison of the two different majorant types must be done indirectly. Probably the best way to judge, which of the two methods performs better in neutron transport is through the sampling efficiencies and sampling violations: if majorant A leads to a higher average sampling efficiency with the same or a lower proportion of majorant exceedings than majorant B, then A can be considered superior to B.

Since the traditional majorant with original SIGMA1 cutoffs is very conservative and, consequently, the majorant exceedings are very rare, it is practical to modify the majorant for the following study. The original multiplier $h = 4.0$ in the cut-off condition of the traditional majorant (Eqs. (15), (16) and (17)) is replaced by $h = 3.0$, which makes the majorant less conservative.

Before the efficiencies can be compared, the confidence level $1 - Q$ must be determined for the revised majorant such that the proportion of majorant exceedings becomes roughly equal to that from calculations with the modified traditional majorant. The task is complicated by the fact that this Q-parameter may differ between the systems and it also depends on whether the proportion of TMS majorant or DBRC majorant exceedings is considered. Reason for this is that while the Q parameter determines the proportion of sampled relative velocities outside the energy range used in the majorant generation, the proportion of majorant exceedings depends also on the cross sections in the rejection sampling criteria. The cross sections, for their part, depend on whether scattering cross sections (DBRC) or total cross sections (TMS) are considered, the nuclides for which the methods are applied, the temperatures of the cross

sections and, additionally, the neutron flux spectrum affects the energies at which these cross sections are applied in the rejection sampling. The Q parameters were determined for each of the three different test cases with trial and error. To rationalize the amount of work, Q parameters were only determined at an accuracy of 10^{-6}.

The results of the calculations are provided in Tables I and II for TMS and DBRC, respectively. For both of the studies, the average sampling efficiencies and proportions of majorant exceedings $P_{\mathrm{err,\ maj}}$ are provided. The statistical deviations of the sampling efficiencies are negligible (< 0.01 %) and are, therefore, not shown in the tables. In addition, the proportions of target velocity samples outside the energy range used in the TMS majorant generation are provided for the TMS calculations. The proportion of target velocity samples for which the target-at-rest energy E' is below $E_{\min}(E)$ is denoted with $P_{\mathrm{err,low}}$ and, correspondingly, the proportion of samples above $E_{\max}(E)$ is $P_{\mathrm{err,high}}$. It should be noted that the proportion of majorant exceedings is significantly lower than the sum of boundary violations, because the cross section corresponding to the "illegal" target velocity sample is only rarely larger than the majorant at resonance energies, where a significant proportion of the interactions takes place. At low energies with $1/v$ cross sections the situation is different and samples violating the lower energy boundary always result in majorant exceedings. Number of active neutron histories was 500 million in all of the calculations.

The results for the TMS calculations, presented in Table I, show that the revised majorant results in slightly higher TMS sampling efficiencies with a lower proportion of erroneous samples than the traditional majorant. The increase in efficiency should also affect the transport calculation times, but the differences are small compared to the uncertainties associated with these measures. The main idea of the revised majorant can be seen in the proportions of upper and lower majorant boundary violations: for the revised majorant the proportion of velocity samples below the lower boundary is equal to the proportion of samples that violated the upper boundary, while the distribution of erroneous samples is non-symmetrical for the traditional majorant.

Instead, the results of the DBRC calculations in Table II show no practical difference between the traditional and the revised majorant. The proportions of erroneous samples are the same within statistical accuracy and also the DBRC sampling efficiencies are practically equal for both of the majorant types.

It should be noted that also the majorant generation times affect the overall performance of the different majorant types. As can be seen in the Tables I and II, the majorant generation times for the revised majorant are about 2–7 times higher than for the traditional majorant,

since the revised boundaries are more complicated to calculate. In typical calculations with good statistics the 0.7 %–1.5 % increase in the TMS sampling efficiency is expected to compensate the extra time spent in the majorant generation, because most of the calculation time is in any case spent in the neutron transport. However, in calculations with poor statistics the traditional majorant may actually outperform the revised majorant. The overhead in the majorant generation could be at least somewhat reduced by optimizing the algorithm used in the calculation of the revised majorant boundaries.

IV.C. Optimal Level of Conservativity in TMS Applications

Determining an optimal level of conservativity for the majorant cross section is problematic, since on the other hand one would like to use as small, or as non-conservative, majorant as possible to get high efficiency, but on the other hand using of a too tight cut-off condition for the thermal motion will introduce significant error in the calculations, which of course should be avoided by all means. Experimenting with the majorants also has shown that the optimal level of conservativity is problem-dependent and, to avoid errors, the determination of the majorant should be based on a realistic transport problem that is as sensitive to the majorant violation errors as possible.

An unambiguous worst-case-scenario is impossible to determine, but some clue on the properties of the problem can be obtained based on previous experience. First of all, the majorant violations tend to have the most effect on the neutron spectrum and k_{eff} in systems in which the neutrons experience a lot of collisions with the fuel material at the energy region of resolved resonances. A good example of such a system is the HTGR test case, introduced in Section IV.A., which involves very small fuel particles dispersed in a graphite matrix[e]. Second, while the temperature difference between T_{base} and the maximum temperature of the system has only moderate effect on the proportion of majorant violations, a larger temperature difference leads to more significant violations, which are expected to have stronger impact on the transport. As 3000 K is usually considered the maximum temperature required in reactor physical analysis, this is chosen as the fuel temperature in the HTGR system. To maximize the temperature difference, the cross sections are kept at $T_{\text{base}} = 0$ K temperature, which also enables re-using of the sampled velocities in the solution of scattering kinetics [4]. Thus,

[e]Since this system is in practice a quasi-homogeneous mixture of moderator and fuel, the probability of a neutron to interact with the fuel material during the slowing-down process is very high compared to, for instance, LWR geometries. In addition, the fact that the moderator atoms in graphite are relatively heavy ($A_{\text{C}} \approx 12$) increases the number of scattering events a neutron experiences during the process compared to lighter moderators like hydrogen. This increases the probability of a neutron to end up at energies corresponding to resonances in the fuel material at some point of the slowing-down process and, thus, makes the interactions more probable on average.

DBRC is not required in these calculations.

The effect of the majorant conservativity on the accuracy of the TMS method is studied in this HTGR system with 3000 K fuel. For the sake of simplicity, the main comparison is based on different k_{eff} estimates that should all agree with the reference solution within statistics as long as the transport is physically valid. The three k_{eff} estimators are

1. the "analog estimator", which is the ratio of source weights in subsequent neutron generations

2. the "implicit estimator", defined

$$k_{\text{eff,imp}} = \frac{\overline{\nu} R_{\text{f}}}{R_{\text{f}} + R_{\text{c}} - R_{(\text{n,xn})} + R_{\text{L}}} , \tag{22}$$

   where $\overline{\nu}$ is the average number of neutrons emitted in a fission, R_f, R_c and R_L are fission, total capture and leakage rates, respectively, and

$$R_{(\text{n,xn})} = \sum_y (y-1) R_{(\text{n,yn})} \tag{23}$$

   is the neutron production rate from (n,xn) reactions.

3. the "collision estimator", which is the ratio of $\overline{\nu} R_{\text{f}}$ to the neutron source size.

In addition, the results are confirmed by comparing the neutron flux spectra of relevant calculations to the reference solution.

The calculations were run using 500 million active neutron histories. The results are provided in Figure 3 for the revised majorant and in Figure 4 for the traditional majorant. The reference value value of k was calculated using 2.5 billion neutron histories and NJOY-broadened cross sections [20]. The neutron flux spectra of two relevant calculations with revised majorants are compared to the reference in Figure 5. The neutron spectra are normalized to constant total flux.

In Figure 3 it can be seen that all three k-estimators agree within statistics with each other and with the reference solution as long as $Q \leq 10^{-4}$. With higher values the k_{eff} estimators deviate from each other significantly and also the k_{eff} values are no longer in agreement with the reference solution. The same effect can be seen in Figure 5: with $Q = 10^{-4}$ the neutron flux spectra are in perfect agreement, but with $Q = 3.2 \times 10^{-4}$ a small positive bias is observed in the lower epithermal region. Thus, it seems that the optimal value for the Q parameter is near $Q = 10^{-4}$. What comes to the results of the traditional majorant in Figure 4, the optimal

boundary is slightly harder to recognize, but side-by-side comparison of neutron spectra and k reveals that $h = 2.8$ is the lowest acceptable value.

IV.D. Optimal Level of Conservativity in DBRC Applications

The same system that was used in the previous section suits also very well in the studying of the effect of the majorant conservativity on the functionality of the DBRC method. As the total effect of the Doppler-Broadening Rejection Correction on the eigenvalue is about 1500 pcm, it is hard to figure out a practical reactor physical problem that would be more sensitive to the correct functionality of the correction.

All the cross sections are NJOY-originated, i.e. no TMS method nor the Doppler preprocessor of Serpent is used in the calculations [24]. Eigenvalue results of the calculations are provided in Figures 6 and 7 for the revised and the traditional majorant, respectively.

Results indicate that the conservativity of the majorant can be decreased even lower than in the TMS case before the effect of the majorant violations on k_{eff} can be recognized. With the revised majorant the highest Q value for which the eigenvalue estimators are still correct is $Q = 3.2 \times 10^{-3}$ and for the traditional majorant the smallest acceptable value seems to be $h = 2.3$. These results were also confirmed by comparing the neutron spectra, which agreed with the reference solution within statistical deviation. The flux comparison for the revised majorant is shown in Figure 8.

IV.E. Performance Results

On basis of the previous results, presented in Sections IV.B.– IV.D., the revised majorant type was chosen as the default majorant in Serpent version 2.1.17 for both TMS and DBRC majorants. The implementation of the traditional majorants was, however, left in the code as a compiler option to provide for easy experimenting in the future. Value of $Q = 2.0 \times 10^{-5}$ was, conservatively, chosen as the default confidence level in the majorant generation for the TMS. In case the traditional majorant generation is activated, the default value for the temperature cut-off is, again conservatively, the same as in the PRIZMA code, $h = 3.0$. It was decided to use the same default values of Q and h also for the DBRC majorants even though the previous results indicate that also less conservative majorants could be used without compromising the accuracy of important reactor physical results. As the computational overhead from DBRC is relatively small, it was decided to be rather safe than sorry in this matter.

In the previous articles on the TMS method [4, 8, 17], the performance of the method has been compared to standard Serpent calculations with reduced optimization, i.e. Serpent

calculations that have been purposely slowed down. This choice was made because Serpent with full optimization takes advantage of pre-calculated macroscopic cross sections and this kind of optimization cannot be used together with the TMS method. Thus, if the performance of TMS was compared to Serpent with full optimization, it would be self-evident that a significant part of the overhead would be caused by the lack of pre-calculated macroscopic cross sections, especially in problems involving hundreds of nuclides. However, the slowing-down of the reference calculations has its own downsides as it was noticed for example in [4], where the TMS method appeared even faster than the reference in a couple of cases. This kind of results make little sense as the TMS should always increase the computational effort compared to conventional transport in fair a comparison due to the sub-unitary sampling efficiency. To get consistent results, it was decided to make an "unfair" comparison for the TMS in the current article and use full optimization in the reference calculations. However, calculation times are provided also for corresponding calculations with reduced optimization, optimization mode 2 to be precise [25]. The performance comparison for the DBRC calculations is more straightforward, since DBRC works inherently with full optimization.

The temperature of the cross sections, T_{base}, was chosen as the minimum temperature of each nuclide in the system in the TMS calculations. Performance measures of the calculations are provided in Table III. The Table also includes results and figures-of-merit (FOM) for two estimators in the TMS cases. First of these estimators is for the total (energy-integrated) capture rate in the corner rods (PWR-Gd and PWR-BU cases) or all fuel material (HTGR case). The second estimator calculates the capture rate around the 6.7 eV resonance of ^{238}U ($6.5 - 6.9$ eV), which was found to be problematic in Reference [17] when using the TMS[f].

The TMS results show that by reducing the conservativity of the majorant from the original $h = 4.0$ value it is possible to save 8–23 % of the transport calculation time without affecting the results. This applies also for the neutron flux spectra and the results of the reaction rate estimators, which are omitted here for the sake of simplicity. The performance is somewhat better for the revised majorant with the chosen conservativity parameters h and Q, but as it can be seen in the proportions of majorant-violating samples, $P_{\text{err,maj,TMS}}$, the revised majorant with $Q = 2 \times 10^{-5}$ also leads to a slightly larger fraction of majorant failures. With the newly implemented revised majorant the overhead from using TMS, unfairly compared to Serpent 4 with full optimization, is 1.24 in the PWR case, 1.18 in the HTGR case and 12.33 in the PWR-BU case.

[f]It was found in [17] that the variances and, consequently, also the Figures-of-Merit for all estimators including the flux estimator are significantly affected by the usage of the TMS method near strong resonances.

The majorant cross section has significantly less effect on the performance of the DBRC method. In Serpent the overhead from the DBRC method is about 4-8 % in these test cases when using the traditional temperature majorant with $h = 4.0$, as suggested by the developers of the DBRC method. By reducing the conservativity of the majorant cross section, this overhead can be reduced by a couple of percents.

It should also be noted that the performance of the TMS method with the old $h = 4.0$ majorant has somewhat improved from the previous results presented in [4]. This is due to many small changes in the implementation, perhaps most important of which was changing from a point-wise to a histogram representation for the temperature majorant cross sections.

V. Summary and Conclusions

In this article, a revised approach for generation of the temperature majorant cross sections was first introduced, and the revised majorants were compared to those generated using the traditional approach. An optimal cut-off condition was sought by applying TMS and DBRC in a reactor system in which the majorant violations are expected to have very large effect on the transport calculation. After finding optimal values for the f and Q parameters, which affect the conservativity of the traditional and revised type majorants, the temperature majorant generation in Serpent 2.1.17 was optimized according to the new results. Finally, the updated version was applied in three thermal reactor systems with different characteristics to estimate the effects of the updated temperature majorants on the performance of the transport calculation.

The difference between the traditional and revised majorants was rather small: In TMS applications the revised majorant resulted in 0.7–1.5 % larger sampling efficiencies than the traditional majorant with practically the same proportion of majorant violations. Instead, no practical difference between the two majorant types was observed in DBRC applications. Thus, switching to more complicated revised majorants does not make any difference in DBRC implementations, but with TMS method the introduction of the revised truncation can bring a slight increase in the performance of the transport calculation. In short calculations the benefit from using the revised boundaries may be lost due to more time consuming majorant generation in the pre-processing phase, but in typical calculations with good statistics the usage of the revised majorants pays off.

What comes to the TMS calculations, the results showed that the calculation times are reduced by about 8–23 % when applying the suggested, less conservative cut-off conditions. In calculations involving only a few resonance absorbers the overhead from using the TMS

method is well-feasible, about 1.2-1.3. However, with numerous temperature-dependent nuclides the overhead compared to a Serpent calculation with full optimization increases to about 12. Most of this slow-down comes from the fact that Serpent normally pre-calculates the macroscopic cross sections and this kind of optimization cannot be applied together with the TMS method as long as all of the nuclides are treated temperature-dependently.

Switching to the less-conservative temperature majorants decreased also the computational overhead from the DBRC method significantly. Nevertheless, since the original overhead from using DBRC in Serpent was only 4–8 %, the overall gain in performance remained small.

It should be kept in mind that reducing the conservativity of the temperature majorants introduces systematic bias in the transport calculation. According to the results of the current study the chosen values for Q and h are conservative enough for the errors to remain statistically insignificant in practical calculations with realistic reactor systems. Thus, the results should be fine as long as for example neutron flux, reaction rates, cross sections or any derived parameter like k is calculated using criticality source simulation.

The same does not necessarily apply when studying very narrow energy regions, for example using mono-energetic external neutron sources. The biases from majorant violations are concentrated at narrow energy intervals in the vicinity of strong resonances, and these errors are lost in the background when integrating over wider intervals. However, with very narrow energy binning and certain energies the bias may become significant. When using mono-energetic neutron sources this kind of errors are, luckily, easy to recognize automatically by analyzing the proportion of majorant violations. In case the proportion seems suspiciously large, it is possible to increase the conservativity of the majorant via user input.

In the light of the results presented above, it seems in any case reasonable to provide the users of Monte Carlo codes with a possibility to manipulate the conservativity of the DBRC and TMS majorants.

Acknowledgments

This work was partly funded from the NUMPS project of the Finnish Academy the KÄÄRME project under the Finnish Research Programme on Nuclear Power Plant Safety SAFIR2014.

REFERENCES

[1] MCNP X-5 Monte Carlo Team, "MCNP — a General Monte Carlo N-Particle Transport Code," Version 5, LA-UR-03-1987, Los Alamos National Laboratory (2003).

[2] B. Becker, R. Dagan and G. Lohnert, "Proof and implementation of the stochastic formula for ideal gas, energy dependent scattering kernel," *Ann. Nucl. Energy*, **36**, 470–474 (2009).

[3] T. Viitanen and J. Leppänen, "Explicit treatment of thermal motion in continuous-energy Monte Carlo tracking routines", *Nucl. Sci. Eng.*, **171**, 165-173 (2012).

[4] T. Viitanen and J. Leppänen, "Target Motion Sampling Temperature Treatment Technique With Elevated Basis Cross Section Temperatures", *Nuc. Sci. Eng.*, Accepted

[5] V.N. Ogibin and A.I. Orlov, "Majorized cross-section method for tracking neutrons in moving media", *Voprosy Atomnoj Nauki i Techniki, Metodoki i Programmy*, **2(16)**, 6–9 (1984), *In Russian.*

[6] Y.Z. Kandiev et al., "PRIZMA Status", *Proc. SNA+MC2013.* Paris, France, 27–31 October, 2013.

[7] D.E. Cullen and C.R. Weisbin, "Exact Doppler Broadening of Tabulated Cross Sections", *Nucl. Sci. Eng.*, **60**, 199–229 (1976).

[8] T. Viitanen and J. Leppänen, "Optimizing the Implementation of the Explicit Treatment of Thermal Motion — How Fast Can It Get?", *Proc. M&C 2013*, Sun Valley, ID, May 5–9, 2013.

[9] R.R. Coveyou, R.R. Bate and R. K. Osborn, "Effect of Moderator Temperature upon Neutron Flux in Infinite, Capturing Medium", *J. Nucl. Energy*, **2**, 153–167 (1956).

[10] E.E. Sunny and W.R. Martin, "On-The-Fly Generation of Differential Resonance Scattering PDF", *Trans. Am. Nucl. Soc.*, **107**, 1124–1127 (2012).

[11] D. Lee, K. Smith and J. Rhodes, "The Impact of ^{238}U Resonance Elastic Scattering Approximations on Thermal Reactor Doppler Reactivity", *Ann. Nucl. Energy*, **36**, 274–280 (2009).

[12] T. Mori and Y. Nagaya, "Comparison of Resonance Elastic Scattering Models Newly Implemented in MVP Continuous-Energy Monte Carlo Code", *J. Nucl. Sci. Tech.*, **46**, 793–798 (2009).

[13] M. Ouisloumen and R. Sanchez, "A Model for Neutron Scattering Off Heavy Isotopes That Accounts for Thermal Agitation Effects", *Nucl. Sci. Eng.*, **107**, 189–200 (1991).

[14] W. Rothenstein, "Proof of the formula for the ideal gas scattering kernel for nuclides with strongly energy dependent scattering cross sections", *Ann. Nucl. Energy*, **31**, 9–23 (2004).

[15] R. Dagan, "On the use of $S(\alpha, \beta)$ tables for nuclides with well pronounced resonances", *Ann. Nucl. Energy*, **32**, 367–377 (2005).

[16] A.N. Ivanov and N.V. Ivanov, "Accounting for the thermal motion of atoms in media in neutron transport simulation by the Monte Carlo method", *Journal Voprosy atomnoj nauki i techniki, Matematicheskoe modelirovanie physicheskikh processov*, **4**, 25-32 (2003).

[17] T. Viitanen and J. Leppänen, "Effect of the Target Motion Sampling Temperature Treatment Method on the Statistics and Performance", *Proc. SNA+MC2013*. Paris, France, 27–31 October, 2013.

[18] T. Viitanen, J. Leppänen and B. Forget, "Target Motion Sampling Temperature Treatment Technique with Track-length Estimators in OpenMC - Preliminary results", PHYSOR 2014, Kyoto, Japan, 28th September – 3rd October, 2014 (submitted).

[19] W. Rothenstein, "Effect of Upscattering by Heavy Nuclides on Doppler Changes of Resonance Absorption", *Proc. ENS Conference 1994*, Tel Aviv, Israel, 23–26 January, 1994.

[20] R. E. MacFarlane and D. W. Muir, "NJOY99.0 Code System for Producing Pointwise and Multigroup Neutron and Photon Cross Sections from ENDF/B Data," PSR-480, Los Alamos National Laboratory (2000).

[21] E. Kreyszig, "Advanced Engineering Mathematics", 8th edition, John Wiley & Sons inc., New York, (1999).

[22] B. Roque et al., "Specification for the Phase 1 of a Depletion Calculation Benchmark devoted to Fuel Cycles", NEA/NSC/DOC(2004)11, OECD/NEA (2004).

[23] M.D. DeHart and A. P. Ulses, "Benchmark Specification for HTGR Fuel Element depletion", NEA/NSC/DOC(2009)13, Nuclear Energy Agency, Organization for Economic Cooperation and Development (2009).

[24] J. Leppänen and T. Viitanen, "New Data Processing Features in the Serpent Monte Carlo Code", *J. Korean Phys. Soc.*, **59**, 1365–1368 (2011).

[25] J. Leppänen and A. Isotalo, "Burnup Calculation Methodology in the Serpent 2 Monte Carlo Code", *Proc. PHYSOR-2012*, Knoxville, TN, 15–20 April, 2012.

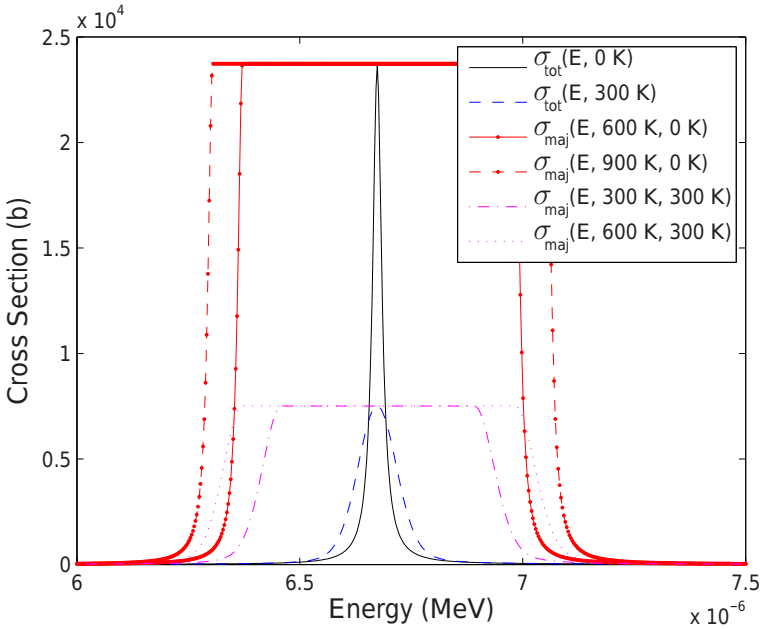

Figure 1 *Majorant cross sections for different basis temperatures T_{base} (0 K and 300 K) and temperature differences (300 K, 600 K and 900 K) for the total cross section of ^{238}U around the 6.7 eV resonance.*

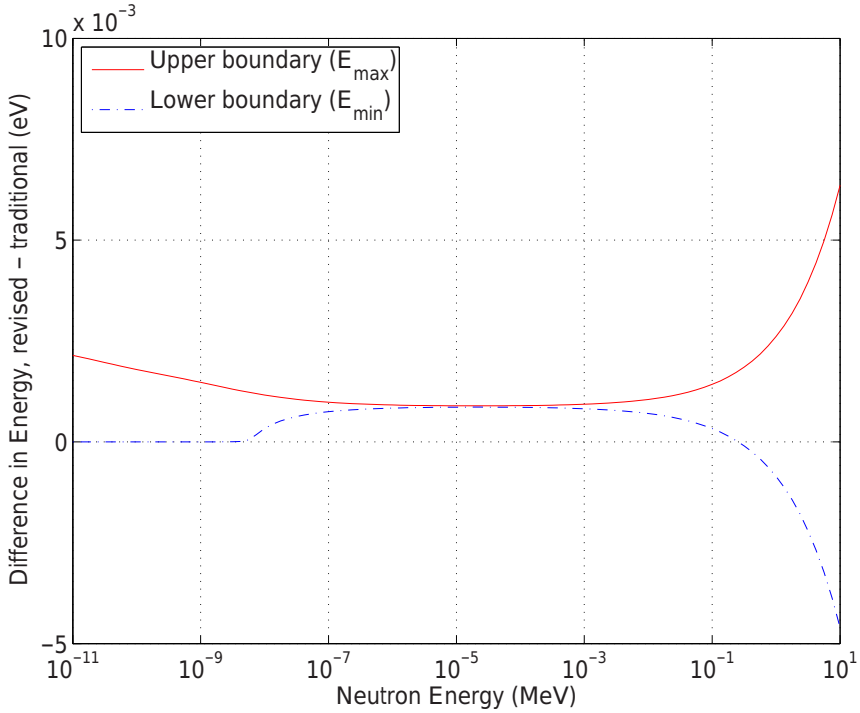

Figure 2 *The energy ranges are defined differently for the revised and the traditional majorant.*

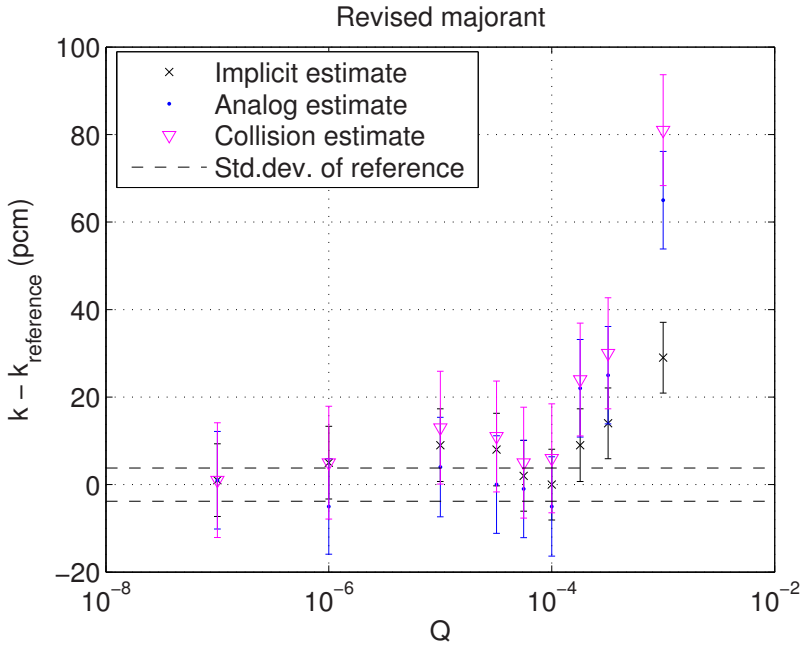

Figure 3 *Effect of the conservativity of the TMS majorant on three* k_{eff} *estimators of a HTGR system. The effect is studied for the revised majorant and, thus, the conservativity is manipulated through the Q parameter. The error bars correspond to two standard deviations, 2* σ*.*

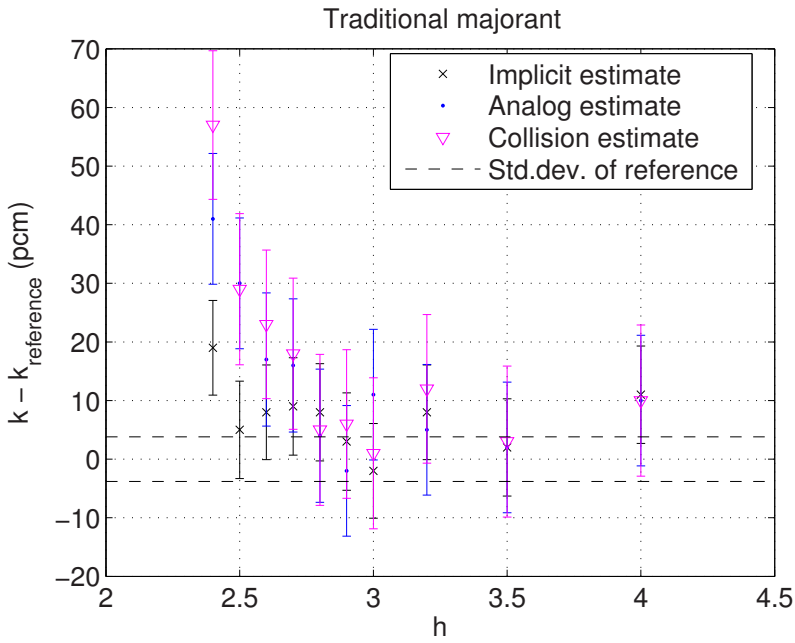

Figure 4 *Effect of the conservativity of the TMS majorant on three different k_{eff} estimators of a HTGR system. The conservativity is manipulated through the h parameter of the traditional majorant.*

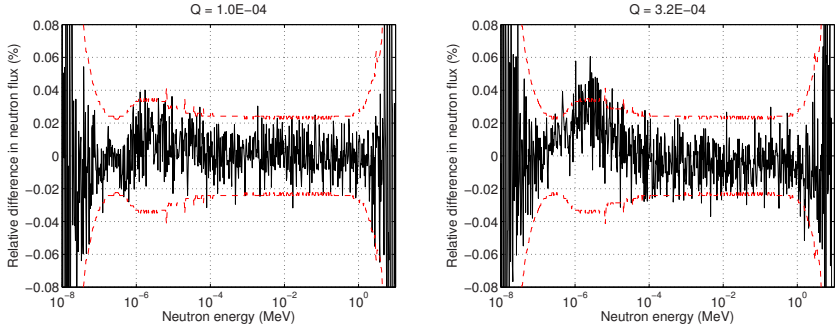

Figure 5 *Comparison of neutron flux spectra between two TMS calculations and NJOY-based reference solution. With Q=1E-4 (left) the flux spectrum corresponds to the reference, but with Q=3.2E-4 (right) significant differences can be recognized. The dashed line corresponds to two standard deviations.*

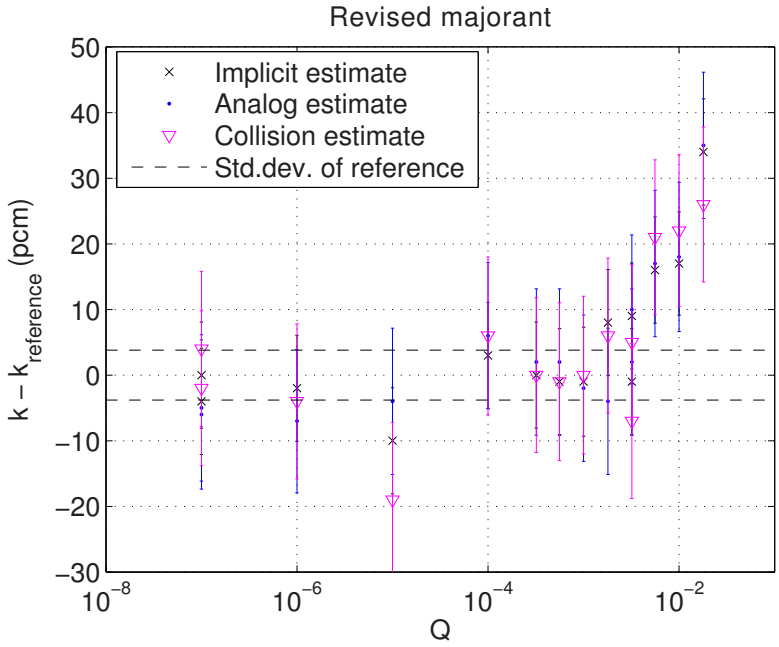

Figure 6 *Effect of the conservativity of the revised DBRC majorant on three k_{eff} estimators of a HTGR system.*

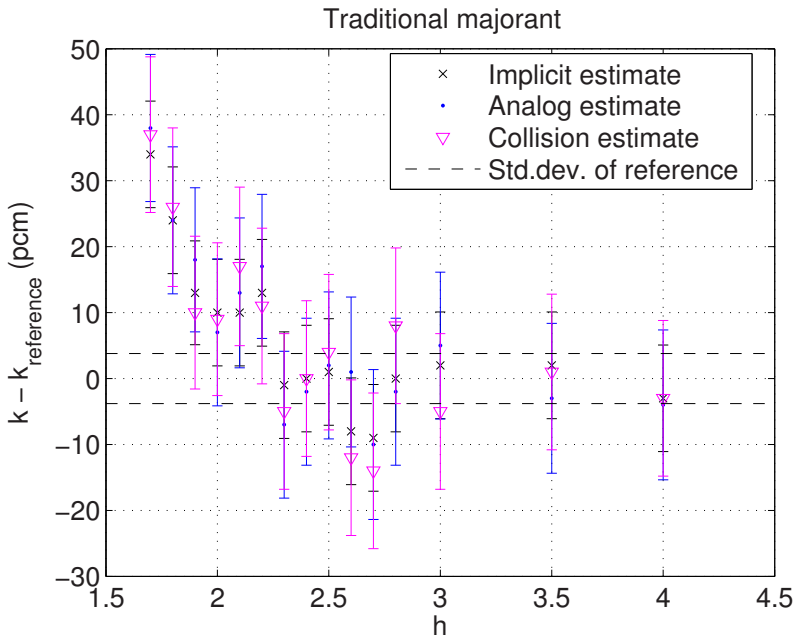

Figure 7 *Effect of the conservativity of the traditional DBRC majorant on three different* k_{eff} *estimators of a HTGR system.*

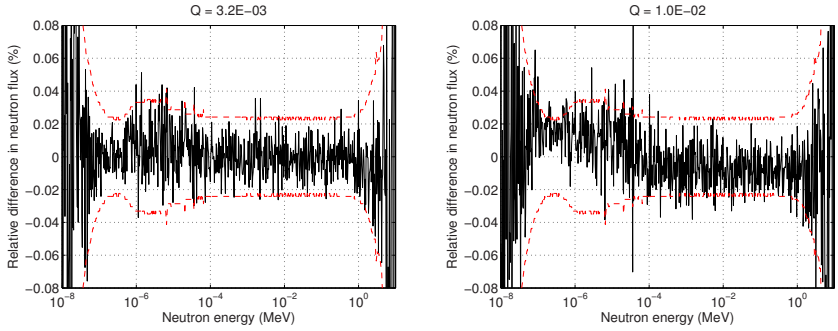

Figure 8 *Comparison of neutron flux spectra between two DBRC calculations and NJOY-based reference solution. With h=3.2E-3 (left) the flux spectrum corresponds to the reference, but with h=1.0E-2 (right) significant differences can be recognized.*

Table I *Performance comparison between traditional and revised majorant when applying TMS method in three thermal systems.*

	PWR-Gd	PWR-BU	HTGR
TMS with traditional majorant, $h = 3.0$			
Majorant generation time (s)	1.08	343.05	0.77
Transport time (h)	3.15	34.62	9.14
k_{eff}	1.15513 ± 6 pcm	0.93453 ± 6 pcm	1.20196 ± 6 pcm
TMS sampling efficiency (%)	51.7	50.4	47.3
$P_{\text{err,maj,TMS}}$	4.02E-07 ± 9E-09	4.43E-07 ± 9E-09	5.13E-07 ± 1E-08
$[P_{\text{err,low}}, P_{\text{err,high}}]$	[9.9E-06, 1.3E-05]	[9.8E-06, 1.3E-05]	[9.3E-06, 1.5E-05]
TMS with revised majorant			
Q	1.8E-05	1.8E-05	1.8E-05
Abs. / Rel. majorant generation time (s/-)	7.92 / 7.36	772.40 / 2.25	3.88 / 5.03
Abs. / Rel. transport time (h/-)	3.11 / 0.99	35.02 / 1.01	8.56 / 0.94
k_{eff}	1.15524 ± 6 pcm	0.93462 ± 6 pcm	1.20206 ± 6 pcm
TMS sampling efficiency (%)	53.0	51.9	48.0
$P_{\text{err,maj,TMS}}$	3.76E-07 ± 8E-09	3.89E-07 ± 8E-09	4.65E-07 ± 1E-08
$[P_{\text{err,low}}, P_{\text{err,high}}]$	[9.0E-06, 9.0E-06]	[8.5E-06, 8.5E-06]	[9.0E-06, 9.1E-06]

Table II *Performance comparison between traditional and revised majorant when applying DBRC method in three thermal systems.*

	PWR-Gd	PWR-BU	HTGR
DBRC with traditional majorant, $h = 3.0$			
Majorant generation time (s)	0.12	18.39	0.09
Transport time (h)	2.35	4.76	6.98
k_{eff}	1.15515 ± 6 pcm	0.93455 ± 6 pcm	1.20200 ± 5 pcm
DBRC sampling efficiency (%)	5.56	5.63	4.49
$P_{\text{err,maj,DBRC}}$	10.0E-08 ± 3E-09	9.9E-08 ± 3E-09	6.0E-08 ± 3E-09
DBRC with revised majorant			
Q	2.2E-05	2.1E-05	2.1E-05
Abs. / Rel. majorant generation time (s/-)	0.64 / 5.26	38.11 / 2.07	0.50 / 5.69
Abs. / Rel. transport time (h/-)			
k_{eff}	1.15512 ± 6 pcm	0.93447 ± 6 pcm	1.20200 ± 5 pcm
DBRC sampling efficiency (%)	5.57	5.63	4.47
$P_{\text{err,maj,DBRC}}$	10.3E-08 ± 3E-09	9.8E-08 ± 3E-09	6.2E-08 ± 3E-09

Table III *Final performance results for three test cases. The relative (rel.) values are calculated with respect to the "Reference" calculation, an ordinary Serpent calculation with DBRC and full optimization. The errors correspond to one sigma.*

	PWR-Gd	PWR-BU	HTGR
Number of active neutron histories	10^9	5×10^8	5×10^8
Reference, h=4.0			
k_{eff}	1.15523	0.93453	1.20248
Δk_{eff} (pcm)	2	2	4
Transport time (h)	5.2	2.7	7.5
Memory requirement (GB)	3.4	91.2	1.1
$P_{\text{err,maj,DBRC}}$	3.3E-11	0.0E+00	0.0E+00
FOM, Total Capture Rate ($\frac{1}{\text{s}}$)	4.1E+04	5.4E+04	1.4E+06
FOM, Capture Rate Around 6.7 eV ($\frac{1}{\text{s}}$)	9.2E+02	8.7E+02	1.1E+05
Reference with reduced optimization			
Abs. / Rel. Transport time (h/-)	7.2 / 1.39	24.4 / 9.04	10.5 / 1.40
Reference without DBRC			
$k - k_{\text{ref}}$ (pcm)	134 ± 3	135 ± 3	717 ± 5
Abs. / Rel. Transport time (h/-)	4.9 / 0.94	2.5 / 0.92	7.2 / 0.97
TMS with Traditional Majorant, h=4.0			
$k_{\text{TMS}} - k_{\text{ref}}$ (pcm)	1 ± 3	0 ± 3	1 ± 5
Abs. / Rel. Transport time (h/-)	7.2 / 1.39	43.0 / 15.96	10.1 / 1.35
Abs. / Rel. Memory requirement (GB/-)	2.5 / 0.72	34.0 / 0.37	1.0 / 0.91
TMS Sampling efficiency (%)	39.3	38.1	38.1
$P_{\text{err,maj,TMS}}$	3.4E-10	3.9E-10	2.4E-10
Abs. / Rel. FOM, Tot. Capt. ($\frac{1}{\text{s}}$/-)	2.9E+04 / 0.72	3.2E+03 / 0.06	1.0E+06 / 0.74
Abs. / Rel. FOM, Capt. Around 6.7 eV ($\frac{1}{\text{s}}$/-)	4.6E+02 / 0.50	3.7E+01 / 0.04	7.3E+04 / 0.65
TMS with Traditional Majorant, h=3.0			
$k_{\text{TMS}} - k_{\text{ref}}$ (pcm)	-2 ± 3	3 ± 3	7 ± 5
Abs. / Rel. Transport time (h/-)	6.6 / 1.26	34.4 / 12.76	9.2 / 1.22
Abs. / Rel. Memory requirement (GB/-)	2.5 / 0.72	34.0 / 0.37	1.0 / 0.91
TMS Sampling efficiency (%)	51.7	50.4	47.4
$P_{\text{err,maj,TMS}}$	3.9E-07	4.5E-07	4.9E-07
Abs. / Rel. FOM, Tot. Capt. ($\frac{1}{\text{s}}$/-)	3.0E+04 / 0.74	4.0E+03 / 0.07	1.2E+06 / 0.86
Abs. / Rel. FOM, Capt. Around 6.7 eV ($\frac{1}{\text{s}}$/-)	4.8E+02 / 0.52	5.1E+01 / 0.06	8.5E+04 / 0.75
TMS with Revised Majorant, $Q = 2 \times 10^{-5}$			
$k_{\text{TMS}} - k_{\text{NJOY}}$ (pcm)	3 ± 3	1 ± 3	-1 ± 5
Abs. / Rel. Transport time (h/-)	6.4 / 1.24	33.2 / 12.33	8.8 / 1.18
Abs. / Rel. Memory requirement (GB/-)	2.5 / 0.72	34.0 / 0.37	1.0 / 0.91
TMS Sampling efficiency (%)	53.2	52.3	48.2
$P_{\text{err,maj,TMS}}$	4.2E-07	4.9E-07	5.2E-07
Abs. / Rel. FOM, Tot. Capt. ($\frac{1}{\text{s}}$/-)	3.1E+04 / 0.75	3.9E+03 / 0.07	1.2E+06 / 0.85
Abs. / Rel. FOM, Capt. Around 6.7 eV ($\frac{1}{\text{s}}$/-)	4.9E+02 / 0.53	4.8E+01 / 0.06	8.4E+04 / 0.74
DBRC with Traditional Majorant, h=3.0			
$k - k_{\text{ref}}$ (pcm)	-1 ± 3	2 ± 3	-10 ± 5
Abs. / Rel. Transport time (h/-)	5.0 / 0.96	2.6 / 0.98	7.4 / 0.99
$P_{\text{err,maj,DBRC}}$	9.0E-08	1.0E-07	5.1E-08
DBRC with Revised Majorant, $Q = 2 \times 10^{-5}$			
$k_{\text{TMS}} - k_{\text{NJOY}}$ (pcm)	-1 ± 3	2 ± 3	0 ± 6
Abs. / Rel. Transport time (h/-)	4.9 / 0.95	2.6 / 0.97	7.3 / 0.98
$P_{\text{err,maj,DBRC}}$	8.2E-08	8.5E-08	5.4E-08

CAPTIONS FOR FIGURES

Figure 1 Majorant cross sections for different basis temperatures T_{base} (0 K and 300 K) and temperature differences (300 K, 600 K and 900 K) for the total cross section of ^{238}U around the 6.7 eV resonance.

Figure 2 The energy ranges are defined differently for the revised and the traditional majorant.

Figure 3 Effect of the conservativity of the TMS majorant on three k_{eff} estimators of a HTGR system. The effect is studied for the revised majorant and, thus, the conservativity is manipulated through the Q parameter. The error bars correspond to two standard deviations, 2 σ.

Figure 4 Effect of the conservativity of the TMS majorant on three different k_{eff} estimators of a HTGR system. The conservativity is manipulated through the h parameter of the traditional majorant.

Figure 5 Comparison of neutron flux spectra between two TMS calculations and NJOY-based reference solution. With Q=1E-4 (left) the flux spectrum corresponds to the reference, but with Q=3.2E-4 (right) significant differences can be recognized. The dashed line corresponds to two standard deviations.

Figure 8 Comparison of neutron flux spectra between two DBRC calculations and NJOY-based reference solution. With h=3.2E-3 (left) the flux spectrum corresponds to the reference, but with h=1.0E-2 (right) significant differences can be recognized.

CAPTIONS FOR TABLES

Table I Performance comparison between traditional and revised majorant when applying TMS method in three thermal systems.

Table II Performance comparison between traditional and revised majorant when applying DBRC method in three thermal systems.

Table III Final performance results for three test cases. The relative (rel.) values are calculated with respect to the "Reference" calculation, an ordinary Serpent calculation with DBRC and full optimization. The errors correspond to one sigma.

FOOTNOTES

a For a complete and up-to-date description, visit Serpent website — http://montecarlo.vtt.fi

b To be precise, also each cross section Σ_x for which $\Sigma_x(E) \geq \Sigma_{\mathrm{maj}}(E)$ can be considered a temperature majorant cross section of $\Sigma(E')$, but usually it is practical to choose the majorant according to Eq. (1).

c Also other ways of dealing with the energy dependence have been introduced: in Ref. [10] a technique based on direct sampling of the secondary neutron velocity has been examined, while in Refs. [11, 12] the correction is done by varying the particle weights. It is also possible to include the effect by using $S(\alpha, \beta)$ tables based on the analytical scattering kernel, which has been covered in sequential Refs. [13–15].

d The multiplication is required for correct modeling of the reaction rates at low energies and is related to the fact that the integral of the distribution from which the target velocities are sampled (Eq. (7)) is greater than unity at low energies. This modification is perhaps the most intuitive in case of potential scatterers with constant low-energy cross sections: these cross sections are increased in the Doppler-broadening process, but the corresponding increase in the reaction rates could not be captured in the TMS transport without multiplying the cross sections by g.

e Since this system is in practice a quasi-homogeneous mixture of moderator and fuel, the probability of a neutron to interact with the fuel material during the slowing-down process is very high compared to, for instance, LWR geometries. In addition, the fact that the moderator atoms in graphite are relatively heavy ($A_{\mathrm{C}} \approx 12$) increases the number of scattering events a neutron experiences during the process compared to lighter moderators like light water. This increases the probability of a neutron to end up at energies corresponding to resonances in the fuel material at some point of the slowing-down process and, thus, makes the interactions more probable on average.

f It was found in [17] that the variances and, consequently, also the Figures-of-Merit for all estimators including the flux estimator are significantly affected by the usage of the TMS method near strong resonances.

PUBLICATION VI

Effect of the target motion sampling temperature treatment method on the statistics and performance

Ann. Nucl. Energy, Accepted for publication Aug 21, 2014.

Annals of Nuclear Energy xxx (2014) xxx–xxx

Contents lists available at ScienceDirect

Annals of Nuclear Energy

journal homepage: www.elsevier.com/locate/anucene

Effect of the Target Motion Sampling temperature treatment method on the statistics and performance

Tuomas Viitanen *, Jaakko Leppänen

VTT Technical Research Centre of Finland, P.O. Box 1000, FI-02044 VTT, Finland

ARTICLE INFO

Article history:
Received 22 April 2014
Received in revised form 14 August 2014
Accepted 14 August 2014
Available online xxxx

Keywords:
Monte Carlo
On-the-fly
Temperature
Collision estimator

ABSTRACT

Target Motion Sampling (TMS) is a stochastic on-the-fly temperature treatment technique that is being developed as a part of the Monte Carlo reactor physics code Serpent. The method provides for modeling of arbitrary temperatures in continuous-energy Monte Carlo tracking routines with only one set of cross sections stored in the computer memory.

Previously, only the performance of the TMS method in terms of CPU time per transported neutron has been discussed. Since the effective cross sections are not calculated at any point of a transport simulation with TMS, reaction rate estimators must be scored using sampled cross sections, which is expected to increase the variances and, consequently, to decrease the figures-of-merit. This paper examines the effects of the TMS on the statistics and performance in practical calculations involving reaction rate estimation with collision estimators.

Against all expectations it turned out that the usage of sampled response values has no practical effect on the performance of reaction rate estimators when using TMS with elevated basis cross section temperatures (EBT), i.e. the usual way. With 0 Kelvin cross sections a significant increase in the variances of capture rate estimators was observed right below the energy region of unresolved resonances, but at these energies the figures-of-merit could be increased using a simple resampling technique to decrease the variances of the responses. It was, however, noticed that the usage of the TMS method increases the statistical deviances of all estimators, including the flux estimator, by tens of percents in the vicinity of very strong resonances. This effect is actually not related to the usage of sampled responses, but is instead an inherent property of the TMS tracking method and concerns both EBT and 0 K calculations.

1. Introduction

The traditional continuous-energy Monte Carlo tracking approach relies on effective cross sections. In other words, the cross sections are Doppler-broadened to match the temperatures of the transport problem beforehand and used as-is throughout the transport simulation. Since cross sections for each nuclide and temperature must be stored separately in the computer memory, the memory requirement of the pre-broadened cross sections may increase to an intolerable magnitude. Particularly, the computer memory becomes a significant limitation when modeling systems with numerous nuclides and temperatures, as is often the case in multi-physics applications of Monte Carlo. To get rid of the memory limitation and, thus, to provide for modeling of systems with complex temperature distributions, on-the-fly temperature treatment techniques are required.

This article discusses a promising on-the-fly temperature treatment technique, in which the effective cross sections are not calculated at any point, but the thermal motion of target nuclei is handled stochastically by sampling target velocities at each collision site. With this approach, only one set of continuous-energy cross sections needs to be stored in the computer memory regardless of the number of temperatures appearing in the system. As a novel feature, the Target Motion Sampling (TMS) temperature treatment method only sees the temperature through an arbitrary variable $T(\mathbf{r}, t)$, which may vary continuously in both space and time. The capability to easily model realistic temperature distributions makes TMS a very attractive temperature treatment technique to be used in multi-physics couplings.

The idea behind this technique was introduced for the first time in English-written journals by the authors in Viitanen and Leppänen (2012b) and it was implemented in the Monte Carlo reactor physics code Serpent[1] shortly afterwards (Viitanen and

* Corresponding author. Tel.: +358 40 763 1963; fax: +358 20 722 5000.
E-mail address: tuomas.viitanen@vtt.fi (T. Viitanen).

[1] A complete and up-to-date description of the Serpent code is found at the project website: http://montecarlo.vtt.fi

http://dx.doi.org/10.1016/j.anucene.2014.08.033
0306-4549/

Please cite this article in press as: Viitanen, T., Leppänen, J. Effect of the Target Motion Sampling temperature treatment method on the statistics and performance. Ann. Nucl. Energy (2014), http://dx.doi.org/10.1016/j.anucene.2014.08.033

Leppänen, 2012a). It was, however, recently learned that a technique similar to TMS has been introduced in a Russian journal already in the 1980s (Ogibin and Orlov, 1984). The development of the TMS method is still on-going, and recently the main focus in the development has been on the optimization of the method (Viitanen and Leppänen, 2013, 2014). Near-future challenges in the development involve at least the extension of the method to the energy range of unresolved resonances and the application of the method together with $S(\alpha,\beta)$ tables for bound-atom scattering.

This work concentrates on an anticipated challenge related to the reaction rate estimators: since the effective cross sections are not available during the transport simulation when tracking with the TMS method, the reaction rate estimators need to be scored using sampled cross sections. As the scores become distributed quantities, the variances of the estimators may increase significantly. On the other hand, the usage of the TMS increases the total number of collisions in a calculation, which has an opposite effect on the variances of collision estimators when considering a constant number of neutron histories. Hence, the total effect of the TMS method on estimator deviances is hard to figure out without testing it in practice.

The effect of the TMS method on statistics and performance of reaction rate estimators is studied in the current work. First, an introduction to the TMS method and reaction rate estimators are provided in Sections 2 and 3, respectively. Four realistic fuel assemblies, used to test the estimators in practice, are presented shortly in Section 4 and selected results of the calculations are provided in Section 5. The last Section 6 is dedicated for summary and conclusions.

2. Target Motion Sampling (TMS) temperature treatment

The TMS temperature treatment technique is basically a tracking scheme that takes the effect of thermal motion into account during the tracking simulation (Viitanen and Leppänen, 2012b, 2014). The neutron path lengths are sampled based on a "temperature majorant" cross section

$$\begin{aligned}\Sigma_{\mathrm{maj}}(E) &= \sum_i \Sigma_{\mathrm{maj},i}(E) \\ &= \sum_i g_i(E,\Delta T_i) \max_{E'\in[E_{\min},E_{\max}]} \Sigma_{\mathrm{tot},i}(E',T_{\mathrm{base}}),\end{aligned} \tag{1}$$

where E is the neutron energy, $T_{\max,i}$ is the maximum temperature of nuclide i, $\Sigma_{\mathrm{tot},i}$ is the macroscopic total cross section of nuclide i, T_{base} is the basis temperature of the cross section and $[E_{\min},E_{\max}]$ is the energy range of thermal motion around E, which corresponds to the temperature difference

$$\Delta T_i = T_{\max,i} - T_{\mathrm{base},i}. \tag{2}$$

The g_i factor in Eq. (1) is the Doppler-broadening integral for constant cross section

$$\begin{aligned}g_i(E,\Delta T) = &\left(1+\frac{1}{2\lambda(\Delta T,A_i)^2E}\right)\mathrm{erf}\left(\lambda(\Delta T,A_i)\sqrt{E}\right) \\ &+\frac{e^{-\lambda(\Delta T,A_i)^2E}}{\sqrt{\pi}\lambda(\Delta T,A_i)\sqrt{E}},\end{aligned} \tag{3}$$

where A_i is the atomic weight ratio of nuclide i,

$$\lambda(\Delta T,A) = \sqrt{\frac{A}{k_{\mathrm{B}}\Delta T}} \tag{4}$$

and k_{B} is the Boltzmann constant (X-5 Monte Carlo Team, 2003).

The energy range of the thermal motion depends on the mass of the target nuclide and the neutron energy E in addition to ΔT. In the current Serpent version, the energy boundaries are chosen similar to the elastic scattering majorant of the Doppler-broadening rejection correction (DBRC) method[2] (Becker et al., 2009). Thus, the minimum energy in the range is

$$E_{\min}(E,\Delta T_i,A_i) = \left(\sqrt{E}-\frac{4}{\lambda(\Delta T,A_i)}\right)^2 \tag{5}$$

and the maximum energy is

$$E_{\max}(E,\Delta T_i,A_i) = \left(\sqrt{E}+\frac{4}{\lambda(\Delta T,A_i)}\right)^2. \tag{6}$$

From (5) and (6) it is also easy to derive a formula for the width of the energy range:

$$E_{\max}-E_{\min} = 16\frac{\sqrt{E}}{\lambda(\Delta T,A_i)} = 16\sqrt{\frac{Ek_{\mathrm{B}}\Delta T}{A_i}}. \tag{7}$$

The path length l and, thus, the next collision point candidate are obtained using inversion sampling

$$l = -\frac{1}{\Sigma_{\mathrm{maj}}(E)}\ln(\xi), \tag{8}$$

where ξ is a uniformly distributed random variable on the unit interval. At the collision point, the target nuclide candidate is first sampled such that the probability of sampling nuclide i is simply

$$P_i = \frac{\Sigma_{\mathrm{maj},i}(E)}{\Sigma_{\mathrm{maj}}(E)}. \tag{9}$$

Then, the target velocity V_{t} and cosine between the directions of the target and neutron μ are sampled from the distribution

$$P(V_{\mathrm{t}},\mu,T-T_{\mathrm{base}},A_i) = \frac{v'}{2v}P_{\mathrm{MB}}(V_{\mathrm{t}},T-T_{\mathrm{base}},A_i), \tag{10}$$

where T is the local temperature at the collision point, v is the LAB-frame speed of the neutron and

$$v' = \sqrt{v^2+V_{\mathrm{t}}^2-2vV_{\mathrm{t}}\mu} \tag{11}$$

is the relative speed of the neutron to the target (target-at-rest velocity). Symbol P_{MB} stands for the Maxwell–Boltzmann distribution for the target speed, defined

$$P_{\mathrm{MB}}(V_{\mathrm{t}},T,A) = \frac{4}{\sqrt{\pi}}\gamma(T,A)^3V_{\mathrm{t}}^2e^{-\gamma(T,A)^2V_{\mathrm{t}}^2}, \tag{12}$$

where

$$\gamma(T,A) = \sqrt{\frac{AM_{\mathrm{n}}}{2k_{\mathrm{B}}T}} \tag{13}$$

and M_{n} is the neutron mass.

The collision point is accepted or rejected according to the rejection sampling criterion

$$\xi < \frac{g_i(E,T-T_{\mathrm{base}})\Sigma_{\mathrm{tot},i}(E',T_{\mathrm{base}})}{\Sigma_{\mathrm{maj},i}(E)}, \tag{14}$$

where E' is the target-at-rest energy corresponding to speed v'. In case the collision is rejected, the tracking proceeds by sampling of a new path length beginning from the current collision point candidate. If the collision is accepted, a reaction is sampled using the cross sections at temperature T_{base} such that the probability of sampling reaction j is

[2] Previous results, published in Viitanen and Leppänen (2013), have shown that the energy boundaries could be chosen in a more efficient way, leading to better performance without compromising the accuracy of the calculations in practice. However, the final implementation of this optimization technique is still incomplete and, therefore, the less efficient DBRC boundaries will have to do for now.

Please cite this article in press as: Viitanen, T., Leppänen, J. Effect of the Target Motion Sampling temperature treatment method on the statistics and performance. Ann. Nucl. Energy (2014), http://dx.doi.org/10.1016/j.anucene.2014.08.033

$$P_j = \frac{\Sigma_{i,j}(E', T_{\text{base}})}{\Sigma_{\text{tot},i}(E', T_{\text{base}})}. \quad (15)$$

The tracking procedure continues according to the sampled reaction.

It has been shown in Viitanen and Leppänen (2012b) that this tracking scheme, with $T_{\text{base}} = 0$K, reproduces the same mean free paths and reaction rates as conventional tracking methods relying on effective, pre-broadened cross sections. The elevating of the basis cross section temperature has been further discussed in Viitanen and Leppänen (2014), where the functionality and feasibility of the TMS technique with $T_{\text{base}} \geqslant 0$ K have been demonstrated in four realistic systems with different characteristics.

3. Reaction rate estimators

3.1. Track-length estimators

The basic idea behind the track-length estimators is that the volume-integrated neutron flux, by definition, equals the total track-length of neutrons. Hence, the neutron track-lengths can be used to estimate the total neutron flux. The track-length estimators are scored every time a neutron draws a track in the volume of interest, i.e. the cell, universe or material in which the reaction rates are calculated. The scores are defined

$$s = fwl_{\text{t}}, \quad (16)$$

where w is the weight of the neutron, l_{t} is the track length of the neutron in the volume of interest and f is the response, which is chosen according to the reaction rate being calculated. For example, $f = 1$ would be used to calculate the total neutron flux, $f = \Sigma_{\text{tot}}(E, T)$ to calculate the total reaction rate and $f = \Sigma_{\gamma,i}(E, T)$ to calculate the radiative capture reaction rate of nuclide i. The scores can be binned with respect of different variables, most commonly energy. For instance, by storing separately the scores for $E \leqslant 1$ eV and $E > 1$ eV it is possible to separate the reactions induced by thermal and fast neutrons from each other (Lux and Koblinger, 1990).

The usage of the track-length estimator is limited by two facts:

1. The track-length estimator involves an assumption that the cross section response used in the scoring (Eq. (16)) represents the whole track length l_{t}. Consequently, the volume in which the estimator is scored must be homogeneous in terms of nuclide composition, density and temperature when using cross sections as responses.
2. The track-lengths l_{t} within the volume of interest must be resolvable.

Because of the first limitation, the track-length estimators are not very well suited with the TMS method. Usage of track-length estimators would prevent the modeling of continuous temperature distributions within material zones, thus vitiating a major advantage of the TMS method. The second limitation is only related to the geometry routine of Serpent, which combines surface-tracking with the Woodcock delta-tracking method (Leppänen, 2010). Since the surface crossings are not recorded with the Woodcock delta-tracking, the track-lengths cannot be resolved without significant extra effort and, thus, the track-length estimators cannot be scored in practice. For this reason, the track-length estimator has not been implemented in Serpent 2 and track-length estimators are not used in the current article.[3]

[3] The functionality of the TMS method together with track-length estimators has not been demonstrated, either.

3.2. Collision estimators

Collision estimators are based on the simulated total reaction rates. As the reaction rate of a partial reaction is related to the total reaction rate simply by the ratio of its cross section to the total cross section, the collision estimators of any reactions can be scored every time a reaction takes place in the neutron transport (Lux and Koblinger, 1990).

With the TMS method, the collision estimators are scored at each collision site, regardless of whether the collision point is accepted or not. The scored values can be written as

$$s = \frac{fw}{\Sigma_{\text{maj}}(E)}, \quad (17)$$

where f is the value of the response and Σ_{maj} is the material-wise TMS majorant cross section.

Again, the effective cross sections are not available in TMS transport and the temperature dependence of the responses must be handled in a different way (Section 3.3). Unlike track-length estimators, collision estimators can be used to score reaction rates in material zones with inhomogeneous temperature distributions. Therefore, they are the natural choice to be used with the TMS temperature treatment technique. All the reaction rates in this article are calculated using collision estimators.

3.3. Distributed responses

One challenge in the scoring of reaction rate estimators is that the effective cross sections used as responses f are, in general, not available at the desired temperature when using the TMS temperature treatment. With track-length estimators the response should be in the homogeneous temperature of the surrounding material, while the local temperature T of the collision point should be used in the scoring of the collision estimators.

The issue is very similar to the basic problem of on-the-fly temperature treatment in Monte Carlo neutron transport—and so is its solution. Analogous to the TMS approach in neutron transport, a cross section in T_{base} temperature corresponding to a target-at-rest energy sampled from Eq. (10) is used. Furthermore the responses must be multiplied with the Doppler-broadening integral for constant cross section, Eq. (3). When scored this way, i.e. using responses

$$f = g_i(E, T - T_{\text{base}})\Sigma_x(E', T_{\text{base}}), \quad (18)$$

the expectation values of the reaction rate estimators are not affected since the sampled cross sections correspond to the effective cross section on average. However, the variances of the estimators increase because the responses become distributed quantities. The variance of the response f depends on the temperature difference between the response and T_{base}: the larger the difference, the wider the distribution of E' and, thus, the larger the variance of $\Sigma_x(E', T_{\text{base}})$.

In the current implementation of the TMS method in Serpent, the implicit estimator of k_{eff} is automatically scored at each collision point. Since the scoring involves calculation of several reaction rates, the velocities of all nuclei in the collision material are always sampled for each collision and the same velocities can be used when scoring reaction rate estimators. Consequently, the extra CPU time spent in the scoring of reaction rate estimators in the current implementation is somewhat smaller than if the target velocities would be sampled separately while scoring the estimators.

It is easy to figure out a variance reduction technique for the responses (18). Instead of using a single sample for the response, one may decrease the variance of the response by using an average of N sampled values,

Please cite this article in press as: Viitanen, T., Leppänen, J. Effect of the Target Motion Sampling temperature treatment method on the statistics and performance. Ann. Nucl. Energy (2014), http://dx.doi.org/10.1016/j.anucene.2014.08.033

$$f = \frac{1}{N}\sum_{n=1}^{N} g_i(E, T - T_{\text{base}})\Sigma_x(E_n', T_{\text{base}}). \quad (19)$$

As N approaches infinity, the value of the response approaches to

$$\iint g_i(E, T - T_{\text{base}})\Sigma_x(v', T_{\text{base}}) \times \frac{1}{g_i(E, T - T_{\text{base}})}\frac{v'}{2v} \times P_{\text{MB}}(V_t, T - T_{\text{base}})\mathrm{d}\mu\mathrm{d}V_t = \Sigma_x(v, T) = \Sigma_x(E, T), \quad (20)$$

i.e. the effective cross section at temperature T. In Eq. (20), the normalized form of the target velocity distribution (10) has been used (Viitanen and Leppänen, 2014). This approach increases the CPU time spent in the sampling of the cross sections as the target velocities need to be resampled in case $N > 1$. Therefore, the total number of samples N should be optimized for the best performance.

Even though the temperature difference between the material and T_{base}, and usage of TMS in general, increases the variances of the scores, it also affects the number of collisions in the transport: An increase in the temperature difference $T_{\max} - T_{\text{base}}$ decreases the sampling efficiency of the rejection sampling criterion (14), which increases the proportion of rejected or "virtual" collisions in the transport. Consequently, the collision estimators are scored more often than in an ordinary calculation with the same number of neutron histories, which has a decreasing effect on the variances of estimators. It is, hence, not self-evident whether the total effect of TMS on the variances of collision estimators is increasing or decreasing.

3.4. Figures-of-merit

What comes to the calculation of reaction rates, it is, in practice, not the amount of statistics obtained per transported neutron but the amount of statistics per spent CPU time that counts. The best quantity to describe the overall performance of a Monte Carlo code in reaction rate estimation is the figure-of-merit, defined

$$\text{FOM} = \frac{1}{\tau\sigma^2}, \quad (21)$$

where τ is the calculation time and σ^2 is the variance of an estimator. Since the variance is, by theory, inversely proportional to τ, the value of FOM should be independent of the total calculation time. Thus, it describes purely the efficiency of the calculational system in the calculation of reaction rates. The higher the FOM, the better the performance.

The usage of the TMS temperature treatment has effect on both parameters τ and σ. The effect of TMS on σ has been previously described. When it comes to τ, it has been examined in Viitanen and Leppänen (2012a, 2013, 2014) that the calculation time required per transported neutron is somewhat higher with the TMS method than with methods relying on effective cross sections. After introduction of reaction rate estimators with the stochastic scoring scheme, the calculational overhead may increase further. Since the usage of TMS increases both σ and τ, it is expected that the figures-of-merit are somewhat worse with the TMS than with conventional transport methods.

4. Test cases

The performance of the TMS method in reaction rate estimation is tested in four systems with different neutron spectra to provide an overall picture of its performance in practice. The test cases are the same as in Viitanen and Leppänen (2014).

4.1. Gd-doped pressurized water reactor assembly (PWR-Gd)

The first "PWR-Gd" case involves a 17 × 17 PWR fuel assembly with 16 Gadolinium-doped fuel rods in an infinite two dimensional lattice. The geometry and material definitions of the fuel assembly are from an NEA benchmark (Roque et al., 2004). The only differences to the benchmark specifications are related to temperatures: the moderator temperature is risen to 600 K for simplicity and the originally flat temperature profiles of the fuel rods are replaced with 3-step distributions such that the pellets are divided into three equi-thick annular regions with temperatures 600, 900, and 1200 K from outside in.

In the PWR-Gd case, the estimators are scored in the fuel material of the four corner rods.

4.2. PWR-Gd assembly at 40 MWd/kgU burnup (PWR-BU)

The second case is abbreviated "PWR-BU" and features the previously introduced "PWR-Gd" bundle irradiated to 40 MWd/kgU burnup. The irradiated material compositions were obtained by running a separate burnup calculation using Serpent 2.1.14. The resulting compositions contain 241 actinide and fission product nuclides with cross sections available in the data libraries.

The estimators are scored in the fuel material of the four corner rods also in the PWR-BU case.

4.3. High temperature gas cooled reactor system (HTGR)

The "HTGR" test case consists of TRISO particles within graphite matrix in an infinite three dimensional lattice. The specifications of the TRISO particles and the composition of the graphite matrix are based on a NEA benchmark for HTGR fuel depletion (DeHart and Ulses, 2009), and the lattice pitch is 0.16341 cm. The fuel kernel in the spherical TRISO particles is divided in two equally thick parts such that the innermost 0.0125 cm is at 1800 K temperature and the outer layer is at 1200 K. The temperature of all other materials is 1200 K.

The estimators in the HTGR case are scored in all of the fuel material.

4.4. Sodium cooled fast reactor assembly (SFR)

The last of the test cases, "SFR", involves a fuel assembly from the sodium cooled fast reactor JOYO in an infinite two dimensional lattice. The specifications of the assembly can be found in Nuclear Energy Agency (2006). The geometry and material definitions correspond to the benchmark definition for the 250 °C core. Again, the fuel temperature is modified such that the inner half (radius) of the fuel pellets is at 1200 K and the outer half at 900 K temperature. All other materials are at 600 K temperature in the model.

In the SFR case, the estimators are scored in the fuel material of all 6 corner rods of the hexagonal fuel assembly.

5. Results

The results are calculated using a development version of Serpent, which is based on Serpent 2.1.14. The cross section library used in the calculations is JEFF-3.1.1 based and it has been processed with NJOY 99.364 using a rather low 0.001 reconstruction tolerance (MacFarlane and Muir, 2000). TMS treatment is used for fuel materials only, and all the other materials are modeled using NJOY-broadened cross sections. In the reference calculations, pre-broadened cross sections are used also for the fuel materials.

The Serpent transport routine is optimized for performance using pre-generated material-wise total cross sections to avoid summation over material compositions during tracking

Please cite this article in press as: Viitanen, T., Leppänen, J. Effect of the Target Motion Sampling temperature treatment method on the statistics and performance. Ann. Nucl. Energy (2014), http://dx.doi.org/10.1016/j.anucene.2014.08.033

(Leppänen, 2009). This method results in a considerable speed-up in calculation, especially when modeling irradiated fuels. The same optimization cannot, however, be used together with the TMS method. Thus, comparing the performance of a typical Serpent calculation to a calculation with the TMS treatment would be somewhat misleading. To provide for fair comparison of the transport methods, the material-wise total cross sections were omitted also from all performance-related reference calculations by running Serpent in optimization mode 2, which has been originally developed for Serpent 2 for the purpose of saving memory in large burnup calculations (Leppänen and Isotalo, 2012).

Since the TMS method is not capable of correctly modeling the unresolved resonances, the energy region of unresolved resonances is handled using infinitely dilute cross sections without any special treatment in all of the calculations. Doppler-broadening rejection correction is used for ^{238}U between 0.4 eV and 20 keV in all of the thermal systems. Because of the recent findings in Viitanen and Leppänen (2014), the use of DBRC was extended in the PWR-BU case to nuclides ^{95}Mo, ^{108}Pd, ^{131}Xe, ^{145}Nd, ^{147}Pm, ^{152}Sm, ^{239}Pu, ^{240}Pu, ^{242}Pu and ^{241}Am in addition to ^{238}U. To be precise, DBRC was used only in the reference calculations and TMS calculations with Elevated Basis Temperatures. When using TMS with 0 K basis cross sections the temperature dependence of the elastic scattering kernel is inherently taken into account (Viitanen and Leppänen, 2014).

All the calculations are made using 12 OpenMP threads on a 3.47 GHz Intel Xeon X5690 processor. The results were normalized to 10^{15} total flux in all of the cases.

5.1. Comparison of reaction rates

The very first thing to do is to ensure that the collision estimators provide, on average, the same results with the TMS method as with conventional tracking methods. This is done by comparing the total reaction rate and capture rate spectra of TMS calculations to reference solutions based on NJOY broadened cross sections. The spectra are scored using 1000 equi-lethargy bins from 10^{-11} to 20 MeV and the calculations are performed using two variations of the TMS method: in the "TMS/0 K" variant, T_{base} equals 0 Kelvin, while the "TMS/EBT" (Elevated Basis Temperature) variant involves basis cross sections at the minimum temperature of each nuclide. The parameters and integral results of these calculations are provided in Table 1.

Because of the similarity of the results, the differences in the total reaction rate and capture rate spectra are provided here only for the HTGR case, which has the best statistics for the whole energy spectrum. In Figs. 1 and 2 it can be seen that the estimator results correspond to the reference solution within statistical accuracy at all energies. Also the integral results presented in Table 1 are in perfect agreement.

The performance measures in Table 1 show that the TMS/EBT method performs very well when calculating energy-integrated reaction rates: the figures-of-merit are practically equal to the reference in two out of four cases, namely in the PWR-Gd and HTGR cases. In the PWR-BU case, about twice the CPU time is required by the TMS/EBT method to obtain the same statistical deviation as in the reference calculation, since sampling the velocities of all 241 nuclides at each collision site takes a lot of calculational effort. In the SFR case the TMS method, a little surprisingly, outperforms the reference. This is due to the fact that the optimization mode 2 of Serpent uses a multi-group delta-tracking majorant cross section in the neutron tracking, which slows down the calculation especially at high neutron energies when compared to the TMS method with a continuous-energy majorant.

The figures-of-merit are much worse with TMS/0 K. For example, to obtain a certain level of statistical accuracy in the most inefficient PWR-BU case, about 12 times more CPU time is required than in a conventional Monte Carlo transport calculation.

Table 1
Integral results and performance measures for the reference solution and two variants of the TMS method in four test cases. The "rel." values in the TMS results are calculated relative to the NJOY based reference solution.

Number of active neutron histories	PWR-Gd 10^9	PWR-BU 5×10^7	HTGR 5×10^8	SFR 10^9
NJOY based reference				
Transport time (h)	7.14	2.27	10.39	15.30
Memory requirement (GB)	2.59	77.45	0.72	1.92
Tot. reaction rate ($\frac{1}{s}$)	2.036E+12	2.020E+12	1.074E+13	1.004E+13
σ (%)	0.014	0.062	0.002	0.003
Capture rate ($\frac{1}{s}$)	1.245E+11	1.931E+11	1.672E+12	1.601E+11
σ (%)	0.029	0.109	0.004	0.005
Tot. reaction rate, FOM ($\frac{1}{s}$)	2.0E+03	3.2E+02	6.7E+04	2.0E+04
Capture rate, FOM ($\frac{1}{s}$)	4.6E+02	1.0E+02	1.7E+04	7.3E+03
TMS/EBT				
Transport time, tot./rel. (h/-)	7.13/1.00	4.50/1.98	10.41/1.00	10.31/0.67
Memory requirement tot./rel. (GB/-)	1.89/0.73	33.44/0.43	0.72/1.00	1.64/0.86
Tot. reaction rate ($\frac{1}{s}$)	2.036E+12	2.014E+12	1.074E+13	1.004E+13
σ (%)	0.014	0.062	0.002	0.003
Capture rate ($\frac{1}{s}$)	1.245E+11	1.927E+11	1.672E+12	1.601E+11
σ (%)	0.028	0.108	0.004	0.005
Tot. reaction rate, FOM, tot./rel. ($\frac{1}{s}$/-)	2.0E+03/1.00	1.6E+02/0.50	6.7E+04/1.00	3.0E+04/1.48
Capture rate, FOM, tot./rel. ($\frac{1}{s}$/-)	5.0E+02/1.07	5.3E+01/0.51	1.7E+04/1.00	1.1E+04/1.49
TMS/0 K				
Transport time, tot./rel. (h/-)	17.81/2.50	25.93/11.42	25.63/2.47	16.24/1.06
Memory requirement tot./rel. (GB/-)	1.98/0.76	40.73/0.53	0.76/1.05	2.42/1.26
Tot. reaction rate ($\frac{1}{s}$)	2.036E+12	2.019E+12	1.073E+13	1.004E+13
σ (%)	0.014	0.061	0.002	0.003
Capture rate ($\frac{1}{s}$)	1.245E+11	1.929E+11	1.672E+12	1.600E+11
σ (%)	0.029	0.111	0.005	0.005
Tot. reaction rate, FOM, tot./rel. ($\frac{1}{s}$/-)	8.0E+02/0.40	2.9E+01/0.09	2.7E+04/0.41	1.9E+04/0.94
Capture rate, FOM, tot./rel. ($\frac{1}{s}$/-)	1.8E+02/0.40	8.7E+00/0.08	4.3E+03/0.26	6.8E+03/0.94

Please cite this article in press as: Viitanen, T., Leppänen, J. Effect of the Target Motion Sampling temperature treatment method on the statistics and performance. Ann. Nucl. Energy (2014), http://dx.doi.org/10.1016/j.anucene.2014.08.033

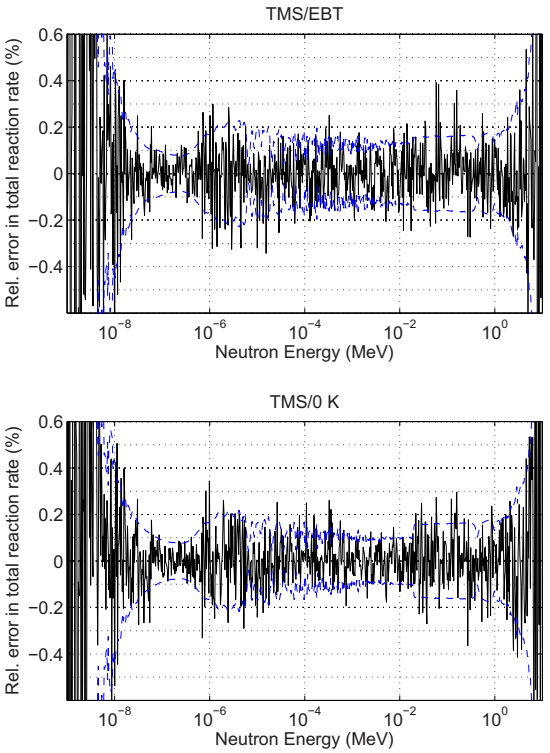

Fig. 1. Differences in total reaction rate spectra compared to an NJOY based reference solution. Results are provided for TMS with two different basis cross section temperatures. The dashed line represents one-sigma standard deviation.

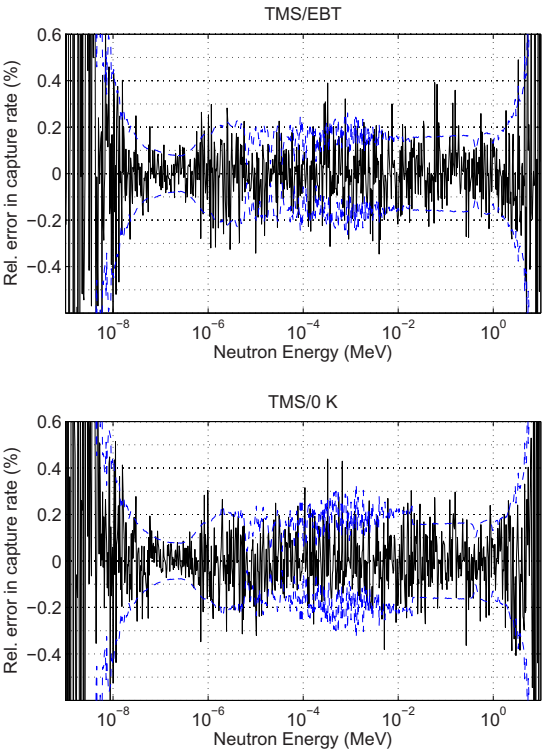

Fig. 2. Differences in capture rate spectra compared to an NJOY based reference solution.

In many cases it is, however, not the energy-integrated reaction rate, but the contribution of a smaller energy region that is of interest. The energy dependence of the variances is examined in the next section.

5.2. Variance spectra

Serpent was run for each of the four test cases with number of resampling, N, ranging from 1 to 100 using 5 million active neutron histories. Again, the calculations were made using two different basis temperatures. For comparison purposes, the results of an NJOY based reference calculation are also provided.

The effect of the response resampling on variances is first examined through the standard deviations of the total reaction rate and capture rate spectra. Since the results are, again, quite similar for all of the test cases, only the results of the PWR-BU test case are provided. Selected results are depicted in Figs. 3–7. The results calculated with 0 K basis are provided mainly to emphasize the effects of the TMS technique on variances: the results in the previous section suggest that EBT variant should always be used for the best performance.

It should also be noted that the plots in Figs. 3–7 represent the statistical deviations, not the figures-of-merit. As can be seen in Table 1, the $N = 1$ calculation with TMS/0 K takes about 11.5 times more calculation time than the reference calculation and changing the N parameter increases the calculation time further by about 10% with $N = 10$ or about 140% with $N = 100$ in the PWR-BU case. Thus, even though it seems that the statistical deviations become slightly smaller with TMS/0 K than with the reference, the figures-of-merit are in fact much worse. With TMS/EBT the calculational overhead to reference is much smaller and, hence, the figures-of-merit would be much closer but still worse than the reference.

Several conclusions can be drawn based on these results:

- In Fig. 3 it can be seen that resampling does not have significant effect on the variances when calculating the total reaction rate. It can also be seen that around 10^{-3} MeV, for instance, the TMS method with 0 K basis results in smaller variances than a conventional calculation with the same number of neutron histories, apparently due to an increase in the number of virtual collisions because of the lowered rejection sampling efficiency. The standard deviation curves are connected above 2×10^{-2} MeV, which corresponds to the lower boundary of the energy region of unresolved resonances for ^{238}U.
- The advantages of resampling can be recognized in Fig. 4, between energies 2×10^{-4} and 2×10^{-2} MeV. The increasing of N decreases the variance of the capture rate estimator. With sufficiently high values of N the standard deviation is approximately halved, decreasing it even below that of the reference calculation. It also seems that at this energy region already a few additional samples decreases the variance of the estimator significantly. Since both the total reaction rate and capture rate estimators are scored equally often, the differences in estimator variances can only be explained by the fact that the total cross section is relatively smooth compared to the capture cross section.

Please cite this article in press as: Viitanen, T., Leppänen, J. Effect of the Target Motion Sampling temperature treatment method on the statistics and performance. Ann. Nucl. Energy (2014), http://dx.doi.org/10.1016/j.anucene.2014.08.033

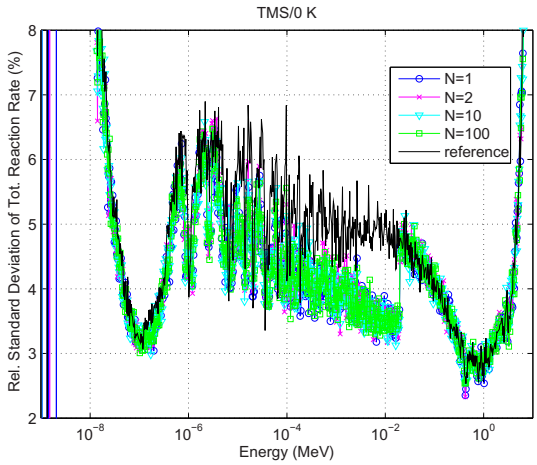

Fig. 3. Relative standard deviations of the total reaction rate spectra for the PWR-BU case. The TMS calculations with different numbers of responses *N* are done using basis cross sections at 0 K. The reference solution is based on NJOY-broadened cross sections.

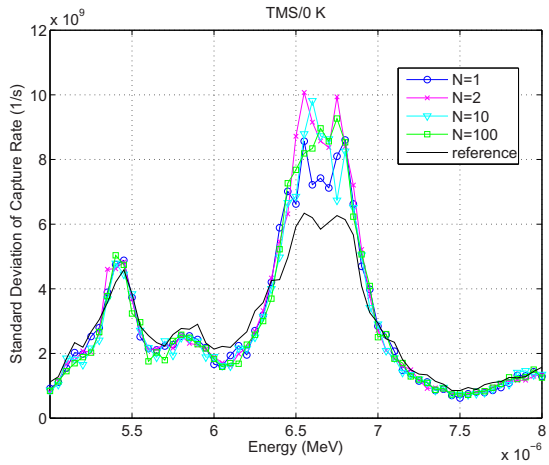

Fig. 5. A selected detail in the capture rate deviation spectrum of the PWR-BU case, calculated using TMS/0 K: the surroundings of the 6.7 eV resonance peak of ^{238}U.

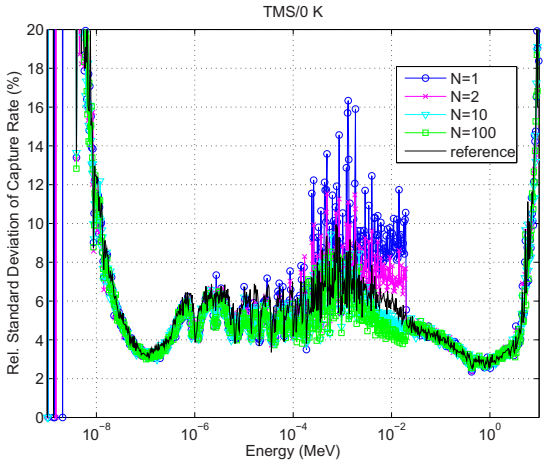

Fig. 4. Relative standard deviations of the capture rate spectra for the PWR-BU case. Zero Kelvin basis cross sections are used in the TMS calculations.

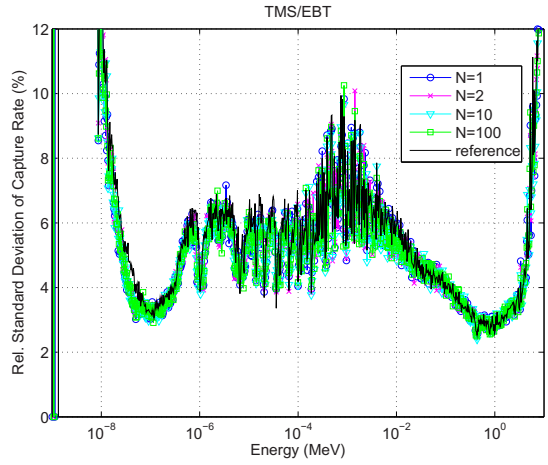

Fig. 6. Relative standard deviations of the capture rate spectra for the PWR-BU case. The TMS calculations are made using elevated basis cross section temperatures (EBT).

- The behavior around the 6.7 eV resonance of ^{238}U in Fig. 5 shows that around very strong resonances the variances in the capture rate are larger than the reference in all calculations with TMS. In fact, it was noticed that with TMS also the statistical deviation of the neutron flux around the strongest resonances is somewhat higher than in an ordinary calculation with effective cross sections, which implies that this behavior is not related to the usage of distributed responses.
- The results in Figs. 6 and 7 show that when using TMS with EBT the value of *N* does not affect the standard deviations at any energy region, in practice. The issue around the strong resonances exists also with EBT, but the standard deviations of the TMS calculations are slightly closer to the reference than in the 0 K cases.

The fact that the quality of the response samples is only important at a particular energy region seems to be related to the energy range of the effect of thermal motion, which according to Eq. (7) is directly proportional to the square root of neutron energy. Since the spacing and average width of the resonances are roughly constant (at least in magnitude) throughout the whole energy spectrum, the broadening of the extent of thermal motion means that the energy region from which the response values are sampled contains a higher number of resonances and the probability of hitting an individual resonance is much smaller than at low energies. This increases significantly the variances of responses, which is also reflected in the estimator results. It should be noted that the energy range defined by Eq. (7) depends also on the mass of the nuclide and the temperature. Hence, the phenomenon is emphasized for light resonance absorber nuclides at high temperatures.

Please cite this article in press as: Viitanen, T., Leppänen, J. Effect of the Target Motion Sampling temperature treatment method on the statistics and performance. Ann. Nucl. Energy (2014), http://dx.doi.org/10.1016/j.anucene.2014.08.033

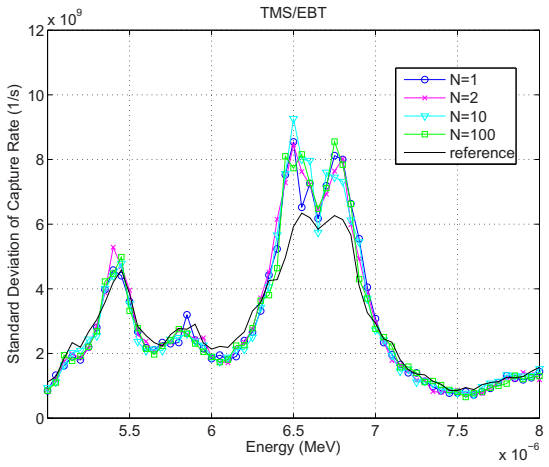

Fig. 7. A selected detail in the capture rate deviation spectrum of the PWR-BU case, calculated using TMS/EBT: the surroundings of the 6.7 eV resonance.

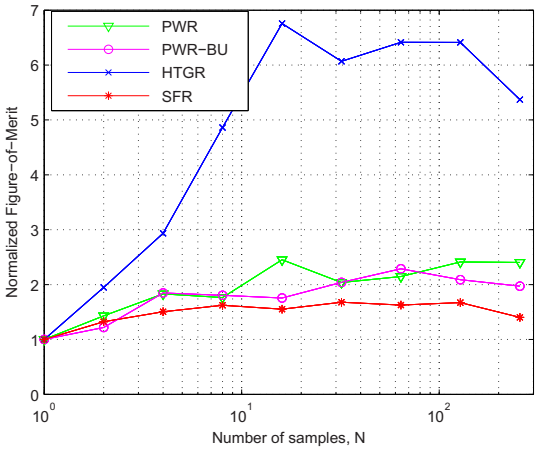

Fig. 8. Normalized figures-of-merit of reaction rate estimators in four test cases, scored using averages of $N = 1 - 256$ response samples. The estimators are scored between 2–4 keV.

5.3. Effect of resampling

In the previous, it was noticed that increasing of the N parameter has a decreasing effect on the variance of the total capture rate between energies 2×10^{-4} and 2×10^{-2} MeV, but only when using TMS/0 K. To examine the corresponding effect on the figures-of-merit, the capture reaction rate between 2–4 keV was estimated with different values of N. Five million active neutron histories were run per each calculation. The results are depicted in Fig. 8.

When resampling is applied only at a narrow energy interval, the value of N has only minor effect on the calculation times. Changing N from 1 to 256 increased the overall calculation time by 64% in the HTGR case, while the extra calculation time was less than 12% in all other cases. The figures-of-merit in Fig. 8 show that the performance of the TMS method in high-energy reaction rate estimation can be significantly increased using the resampling method. With optimal number of samples N the figure-of-merit can be increased even by a factor of six in the HTGR case and by a factor of about 1.5–2 in other systems.

Table 2
Figures-of-merit for a capture rate estimator scored around the 6.7 eV resonance of ^{238}U.

	PWR		PWR-BU		HTGR	
	Abs.	Rel.	Abs.	Rel.	Abs.	Rel.
NJOY Based Reference	1.08E+03	1.00	8.66E+01	1.00	1.23E+05	1.00
TMS/EBT	5.09E+02	0.47	3.49E+01	0.40	6.71E+04	0.54
TMS/0 K	2.12E+02	0.20	6.14E+00	0.07	2.75E+04	0.22

5.4. Figures-of-merit near strong resonances

To express the importance of the previously-discovered effect around strong resonances also in terms of figures-of-merit, the capture rate around the 6.7 eV resonance of ^{238}U was calculated using a single energy bin between 6.5–6.9 eV. The results for the thermal systems are provided in Table 2.

The figures-of-merit for TMS/0 K are in any case significantly smaller than for reference because of longer calculation times, but those for TMS/EBT should, in general, be very close to the reference in the light of the previous results. Hence, based on the TMS/EBT results in Table 2 it can be concluded that the whole 50% decrease in figures-of-merit around strong resonances is caused by the newly-found behavior.

According to the current understanding, the behavior is caused by a relative increase in TMS score variances in case of highly probable reactions. When considering a constant number of neutron histories, the usage of TMS *usually* decreases the variances because TMS transport adds virtual collisions, at which the collision estimators are scored, along the neutron tracks. Specifically, this effect adds virtual collisions also for such neutrons that do not experience any actual collisions within a material region in which the estimators are scored. Since a couple of scores from virtual collisions is much better for the statistics than no scores at all, the use of TMS in many cases decreases the estimator variances.

However, the situation becomes a little different at energies where the cross sections are very high and, correspondingly, the mean free paths are very small. Near strong resonances the probability of a neutron to experience a real collision is near 100% and, therefore, it is very likely to get one collision estimator score out of each neutron track in the material zone of interest even with conventional tracking methods. It turns out that individual scores corresponding to the actual collisions (conventional transport) result in smaller estimator variances than sums of n scores corresponding to the numerous virtual collisions along the way to the reaction site (TMS), since n is in fact a random variable. Consequently, the TMS method results in slightly poorer estimator statistics near strong resonances and there is, in practice, nothing to do about it. Hopefully, a more rigorous description of the phenomenon will be provided in the future.

6. Summary and conclusions

In this work, the effect of the TMS temperature treatment method on the performance of total reaction rate and capture rate estimators has been studied. Because of a limitation in the geometry routine of the Serpent Monte Carlo code, the study was, at this point, limited to collision estimators only. To better understand the effect of distributed cross section responses on the variances of the estimators, a resampling technique was introduced to decrease the response variances. This technique is simply based on using an

Please cite this article in press as: Viitanen, T., Leppänen, J. Effect of the Target Motion Sampling temperature treatment method on the statistics and performance. Ann. Nucl. Energy (2014), http://dx.doi.org/10.1016/j.anucene.2014.08.033

average of N response samples instead of an individual value in the estimator scoring.

The reaction rate results calculated using the TMS method agreed with the NJOY based reference solution within statistical accuracy throughout the energy spectrum. By examining closely the deviance spectra calculated using the response resampling technique with different values for N, it was noticed that the usage of sampled response function values only had practical effect on the estimator variances when scoring the capture rate estimator at energies between 2×10^{-4} and 2×10^{-2} MeV and the effect was only present when TMS method was used with 0 Kelvin cross sections. With elevated basis temperatures (EBT) or with total reaction rate estimators the "quality" of the responses had no effect on the estimator variances.

The only energy region in which the TMS with EBT performed notably worse than the reference was near very strong resonances: in the vicinity of resonances the statistical deviations of all estimators, including the flux estimator, increased above the reference. This behavior decreased the figures-of-merit near very strong resonances by about 50% compared to the reference, while the performance was practically equal further away from the strong resonances. The effect is, according to current knowledge, caused by the fact that the summing over a random number of scores from virtual collisions results in higher estimator variances than usage of individual scores from actual collisions if the probability of a neutron to experience an actual collision is very high.

It seems that the usage of sampled response values has much smaller effect on the variances of estimators than anticipated beforehand by the authors. In those cases, where the usage of sampled responses significantly deteriorated the variances of the estimators, the performance could be effectively boosted using the response resampling technique. However, it should be noted that in the current study these cases were always associated with the usage of TMS with 0 Kelvin basis temperatures. In practical calculations, the EBT version will be always used and, thus, the resampling will be futile.

In summary, the TMS method with EBT seems to perform very well in the calculation of reaction rates and the performance seems to be governed by the efficiency of the neutron tracking. It is, however, possible that new issues would emerge if more exotic materials and reactions would be investigated: this study was only limited to the behavior of total reaction rate and capture rate estimators in typical fuel materials. The applicability of the method with track length estimators is considered a very important topic and is to be examined in the near future.

Acknowledgements

This work is partly funded through the NUMPS project of the Finnish Academy and KÄÄRME project of the Finnish Research Programme on Nuclear Power Plant Safety, SAFIR2014.

References

Becker, B., Dagan, R., Lohnert, G., 2009. Proof and implementation of the stochastic formula for ideal gas, energy dependent scattering kernel. Ann. Nucl. Energy 36, 470–474.

DeHart, M.D., Ulses, A.P., 2009. Benchmark specification for HTGR fuel element depletion. Tech. Rep. NEA/NSC/DOC(2009)13, Nuclear Energy Agency.

Leppänen, J., 2009. Two practical methods for unionized energy grid construction in continuous-energy Monte Carlo neutron transport calculation. Ann. Nucl. Energy 36, 878–885.

Leppänen, J., 2010. Performance of Woodcock delta-tracking in lattice physics applications using the Serpent Monte Carlo reactor physics burnup calculation code. Ann. Nucl. Energy 37, 715–722.

Leppänen, J., Isotalo, A., 2012. Burnup calculation methodology in the Serpent 2 Monte Carlo code. In: PHYSOR-2012. Knoxville, TN, Apr. 15–20, 2012.

Lux, I., Koblinger, L., 1990. Monte Carlo Particle Transport Methods: Neutron and Photon Calculations. CRC Press, Boca Raton, Florida.

MacFarlane, R.E., Muir, D.W., 2000. NJOY99.0 code system for producing pointwise and multigroup neutron and photon cross sections from ENDF/B data. Tech. Rep. PSR-480, Los Alamos National Laboratory.

Nuclear Energy Agency, 2006. Japan's experimental fast reactor Joyo Mk-I core: sodium-cooled uranium-plutonium mixed oxide fueled fast core surrounded by UO2 blanket, international handbook of evaluated reactor physics benchmark experiments. Tech. Rep. NEA/NSC/DOC(2006)1, Nuclear Energy Agency.

Ogibin, V., Orlov, A., 1984. Majorized cross-section method for tracking neutrons in moving media. Voprosy Atomnoj Nauki i Techniki, Metodoki i Programmy 2 (16), 6–9, in Russian.

Roque, B., et al., 2004. Specification for the phase 1 of a depletion calculation benchmark devoted to fuel cycles. Tech. Rep. NEA/NSC/DOC(2004)11, Nuclear Energy Agency.

Viitanen, T., Leppänen, J., 2012a. Explicit temperature treatment in Monte Carlo neutron tracking routines – first results. In: PHYSOR-2012. Knoxville, TN, Apr. 15–20, 2012.

Viitanen, T., Leppänen, J., 2012b. Explicit treatment of thermal motion in continuous-energy Monte Carlo tracking routines. Nucl. Sci. Eng. 171, 165–173.

Viitanen, T., Leppänen, J., 2013. Optimizing the implementation of the explicit treatment of thermal motion – how fast can it get? In: M&C 2013. Sun Valley, ID, May 5–9, 2013.

Viitanen, T., Leppänen, J., 2014. Target motion sampling temperature treatment technique with elevated basis cross section temperatures. Nucl. Sci. Eng. 177, 77–89.

X-5 Monte Carlo Team, 2003. MCNP—a general Monte Carlo n-particle transport code, version 5. Tech. Rep. LA-UR-03-1987, Los Alamos National Laboratory.

Please cite this article in press as: Viitanen, T., Leppänen, J. Effect of the Target Motion Sampling temperature treatment method on the statistics and performance. Ann. Nucl. Energy (2014), http://dx.doi.org/10.1016/j.anucene.2014.08.033

PUBLICATION VII

Target motion sampling temperature treatment technique with track-length estimators in OpenMC – Preliminary results

In proc. PHYSOR-2014, Kyoto, Japan,
Sep. 28 – Oct 3, 2014.

PHYSOR 2014 - The Role of Reactor Physics toward a Sustainable Future
The Westin Miyako, Kyoto, Japan, September 28 - October 3, 2014, on CD-ROM (2014)

TARGET MOTION SAMPLING TEMPERATURE TREATMENT TECHNIQUE WITH TRACK-LENGTH ESTIMATORS IN OPENMC — PRELIMINARY RESULTS

Tuomas Viitanen and Jaakko Leppänen
VTT Technical Research Centre of Finland
P.O. Box 1000, FI-02044 VTT, Finland
tuomas.viitanen@vtt.fi

Benoit Forget
Massachusetts Institute of Technology, Department of Nuclear Science and Engineering
77 Massachusetts Avenue, 24-107, Cambridge, MA 02139, United States

ABSTRACT

This paper examines the applicability of the Target Motion Sampling (TMS) temperature treatment method together with track-length estimators. Several track-length estimator based quantities are calculated in four test cases using a preliminary implementation of the method in OpenMC. The results are compared to an NJOY-based reference. The study reveals a statistically significant bias in the estimator results, but the errors were found to only affect limited energy regions, and their magnitude is relatively small as long as energy-integrated estimators are considered.

Key Words: **on-the-fly, Doppler-broadening, track-length estimator, TMS, OpenMC**

1. INTRODUCTION

Target Motion Sampling (TMS) temperature treatment technique is a stochastic method for taking the effect of the thermal motion of nuclides on path lengths and reaction rates into account on-the-fly during a Monte Carlo neutron tracking calculation. The method provides for modeling of arbitrary material temperatures with only one set of cross sections stored in the computer memory, significantly decreasing the memory demand of coupled multi-physics calculations involving detailed temperature distributions. Currently, the method is only able to deal with the energy region of resolved resonances and the thermal region of non-bound nuclides, but there are plans to extend the method to $S(\alpha, \beta)$ and the region of unresolved resonances in the future.

Previously, the TMS method has only been studied as a part of the Serpent 2 Monte Carlo code. The implementation of the method in Serpent has been found to be both accurate and well-feasible in terms of performance [1]. Since the calculation of reactor-physical parameters in Serpent relies on collision estimators, the functionality of the TMS method has not previously been studied together with track-length estimators. As there has been discussion whether or not the TMS method can be used together with track-length estimators in the first place, it was decided to scratch the surface of this important topic with a simple hands-on study.

The main application of the TMS method in Serpent is related to the multi-physics interface. Since this interface relies strongly on rejection sampling techniques that can only be applied together with the collision estimators, implementation of the track-length estimators in Serpent only for the purpose of the current study was considered pointless. Hence, the open-source Monte Carlo code OpenMC was chosen as the testing platform [3, 4]. The TMS method was implemented in a currently non-public branch of the OpenMC, primarily, to study the TMS method together with the track-length estimators and, secondarily, to test the performance of the method in a new code. The very first results, including problems that are recognized but not yet solved, are presented in the current article.

2. METHODOLOGY

2.1. OpenMC Monte Carlo Code

OpenMC is an open-source Monte Carlo code originating from the Massachusetts Institute of Technology. The code development has strong emphasis on efficient high-performance computing with current and future parallel computers. The focus on massive parallelization has affected many of the techniques implemented in the code, including for instance the efficiently parallelizable fission bank algorithm and the double-indexing based implementation of the unionized energy grid, which significantly speeds up cross section data retrieval with only a small increase in the memory requirement [3, 5, 6].

OpenMC was the natural choice for the current study for a couple of reasons. First of all, OpenMC, unlike Serpent, uses track-length estimators in the estimation of reaction rates, k_{eff} etc., which makes the study possible in the first place. Second, the source code of OpenMC is freely and easily accessible through the GitHub hosting service. In addition, OpenMC uses the same ACE cross section data format as MCNP and Serpent, significantly facilitating inter-code comparisons.

Since in OpenMC the material-wise macroscopic cross sections are calculated on-the-fly during transport, the code also acts as a very good reference for measuring the performance of the TMS method. This is not the case with the Serpent Monte Carlo code in which the macroscopic cross sections are normally precalculated in the problem initialization phase. As this optimization tweak cannot be utilized together with the TMS method, a normal Serpent calculation does not provide a fair reference for the TMS method, and artificial slowing-down of the Serpent calculations in the hope of a better performance reference, as it has been done for example in Reference [1], has its own issues.

2.2. TMS Temperature Treatment Method

Target Motion Sampling (TMS) temperature treatment technique was introduced for the first time in English-written journals in 2012 [7], but it was recently learned that a similar method has been presented already in 1984 in the Soviet Russia [8] and has been routinely used in Russian Monte Carlo

codes for many years. The efficiency and optimization of the method has been further discussed in References [1] and [9].

The TMS method is, contrary to other recently-developed on-the-fly temperature treatment techniques [10, 11], in fact a neutron tracking rather than a Doppler-broadening technique. Thus, the Doppler-broadened, effective cross sections are not calculated at any point of the transport calculation, but instead the temperature corrections are based on sampling target velocities at collision sites and using the available cross sections to determine the reaction probabilities in target-at-rest frame. To make this possible, a majorant-based rejection sampling technique must be applied in the sampling of path lengths, as described in Reference [1].

In the current study, "traditional" or DBRC-style truncation of the Maxwellian is used in the generation of the majorant cross section [9]. Thus, the energy range of thermal motion around neutron energy E is defined by limits

$$E_{\min,n}(E) = \left(\sqrt{E} - h\sqrt{\frac{k_{\mathrm{B}}\Delta T_n}{A_n}}\right)^2 \tag{1}$$

$$E_{\max,n}(E) = \left(\sqrt{E} + h\sqrt{\frac{k_{\mathrm{B}}\Delta T_n}{A_n}}\right)^2 , \tag{2}$$

where A_n is the atomic weight ratio of nuclide n,

$$\Delta T_n = T_{\max,n} - T_{\mathrm{base}} \tag{3}$$

is the temperature difference between the maximum temperature of the nuclide $T_{\max,n}$ and the cross sections T_{base}, k_{B} is the Boltzmann constant and h specifies the range of thermal motion in terms of dimensionless velocity, similar to the truncation originally used in the Sigma1 kernel broadening method [12]. In other words, h defines the conservativity of the majorant (see Section 2.4).

2.3. Track-length Estimators

The basic idea behind track-lengths is the fact that the integral of neutron flux over a volume is equal to the total track-length of neutrons within the volume in a time interval. Consequently, by keeping track of the neutron track-lengths l during a Monte Carlo transport calculation it is possible to gain information on the spatially integrated neutron flux. When scoring the neutron flux using track-length estimators, the score s_i corresponding to track-length i is defined

$$s_i = w_i l_i \,, \tag{4}$$

where w_i is the neutron weight, and the estimator for the neutron flux Φ is simply the (normalized) sum of the scores obtained during the transport simulation. Furthermore, the scores can be binned with respect of, for example, energy or spatial domain to gain information on the neutron spectrum or the spatial flux distribution.

The estimators can also be used to calculate reaction rates and other integrals of type

$$\int_t \int_V \int_E f(E,\overline{r})\Phi(E,\overline{r}) dt d^3r dE \,, \tag{5}$$

where the integration is carried over time, some spatial volume and an energy interval, and $f(E,\overline{r})$ is a response function. In this case the scores are multiplied by the value of the response function f_i corresponding to the track-length, i.e.

$$s_i = w_i f_i l_i \,. \tag{6}$$

For example, when calculating the capture reaction rate the value of the response f_i would be the macroscopic capture cross section in the material zone of the neutron track l_i corresponding to neutron energy E, $f_i = \Sigma_\gamma(E,\overline{r},T)$. When using track-length estimators in the estimation of quantities other than the neutron flux (for which $f_i = 1.0$), the value of the response must represent the whole track-length l_i and, therefore, the material zones in the Monte Carlo transport must be homogeneous with respect to density, nuclide composition and temperature T.

With the TMS temperature treatment method, the effective cross sections at the temperature of the material zone T are not available in general. Hence, the scoring of the estimators must be somehow based on the cross sections at temperature $T_{\mathrm{base}} \leq T$. What comes to *collision* estimators, it was demonstrated in [2] that the effect of thermal motion on cross section responses can be taken into account by first sampling target velocities and then using target-at-rest frame cross sections at T_{base} as responses, similar to the basic idea behind the TMS method. To take also the low-energy effects of thermal motion into account, the responses must be additionally multiplied by the Doppler-integral for constant cross section

$$g_n(E,\Delta T) = \Big(1+\frac{k_{\mathrm{B}}\Delta T}{2A_nE}\Big)\mathrm{erf}\Big(\sqrt{\frac{A_nE}{k_{\mathrm{B}}\Delta T}}\Big) + \sqrt{\frac{k_{\mathrm{B}}\Delta T}{\pi A_nE}}e^{-A_nE/(k_{\mathrm{B}}\Delta T)} \,. \tag{7}$$

Thus, when scoring the total capture reaction rate within TMS transport, the responses become

$$f_i = \sum_n g_n(E, T-T_{\mathrm{base}})\Sigma_{\gamma,n}(E'_n,\overline{r},T_{\mathrm{base}}) \,, \tag{8}$$

where E'_n are the sampled target-at-rest energies for nuclides n.

In the current work a similar approach is applied for the track-length estimators. However, some problems are expected due to the usage of non-representative cross section responses in the scoring. To demonstrate the problem, let us consider N monoenergetic neutron tracks with energy E_{m} that are used to estimate the reaction rate of reaction r. In conventional neutron transport the expected value (EV) of the estimator is

$$\begin{aligned} EV[R_{\mathrm{eff}}] \quad &= EV[\sum_i^N s_i] = EV[w_1\Sigma_{\mathrm{eff},r}(E_{\mathrm{m}},\overline{r},T)l_1 + w_2\Sigma_{\mathrm{eff},r}(E_{\mathrm{m}},\overline{r},T)l_2 + \dots] \\ &= \Sigma_{\mathrm{eff},r}(E_{\mathrm{m}},\overline{r},T)EV[\sum_i^N w_i l_i] \end{aligned} \tag{9}$$

where $\Sigma_{\mathrm{eff},r}(E_{\mathrm{m}},T)$ is the effective cross section of reaction r at material temperature T. With TMS transport the effective cross sections must be approximated with sampled cross section responses and the corresponding EV becomes

$$\begin{aligned} EV[R_{\mathrm{TMS}}] \quad &= EV[w_1 g_n(E_{\mathrm{m}},\Delta T)\Sigma_r(E'_1,\overline{r},T_{\mathrm{base}})l_1 + w_2 g_n(E_{\mathrm{m}},\Delta T)\Sigma_r(E'_2,\overline{r},T_{\mathrm{base}})l_2 + \dots] \\ &= EV[\sum_i^N w_i g_n(E_{\mathrm{m}},\Delta T)\Sigma_r(E'_i,\overline{r},T_{\mathrm{base}})l_i] \,, \end{aligned} \tag{10}$$

where n is the target nuclide of reaction r. If the track-lengths were independent of the sampled responses, the expected value in (10) would correspond to [13]

$$\begin{aligned} EV[\sum_i^N w_i g_n(E_\mathrm{m}, \Delta T)\Sigma_r(E_i', \overline{r}, T_\mathrm{base})l_i] &= EV[g_n(E_\mathrm{m}, \Delta T)\Sigma_r(E_i', \overline{r}, T_\mathrm{base})]EV[\sum_i^N w_i l_i] \\ &= \Sigma_{\mathrm{eff},r}(E_\mathrm{m}, \overline{r}, T)EV[\sum_i^N w_i l_i]\,, \end{aligned} \tag{11}$$

i.e. the correct expected value. However, the sampled cross section responses are also used in the neutron tracking process while determining whether a collision point candidate is accepted, terminating the neutron track and ultimately defining the track-length, or rejected, in which case the tracking proceeds by sampling of a new collision point candidate. Consequently, the track-lengths and responses are at least somewhat correlated, meaning that Equation (11) does not hold. This may introduce bias in the estimator results. The correlation effects are emphasized if the response reaction r has significant impact on the neutron transport process and involves a strongly energy-dependent cross section. The basic cause for the problem persists also when calculating energy-integrated estimators.

To reduce the correlations, all of the information on sampled cross sections obtained along each track-length is utilized instead of using only one cross section sample per nuclide per score. In practice, every time the velocity of a target nuclide is sampled during the TMS tracking process, the corresponding target-at-rest cross sections are used to accumulate nuclide-wise cross section sums and the average of the cross sections (multiplied by g_n) is used as the response when finally scoring the track-length estimator. In case the cross sections for some nuclides have not been sampled even once before the track ends, cross sections for these nuclides are sampled prior to scoring the estimator.

2.4. Implementation of TMS in OpenMC

The Target Motion Sampling (TMS) temperature treatment method was implemented in the OpenMC Monte Carlo code using the Elevated Basis Temperature approach, meaning that the basis cross sections can be at any temperature between zero Kelvin and the minimum temperature of the nuclei in the system. In the original TMS method the basis cross sections were forced to zero Kelvin, but it was later realized that the performance of the method can be significantly increased by elevating the basis cross section temperature [1]. The method was implemented such that the TMS method is only used for user-specified materials and the remaining materials are treated normally using pre-broadened cross sections.

The calculation of the nuclide-wise majorant cross sections is done in the problem initialization phase and the cross sections are kept in the computer memory. The majorant boundaries are chosen according to the "traditional" method (Equations (1)–(2)), which is based on the truncation of the Maxwell-Boltzmann distribution. The studies performed in [9] showed that the conservativity of the majorant can be decreased by changing the value of the h parameter in Equations (1)–(2) from original value of $h = 4.0$ to $h = 3.0$. This increases the performance of the TMS method without affecting the neutron transport in practice.

The usage of TMS slightly increases the memory consumption of OpenMC, because nuclide-wise majorant cross sections and the sums of sampled cross sections used in the scoring of the estimators are stored, in addition to the normal data. The memory consumption of the sampled cross sections is very small, so in practice the increase in memory consumption comes from one additional cross section to be scored per nuclide. As the number of nuclides in problems involving burned fuel is around 300 and the number of points in the nuclide-wise energy grid is usually below 200 000, the increase in memory consumption should be less than 100 MB, multiplied by the number of parallel MPI processes.

3. TEST CASES

The first "PWR-Gd" case involves a 17x17 PWR fuel assembly with 16 Gadolinium-doped fuel rods in an infinite two dimensional lattice. The geometry and material definitions of the fuel assembly are from an NEA benchmark [14]. The only differences to the benchmark specifications are related to temperatures: the moderator temperature is risen to 600 K for simplicity and the originally flat temperature profiles of the fuel rods are replaced with 3-step distributions such that the pellets are divided into three equi-thick annular regions with temperatures 600 K, 900 K and 1200 K from outside in.

The second case is abbreviated "PWR-BU" and features the previously introduced "PWR-Gd" bundle irradiated to 40 MWd/kgU burnup. The irradiated material compositions were obtained by running a burnup calculation using Serpent 2.1.14. The resulting compositions contain 241 actinide and fission product nuclides with cross sections available in the data libraries.

The "HTGR" test case consists of TRISO particles within graphite matrix in an infinite three dimensional lattice. The specifications of the TRISO particles and the composition of the graphite matrix are based on a NEA benchmark for HTGR fuel depletion [15], and the lattice pitch is 0.16341 cm. The fuel kernel in the spherical TRISO particles is divided in two equally thick parts such that the innermost 0.0125 cm is at 1800 K temperature and the outer layer is at 1200 K. The temperature of all other materials is 1200 K.

The last of the test cases, "SFR", involves a fuel assembly from the sodium cooled fast reactor JOYO in an infinite two dimensional lattice. The specifications of the assembly can be found in [16]. The geometry and material definitions correspond to the benchmark definition for the $250^{\circ}\mathrm{C}$ core. Again, the fuel temperature is modified such that the inner half (radius) of the fuel pellets is at 1200 K and the outer half at 900 K temperature. All other materials are at 600 K temperature in the model.

4. RESULTS

The calculations were made using the development branch version of OpenMC 0.5.2 with extended xml support and the TMS temperature treatment method preliminarily implemented. It is empha-

sized that the implementation is not yet working correctly. Hence all results, particularly those considering the performance of the method, are very preliminary. Fixing the present problems in the implementation is expected to slightly decrease the performance.

The TMS method is used only for the fuel materials, while other materials are treated conventionally using NJOY-broadened cross sections. The basis temperature of the cross sections for the TMS treatment T_{base} equals the minimum temperature of the fuel material in each system. In the reference calculations all materials are modeled using NJOY cross sections as-is. The only difference between the TMS calculation and the reference is in the modelling technique of the thermal motion, i.e. the materials, the geometry definitions and the temperature profiles are identical. Probability table treatment for unresolved resonances is turned off in all of the calculations.

OpenMC was run using MPI parallelization on 12 Intel Xeon CPUs running at 3.47 GHz with the exception that the HTGR-case was run using only one processor due to an unidentified problem that caused random termination of the calculations for this test case. The cross section library is based on JEFF-3.1.1 and has been processed with NJOY using 0.001 reconstruction tolerance for high accuracy.

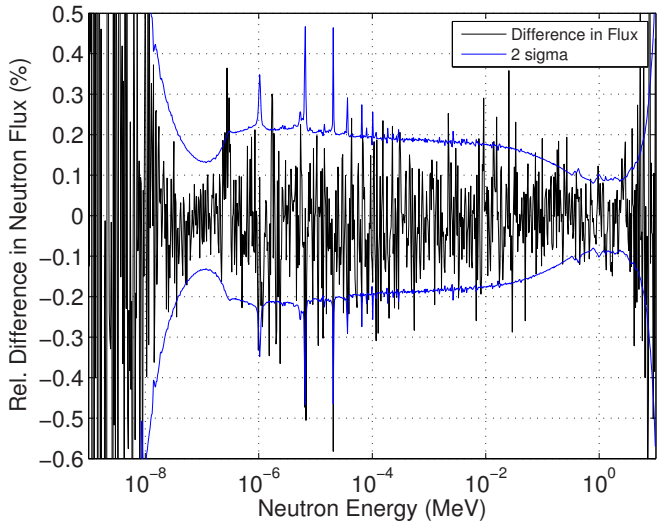

Figure 1. Comparison of the neutron spectra of the PWR-BU case between the TMS calculation and the reference.

4.1. Checking the Implementation

The very first thing to do is to check that the neutron transport with TMS is working properly. Almost all of the output parameters of OpenMC are calculated using track-length estimators, scored with sampled and, thus, potentially non-representative responses as described in Section 2.3. Since this kind of results may be biased, the validity of the implementation can only be checked via

neutron flux estimators for which the values of the responses are known to properly represent the track-lengths ($f_i = 1.0$).

The neutron flux spectra between a TMS calculation and the reference were compared in all of the four test cases and the comparison for the PWR-BU case is shown in Figure 1. Neutron flux spectra were in agreement in all of the four test cases, which indicates that the neutron transport is working properly.

4.2. Integral and Performance Results

The results of energy-integrated parameters and performance measures are provided in Table I. To emphasize the potential biases related to TMS and track-length estimators the reaction rates estimators were scored in fuel materials only. The combined k_{eff}, provided in Table I, is a combination of different track-length estimator based multiplication factors that OpenMC calculates by default.

Table I. Performance measures and integral results. The statistical deviations correspond to one sigma.

	PWR-Gd	**PWR-BU**	**HTGR**	**SFR**
Number of Neutrons	5×10^8	2×10^8	1×10^7	2.5×10^8
Reference Calculation				
Combined k_{eff}	1.15612 ± 4 pcm	0.93621 ± 6 pcm	1.21053 ± 29 pcm	1.78781 ± 4 pcm
Transport time (h)	2.4	13.5	9.5	4.7
XS Memory size (MB)	68	382	31	78
Tot. reaction rate (1/s)	5.7107 ± 1E-4	5.8728 ± 1E-4	3.1481 ± 6E-4	20.1789 ± 9E-4
Figure-of-Merit	4.64E+5	5.50E+4	9.48E+2	3.27E+4
Tot. absorption rate (1/s)	0.92494 ± 3E-5	0.92023 ± 4E-5	0.98426 ± 3E-4	0.98248 ± 5E-5
Figure-of-Merit	9.75E+4	1.20E+4	3.31E+2	2.30E+4
TMS Calculation				
Δk_{eff} (pcm)	5 ± 6	**-32** ± 8	-34 ± 41	3 ± 6
Transport time, abs/rel (h/-)	2.6 / 1.09	14.0 / 1.04	9.6 / 1.02	4.8 / 1.01
XS Memory size, abs/rel (MB/-)	32 / 0.47	136 / 0.36	16 / 0.51	50 / 0.64
Tot. reaction rate (1/s)	5.7088 ± 1E-4	5.8707 ± 1E-4	3.1455 ± 6E-4	20.1811 ± 9E-4
Figure-of-Merit, abs/rel	4.15E+5 / 0.90	5.28E+4 / 0.96	9.38E+2 / 0.99	3.24E+4 / 0.99
Tot. absorption rate (1/s)	0.92431 ± 3E-5	0.91938 ± 4E-5	0.9830 ± 3E-4	0.98252 ± 5E-5
Figure-of-Merit, abs/rel	9.02E+4 / 0.92	1.15E+4 / 0.96	3.40E+2 / 1.03	2.27E+4 / 0.99

The results show that in three cases out of four the k_{eff} estimate of the TMS calculation agrees with the reference within statistics. For the PWR-BU case the difference is 32 pcm, which is a relatively small error, but still statistically significant. Small biases can also be seen in the reaction rate estimators of the three thermal systems: the TMS results are consistently slightly smaller than the reference, but the errors are again small, less than 0.1 %. In the SFR case the estimators agree within statistics. The overhead from the TMS method varies between 1.01–1.09 for this preliminary implementation.

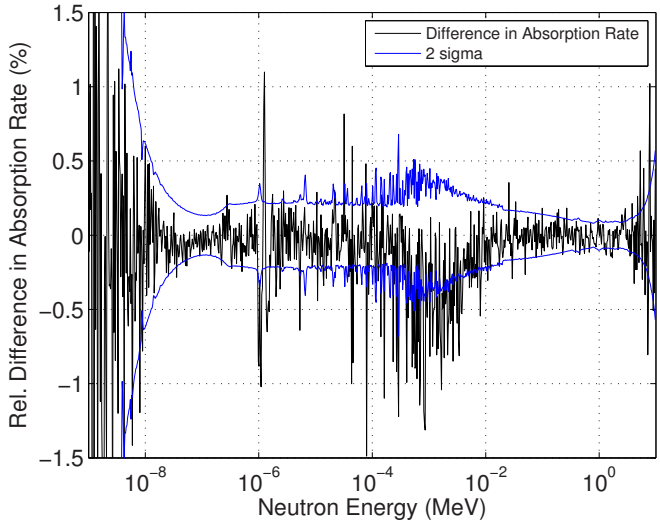

Figure 2. Comparison of the absorption spectra of the PWR-BU case between the TMS calculation and the reference.

4.3. Comparison of Reaction Rate Spectra

As the usage of track-length estimators together with the TMS method clearly introduces a small bias in some of the energy-integrated results, it is beneficial to take a look at the reaction rate spectra to get more information on the origin of the error. The absorption spectra for the PWR-BU case are compared in Figure 2. In this plot a region of negative bias can be seen in the surroundings of 1 keV and, additionally, several narrow error peaks can be recognized. The biases were otherwise similar in all of the thermal systems, but the lowest 1 eV bias peak was only present in the PWR-BU system.

The bias around 1 keV was studied further by calculating reaction rate spectra for the partial absorption reactions. It was noticed that the main contribution to the bias comes from $^{238}\mathrm{U}$. On the other hand, the absorption rate of $^{234}\mathrm{U}$ did not have any contribution to the bias even though it has a strongly energy-dependent cross section. These observations indicate that the bias originates from correlations between the track-lengths and the sampled cross sections and is specific to "important" nuclides, as anticipated. It also seems that there are no coarse errors in the implementation of the track-length estimators.

The 1 eV bias peak of the PWR-BU was traced back to nuclides $^{103}\mathrm{Rh}$, $^{239}\mathrm{Pu}$ and isotopes of Sm, which are only present in the PWR-BU case. Excluding $^{103}\mathrm{Rh}$ from the fuel compositions (both TMS and reference) made the positive part of the error peak disappear, and the negative part disappeared after removing $^{239}\mathrm{Pu}$ and Sm.

5. CONCLUSIONS AND FUTURE PROSPECTS

In the current study, the applicability of the TMS method together with track-length estimators was studied in four systems with different neutron spectra and characteristics. The calculations were performed using a preliminary implementation of the TMS method in the OpenMC Monte Carlo code.

Comparison of neutron fluxes in Section 4.1 showed that the implementation of the TMS is working correctly what comes to the neutron transport. Instead, a small but clear bias can be seen in the reaction rates and their derivatives that are calculated in OpenMC using track-length estimators. By comparing the reaction rate spectra it was noticed that the bias concerns a rather narrow energy region around 1 keV and, additionally, some individual resonances. The bias seems to originate from correlations between the track-lengths and the sampled cross sections that are used as responses. Since a negative correlation exists between the sampled cross section responses and corresponding track-lengths, a negative bias emerges in the estimator results at certain energies. However, also positive bias peaks were observed at a few narrow energy intervals. The exact origin of the positive peaks was not identified within the current study.

In general, using TMS-originated, sampled cross sections as responses in the scoring of the track-length estimators had surprisingly small effect on the accuracy of the reaction rates, at least when energy-integrated values are considered. Nevertheless, some unacceptable bias exists in the results and this bias must be removed before the implementation can be considered complete and the TMS method can be included in the official version of OpenMC.

It should be possible to fix the problems by, first, finding a way to recognize the problematic energy regions and cross sections and, then, increasing the number of cross section samples per response within these energy regions by artificially increasing the majorant cross sections. Since the bias exists only at a relatively narrow energy spectrum and sampling cross sections is computationally cheap, this brute-force approach should have only minor effect on the overall performance of the method. However, before proceeding on this path, the topic will be discussed together with the developers of the PRIZMA Monte Carlo code, who have previous experience on the application of track-length estimators together with a tracking method similar to TMS.

ACKNOWLEDGMENTS

This work was partly funded from the NUMPS project of the Finnish Academy and the KÄÄRME project under the Finnish Research Programme on Nuclear Power Plant Safety SAFIR2014. The first author would also like to thank MIT for hosting a productive four-week visit in the fall 2013 and all the fellow colleagues at MIT, especially Bryan Herman, for the invaluable help with the OpenMC code.

REFERENCES

[1] T. Viitanen and J. Leppänen, "Target Motion Sampling Temperature Treatment Technique With Elevated Basis Cross Section Temperatures", *Nuc. Sci. Eng.*, Accepted

[2] T. Viitanen and J. Leppänen, "Effect of the Target Motion Sampling Temperature Treatment Method on the Statistics and Performance", *Proc. SNA+MC2013*. Paris, France, 27–31 October (2013).

[3] P.K. Romano and B. Forget, "The OpenMC Monte Carlo Particle Transport Code", *Ann. Nucl. Energy*, **51**: pp. 274–281 (2013).

[4] The OpenMC Website, `http://mit-crpg.github.io/openmc/`

[5] P.K. Romano and B. Forget, "Parallel Fission Bank Algorithms in Monte Carlo Criticality Calculations", *Nucl. Sci. Eng.*, **170**: pp.125–135 (2012).

[6] J. Leppänen, "Two practical methods for unioninzed energy grid construction in continuous-energy Monte Carlo calculation", *Ann. Nucl. Energy*, **36**: pp. 878–885 (2009).

[7] T. Viitanen and J. Leppänen, "Explicit treatment of thermal motion in continuous-energy Monte Carlo tracking routines", *Nucl. Sci. Eng.*, **171**: pp. 165-173 (2012).

[8] V.N. Ogibin and A.I. Orlov, "Majorized cross-section method for tracking neutrons in moving media", *Voprosy Atomnoj Nauki i Techniki, Metodoki i Programmy*, **2(16)**: pp. 6–9 (1984), *In Russian*.

[9] T. Viitanen and J. Leppänen, "Temperature Majorant Cross Sections in Monte Carlo Neutron Tracking", *Nucl. Sci. Eng.*, in preparation

[10] G. Yesilyurt, W.R. Martin and F.B. Brown, "On-the-Fly Doppler Broadening for Monte Carlo Codes", *Nucl. Sci. Eng.*, **171**: pp. 239–257 (2012).

[11] B. Forget, S. Xu and K. Smith, "Direct Doppler broadening in Monte Carlo simulations using the multipole representation", *Ann. Nucl. Energy*, **64**: pp. 78–85, (2014).

[12] D. E. Cullen and C. R. Weisbin, "Exact Doppler Broadening of Tabulated Cross Sections", *Nucl. Sci. Eng.*, **60**, 199–229 (1976).

[13] E. Kreyszig, "Advanced Engineering Mathematics", 8th edition, John Wiley & Sons inc., New York, (1999).

[14] B. Roque et al., "Specification for the Phase 1 of a Depletion Calculation Benchmark devoted to Fuel Cycles", NEA/NSC/DOC(2004)11, OECD/NEA (2004).

[15] M. D. DeHart and A. P. Ulses, "Benchmark Specification for HTGR Fuel Element depletion", NEA/NSC/DOC(2009)13, Nuclear Energy Agency, Organization for Economic Cooperation and Development (2009).

[16] "Japan's experimental fast reactor Joyo Mk-ICore: Sodium-Cooled Uranium-Plutonium Mixed Oxide Fueled Fast Core Surrounded by UO2 Blanket", International Handbook of Evaluated Reactor Physics Benchmark Experiments, NEA/NSC/DOC(2006)1, Nuclear Energy Agency (2006).

Series title and number

VTT Science 84

Title	**Development of a stochastic temperature treatment method for Monte Carlo neutron tracking**
Author(s)	Tuomas Viitanen
Abstract	Thermal motion of nuclides has a significant effect on the reaction probabilities and scattering kinematics of neutrons. Since also the nuclides in nuclear reactor materials are in constant thermal motion, the temperature-induced effects need to be taken into account in all neutron transport calculations. This task is notably complicated by the fact that the temperature distributions within operating power reactors are always non-uniform. With conventional transport methods, accurate modeling of temperature distributions within a reactor is cumbersome. The temperature distributions that are in reality continuous in space need to be approximated with regions of uniform temperature. More importantly, pre-generated temperature-dependent data on reaction probabilities must be stored in the computer memory at each temperature appearing in the system, which restricts the feasible level of detail in the modeling of temperature distributions. This thesis covers the previous development of a temperature treatment technique for modeling the effects of thermal motion on-the-fly during Monte Carlo neutron transport calculation. Thus, the Target Motion Sampling (TMS) temperature treatment technique is capable of modeling arbitrary temperature distributions such that the memory footprint of the interaction data is unaffected by the resolution of the temperature discretization. As a very convenient additional feature the TMS technique also provides for modeling of continuous temperature distributions as-is, making the discretization of temperature distributions unnecessary altogether. The basic idea of the TMS technique is introduced, and the results are shown to be in accordance with reference solutions calculated with conventional neutron transport methods. The TMS method is developed further by optimizing its implementation, and the performance is compared against conventional neutron transport methods in different reactor systems. The results show that the TMS method significantly facilitates the modeling of complex temperature distributions in nuclear reactors without compromising the accuracy of the calculations. The method also proves to be well-feasible in terms of performance, especially as long as the number of temperature-dependent nuclides remains relatively small.
ISBN, ISSN	ISBN 978-951-38-8242-6 (Soft back ed.) ISBN 978-951-38-8243-3 (URL: http://www.vtt.fi/publications/index.jsp) ISSN-L 2242-119X ISSN 2242-119X (Print) ISSN 2242-1203 (Online)
Date	April 2015
Language	English, Finnish abstract
Pages	65 p. + app. 120 p.
Name of the project	
Commissioned by	
Keywords	Monte Carlo, neutron tracking, temperature, Doppler-broadening, DBRC, Target Motion Sampling, TMS, temperature majorant cross section
Publisher	VTT Technical Research Centre of Finland Ltd P.O. Box 1000, FI-02044 VTT, Finland, Tel. 020 722 111

Julkaisun sarja ja numero

VTT Science 84

Nimeke	**Stokastinen menetelmä lämpöliikkeen huomioimiseen Monte Carlo -neutronikuljetuslaskun aikana**
Tekijä(t)	Tuomas Viitanen
Tiivistelmä	Lämpöliike vaikuttaa merkittävästi sekä neutronien todennäköisyyteen vuorovaikuttaa nuklidien kanssa että nuklidien sirotusominaisuuksiin. Koska myös ydinreaktorin polttoaine ja muut reaktorimateriaalit ovat jatkuvassa lämpöliikkeessä, lämpötilan vaikutus täytyy huomioida käytännössä kaikissa neutronikuljetuslaskuissa. Tarkoissa reaktorifysiikka-analyyseissä täytyy lisäksi ottaa huomioon, että tehoajolla olevassa ydinreaktorissa lämpötilajakauma on epätasainen polttoaineen lämmöntuotannon vuoksi. Lämpötilajakaumien yksityiskohtainen mallinnus on hankalaa perinteisillä neutronikuljetusmenetelmillä. Ensinnäkin jatkuvat lämpötilajakaumat joudutaan mallintamaan likimääräisesti joukkona tasalämpöisiä alueita. Toiseksi neutronien vuorovaikutustodennäköisyydet täytyy tallentaa tietokoneen muistiin erikseen jokaisessa mallin lämpötilassa, joten tietokoneiden muistikapasiteetti rajoittaa merkittävästi mallinnettavissa olevien lämpötila-alueiden lukumäärää ja siten myös mallin tarkkuutta. Tässä väitöskirjassa on kehitetty Target Motion Sampling (TMS) -tekniikka, jonka avulla lämpötilan vaikutus reaktiotodennäköisyyksiin voidaan ottaa huomioon Monte Carlo -neutronikuljetuslaskun aikana. Uutta menetelmää käytettäessä vuorovaikutustodennäköisyydet tallennetaan tietokoneen muistiin ainoastaan yhdessä lämpötilassa riippumatta mallissa esiintyvien lämpötilojen määrästä, jolloin tietokoneiden muistikapasiteetti ei enää rajoita lämpötilajakaumien mallinnustarkkuutta. Lisäksi TMS-tekniikkaa käytettäessä jatkuvat lämpötilajakaumat voidaan mallintaa tarkasti myös sellaisenaan, jakamatta geometriaa tasalämpöisiin alueisiin. Väitöskirjassa esitellään ensin TMS-tekniikan perusidea ja osoitetaan, että TMS-tekniikalla ja perinteisillä kuljetusmenetelmillä päästään tilastollisen vaihtelun puitteissa samaan lopputulokseen. Tämän jälkeen menetelmää optimoidaan, ja sen suorituskykyä tutkitaan mallintamalla erilaisia reaktoreita. TMS-menetelmän käytön havaitaan helpottavan huomattavasti monimutkaisten lämpötilajakaumien mallinnusta vaikuttamatta tulosten tarkkuuteen. Menetelmä on hyvin käyttökelpoinen myös tehokkuutensa puolesta erityisesti silloin, kun mallissa olevien nuklidien määrä on suhteellisen pieni.
ISBN, ISSN	ISBN 978-951-38-8242-6 (nid.) ISBN 978-951-38-8243-3 (URL: http://www.vtt.fi/publications/index.jsp) ISSN-L 2242-119X ISSN 2242-119X (Painettu) ISSN 2242-1203 (Verkkojulkaisu)
Julkaisuaika	Huhtikuu 2015
Kieli	Englanti, suomenkielinen tiivistelmä
Sivumäärä	65 s. + liitt. 120 s.
Projektin nimi	
Rahoittajat	
Avainsanat	Monte Carlo, neutronikuljetus, lämpötila, Doppler-leveneminen, DBRC, Target Motion Sampling, TMS
Julkaisija	Teknologian tutkimuskeskus VTT Oy PL 1000, 02044 VTT, puh. 020 722 111

Development of a stochastic temperature treatment technique for Monte Carlo neutron tracking

Nuclear fission reactors are based on a self-sustaining fission chain reaction, carried on by neutrons. Since the reaction probabilities and scattering kinematics of neutrons are strongly affected by the thermal motion of target nuclides, the temperatures of nuclear reactor materials need to be taken into account in all reactor physical analyses. Detailed modeling of the temperature distributions within operating nuclear reactors is often problematic when using traditional neutron transport methods, which require the interaction probability data to be stored in the computer memory separately at each temperature appearing in the system. Consequently, the feasible level of detail in the temperature distributions is always restricted by the memory capacity of computers.

This thesis covers the previous development of the Target Motion Sampling (TMS) temperature treatment technique, which is capable of taking the effects of thermal motion on interaction probabilities into account on-the-fly during Monte Carlo neutron transport calculation. With the TMS method, arbitrary temperature distributions can be modeled based on interaction probability data at one temperature only, which significantly facilitates high-fidelity neutron transport calculations. The results suggest that the TMS method is both accurate and well-feasible in terms of performance, and thus it can be considered a practical temperature treatment technique for Monte Carlo neutron tracking.

ISBN 978-951-38-8242-6 (Soft back ed.)
ISBN 978-951-38-8243-3 (URL: http://www.vtt.fi/publications/index.jsp)
ISSN-L 2242-119X
ISSN 2242-119X (Print)
ISSN 2242-1203 (Online)